The molecular and cellular consequences of AsiDNA™ combined with radiotherapy on healthy tissue

Anouk Sesink

THÈSE DE DOCTORAT

NNT : 2023UPASL101

université PARIS-SACLAY

The molecular and cellular consequences of AsiDNA™ combined with radiotherapy on healthy tissue

Conséquences moléculaires et cellulaires d'AsiDNA™ combinée à la radiothérapie sur les tissus sains

Thèse de doctorat de l'université Paris-Saclay

École doctorale n° 582 Cancérologie : Biologie - Médecine - Santé (CBMS)
Spécialité de doctorat : Sciences du cancer
Graduate School : Life Sciences and Health. Référent : Faculté de médecine

Thèse préparée dans l'unité de recherche **Signalisation radiobiologie et cancer (Université Paris-Saclay, Inserm, CNRS)**, sous la direction de **Pierre-Marie GIRARD**, PhD, HDR,

Thèse soutenue à Paris-Saclay le 10 Novembre 2023, par

Anouk SESINK

Composition du Jury

Membres du jury avec voix délibérative

Pr. Anne-Helene Monsoro-Burq Professor, Université Paris-Saclay	Présidente
Pr. Marie-Catherine VOZENIN Professor, Université de Lausanne	Rapporteure and Examinatrice
Dr. Geoffrey HIGGINS Associate Professor, University of Oxford	Rapporteur and Examinateur
Dr. Laure MARIGNOL Professor, University of Dublin	Examinatrice
Dr. Kristoffer PETERSSON Principal investigator, University of Oxford	Examinateur
Pr. Laurent QUERO Professor, Université Paris Cité	Examinateur

université PARIS-SACLAY

ÉCOLE DOCTORALE
Cancérologie : biologie - médecine - santé (CBMS)

Invited jury member: Dr. Wael Jdey from 

Host institution: 

Funders: 

Voor mijn ouders.

To my parents.

'Life is not easy for any of us. But what of that? We must have perseverance and above all confidence in ourselves. We must believe that we are gifted for something, and that this thing must be attained.''

- *Maria Salomea (Marie) Skłodowska-Curie*

''I am among those who think that science has great beauty. A scientist in his laboratory is not only a technician: he is also a child placed before natural phenomena which impress him like a fairy tale. We should not allow it to be believed that all scientific progress can be reduced to mechanisms, machines, gearings, even though such machinery has its own beauty.''

- *Maria Salomea (Marie) Skłodowska-Curie*

Acknowledgements

My PhD adventure has truly been a roller-coaster and many of my successes have been with the great help of my colleagues and friends. In this acknowledgement I would like to express my great gratitude to all that have been important within the progress of my PhD.

First of all, I would like to thank my supervisor, **Dr. Pierre-Marie Girard**. I am thankful for all the support and opportunities I received throughout my PhD. I am very grateful for your guidance and encouragement along the way. I would like to express my thankfulness to the members of the scientific community who have invested their time, knowledge, and advice into my work. I would like to thank the rapporteurs of my PhD jury, **Dr. Geoffrey Higgins** and **Prof. Marie-Catherine Vozenin**, for their time evaluating my thesis. I also thank my examinateurs, **Prof. Anne-Helene Monsoro-Burq, Dr. Kristoffer Petersson, Dr. Laure Marignol** and **Prof. Laurent Quero** for kindly participating in my PhD jury. Furthermore, I would like to thank my monitoring committee meeting members **Prof. Marc Vooijs, Dr. Mark Hill** and **Dr. Wael Jdey** for their continues time and feedback throughout my PhD development.

In addition, I would like to thank unit **U1021** at Institut Curie, especially **Sandrine Bourgeois** and **Veronique Piveux** for ensuring everything was running smoothly. A massive thank you to **Sophie Leboucher** for her great support in histology and a big thank you to **Charlène Lasgi** for the support at the FACS platform together with the microscopy platform at Orsay.

Thank you to the doctorial school **Cancerologie: biologie – medicine – sante (CBMS), Institut Curie** and **Universite Paris-Saclay**, for providing me with the opportunity to conduct my PhD project. A special thank you to the **H2020 MDCA-ITN THERADNET** program, ran by **Prof. Martin Pruschy** and to **Fondation pour la recherche sur le cancer ARC** for the funding to pursue my PhD. I also would like to thank **Dr. Wael Jdey** and **Valerio Therapeutics** for providing not only the AsiDNA™ molecules but regular fruitful meetings dedicated to brainstorm and excel in the research.

I would like to thank all the current and former members of team Dutreix and team Londono that I had the great opportunity of working alongside them. With this I would like to highlight **Dr. Sophie Heinrich** for her great support during irradiations and always being keen to answer my many radiation physics questions. Furthermore, I would like to thank **Dr. Charles Fouillade**, **Dr. Vincent Favaudon** and **Maxime Dubail** for their great advice on FLASH radiotherapy,

radiation induced lung fibrosis and precision cut lung slices. I also would like to thank **Juliette Soulier**, **Directeur de recherche José Arturo Londono Vallejo**, **Dr. Delphine Javelaud** and **Nathalie Berthault** for their great support with single cell RNA sequencing and support in and outside of the lab. In addition, I would like to thank **Dr. Marie Dutreix**, not only the developer of the first concepts of AsiDNA™ but also a person I could always ask for advice and guidance throughout my PhD. A special thank you to **Ayan Mallick, Hugo Laporte, Jessica Bastian** and **Manon Delemazure** who really made my last year a very pleasant environment to work in. They provided much support as well as many fun times. And finally, I would like to thank **Margaux Becerra** who has not only supported me a great deal in my PhD project but also became a friend.

Throughout my PhD journey I have been part of the International Network for Training and Innovation in Therapeutic Radiation (THERADNET) where, together with fellow early-stage researchers, we excelled in our PhD progression together. I would like to thank all the Doctors and professors within this network for continues advice and discussions throughout my PhD development that have tremendously contributed to the improvement of my PhD project. I would also greatly like to thank all the early-stage researchers within this network, especially **Justin Rondeau, Elia Prades Sagarra, Nicole Machado** and **Eleanor Hawkins**. You have provided me with much joy during the meeting, hands-on advice and listened to all the ups and downs over the last 4 years.

I would like to thank the friends that I made during my previous adventures in the UK that still are very dear to me and have been supporting me throughout. Firstly, I would like to thank my fellow friends and MSc students **Dr. Janine Deblasi, Dr. Ryan Zitter, Collin Larkin, Yi-Chun Wang** and **Dr. Ayesha Khan** for our great radiation research adventures, advice and allowing me to explore and learn from their cultures. Secondly, I would like to thank **Dr. Susan Kilgas** and **Dr. Tiffany Ma**, two talented scientists that have been true inspirations for me during my MSc and PhD. Thank you for all the advice, guidance, support and all the fun times we shared together. During my time in Paris, I am very grateful to have made many friends that made my experience here incredible. Thank you to Eleanor Hawkins for her friendship and sharing our PhD journey together. Thank you to **Enci Kovacs**, **Dr. Marton Kovacs** and **Gertjan Laenen** for all the interesting discussions, exploring Paris and its culture together including many terraces. Furthermore, I would like to thank **Margaux Becerra** who has become a true friend, a partner in crime in and outside of the lab, with our shared passion for music, tattoos, traveling, and

her unstoppable ambition to alter my opinion about France. And finally, I must thank **Dr. Tina Karagyozova**, who truly became my little family in Paris. You have been so patient and loving with me throughout the last 3 years and provided me with much advice, a shoulder to cry or complain on and exciting scientific discussions that sometimes could last until deep in the night. You are truly one of the kindest and brightest minds I know and inspires me every day.
Going back to my origins, I will finish in Dutch. Hierbij wil ik graag **Lisa van de Ven, Mariem Bencharra, Eline van de Ven** en **Barbara Hoefeijzers** bedanken die me vanuit Nederland veel steun hebben verleend en mijn nieuwe thuis in Parijs hebben bezocht. Daarnaast wil ik de vriendengroep bedanken, specifiek **Kim Zumker, Dries Zumker** en **Nick Timmermans**. De globale pandemie was helaas niet de enige zware tijd tijdens mijn promotie. In 2021 verloren vele van mijn vrienden waaronder ikzelf, plotseling een goede vriend, **Freek Drenth**. Daarom wil ik hem uitzonderlijk bedanken voor zijn vriendschap en steun.
Graag sluit ik af met het bedanken van de belangrijkste personen in mijn leven, mijn familie. Ik wil mijn broertje bedanken, **Thijs Sesink**, en mijn grootouders, **Franz** en **Mien Kreuz,** voor al de support en ervoor zorgen dat Vessem altijd een thuis voor mij blijft. Ook bedank ik de rest van familie Kreuz en Sesink voor alle steun en interesse in mijn educatie. Tenslotte, **Mam (Sabine Sesink)** en **pap (John Sesink),** ontzettend bedankt voor de eindeloze liefde, steun, advies en een luisterend die jullie gegeven hebben en nog steeds geven tijdens mijn gehele leven. Of het nou het aanvechten van het Nederlandse educatie systeem was voor betere ondersteuning van mijn dyslexie, al mijn theatervoorstellingen bijwonen of weer op vakantie moeten naar een onverwacht land vanwege mijn stages of studies. Zoals ze in het Brabants zeggen, gullie deed ut gelijk, echt hardstikke bedankt!

September, Orsay 2023

Anouk Sesink

Résumé

Contexte/objectifs : La radiothérapie et la chimiothérapie sont couramment utilisées dans les traitements anticancéreux à visée curative. Cependant, les effets secondaires, parfois graves, qui y sont associés empêchent souvent de mener à bien le plan de traitement initial. Bien que les normes de soins actuelles aient réduit la fréquence des lésions graves, leur efficacité reste sous-optimale. Des études antérieures ont révélé qu'AsiDNA™, une courte molécule d'ADN double brin capable d'interférer avec la machinerie de réparation de l'ADN, sensibilise les cellules tumorales in vitro et in vivo à la chimio- et radio-thérapie, sans augmenter la sensibilité des tissus normaux. Ces observations nous ont amenés à évaluer le potentiel d'AsiDNA™ à protéger les tissus sains des toxicités induites par les radiations et à explorer son comportement dans les cellules normales.

Méthodes : In vitro, nous avons combiné des analyses par cytométrie de flux, par Western blot, par immunofluorescence et par invalidation de l'expression de certains gènes dans des cellules normales et tumorales pour étudier l'impact d'un traitement par AsiDNA™ sur l'arrêt du cycle cellulaire. En outre, nous avons étudié la survie des cellules normales et tumorales en réponse à une chimiothérapie ou une irradiation combinée ou non à AsiDNA™ pour évaluer un rôle protecteur d'AsiDNA™. Nous avons utilisé un biomarqueur de l'activité d'AsiDNA™ (γ-H2AX) pour explorer l'activité d'AsiDNA™ dans les différentes phases du cycle cellulaire et dans des cellules en prolifération ou quiescentes. In vivo, nous avons combiné le traitement par AsiDNA™ avec la radiothérapie FLASH et conventionnelle (FLASH-RT versus CONV-RT) sur des souris C57BL6/J. La toxicité aiguë radio-induite a été examinée en quantifiant la survie des cryptes de l'intestin après une irradiation abdominale. La toxicité tardive radio-induite a été examinée par le suivi de la survie des animaux au cours du temps et l'apparition de la fibrose pulmonaire après une irradiation du thorax. En parallèle, le niveau d'expression de cytokines inflammatoires dans le plasma sanguin a été mesuré de 2 semaines à 5 mois après l'irradiation du thorax des souris, et une étude préliminaire de séquençage de l'ARN sur cellule unique menée pour identifier les signatures génétiques pro-fibrotiques des poumons irradiés. Enfin, des coupes histologiques de l'intestin de souris C57BL6/J sauvages ainsi que des coupes ex vivo de poumons issus de souris C57BL6/J délétées ou non pour p53 ont été utilisés pour identifier le mécanisme de radio-protection par AsiDNA™ dans les modèles de réponse précoce et tardive.

Résultats : In vitro, AsiDNA™ pénètre dans les cellules normales et tumorales mais n'induit un arrêt du cycle cellulaire en G1/S que dans les cellules normales. Nous avons révélé que cet arrêt est dépendant des protéines DNA-PK/p53/p21 et qu'il est absent dans les cellules tumorales. Nous montrons que si la phosphorylation de l'histone H2AX, un biomarqueur de l'activité d'AsiDNA™ dans les cellules, est détectée assez rapidement après l'ajout d'AsiDNA™ aux cellules, celle-ci n'a lieu qu'en phase G1 du cycle cellulaire, bien qu'AsiDNA™ pénètre dans toutes les cellules. En outre, l'arrêt en G1/S est indépendant de la phosphorylation d'H2AX. Par ailleurs, nous montrons que l'activité d'AsiDNA™ est fortement réduite dans les cellules quiescentes par rapport aux cellules en division. Le mécanisme sous-jacent est toujours en cours d'étude. In vitro, l'association d'AsiDNA™ à de la chimiothérapie ou de la radiothérapie augmente la survie des cellules saines et prolifératives, ce qui n'est pas le cas des cellules tumorales ou des cellules normales déficientes en p53. In vivo, nous montrons un rôle radioprotecteur d'AsiDNA™. En effet, l'association d'AsiDNA™ avec CONV-RT a retardé l'apparition de la fibrose pulmonaire et augmenté la survie des cryptes dans l'intestin par rapport à CONV-RT seule. Un effet protecteur est aussi observé avec FLASH-RT seul qui n'est pas amélioré si AsiDNA™ est associée à FLASH-RT. Le séquençage de l'ARN en cellule unique du poumon irradié a révélé une signature génétique pro-fibrotique présente dans les fibroblastes et les macrophages alvéolaires en réponse à la radiothérapie CONV. Cette signature est réduite lors de la radiothérapie CONV combinée au traitement AsiDNA™ et au traitement radiothérapeutique FLASH seul. L'activation des cytokines inflammatoires observée dans le plasma sanguin après l'irradiation du thorax a révélé une synergie unique entre la radiothérapie combinée au traitement AsiDNA™, avec une augmentation de l'IFN-γ, du TNF-α et du GM-CSF. En outre, un mécanisme d'arrêt de cycle en phase G1/S impliquant DNA-PK, p53 et p21 a été observé dans les modèles in vivo de l'intestin et ex vivo de coupes de poumon, comparables à celui identifié in vitro.

Conclusion : Ces résultats suggèrent que, grâce à l'arrêt du cycle cellulaire en G1/S induit par AsiDNA™ sur des cellules normales en division in vivo, la combinaison d'AsiDNA™ avec diverses modalités d'irradiation réduit la toxicité induite par l'irradiation. Ce mécanisme est absent dans les cellules tumorales, dans lesquelles AsiDNA™ fonctionne comme un radiosensibilisateur, offrant ainsi une opportunité unique d'utiliser AsiDNA™ en oncologie pour une augmentation bilatérale de la fenêtre thérapeutique.

Summary

Background/Aims: Radiotherapy and chemotherapy are customary implemented in cancer treatments with curative intent. However, the associated severe side effects often interfere with the completion of the initial treatment plan. Although the current standard of care reduced the frequency of severe injuries, their efficacy is still suboptimal. Previous studies have uncovered that AsiDNA™, a short double-stranded DNA molecule able to interfere with the DNA repair machinery, chemo- and radio-sensitizes tumour cells in vitro and in vivo, with no increased normal tissue sensitivity. These observations led us to assess the potential of AsiDNA™ to protect healthy tissues from radiation induced toxicities and explore its behaviour in normal cells.

Methods: In vitro, we combined flow cytometry, Western blot, immunofluorescence, and gene expression invalidation analyses in normal and tumour cells to study the impact of AsiDNA™ treatment on cell cycle arrest. In addition, we studied the survival of normal and tumour cells in response to chemotherapy or irradiation combined or not with AsiDNA™ to assess a protective role of AsiDNA™. We used a biomarker of AsiDNA™ activity (γ-H2AX) to explore AsiDNA™ activity in different phases of the cell cycle and in proliferating or quiescent cells. In vivo, we combined AsiDNA™ treatment with FLASH and conventional radiotherapy (FLASH-RT versus CONV-RT) in C57BL6/J mice. Acute radiation-induced toxicity was examined by quantifying the survival of intestinal crypts after abdominal irradiation. Late radiation-induced toxicity was examined by monitoring animal survival over time and the appearance of pulmonary fibrosis after thoracic irradiation. In parallel, the level of inflammatory cytokine expression in blood plasma was measured from 2 weeks to 5 months after all thorax irradiation of mice, and a preliminary single-cell RNA-sequencing study was conducted to identify pro-fibrotic genetic signatures of irradiated lungs. Finally, histological sections of the intestine of wild-type C57BL6/J mice, as well as ex vivo sections of lungs from p53-deficient and wild-type C57BL6/J mice were used to identify the mechanism of radioprotection by AsiDNA™ in early and late responding models.

Results: In vitro, AsiDNA™ penetrates normal and tumour cells, however, induces G1/S cell cycle arrest only in normal cells. We reveal that this arrest is DNA-PK/p53/p21-dependent and absent in tumour cells. We show that while phosphorylation of histone H2AX, a biomarker of AsiDNA™ activity in cells, is detected quickly after AsiDNA™ is added to cells, this only occurs

in G1 phase of the cell cycle. Moreover, G1/S arrest is independent of H2AX phosphorylation. Furthermore, we show that AsiDNA™ activity is strongly reduced in quiescent cells compared to dividing cells, and the underlying mechanism is still under investigation. In vitro, the combination of AsiDNA™ with chemotherapy or radiotherapy increases the survival of healthy, proliferative cells, which is not the case for tumour cells or normal p53-deficient cells. In vivo, we show a radioprotective role of AsiDNA™. Indeed, the combination of AsiDNA™ with CONV-RT delayed the onset of pulmonary fibrosis and increased crypt survival in the intestine compared with CONV-RT in standalone. A protective effect was also observed with FLASH-RT alone, which was not enhanced if AsiDNA™ was combined with FLASH-RT. Single-cell RNA sequencing of irradiated lung revealed a pro-fibrotic genetic signature present in fibroblasts and alveolar macrophages in response to CONV radiotherapy. This signature is reduced in response to CONV-RT combined with AsiDNA™ and FLASH-RT. The activation of inflammatory cytokines observed in blood plasma after thorax irradiation revealed a unique synergy between radiotherapy combined with AsiDNA™ treatment, with an increase in IFN-γ, TNF-α and GM-CSF. In addition, a G1/S phase cycle arrest mechanism involving DNA-PK, p53 and p21 was detected in vivo in gut and ex vivo in precision cut lung slices, comparable to that identified in vitro.

Conclusion: These results suggest that due to the G1/S cell cycle arrest induced by AsiDNA™ on dividing normal cells in vivo, the combination of AsiDNA™ with various irradiation modalities reduces irradiation-induced toxicity. This mechanism is absent in tumour cells, in which AsiDNA™ functions as a radiosensitizer, offering a unique opportunity to use AsiDNA™ in oncology for a bilateral increase in the therapeutic window.

Contents

List of figures

List of tables

Abbreviations

3D-CRT	Three-dimensional conformal radiotherapy
5-FU	5-fluoruracil
AM	Alveolar macrophages
ASR	Age-standardised rate
ATM	Ataxia-telangiectasia mutated
ATR	Ataxia telangiectasia and Rad3 related
AT1	Alveolar type 1
AT2	Alveolar type 2
BBB	Blood brain barrier
BRCA	Breast cancer susceptibility protein
CBC	Crypt-base-columnar cells
Cdk	Cyclin dependent kinases
CECs	Crypt epithelial cells
Chk1	Checkpoint kinase 1
Chk2	Checkpoint kinase 2
CONV-RT	Conventional radiotherapy
CT	Computed tomography
CTD	C-terminal domain
DBD	DNA-binding domain
DC	Dendritic cells
DDR	DNA damage response
DNA-PK	DNA-dependent protein kinase
DPS	Darinaparsin
DSBs	Double stranded breaks
ECM	Extracellular matrix
EC	Endothelial cells
EMT	Endothelial mesenchymal transition
FDA	Food and drug administration
FLASH-RT	FLASH radiotherapy

FSU	Functional subunits
GI	Gastrointestinal
GM-CSF	Granulocyte-macrophage colony-stimulating factor
HCC	Human hepatocellular carcinoma
HR	Homologous recombination
Hsp90-p	Heat shock protein 90 phosphorylation
HSPCs	Hematopoietic stem/progenitor cells
HT	Helical tomotherapy
IL	Interleukin
IM	Interstitial macrophages
IMPT	Intensity-Modulated Proton Therapy
IMRT	Intensity modulated radiotherapy
IV	Intravenous
KGF	Keratinocyte growth factor
LDL-R	Low-density lipoprotein receptor
LET	Linear energy transfer
MAPK	Mitogen-activated protein kinases
MBRT	Minibeam radiotherapy
MDM2	Mouse double minute 2 homolog
MRC-5	Primary human lung fibroblasts
MRI	Magnetic resonance imaging
NF-κB	nuclear factor-kappa B
NHEJ	Non-homologous end-joining
NHSF/BJ	Normal human skin fibroblasts
NK cells	Natural killer cells
NO	Nitric oxide
NSCLC	Non-small cell lung cancer
NTD	N-terminal transactivation domain
OARs	Organs at risk
OD	Oligomerization domain
OER	Oxygen enhancement ratio
PARP	Poly(ADP-ribose) polymerase

PBT	Proton beam therapy
PCLS	Precision cut lung slices
PCNA	proliferating cell nuclear antigen
PD-1	Programmed cell death protein 1
PD-L1	Programmed death-ligand 1
PDGF	Platelet-derived growth factor
PET	Positron emission tomography
PFA	Paraformaldehyde
pMBRT	Proton Minibeam radiotherapy
PR	Proline-rich domain
PTM	Post translational modification
PUMA	P53 upregulated modulator of apoptosis
RILI	Radiation induced lung injury
ROO	Peroxyl radicals
ROS	Reactive Oxygen Species
RPE-hTERT	Retinal pigment epithelium human telomerase reverse transcriptase
scRNA-seq	Single cell RNA sequencing
SH	Sulfhydryl
SMC	Smooth muscle cells
SSBR	Single stranded break repair
ssDNA	Single-stranded DNA
SSBs	Single stranded breaks
SV40	Large T-antigen simian virus 40
TACE	Trans arterial chemoembolization
TA	Transit-amplifying
TAD	Transactivation domain
TGF-β	Transforming Growth Factor-β
TNF-α	Tumour necrosis factor-α
UV	Ultraviolet
VEGFR	Vascular endothelial growth factor receptor
VMAT	Volumetric modulated arc therapy

XRCC	X-ray repair cross-complementing protein
γH2AX	Gamma Histone H2A variant

I. INTRODUCTION

1. Standard of care

1.1. The status of cancer incidences within the population

Worldwide, the second biggest mortality cause is cancer. It is estimated that global cancer rates will increase 47% by 2040, paired with an alarming increase in the need for preventive measures, treatment availability, and increased cancer-related mortality rates [1]. Following the information provided by the world health organization, the estimated age-standardized cancer incidence worldwide in 2020 identified an incidence rate above 250 cases per 100.000 citizens in the western world (Figure 1A). In Europe, the estimated mortality rate in 2020 reached almost 2 million people, of which 19.6% lung cancer, 12.5% colorectal cancer, 7.3% breast cancer and 6.8% pancreatic cancer (Figure 1B-C). The demographic changes estimated that by 2040 the incidence of new cancer cases in Europe will rise from 4.4M up to 5.32M. (Figure 1D). This stresses the emerging cancer related mortality rates that society will encounter in the future, underlining the importance of enhancing cancer treatment modalities and improving the standard of care.

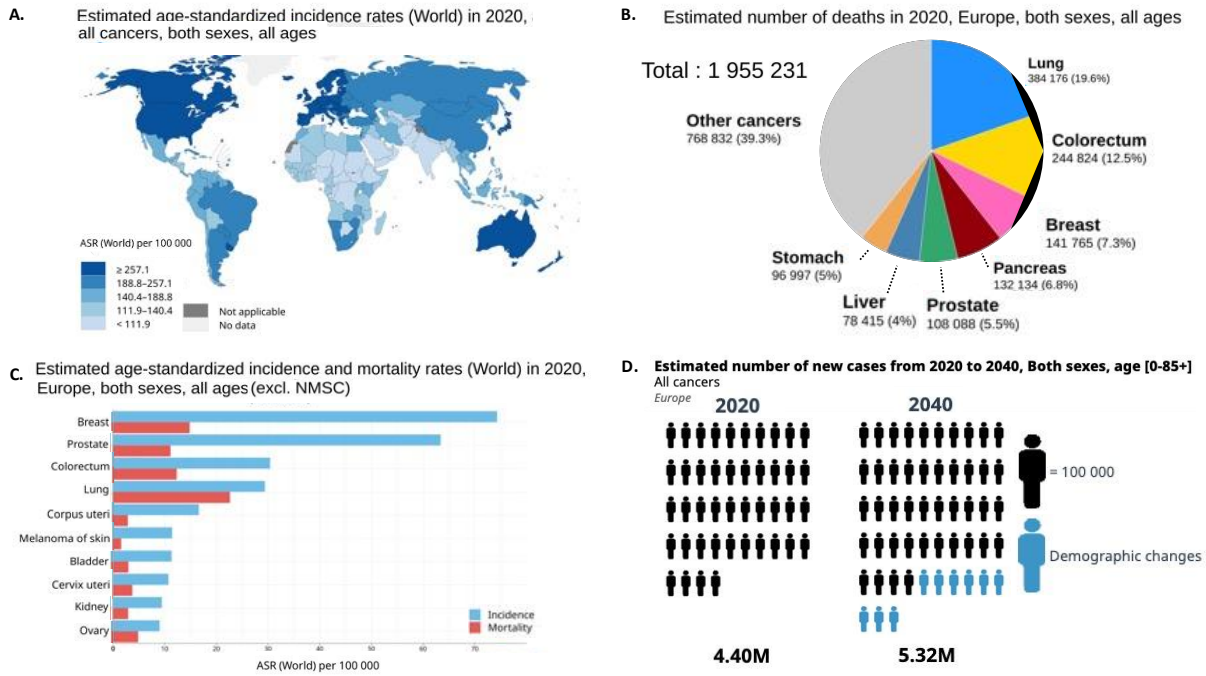

Figure 1: Global and European statistics on current and future estimations of cancer incidences.

Incidence rates are presented for all cancers, both sexes and of all ages. (a) Global map estimated age-standardized incidence rates in 2020 presented in age-standardised rate (ASR) per 100.000 citizens per country. (b) Pie chart representing estimated number of cancer related deaths in 2020 in Europe, including lung, colorectum, breast, pancreas, prostate, stomach, liver, and other cancers. (c) Histogram representing

estimated number of cancer related incidences and deaths in 2020 in Europe represented in ASR (World) per 100.000 citizens, including breast, prostate, colorectum, lung, corpus uteri, skin, bladder, cervix uteri, kidney, and ovary. (d) Visual illustration of estimated number of overall new cancer cases from 2020 to 2040 in Europe. (Data provided by World Health Organization, Global Cancer Observatory: https://gco.iarc.fr/, accessed August 2023)

1.2. Standard of Care

Standard of care refers to the developed and published evidence-based standards that are at the base of the treatment modality and are different for every cancer type. Most standard of care protocols use combined treatments of chemotherapy, radiotherapy, and surgery. As scientific research is continuously enhancing aspects within the treatment modalities, changes can be made to the standard of care. For this, new methods or drugs need to prove to be beneficial combined with the standard of care in clinical trials compared to the standard of care standalone.

1.2.1. Chemotherapy

Chemotherapy is perhaps the most known therapy in cancer treatment. During chemotherapy, chemotherapeutic agents are given to the patient as neoadjuvant, before surgery or radiotherapy, and/or as adjuvant, after surgery or radiotherapy. Chemotherapeutic agents can be administered by intravenous (IV) or oral administration, depending on the drug and is overall considered a systemic treatment. The agents can be divided in 4 classes of chemotherapy depending on its mechanism of action: antimicrotubular agents, antimetabolites, topoisomerase inhibitors including anthracyclines and alkylating agents. Overall, chemotherapeutic agents impact cell growth and tumour cell division, striving for elimination of tumour invasion or metastasis. By affecting cell growth, normal dividing cells are also injured by the treatment, and chemotherapy is therefore often accompanied with severe adverse effects [2]. Although effective in decreasing tumour volume and affecting possible escaped tumour cells, the treatment alone is often not enough for complete tumour control and chemotherapeutics are combined with surgery and radiotherapy.

1.2.2. Surgery

Surgical resection is the most effective treatment modality in the removal of cancer and is necessary for approximately 80% of diagnosed cancer patients [3]. During surgical resection,

the tumour and its nearby surrounding is manually removed. The resection edges of the removed mass are assessed using histology to ensure that all edges are clean, limiting the possibility of incomplete tumour removal [4]. However, some tumour locations are difficult or impossible to undergo operations, for example the brain and the brain stem, with radiotherapy treatment as only available local treatment modality.

1.2.3. Radiotherapy

Over half of diagnosed cancer patients will receive radiotherapy in their treatment plan, this can increase to 83% of patients for breast cancer and 92% with tumours in the central nervous system [5]. The local treatment is essential for cancer treatment and greatly contributes to patients cure and palliative care. In the next chapters we will unravel the structure of an ionization event, different radiation modalities, the impact of radiotherapy to the normal tissue and how to implement drug treatments to decrease normal tissue toxicity while maintaining tumour control or enhance tumour radiosensitivity with limiting the affects to the normal tissue.

2. The different phases of an ionizing radiation event

Most cancer patients receive radiotherapy during their treatment regimen. It is a common practice and categorized as a local treatment. However, ionization events during radiotherapy treatment are not simple events and consist of a complex multidisciplinary occurrence. When dissecting the different aspects of radiation events, we encounter physics, chemistry, and biology.

2.1. Physics

Ionizing radiation applied to a subject or matter results in the release of large quantities of energy that is transferred to electrons, ejecting them from their atomic orbital. This process is known as an ionization event. Radiation classification can be divided into electromagnetic and particle radiation. Electromagnetic radiation consists of waves or bundles of energy identified as X-or γ-rays. Although the consistency of X- and γ-ray photons are identical, their origins differ. Gamma-rays are produced from within an atom's nucleus after a radioactive decay, whereas X-rays are emitted when orbital electrons rearrange or through the interaction of a free electron with the atom. In the latter case, X-rays can be produced in linear accelerators, with high energy electrons striking a high Z metal target [6]. X- and γ-rays are massless bundles or waves of energy that can be deposited all at once in matter to produce charged particles that, in turn, can result in an indirect ionization event. Particulate radiation comprises of particles with a mass and include protons (positively charged), α-particles (positively charged), electrons (negatively charged), heavy ions (positively charged) and neutrons (uncharged). Charged particles deposit small fractions of their energy regularly along their path, creating (direct) ionization tracks. The track structure and therefore the energy deposition per unit distance differs for each particle, with average low linear energy transfer (LET, expressed in keV/μm) for electrons and high LET for alpha particles (Figure 2).

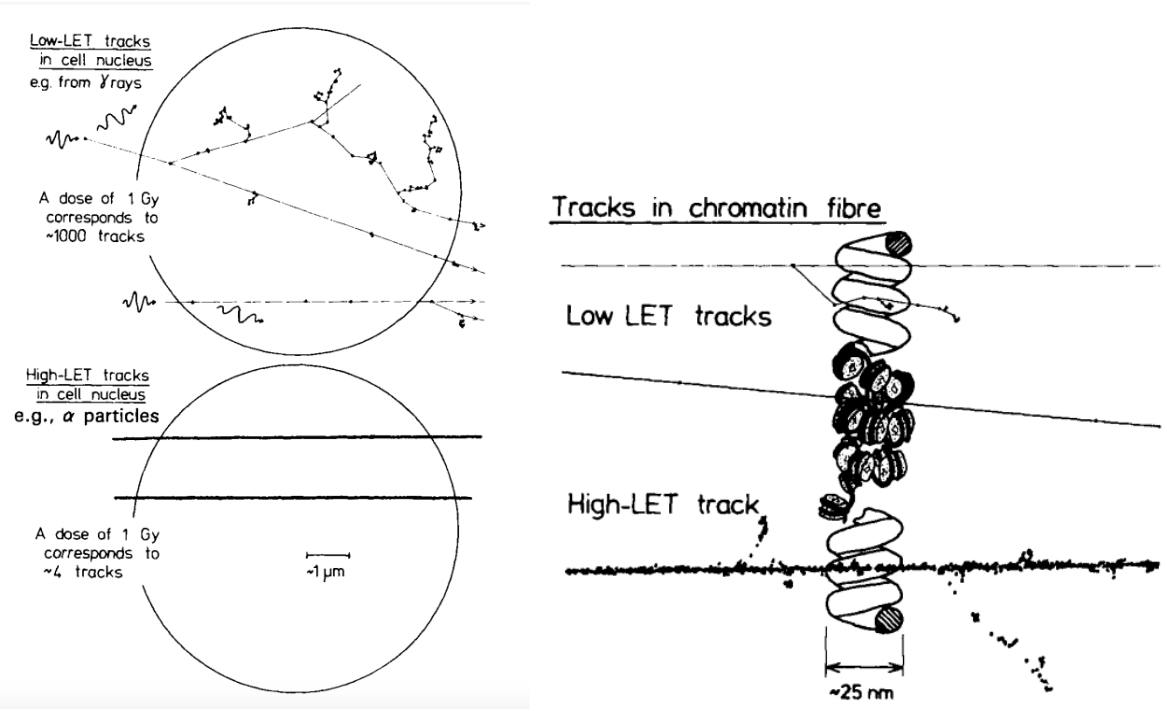

Figure 2: Low and high LET tracks.

Illustration of secondary electrons from γ-ray low LET tracks and α-particle high LET tracks in a cell nucleus scale representation (left, 1 μm scale bar) and chromatin fibre scale representation (right, 25nm fibre) [7].

2.2. Chemistry

A large fraction of the interaction events of radiation with living matter results in the breakage of water molecules (a process known as water radiolysis), generating free radicals, including the primary production of $H_2O^{\bullet}$, H_2O^{+} and e^{-}, secondary production of $H^{\bullet}$, $HO^{\bullet}$, H^{2}, H_3O^{+} and e_{-aq}, and tertiary production of H_2O_2, H_2, H_3O^{+}, OH^{-}, $HO2^{\bullet}$, $HO^{\bullet}$, $H^{\bullet}$ and e_{-aq} (Figure 3). The radiolytic products can interact with oxygen creating additional radiolytic products together with Reactive Oxygen species (ROS) HO_2^{-}, O_2^{-} and $O_2^{\bullet}$- [8], [9]. All generated radicalized species have their own unique diffusion rate and lifetime. An important reaction is the interaction of $^{\bullet}OH$ with a carbon-centred substrate, resulting in the release of a $H^{\bullet}$ and a carbon-centred radical. In turn, carbon-centred radicals can interact with oxygen molecules, resulting in peroxyl radical ($ROO^{\bullet}$) formation. This radical is relatively long lived and therefore is susceptible to reach DNA molecules, proteins, and lipids within cells, to which they can create substantial damages [9].

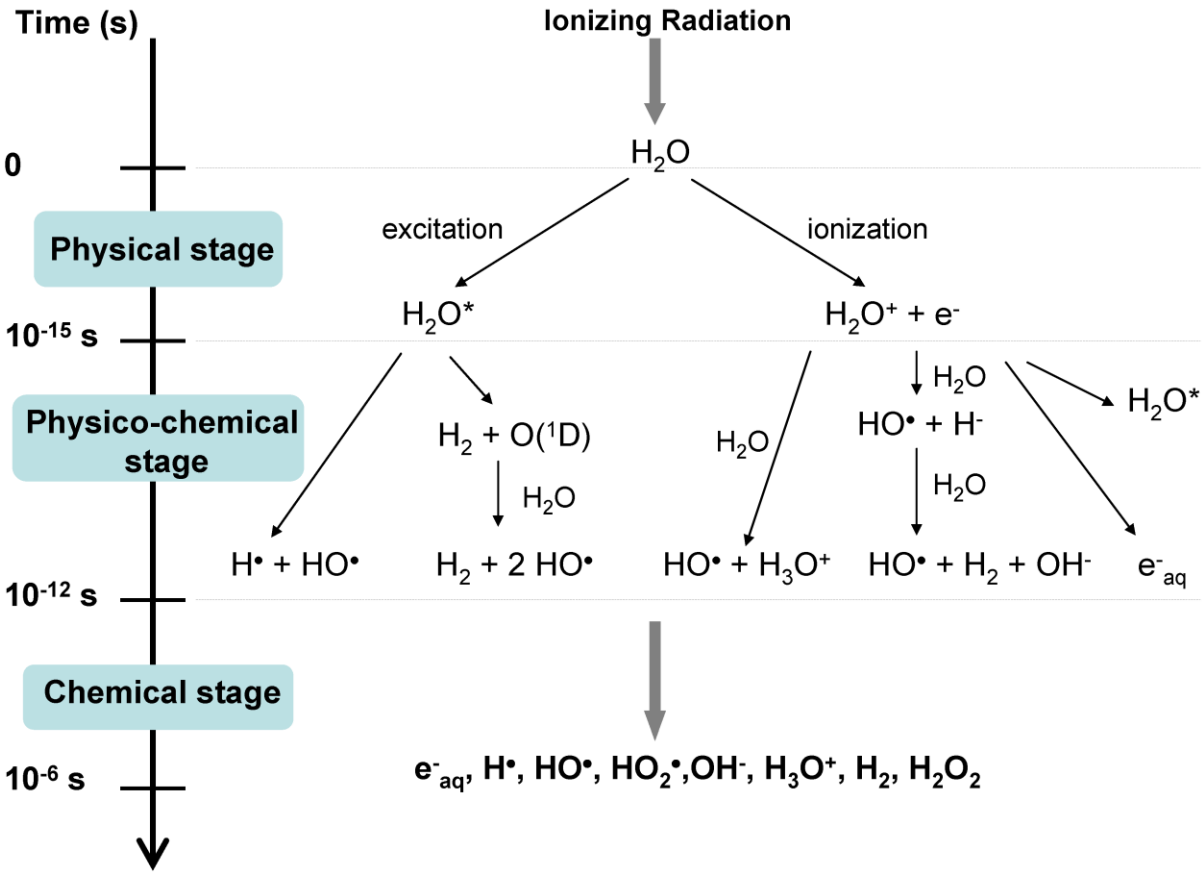

Figure 3: Schematic presentation of the radiolysis of water.

The radiolysis of water separated by physical, physico-chemical, and chemical stage. The illustration represents the primary, secondary, and tertiary production of free radicals with a time scale is represented from 0 – 10^{-6} seconds [8].

2.3. Biology

The interaction between ROS or additional radicals, such as peroxyl radicals, and DNA molecules result in damage, characterized as indirect damage. The direct deposit of energy to DNA molecules during an ionization event is characterized as direct damage. Both damages contribute to the formation of complex clustered DNA damages. On average, 1 Gy of photon irradiation can induce 40 double stranded breaks (DSBs), 1000 single stranded breaks (SSBs), over 2000 base damages and 30 DNA-DNA crosslinks, per cell [10]. High-LET particles are more prone to create clustered direct damages (by definition). The complex clustered DNA damage is challenging to repair and can result in mutation formation or cell death by apoptosis [11], necrosis [12], autophagy [13], senescence [14], or mitotic catastrophe [15].

A secondary response to induce cell death is through the bystander effect. Cells directly damaged by the initial ionization event can communicate the magnitude of its injury to

surrounding cells, mainly through gap-junctions [16]. The communication to non-irradiated cells has been demonstrated to result in mutations, modifications in gene expression, induction of chromosomal aberrations and even cell death [17], [18].

2.4. The linear quadratic model

An aspect used in the measurement of tissue and tumour response following radiotherapy is the concept of the linear quadratic model providing the α/β ratio. The simplified model uses two components of cell killing, one depending on the dose (αD) and one depending on the square of the dose (βD^2). The model uses the formula:

$$S = e^{-\alpha D - \beta D^2}$$

where S is the cell survival rate after a dose D in the context of clonogenic assays. Additionally, if the linear and the quadratic contribution to the killing of the cell are equal at a specific dose, this dose is the α/β ratio. With the implementation in biological experiments, it has been proposed that α represents the proportion of cell deaths caused by a single, lethal, DSB event, whereas β represents the proportion of cell deaths originated from the combination by two sublethal events, for instance SSBs forming a DSB together (Figure 4) [6], [19]. The sublethal events may however be repairable if the treatment is fractionated and protracted.

Within that framework, we can easily calculate the dose *D* for which lethal events and sublethal events contribute equally to cell death: $\alpha D = \beta D^2$ *implies* $D = \alpha/\beta$. Indicating that for any dose $> \alpha/\beta$, the accumulation of sublethal damages contribute more to cell killing, and vice versa. The threshold value of α/β depends on the cell type and on the radiation type, ranging typically from 1 to 15 Gy. When the typical dose of 2 Gy/fraction is used:

- In low α/β tissues, $\alpha/\beta < 2$ Gy, and lethal, unrepairable events are mostly responsible for cell death [19].
- In high α/β tissues, $\alpha/\beta > 2$ Gy, and sublethal repairable events are mostly responsible for cell death [19].

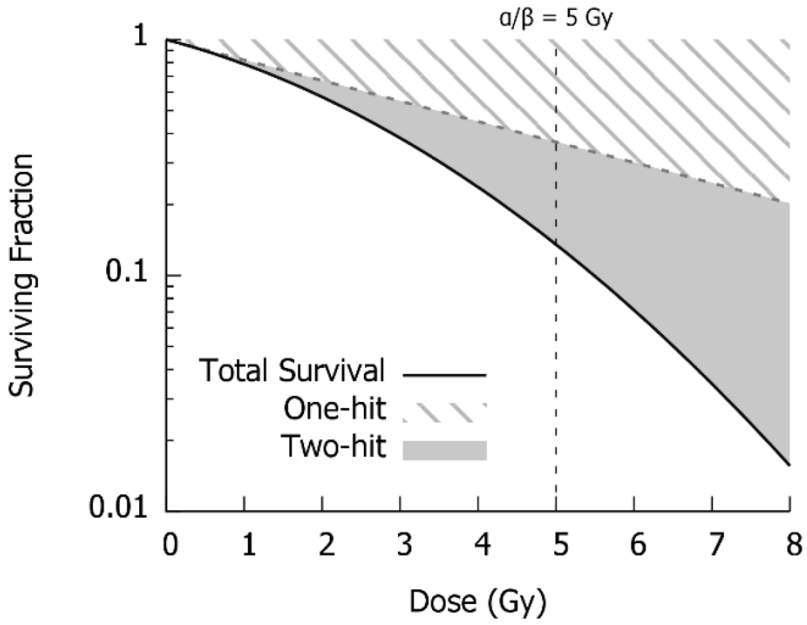

Figure 4: The linear quadratic dose response model.

The one hit linear component α is represented with the dotted line and the two-hit quadratic component β is represented in gray. The data is represented in Surviving fraction vs. dose in Gy with an α/β ratio of 5 Gy [19].

3. Radiotherapy modalities

The implementation of radiation to fight cancer differs with treatment regimes, particles used, type of tumour, its location and additional patient characteristics. The choice of particles used depends on the locations of the organs at risk, the type of tumour and unfortunately often on the feasibility of the radiation types.

3.1. Internal radiotherapy

During internal radiotherapy, radioactive isotopes are inserted to deposit locally their energy over short distances. Common applications for this, is the use of radioactive iodine to treat hyperthyroidism and thyroid cancer, where radioactive iodine is supplemented to patients through ingested supplements, absorbed into the blood, filtered from the blood by the cancerous thyroid, and when stored deposits gamma irradiation [20]. Due to its 8-day physical half-life, patients undergo internal radiotherapy, isolated but often within the comfort of their home. Another conventional internal radiotherapy treatment is brachytherapy. Here, radioactive seeds are manually inserted into the tumour and have been implemented for the treatment of prostate cancer, skin cancers, breast cancer and ovarian cancer. Various isotopes have been used depositing decay of electron capture of β- creating γ-rays with energy ranging from 21 up to 970 keV and half-lives from 10 days up to 28 years [21]. Internal radiotherapy is limited in its usability merely for reachable tumours or organs accumulating unique substances, and in most cases, external radiotherapy is implemented.

3.2. External radiotherapy

Particles or electromagnetic radiation, implemented during external radiotherapy, all have their own characteristic dose distribution as visible in Figure 5 [22]. Low energy electrons interact rapidly with the encountered matter, diffusing their dose and are therefore low in a dose-depth deposition in tissues. Electrons allocate the dose to the skin surface and tissues close underneath and are therefore applicable for the treatment of melanomas and subcutaneous located tumours. Although still in the early phases of development, current research is ongoing in creating accelerators capable of generating high energy electrons, enhancing the tissue depth of the particles to reach deep seated tumours [23]. As protons are bundles or waves of energy, interaction is needed for the reaction of free electrons. The dose

is distributed further in the tissue with a long dose delivery tail. Photon irradiation can reach deep seated tissues and can therefore reach tumours located throughout the body. However, the extended tail of additional dose increases the radiation dose delivered to the normal tissue.

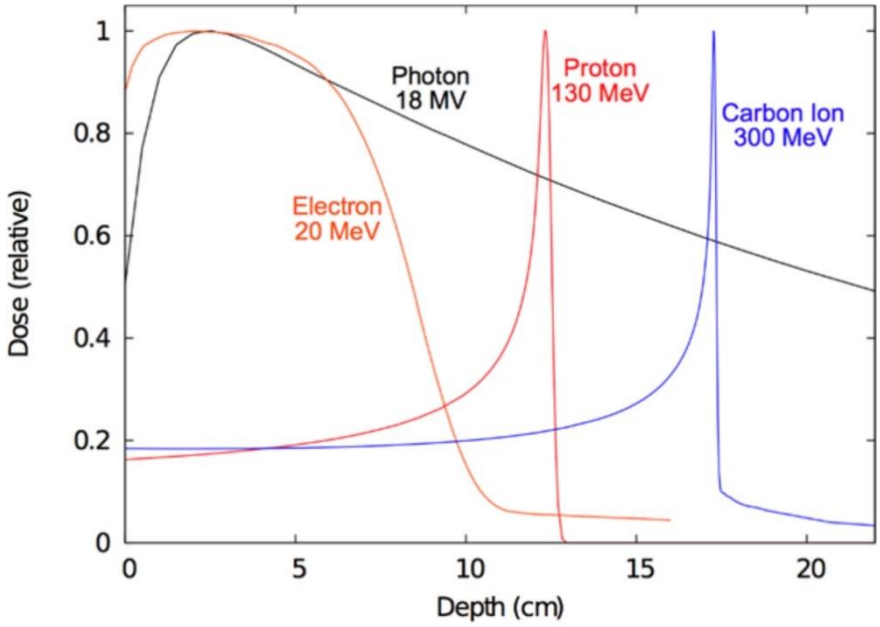

Figure 5: Dose distribution of various radiation modalities.

Distribution of 20 MeV Electron, 18 MV Photon, 130 MeV Proton and 300 MeV Carbon ion represented with depth in cm and expressed in relative radiation dose [22].

3.3. Photon Radiotherapy

Since the discovery of x-rays by Wilhelm Rontgen in 1895, and its immediate first application for medical imaging and therapeutic use in 1896, imaging and radiation therapy have been inseparably intertwined. Early radiotherapy treatment based its localization on bone structure as it was the only clear detectible imaging available at that time and with improvements in imaging, radiotherapy advances were made in parallel. The progression made in the delivery of external radiotherapy has been focused on reducing the dose to the normal tissue while delivering the optimum dose to the tumour. With this, technology has improved enabling the application of radiation from different angles and based its target on previously collected tumour imaging, identifying the location and shape of the tumour.

3.4. From tumour reconstruction to 360 arc rotations

The implementation of modern-day computer power was quickly implemented in treatment planning by utilizing CT, magnetic resonance imaging (MRI), positron emission tomography (PET) or PET-CT imaging to generate a 3-dimensional (3D) reconstruction of the tumour shape, its location, and nearby organs at risk (OARs). By utilizing this generated 3D model, a highly accurate delivery plan can be designed, known as 3D conformal radiotherapy (3D-CRT). The method has made it possible to increase radiation doses, and improve tumour control [24], [25]. 3D-CRT can deliver radiation from various angles but requires forward treatment planning. With this, beam parameters and radiation set-up are designed and calculated with a uniform dose. With this method, normal toxicity was reduced compared to standard conventional radiotherapy. However, OARs close to the tumour were often unavoidable in the treatment delivery.

To reduce radiation dose delivered to the OARs, intensity modulated radiotherapy (IMRT) was introduced. With the identical core principles to 3D-CRT, IMRT uses furthermore inverse treatment planning where firstly the desired dose to the target and normal tissue is set. Secondly, the radiation field is altered to achieve the desired doses using a rotating gantry and multileaf collimator. The collimator can alter its shape during the radiation, creating a pencil beam, able to precisely deliver the desired dose [26], [27]. Using IMRT instead of 3D-CRT, OARs closer located to the tumour receive less dose and this resulted in improved treatment outcomes in numerous studies [28]–[32]. Optimizations of IMRT resulted in helical tomotherapy (HT) and volumetric modulated arc therapy (VMAT). HT uses an increased number of independent beam angles for treatment delivery and a movable bed, resulting in a smoother and more precise dose coverage of the tumour [33]. VMAT uses a single radiation beam in a 360-degree rotation of the arc in which the radiation continuously rotates around the patient and is therefore quicker in delivery [34]. The implications of IMRT, HT and VMAT all have reduced normal tissue toxicity and optimum dose coverage of tumours. However clinical trials revealed variable benefits or disadvantages, depending on the treatment delivery variables and additional complications with increased low dose baths to the normal tissue and increased dosimetry complexity [35]–[38]. Overall, it is evident that the decision for its implementation will depend on individualized patient care, selecting the most suitable treatment to achieve the desired dose coverage and on the accessibility and coverage of the machines that have the capacity to conduct the treatment protocols.

3.5. Particle radiotherapy

Protons and heavy ions, including carbon ions, are quite interesting with its representation of a Bragg peak. The loaded particles travel at a high speed through the tissue and upon interaction slow down. Only once the particles are decelerated enough, they distribute the dose in the tissue in vast amounts with a sharp dose cut off, identified as the Bragg peak, reducing radiation to the tissue located behind the tumour.

The implementation of proton beam therapy (PBT) for cancer treatment utilizes the Bragg peak into a spread-out Bragg peak, where different proton energies are generated correlated to different depths, covering the tumour (Figure 6) [39]. Its first use was implemented for treatments of unrespectable cancers or tumours in proximity with organs at risk, often in children, and draws upon its advantage of the sharp dose cut off after the Bragg peak. PBT has similar beam implementations as photon irradiations including IMRT based Intensity-Modulated Proton Therapy (IMPT). IMPT implements functions identical to those of IMRT but with the use of protons instead of photons. Recent studies have revealed that IMPT decreased the probability of normal tissue toxicity compared to IMRT in patients treated with stage III non-small cell lung cancer and revealed to significantly reduce dose delivery to various organs compared to 3D-CRT [40], [41].

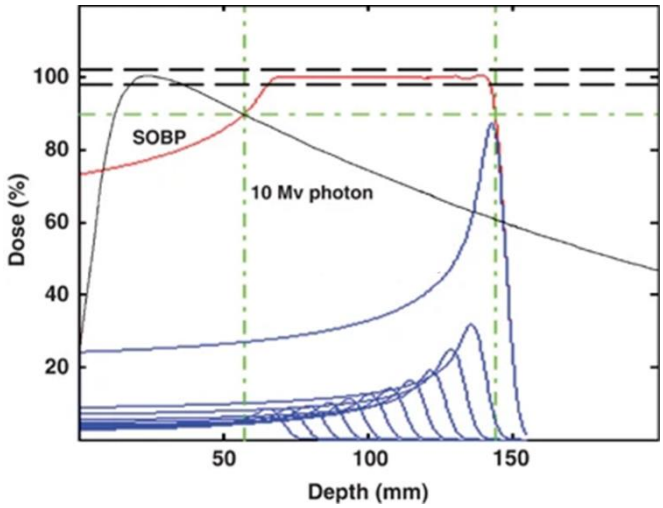

Figure 6: Dose depth distribution of various external beam radiation modalities.

Dose depth distribution of the spread-out Bragg peak (SOBP, red) containing proton induced Bragg peaks with a range of energies (blue) and a 10 Mv photon beam (black). Dose is presented in percentage and depth in mm [39] .

However, the accelerators required for the generation of these particles are big, expensive, and therefore often inaccessible. Another matter of concern with respect to proton and heavy ion therapy compared to photon therapy, is that the high precision of dose delivery result in high doses to the tumour but are therefore sensitive to the delivery of high doses to the normal tissue if the target moves. Overall, the delivery of external radiotherapy has tremendously progressed over the decades, due to the implications of various treatment delivery techniques.

4. Novel developments in radiotherapy

Radiotherapy has evolved drastically over the decades providing big advances in tumour control and reduced normal tissue toxicity. Although less severe than decades ago, normal tissue radiation toxicity still occurs frequently, affecting patients' welfare and reducing the change of completing the initial treatment plan. Recent studies have therefore been focussing on changes in dose delivery to reduce normal tissue toxicity while maintaining or enhancing tumour control.

4.1. The peaks and valleys of minibeam radiotherapy

A novel radiotherapy approach is the use of distinct spatial distributions, identified as minibeam and microbeam radiotherapy [42], [43]. Minibeam radiotherapy (MBRT) consist of delivering the radiation in spatial fractions of 500-700μm in field size with 1 to 3 mm spacing in between the beams. This creates a dose distribution over the tumour known as the peaks and valleys. Tissue within the peaks receive a direct fraction of radiation and are exposed to the maximum dose given, the tissue in the valleys do not receive radiation from the initial beam but do receive a minimum amount of scattered radiation from the peak areas [43], [44]. Although it has been proven to function with x-ray irradiation, the maintaining of peaks and valleys is difficult due to increased scattering and error prone irradiation due to increased geometry complexity. Therefore, the implementation of MBRT is currently focussed on proton therapy (pMBRT) using pencil beam scanning or passive scattering. Interestingly, this method of radiotherapy delivery revealed to decrease normal tissue toxicity while maintaining control of tumour growth [42], [44], [45]. The study of Prezado et al (2017) [46] revealed that rats receiving whole brain irradiation using pMBRT displayed a significant decrease in brain damage compared to standard PRT. In parallel, an increase in tumour control was achieved using pMBRT in glioma bearing rats in comparison to standard PRT [47]. Evidence have been provided that different biological mechanisms parallel to physical parameters such as dose volume effects, are involved in the development of the minibeam reduced normal tissue toxicity including cell signalling, the bystander effect, vascularisation and even the involvement of the immune system [48]–[52]. Nevertheless, the biological response to spatial fractionation remains to be fully identified.

4.2. Ultra-high dose rates in FLASH radiotherapy

Another novel radiotherapy technique that has recently emerged as a novel field within the radiation research community is ultra-high dose rate radiotherapy, identified as FLASH radiotherapy. FLASH radiotherapy is characterised by the application of an ultra-high dose rate, almost instantaneously (within milliseconds) unlike low dose rate (within min) used in conventional radiotherapy (CONV-RT). Various studies of FLASH-RT have revealed a tremendous diminishment of normal tissue toxicities together with maintaining equal tumour control, compared to CONV-RT [53].

The concept first arose from preliminary research conducted in the 60s and was rediscovered by Favaudon et. al. (2014), providing in addition evidence for equal tumour control [54]. Within this research, the recurrence of lung fibrosis was examined in C57BL/6J mice after receiving CONV or FLASH irradiation. Mice underwent thoracic irradiation using a single fraction of 17 Gy or the CONV-RT equivalent of 17 Gy with a dose-rate of 0.03 Gy/sec. CONV-RT resulted in a severe increase in pulmonary fibrosis 36 weeks post radiotherapy (Figure 7A). In comparison, FLASH-RT with an average dose rate of 40-60 Gy/s (in-pulse dose-rate $\approx 10^6$ Gy/s) resulted in low to zero induction of pulmonary fibrosis in the irradiated mice [54]. The decrease in normal tissue toxicity was further examined using FLASH-electrons and FLASH-x-rays, both reporting a neuroprotective effect after FLASH-RT in mice compared to CONV-RT [55], [56]. The FLASH effect, described as the sparing of healthy tissue after FLASH-RT, has been identified in numerous additional tissues including the skin and the intestine of mice (Figure 7B-D). The initial studies were conducted using FLASH-RT with low energy electrons, and similar normal tissue protection were later confirmed using FLASH-RT with proton irradiation [57]–[63]. Translation was made to larger in vivo models using mini-pigs, and cats diagnosed with squamous cell carcinoma of the nasal planum [64]. A protection of the normal tissue was observed in pig skin characterised by a lack of fibronecrosis development after FLASH-RT compared with CONV-RT. FLASH-RT applied to cat's squamous cell carcinoma resulted in mild mucositis, no acute toxicity and progression free survival above 80% at 16 months' post treatment [64]. However, optimisation of radiation delivery is required to prevent later identified chronic toxicities.

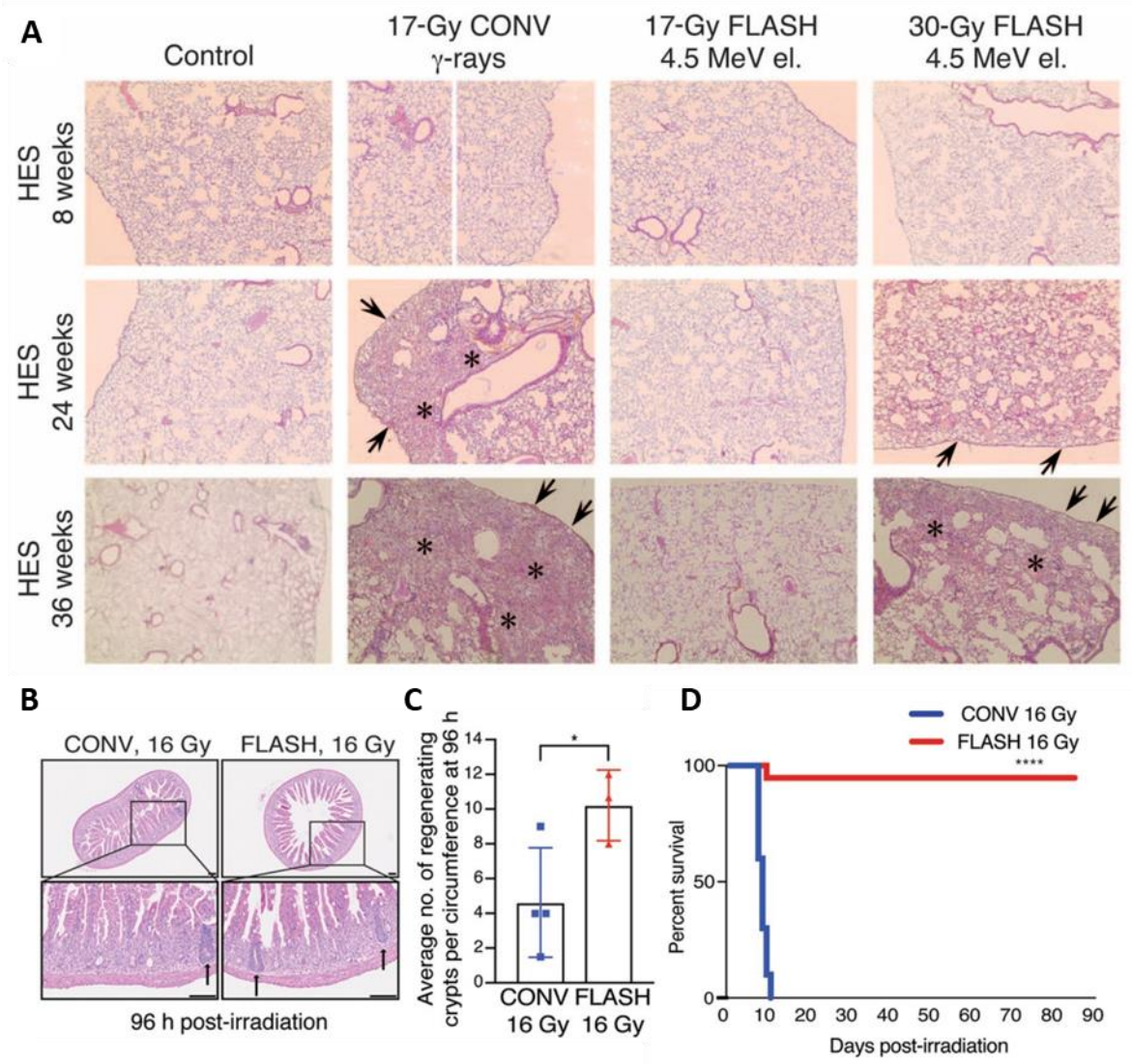

Figure 7: Identification of the FLASH effect in the lung and intestine.

(A) C57BL/6J mice received thorax irradiation of 17 Gy CONV/FLASH-IR or 30 Gy FLASH-IR, delivered in a single fraction. Hematoxylin-eosin staining of lungs performed on lung sections 8-, 24- and 36-weeks following radiotherapy. Arrows are indicating subpleural fibrosis regions and stars indicating intraparenchymal fibrosis regions [54]. *C57BL/6J mice received abdominal irradiation of 16 Gy CONV/FLASH-IR (B) with example Hematoxylin-eosin staining of jejunal sections 96h following irradiation, arrows indicating healthy crypts and (C) quantification of average remaining crypts. (D) Kaplan-Meier survival curve of mice following radiotherapy* [59].

4.2.1. Radiation parameters and mechanism identification

Recent studies have been dedicated to identifying the physical and biological parameters needed to generate the FLASH effect. The study of Montay-Gruel et al. (2017) pioneered by identifying the importance of the dose rate. Whole brain irradiation was performed with mean

dose rates of 100 Gy/s down to 0.1 Gy/s. Decrease in recognition ratio was observed below a dose rate of 30 Gy/s at 2 months following RT [55].

Additional research identified evidence for the dependency of the FLASH effect on oxygen concentrations in the normal tissue. Mice received CONV or FLASH-RT on oxygen breathing, resulting in a loss of the FLASH effect when oxygen breathing was combined with FLASH-RT [65]. The results gave rise to the oxygen depletion hypothesis. This hypothesis states that the fast delivery of radiation during FLASH-RT results in a temporary hypoxia explicitly in the normal tissue, resulting in increased radio resistance. Continuing research did identify oxygen depletion following FLASH-RT, but the depletion level was not significantly different from that expected from the known radiolytic yield of oxygen consumption by H● and e_{-aq} radicals. The depletion was too small to be responsible for a clinically relevant hypoxic scenario and for the solitary source of the FLASH effect [66]. The theoretical physiochemical model of Labarbe et. al. (2020) [9] also argued against the oxygen depletion hypothesis, highlighted the role of peroxyl radical ROO● production and supported free radical recombination as the source of the FLASH effect [9].

Additional examination revealed an impact on water hydrolysis following electron and proton FLASH-RT. The study identified significant decrease in H_2O_2 production after FLASH proton and electron irradiation in water [67]. However, there is a general agreement among radiobiologists that sub-millimolar amounts of H_2O_2 are not harmful to cells and tissues, and the physical and physico-chemical parameters for FLASH-RT are still far from identified.

As the FLASH effect is identified as an in vivo normal tissue response, the involvement of the immune system has been hypothesized. This hypothesis was rapidly disproven with a FLASH effect observed in both immunocompetent [54], [59], [68], [69], immunodeficient mice [69] and nude mice [69], [70] and is therefore not dependent on the immune response. However, the immune system of tumour-bearing mice and rats does reveal a differential response following FLASH-RT compared to CONV-RT, providing evidence of a possible beneficial impact of FLASH-RT on tumour control through the immune system [71]–[73]. This was exploited in the study of Eggold at al. (2022) [74]. Tumour bearing mice were treated with the combination of FLASH-RT and αPD-1 antibody, blocking the Programmed cell death protein 1 (PD-1)/ Programmed death-ligand 1 (PD-L1) immune checkpoint. FLASH-RT revealed an increased infiltration of antitumoral T cells and enhanced the efficacy of the αPD-1 antibody while maintaining the FLASH effect in the normal tissue [74]. Nevertheless, the study of Cunningham

et al. 2021 [68] revealed no difference in tumour response of CD8+ infiltrated and non-infiltrated oral carcinoma tumours following FLASH-or CONV-RT. Despite the repeatable promising in vivo results displayed after FLASH-RT, the immune system does not indicate to play a major role in the FLASH effect (i.e. sparing of the healthy tissue), while its contribution to tumour control following FLASH-RT needs further investigation.

4.2.2. Translation to the clinic

With the convincing results observed in pre-clinical research the connection was made in 2019 for the first patient to receive FLASH irradiation [75]. The patient suffered from CD30+ T-cell cutaneous lymphoma and agreed to receive FLASH radiotherapy on the 3.5-cm ulcero-infiltrated tumour located on the forearm by applying 15 Gy in 10 pulses of 1 us. The treatment revealed a mild epithelitis (grade 1) and grade 1 oedema together with a complete tumour response 36 days after FLASH-RT, compared to the average complete response 5 months after CONV-RT [75]. In addition, the first clinical trial using proton FLASH for palliative treatment of patients bearing bone metastasis was concluded in 2022 [76]. The study identified the feasibility and safety of FLASH-RT use for patients with equal efficacy and adverse effects following FLASH-RT compared to the standard of care. These promising results support the development of FLASH-RT from pre-clinical to clinical applications.

Moreover, research by Montay-Gruel et al. [70] and Alaghband et al. [77], showed that FLASH hypo-fractionated treatment plans resulted in maintaining the FLASH effect. Interestingly, recent work of Limoli at al. (2023) pioneered in applying hyper fractionated radiotherapy in FLASH settings, where the FLASH effect, identified by preservation of cognitive functions, remained with 10 fractions of 3 Gy [78]. These studies provide evidence that both hypo- and hyper-fractionated radiotherapy can produce the FLASH effect, giving rise to an optimistic outlook in its potential for future clinical applications. Nevertheless, the current standard of care using CONV dose rates does not only use fractionated radiotherapy, but also exploits 3D imaging, rotating gantries, image-guided radiotherapy with possible tracking of tumour and organ movements, and millimetre thin radiation beams that are all still absent in current FLASH-RT treatments. Another vital aspect where any knowledge is still completely lacking is treatment modalities of FLASH-RT combined with commonly used chemotherapies. It is crucial to add combined treatment modalities and the current additional CONV-RT parameters to FLASH-RT to be applicable in future clinical settings.

5. Normal tissue toxicities in response to Ionizing radiation

Radiation can induce significant damage to tissues and organs in the human body. The toxicity exhibited post radiotherapy is derived from post radiation induced cell damage. Minutes to days following irradiation, DNA and additional cellular damage results in cell cycle arrest and the induction of the DNA repair machineries. Successful repair results in cell survival and no additional implications. However, ineffective, or inaccurate repair can result in mutation formation with the cell transformation at long term to a malignant subtype, although rarely observed [79]. Additionally, unsuccessful repair can result in senescence or cell death. Within days to weeks post radiation exposure, the loss of cells or their function in the normal tissue leads to the loss of epithelial and mucosal barriers, an acute inflammatory response, and a severe decrease in blood cell count. Months to years post radiation exposure, late vascular damage and atrophy can occur as well as the continuation of the acute inflammation developing into chronic inflammation supporting fibrosis formation and loss of organ functions (Figure 8).

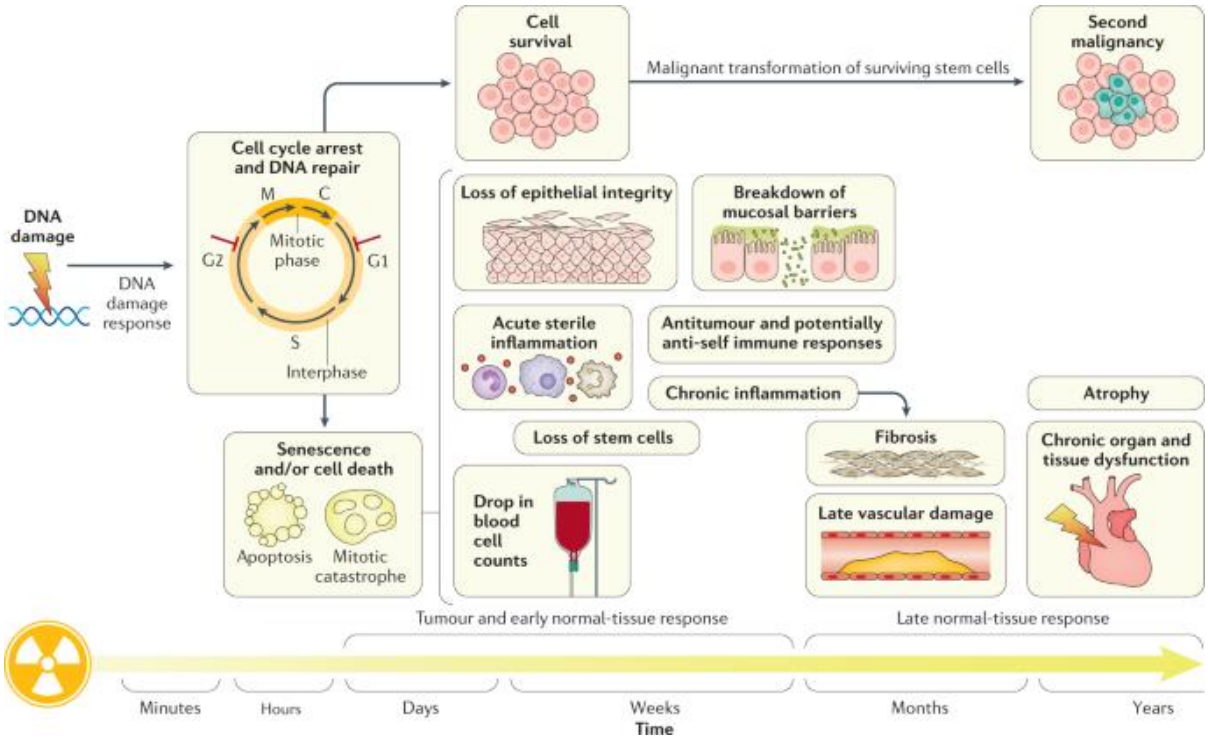

Figure 8: Schematic illustration of normal tissue toxicity following a radiation event.

Damage is induced on the DNA followed by a DNA damage response within minutes. Cells will undergo cell cycle arrest to attempt repair of the damage resulting in senescence or cell death by apoptosis or mitotic catastrophe following unsuccessful repair or cell survival following successful repair, hours after

radiotherapy. Days to weeks following irradiation, tumour and early normal tissue responses occur with loss of epithelial integrity, acute sterile inflammation, decrease in blood cell counts, decrease in stem cells, breakdown of mucosal barriers and antitumour immune responses. Months to years following irradiation, late normal tissue responses can appear with chronic inflammation, fibrosis formation, late vascular damage, atrophy, chronic organ, and tissue dysfunction and possible development of second malignancies [80].

The response of the normal tissue to radiation varies depending on the tissue type, patient's characteristics, radiotherapy parameters and additional treatment modalities. The identification of the tissue type depends on various characteristics and can have an acute or late response to radiotherapy. An acute response is directly correlated to cell death, identified with early effects. Acute responses can be found in vast dividing tissues including the intestine, and upon stem cell survival, full recovery can be expected. Late response is dependent on various mechanisms including fibrosis formation and vascular damage and occurs in tissues with low to absence of cell division, including the lung, making tissue repair improbable. These late effects appear months to years post radiotherapy [81]. Nevertheless, severe damage to early responding tissues can furthermore result in a consequential late response. If early responding tissues are unable to fully repair, this results in chronic deteriorating toxicity [81]. An overview of organs and their relative radiation-induced toxicities can be found in table 1.

5.1. Organs at risk

An organ located near a tumour that holds the capacity of developing normal tissue toxicities following radiation exposure, is classified as an organ at risk (OAR). During treatment planning, OARs are identified and considered during the treatment design to limit the radiation delivered to the OARs [82]. The acute or late response and the hierarchical structure of the identified OAR is important to determine what dose and radiation treatment regime is best tolerated by this organ. Acute responding tissues have a high α/β ratio (> 7 Gy). They are therefore less sensitive to the implementation of fractionated therapy and more sensitive to the total duration of the treatment plan. In contrast, late responding tissues have a low α/β ratio (< 7 Gy). They are therefore more sensitive to fractionated radiotherapy and less sensitive to the duration of the complete treatment plan [19], [83].

5.2. Functional subunits

Organs can have different structure hierarchies that have an additional impact on their radiation toxicity. The structure hierarchy has been categorized as serial organs, parallel organs, and complex organs, all composed of functional subunits (FSU). Each functional subunit consists of a stem cell maintaining the tissue generation of this subset of cells. If treatment results in the loss of the stem cell, the FSU will become inactive. The structuring of the FSUs in tissues therefore impacts the maintenance or loss of organ function upon damage. Serial organs, including the spinal cord, will undergo a complete loss of organ function if one FSU is inactive. High doses to small volumes should therefore be avoided. In parallel organs, including the lung, a loss of one FSU merely results in the inactivation of the FSU with minimum loss of organ function. High doses to small volumes are therefore well tolerated within these organs. Some tissues, including the skin, are more complex and therefore are characterized by a complex hierarchy. However, categorized complex organs generally display comparable behaviour as the parallel organ response [84]. Although in current treatment planning the structural hierarchy of OARs are implemented by allocated maximum doses allowed to deliver to the identified OARs, there is still no applied model available that can accurately predict the normal tissue toxicity. The current knowledge regarding normal tissue radiation toxicity is far from complete and further research is crucial to establish noticeable differences for patients' well-being.

Table 1: Normal tissue toxicity categorized per organ, response and α/β ratio

The table is adapted from Kehwar et al. (2005) [83].

Organ	α/β (Gy) [83]	Early/late responding	Toxicity	
Kidney	**2.5-3.5**	**late**	**Nephropathy and nephrosclerosis**	[85]
Brain and brain stem	**2.1**	**late**	**vascular abnormalities resulting in infarction, necrosis, cognitive impairment, and gliosis**	[86]
Ear	**3**	**intermediate**	**Stenosis, otitis media with effusion, fibrosis, necrosis, hearing loss, and Meneire syntrome**	[87]
Oesophagus	**3**	**early/late**	**esophagitis, ulceration, and dysphagia**	[88]
Heart	**2**	**late**	**coronary artery disease, pericarditis, cardiac conduction abnormality, cardiomyopathy, and valvular heart disease**	[89]
Bladder	**3.4-6**	**early/late**	**necrosis, haemorrhages, urethral stenosis, haematuria, contracture, nocturia, erectile dysfunction and incontinence**	[90]
Larynx	**3.8**	**late**	**oedema, loss of vocal function, fibrosis, difficulty swallowing**	[91]
Liver	**1.5**	**intermediate**	**fibrosis and hepatic injury**	[92]
Lung	**3.8-6.9**	**late**	**pneumonitis and pulmonary fibrosis**	[93]
Skin	**1.9-2.3**	**early**	**Inflammation with telangiectasia, oedema, erythema, radiation dermatitis, atrophy, ulceration, and necrosis**	[94]
Small intestine	**6.0-8.3**	**early/late**	**nausea, vomiting, abdominal pain, diarrhoea, haemorrhage, epithelial atrophy, ischemia, anorexia, fibrosis, and intestinal obstructions**	[95]
Colon	**3.1-5**	**early/late**	**diarrhoea, rectal and abdominal pain, haemorrhage, tenesmus, urgency, incontinence, sepsis, fistulation, perforation, and rectal discharge**	[95]
Spinal cord	**<3.8**	**late**	**neural toxicity, infarction, necrosis, Lhermitte syndrome, paraesthesia, and myelopathy**	[96]
Stomach	**7.0-10.0**	**early**	**Nausea, vomiting, abdominal pain, dyspepsia, haemorrhage, ulceration and rarely fibrosis**	[95]
eye/eye lens	**1.2**	**late**	**ocular dryness, damaged meibomian glands, fibrosis, epiphora, blepharitis, ciliary disease, madarosis, iritis, corneal oedema, cataracts, and blindness**	[97]
optic nerve	**3**	**late**	**Neuritis and optic neuropathy**	[97]
retina	**3**	**late**	**macular oedema, papillary inflammation, retinopathy, and hard exudates**	[97]
rectum	**3.9**	**late**	**diarrhoea, rectal and abdominal pain, haemorrhage, tenesmus, ulceration, incontinence, sepsis, fistulation, stenosis, and perforation**	[95]
Parotid glands	**3**	**late**	**Xerostomia, decreased saliva production, ulceration, and indirectly mucositis in the oral cavity**	[98]

Thyroid gland	**3**	**late**	**hypothyroidism**	[99]
bone	**1.8-2.8**	**intermediate**	**decrease bone density, increased osteoclast activity, pathologic fractures, osteoradionecrosis, and pancytopenia**	[100]
Testis		**intermediate**	**seminiferous tubule atrophy, oligospermia, azoospermia and infertility**	[101]
ovaries	**10**	**early/late**	**vasculature damage, atrophy, fibrosis, acceleration of reproductive aging, sub- and infertility (depending on growth phase of oocyte), pregnancy complications**	[102]–[104]

6. The lung, a model for late radiation toxicity

6.1. The anatomy of the lung

The human lung contains 5 lobes, all connected by the trachea. The left lung consists of the superior and inferior lobe and has a cardiac notch to encompass the heart. The right lung contains the superior lobe, the middle lobe, and the inferior lobe. The trachea starts from the Larynx and splits up into 2 primary bronchi and branches into the secondary bronchi, the tertiary bronchi, bronchioles, and the small nodules of the alveoli (Figure 9). The grape-like structures are tightly surrounded by capillaries and are responsible for the O_2-CO_2 gas exchange with the cardiovascular system (Figure 9) [105]. A simplified composition of the alveoli consists mainly of ciliated cells, club cells, fibroblasts, alveolar type 1 (AT1) cells, alveolar type 2 (AT2) cells, endothelial cells, alveolar M1 and M2 macrophages, mesenchymal alveolar niche cells (MANC), mesenchymal Wnt2+/ Platelet-derived growth factor receptor α+ (PDGFRα+) cells and Axin2 myofibrogenic progenitor (AMP) cells (Figure 9). AT1 cells are the main cells facilitating the gas-exchange while AT2 cells excrete surfactant to maintain surface tension homeostasis [106]. Ciliated cells contain small cilia, enabling it to function in clearance. The cilia traffic mucus and various other debris upstream of the lungs for removal [107]. Club cells are responsible for the protection of the lining of the lung by secreting a mucus-like layer that can degrade inhaled toxins, supports the surfactant, and ensures a barrier between the lung microbiota and alveolar lining, limiting infections [108]. Fibroblasts are responsible for the maintenance of the extracellular matrix (ECM) homeostasis in between the alveoli and the capillary [109]. Endothelial cells (EC) form the lining of the capillary and form a semipermeable barrier, facilitating gas-exchange, fluid exchange and enabling the accessibility of immune cells to the alveoli if needed [106]. The alveolar macrophages, M1 and M2, are responsible for the maintenance of a healthy lung environment by supporting lung microbiota and removing additional contaminations [110]. Mesenchymal MANC and Wnt2+/PDGFRα+ cells support the alveolar growth and its regeneration, and act in stimulating repair following tissue injury. Finally, AMP cells support airway smooth muscle cells and can contribute to myofibroblast development following injury [111]. Recent studies have found, using single cell RNA sequencing, that the lung consists of at least 58 different molecular cell types, highlighting the fact that there is still much unknown about this vast complex organ and its response to injury [112].

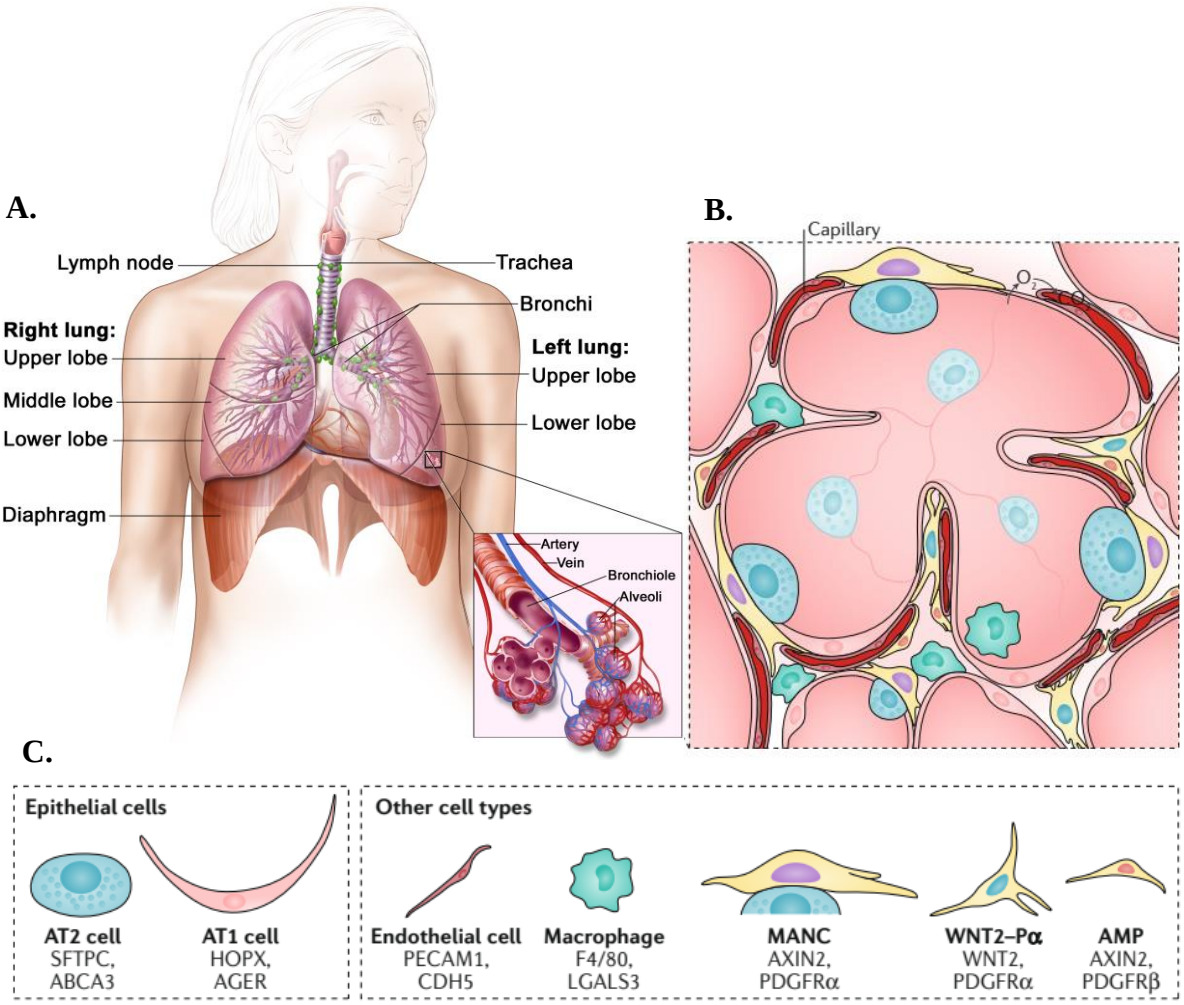

Figure 9: Illustration of the lung composition.

(A) The different lobes of the human lung. (B) Small airways lead to individual alveoli, each enclosed with a capillary plexus. (C) Alveoli cell composition containing AT2, AT1, Endothelial cells, Macrophages, MANC, WNT2-Pa and AMP cells [113], [114].

6.2. Radiation-induced lung injury

Radiation-induced lung injury (RILI) is one of the most common normal tissue toxicities observed in patients post lung irradiation and consists of 3 distinctive phases: the asymptomatic early/latent phase, the acute reversible phase, and the irreversible late phase [115]. During the early phase, the initial direct and indirect radiation damage causes cell death, and the activation of epithelial and endothelial cells, releasing inflammatory cytokines, and triggering the recruitment of immune cells.

6.2.1. Radiation pneumonitis

Radiation pneumonitis is characterized by the loss of alveolar barrier function, resulting in changes within the microenvironment, immune activation through inflammatory cytokine activation and fibrotic cytokine activation, additional ROS production, and cell damage. Radiotherapy to the normal tissue creates tissue damage, mimicking a wound, and causing an imbalance of the cytokine equilibrium. Numerous cytokines have been highlighted to function in contributing to a pro-fibrotic environment including numerous interleukins (IL-1α, IL-1β, IL-4, IL-5, IL-6, IL-8, IL-11, IL-13, IL-17α, IL-18, IL-23, IL-25 and IL-33), tumour necrosis factor- α (TNF-α) and transforming growth factor-β (TGF-β). TNF-α promotes the pneumonitis phase and is secreted upon damage by various immune cells. The cytokine stimulates apoptosis, necrosis and activates nuclear factor-kappa B (NF-κB), resulting in increased inflammation [116]. However, in later stages of RILI, TNF-α indicates to have an opposite effect in which inhibition of the TNF pathway increased collagen production, promoting a pro-fibrotic environment and expression of the TNF pathway resulted in limiting fibrosis development [117]. A vast recruitment of immune cell infiltration occurs together with increase exhaustion of the alveolar space, resulting in partial loss of tissue integrity [118]. In addition, there is an alteration in cell-cell interaction and decrease in lung perfusion [119]–[122]. In addition, the early onset of myofibroblasts occurs. Myofibroblasts can derive from fibroblasts, circulating fibroblasts fibrocytes or AT2 cells after endothelial-mesenchymal transition (EMT) [123]. Myofibroblasts have a high affinity to produce collagen and additional ECM proteins, remodelling the tissue structure. The severity and onset of pneumonitis depends on numerous factors including the radiation volume, dose, dose delivery and patient risk factors [124]. Its diagnosis exclusively depends on general respiratory symptoms, lung biopsy and the early onset of lung structural changes detected with computed tomography (CT) imaging. To fight pneumonitis symptoms, steroid treatment can be administered. Nevertheless, a loss of symptoms does not decrease the development of later onset of pulmonary fibrosis [125], [126].

6.2.2. Radiation fibrosis

Finally, the irreversibility of pulmonary fibrosis characterizes the lung as a late responding radiation toxicity organ [118]. Fibroblasts and AT2 cells continue in the transitioning to myofibroblast, resulting into a vast increase in collagen production, production of ECM protein and, ultimately a modification of the ECM. There is furthermore a continuation of additional

immune cell infiltration, stimulating a pro-inflammatory environment. Eventually, the distinct alteration of the ECM transforms the flexible lung tissue into rigid ''scar-like'' tissue, resulting in a complete and irreversible loss of the organ function in the affected area. The current diagnosis of pulmonary fibrosis is established in detecting clear structural changes in lung density using CT images.

Cytokine TGF-β fulfils numerous roles in driving RILI during fibrosis development by promoting deposition of ECM and collagen [127]. The main isoform, TGF-β1, stimulates fibroblasts, neutrophils, monocytes and T-cells to secrete TNF-α, IL-1, fibroblast growth factor and additional TGF-β1 protein secretion together with directly stimulation of ECM protein release by fibroblasts [128]. The inflammatory cytokine is furthermore responsible for the stimulation of the fibroblast myofibroblast transition through Smad-mediated signalling [129]. It functions in remodelling of the ECM and the alveoli structure, partly through Rho kinase activation, promoting fibrosis [130]. A loss of functioning Smad3 resulted in a decrease in fibrosis formation following radiation exposure in mice and could be an interesting target to reduce radiation induced toxicity [131]. In addition, the cytokine has an impact on the immune response by inhibiting the activation of lymphocytes and leukocytes and enables further production of ROS [132]. Increased level of TGF-β protein in the serum has therefore been identified as a poor prognosis for the development of pulmonary fibrosis. As TGF-β has been linked in promoting both lung fibrosis formation and tumour progression, targeting of the TGF-β pathway is currently a favourable approach in reducing lung fibrosis. Previous clinical trials include the targeting of protein angiotensin II, an important regulator of both TGF-β and α- smooth muscle actin. Within these trials, grade 2 and higher pneumonitis was reduced after treatment with Angiotensin II receptor blocker ACE in non-small cell lung cancer patients treated with thoracic radiotherapy [133]. Similarly, patients treated with scavenging agent ambroxol displayed an inhibition of TGF- β1 and TNF-α and successfully reduced the loss of lung diffusion capacity in patients receiving radiotherapy [134].

7. The small intestine, a model for acute radiation toxicity

7.1. The anatomy of the small intestine

The small intestine starts from the duodenum, continuing into the jejunum and finally the Ileum, before reaching the appendix (Figure 10, left panel). The structure of the intestine is characterized by crypts and villi, specially intended to increase the surface for maximum nutrient uptake. The villi consist mainly of enterocytes and some additional goblet, enteroendocrine and tuft cells (Figure 10, right panel) [135]. This layer of the villi mainly contains enterocytes, responsible for the exchange of nutrients between the intestine space and the blood, supported by a stromal cell layer. The goblet cells are responsible for the production of the mucus layer that covers both the villi as well as the crypts. This layer protects the single cell layer against infiltration of gut bacteria that can lead to infections [136], [137]. The enteroendocrine cells are responsible for the production of various hormones, responsible for stimulating the nutrient transport and the scarce tuft cells facilitate the monitoring of the intestinal substance [137]. The top of the crypts, connecting the villi to the crypts, contains a layer of transit-amplifying (TA) cells. These cells still maintain limited cell divisions before they differentiate into the various cells in the villi. The base of the crypt contains paneth cells together with intestinal stem cells. Paneth cells, characterized by its granules in the cytoplasm, are activated upon bacterial stimuli. Paneth cells can release their granule content, containing antimicrobial proteins, ensuring the homeostasis of the gut microbiota [137]. Finally, the intestinal stem cells are responsible for the regeneration of the intestine and villi. The stem cells are identified as Lgr5 stem cells, located in position 1-4 and responsible for homeostasis regeneration together with Bmi1 stem cells, located in position +4 and only functional following intestinal damage [137], [138]. The study of Barker et al. (2007) identified that the Lgr5 positive stem cells crypt-base-columnar cells (CBCs) in position +1-3 can generate all epithelial differentiated cells present within the intestinal villi [139]. The cells can divide unconditionally, generating a limitless supply of TA cells. It is therefore crucial that after damage implication, like radiotherapy, these cells survive to restore the intestinal wall. The lamina propria connects the intestinal lumen with the muscle layer below and consists of fibroblasts, ECM and hosts immune cells (Figure 10, right panel).

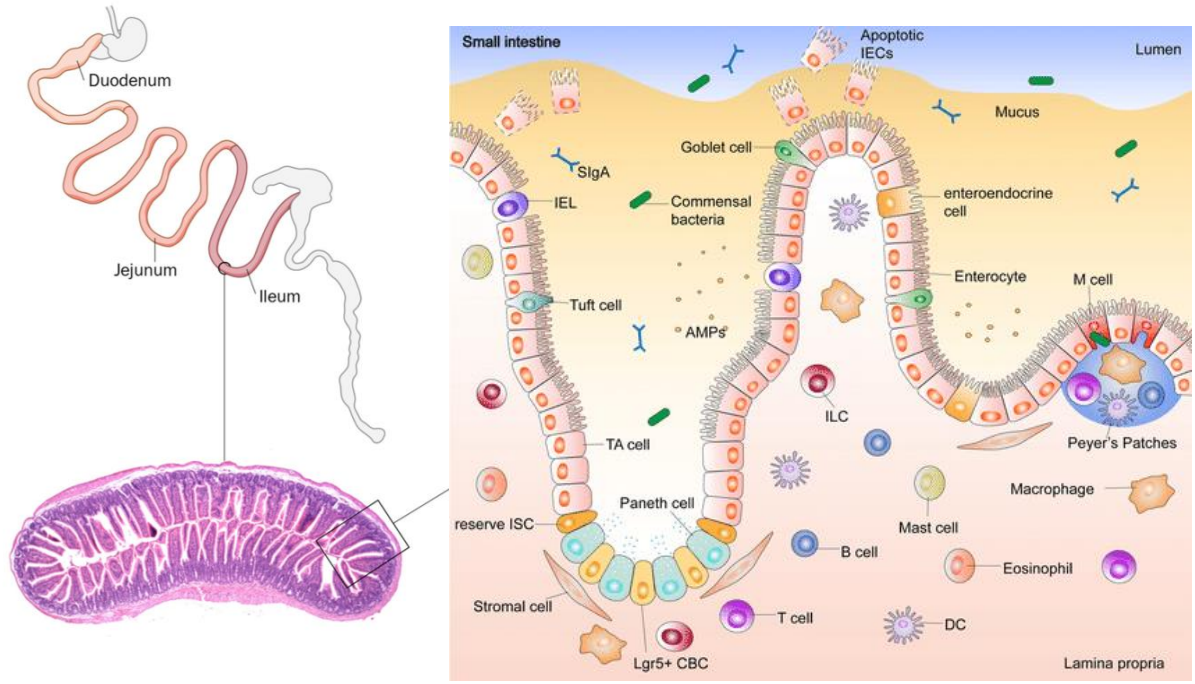

Figure 10: Illustration of the small intestine of mice.

The small intestine divided into the duodenum, jejunum, and Ileum (left) is constructed of crypts and villi, containing stem cells, enterocytes, goblet cells, mucus membrane, inflammatory cells, lamina propria, lymph nodes and lacteal with capillaries (right) [135], [140].

7.2. Radiation-induced intestine toxicity

Toxicity to the intestine is a relative common normal tissue radiation injury. During radiotherapy of the abdominal space, pelvic area or thoracic area, the intestine is often an organ at risk, receiving a considerable amount of undesired treatment [141]. Up to 90% of patients, with the intestine as an organ at risk, experience symptoms of which 15% develop severe chronic complications years after radiotherapy [142]–[144]. The intestine toxicity is depending on numerous factors including the dose, radiation type, the tissue volume, and the treatment protocol. Recently, age has furthermore indicated to contribute to the severity of the intestine toxicity [145]. Generally, the intestine is considered early responding tissue, however, its toxicity is also presented in late responding irreversible chronic injuries [143].

In acute radiation intestine toxicity, known as radiation enteropathy, patients present with mucositis symptoms including diarrhoea, constipation, and haemorrhages. The symptoms appear within hours or days post radiotherapy, vastly impacting patients' welfare [142], [146]. During radiotherapy, direct and indirect events through direct ionization and indirect damage through ROS, results in damage to the DNA, proteins, and additional changes in the rapidly

dividing intestinal epithelium. If repaired improper, this leads to senescence, compensatory proliferative reactions, or cell death, leading to mucositis, a complete destruction of the epithelial barrier characterized as the mucosal breakdown [142]. Gut microbiota can obtain direct contact with the lamina propria, resulting in a severe inflammatory response [147]. In parallel, the damaged vascular epithelium initiates the production of inflammatory cytokines including TGF-β and TNF-α [148], [149]. This collectively recruits T lymphocytes, macrophages, neutrophils, leukocytes, and monocytes, further activating the inflammatory response, increased ROS production, resulting in additional tissue damage and even degradation of the lamina propria [147], [150], [151]. The intestine is considered an early responding tissue, however the sensitivity against radiation induced toxicity varies depending on the cell type within the crypt. Intestinal stem cells at position +4 are very sensitive and undergo rapid apoptosis (4-6h) that occurs at exposure to 1 Gy IR [152]. In parallel, Lgr5+ stem cells revealed to be radioresistant. The crucial aspect to enable any intestine recovery is the survival of the stem cells, known as the Lgr5+ CBC cells, at the bottom of the crypts. The study of Hua et al. (2012) revealed that Lgr5+ CBC cells contain a DNA repair-mediated resistance against radiation induced toxicity. The study displayed in vivo a faster clearance of histone 2AX at serine 139 (termed γH2AX), Breast cancer susceptibility protein 1 (BRCA1), RAD51 and DNA-dependent protein kinase (DNA-PK) foci in the CBCs compared to villus cells or TA cells, indicating increased repair capacities in both the homologous recombination (HR) and NHEJ repair pathways [153]. Following radiation exposure, only high doses of exposure (8-15 Gy) are correlated with a depletion of CBCs, resulting in abandoned gastrointestinal (GI) toxicity [154]. The depletion of Intestinal stem cells located on +4 (ISCs) at lower doses did not result in intestinal injury [154]. Strikingly, it has recently been discovered that following the depletion of CBC cells, daughter cells of Lgr5+ CBCs can de-differentiate to create a new group of Lgr5+ CBC cells in order to maintain homeostasis and reduce GI toxicity [155]–[157].

If tissue recovery is unsuccessful, the additional inflammatory response, ROS production and tissue damage continues, resulting in chronic toxicity. Late toxicity occurs months to years after radiotherapy, is progressive and chronic. During this phase, there is a depletion of stem cells, continued proliferation and inflammatory response leading to drastic changes in the ECM. This results in loss of GI function, fibrosis, intestinal dysmotility, vascular sclerosis, mucosal dysfunction, irreversible mucosal atrophy, and chronic radiation enteritis [142]. Radiation enteritis is driven by an imbalance in proinflammatory cytokines IL-1b, TNF-a and IL-6 within

the muscularis layer. Consequently, this results in expression of IL-8 by the surrounding cells, resulting in neutrophil recruitment and accumulation [158]. The treatment for chronic intestine toxicity is surgical removal, accompanied by high mortality rate and the increase in early injuries has been linked to higher probability of late toxicity [159], [160]. The radiation regimen of commonly used hypofractionation containing 2 Gy per fractions given up to 7 weeks, results in recurring injuries causing a continues recruitment of immune cells, direct tissue damage and pathophysiologic responses [142]. TGF-β expression, as described priorly in chapter 5.2.2., promotes fibroblast in deposition of ECM and collagen, driving fibrosis formation. Interestingly, radiation-induced enteropathy is not correlated to the activation of the Smad pathway as described in lung fibrosis. It is however a result of low levels of TGF-β1 that activate the Rho/ROCK pathway, resulting in increased CCN2 gene expression and fibrosis [161].

Categorizing the intestine as an early responding tissue needs to be reconsidered to limit the ignorance of acute damage on the tremendous complications it has for patients' long term. Currently, no clinically approved drugs against GI toxicity are available. However, some promising results have been obtained in the decrease of acute GI toxicity following radiotherapy treatment in patients by using statins or statins with ACE inhibitors [162]. The standard diagnosis of acute intestine injury remains far from optimal, and solitary based on symptoms. Interestingly, recent studies have found that citrulline detection in plasma can be a suitable tool for diagnosis [163]. Citrulline is produced by enterocytes and therefore citrulline detection in plasma is a direct measure for the intestinal enterocyte population. Increased intestinal damage results in less enterocytes, decreasing the citrulline concentration. This can be used for damage observation and exploited to monitor drug effectiveness against intestine toxicity in a relative non-invasive manner.

8. The cell cycle of the normal tissue and the impact of radiotherapy

8.1. The cell cycle mechanism

The human body is composed of dividing and non-dividing cells, but the vast majority are non-dividing cells that sustain outside of an active cell cycle. Certain non-dividing cells (e.g. senescent or terminally differentiated cells) are irreversibly arrested (e.g. erythrocytes). In contrast, a subset of non-dividing cells, quiescent cells are arrested in G0 phase of the cell cycle and are capable of reactivation, entering the proliferative cell cycle in response to physiological growth signals [164]. The division and proliferation of tumour and normal cells are identified in 4 stages (G1, S, G2, and M phases), collectively known as the cell cycle (Figure 11). In the first stage G1, supported by cyclin D, cells synthesize the required material for DNA replication, expands its size and examines if the environment is desirable to facilitate cell division. To continue to the second division state S, a checkpoint examines the environment including growth factor and nutrient availability, DNA damage, the expansion of the cell and the necessary synthesized proteins. The G1/S checkpoint is regulated by cyclin D and cyclin dependent kinases (Cdk) 4/6 where the complex phosphorylates and inactivate the retinoblastoma protein (Rb), resulting in the release of transcription factor E2F, promoting transcription of S phase transition proteins including cyclin E. Cyclin E activates Cdk2 resulting in degradation of p27 and synthesis of cyclin A, ensuring S phase transition. As the cell cycle progresses from late G1 to early S-phase, cyclin E is degraded, cyclin A and cdk2 form the cyclin A-Cdk2 complex, resulting in the promotion of DNA replication [165]–[168]. During S-phase, the complete genome is duplicated [169].

As DNA replication in eukaryotes is achieved by the activation of multiple replication origins, which needs to be precisely coordinated in space and time, there is a tight interplay between the DNA replication program and the intra-S-phase checkpoint. This intra-S-phase checkpoint monitors the integrity of DNA synthesis and is activated when replication forks are stalled [170], [171].

In the G2 phase, the cell undergoes extended cell growth and protein synthesis to accompany the 2 formed daughter cells. Cyclin A forms a complex with Cdk1 ensuring the stabilization of cyclin B-Cdk1 complex. This complex is necessary to ender cells into the M-phase, and it promotes the expression of maturation/mitosis promoting factors [172], [173]. Here, the G2/M

checkpoint is in place to ensure that no incomplete DNA replication or additional DNA damage is present that can interfere with mitosis. G2/M arrest is commonly observed after irradiation [174]. If the repair is unsuccessful, this will result in cell death. However, if the repair is successful, cells can enter mitosis.

The M-phase/mitosis is responsible for the separation of the chromosomes and the final formation of the new daughter cells. The mitosis is divided into prophase, metaphase, anaphase, telophase, and cytokinesis. During prophase the chromosomes condenses, forming per chromosome the 2-sister chromatid connected by the centromere and the cell starts the formation of the mitotic spindle containing centrosomes and the growth of microtubules. During the prometaphase the nucleus is opened, exposing the chromosomes to the mitotic spindle. The mitotic spindle becomes attached to the kinetochores on the centromeres. During the metaphase, the mitotic spindle and the chromosomes are organized and in an equilibrium with both centromeres on opposite cell poles and the arranged chromosomes forming the metaplate plate in the centre of the cell [175]. The M checkpoint ensures that each sister chromatid is connected to the correct part of the mitotic spindle to allow the correct segregation of the sister chromatins. The cell will go into the anaphase where protein Esp1 separates the sister chromatids from each other by cleaving of the connective cohesions. This is followed by the pulling of each chromatid towards the centromere and elongation of the cell itself. During the final stages of telophase and cytokinesis new nuclei are formed and the cytoplasm is divided using the cleavage furrow, eventually resulting in the complete formation of 2 new daughter cells [176], [177].

In 2006 a new cytokinesis checkpoint was discovered by Norden at all. in S. cerevisiae, regulated by Aurora-B kinase [178]. The checkpoint examines the development of any chromosome bridges that could result in aneuploid cell progeny or introducing abscission resulting in genomic instability [178]–[180].

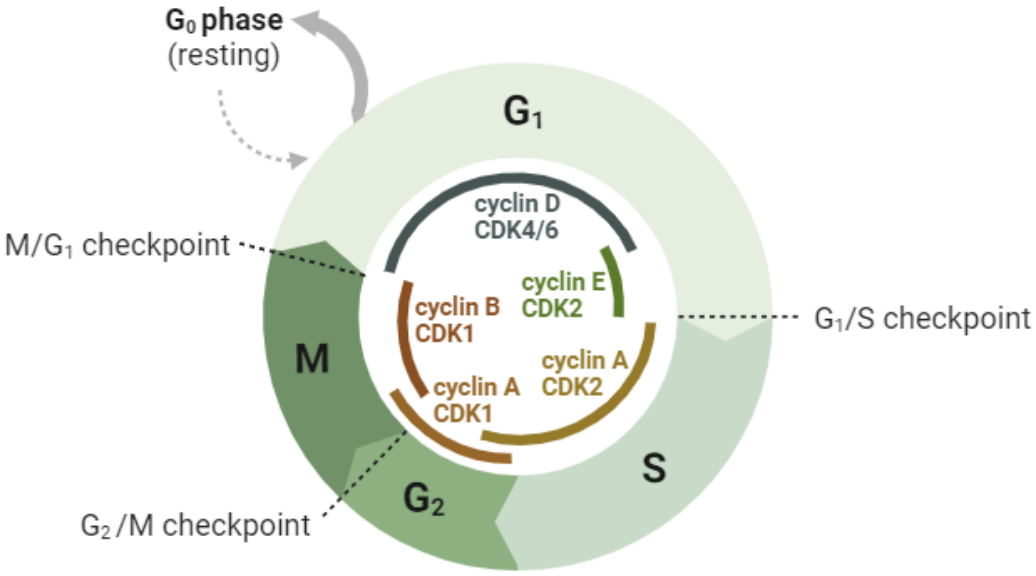

Figure 11: Cell cycle progression.

Cell cycle progression from G1-phase, facilitated by cyclin D/CDK4/6 and cyclin E/CDK2 followed by S-phase with cyclin A/CDK2, G2-phase with cyclin A/CDK1 and M-phase with cyclin B/CDK1 together with its allocated checkpoints. (Created with BioRender.com)

8.2. Cell cycle sensitivity to radiotherapy

As the DNA content of cells, and therefore also its utilized DNA repair pathway, drastically changes throughout the cell cycle, the sensitivity of cells to radiation-induced damage can fluctuate depending on the cell phase. This was tested in early research by Sinclair and later by Vos where the studies examined the radiation sensitivity of cells depending on the cell cycle phase [181]–[184]. Chinese hamster cells and human kidney cells were synchronized and irradiated at different phases of the cell cycle (Figure 12). Sinclair published in 1968 extensive research displaying the cell phase sensitivities following radiation of various cell lines [181]. The research concluded the following points on the cell survival in various cell cycle phases that are still highlighted in scientific texts today. First, on average mitosis appears to be the most radiosensitive phase. Second, if G1 in the cells occurs for a longer period, radio resistance is on average observed in early G1 phase. Third, overall highest radio resistance is observed in mid S-phase. Lastly, G2 phase and mitosis carry equally high radiosensitivity (Figure 12) [181]–[184]. However, in the observation of the cell phase sensitivities of the different cell lines, it appears that the degree of radiosensitivity in the cell phases is cell line specific. Although current research repeating the experiments is lacking, with current knowledge of the

complexity of both tumour and normal cells, it is hypothesized that similar results will obtain to be cell line specific. Nevertheless, it can be concluded that the sensitivity of cells following radiation is influenced by the cell cycle state of the cell following irradiation.

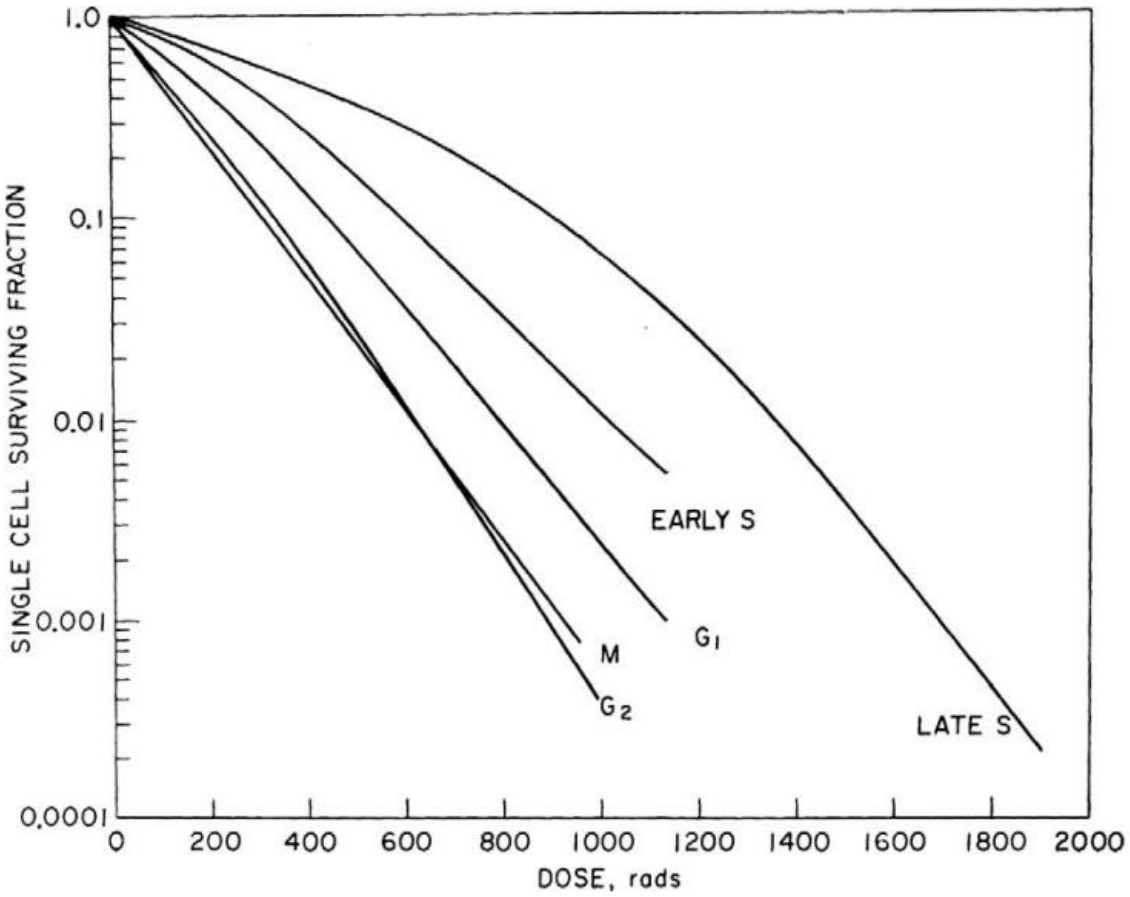

Figure 12: Cell survival sensitivities throughout the cell cycle.

Synchronized Chinese hamster cells displayed changes in cell survival depending on the cell cycle phase during irradiation. Late S phase displayed least sensitive, with G1 phase as moderate sensitivity and G2 phase and mitosis as highly sensitive following radiotherapy [182].

8.3. Exploiting the cell cycle arrest for protection against toxicities

Cancer cells multiply faster than normal cells in the body. Because radiation is most harmful to quickly growing cells, radiation therapy is more detrimental to cancer cells than normal cells. Furthermore, with radiosensitivity variable through the cell cycle and commonly lack of sufficient cell cycle checkpoints in tumour cells, it is interesting to exploit this difference to enhance the therapeutic window. The study of Chen et al (2000) revealed preliminary data on

exploiting the G1 arrest for normal tissue protection in vitro [185]. Normal and cancer epithelial cells were treated with low doses of staurosporine (non-selective protein kinase inhibitor) introducing G0/G1 arrest explicitly in normal cells. Cells were thereafter treated with lethal doses of doxorubicin, an anthracycline drug, resulting in tumour cells toxicity. However, normal epithelial cells resumed proliferation after the drug was removed with little to no toxicity. Similar results were obtained by Price et al (2004) [186]. Mouse kidney proximal tubule cells were treated with p21-adenovirus or Cdk2/5 inhibitor Roscovitine resulting in G1/S and G2/M arrests. Lower cisplatin-induced cell death was observed in treated cells compared to untreated cells. However, the study indicated that the protection against cisplatin induced toxicity is through reduction of apoptosis and not the cell cycle arrest. Interesting in vivo results were obtained by the study of Mull et al (2019) [187]. Using BrdU incorporation and western blot analysis, the authors showed that the compound UCN-01 induced a reversible G1 arrest in the small intestine of nude mice. Interestingly, the combined treatment of UCN-01 and chemotherapeutic 5-fluoruracil (5-FU) resulted in a significant increase in the survival of mice, while it triggered a significant decrease in tumour control on mice bearing MDA-MB-468 tumours. Further research described protection of normal fibroblasts from polyploidy and nuclear morphology abnormalities induced by the aurora kinase inhibitor VX-680, if the cells were pre-treated with the potent p53 activator, actinomycin D [188]. However, p53 proficient tumour cells also displayed some degree of protection [188]. In vivo administration of G1T28 to mice, a potent and selective Cdk4/6 inhibitor that inhibits the phosphorylation of RB inducing an exclusive, reversible G1 arrest, resulted in the inhibition of bone marrow cell proliferation [189]. Pre-treatment of mice with G1T28 allowed a faster recovery of complete blood counts while maintaining tumour control following 5-FU treatment [189].

The progress in reducing radiation-induced toxicity by exploiting normal cells cell cycle arrest was achieved by Johnson in 2010 and Tian in 2013 [190], [191]. The research of Tian et al. (2013) demonstrated that pre-treatment of prostate cancer-bearing mice with the drug darinaparsin (DPS), which arrests the cell cycle of crypts epithelial cells (CECs) at both G1/S and G2/M checkpoints, improved intestinal function as evidenced by increased body weight and animal survival while sensitizing prostate cancer cells [190]. The authors suggested that DPS-activated cell cycle arrest in CECs may be at least one of the mechanisms responsible for DPS-mediated radioprotection. In another study, Johnson et al. (2010) revealed similar radioprotection of proliferating hematopoietic stem/progenitor cells (HSPCs) in vivo by

Cdk4/6 inhibitors. The combined radiation and inhibitor treatment resulted in a decrease in hematopoietic toxicity with increased survival compared to standalone irradiation, providing evidence of a protection by normal cell cycle arrest [191]. This research provides preliminary evidence that the cell cycle can be exploited to reduce normal tissue toxicity while maintaining tumour control.

9. P53, the guardian of the genome

The p53 protein was first discovered as co-immunoprecipitating with large T-antigen when examining the mechanism in which large T-antigen simian virus 40 (SV40) can transform normal cells into malignant cells, explaining that for a long time, the p53 gene was thought to be an oncogene [192], [193]. The research of Donehower et al (1992) revealed that p53 knock-out mice did not display any development defects but developed tumours early on [194]. It is therefore not surprising that p53 is mutated in over 50% of human cancers [195]. The gaining of a p53 mutation is highly favourable for tumour cells, the p53 pathway loss results in a survival advantage where tumour cells can bypass cell cycle checkpoints for DNA damage and oncogenic signals and can undergo unlimited cell divisions. Eventually, the research of Baker in 1989 identified p53 as a tumour suppressor gene [196], [197].

9.1. The structure of the p53 protein

The p53 protein contains 5 regions of main importance, the DNA binding, the transactivation, the tetramerization, the proline-rich and the regulatory domains (Figure 13) [198]. The transactivation domain is divided into Transactivation domain (TAD) 1 and 2, located at the N-terminus of the protein and binds to various cofactors required for the suppression of tumorigenesis, including mouse double minute 2 homolog (MDM2). Mutations in TAD1 modify the p53 protein drastically resulting in a loss of function. Modifications in TAD2 are less severe and the p53 protein remains almost to complete capacity [199].

The proline-rich domain is needed for p53s capacity to bind to DNA and for the protein's stability. Deletions within this domain destabilizes the protein, making it prone for degradation [200]. The central core region of the protein contains the DNA-binding domain (DBD), allowing p53 to function as a transcription factor. The DNA-binding domain can recognize a specific sequence on the DNA identified as the p53 responsive element [201]. The tetramerization domain is located at the c-terminus of the p53 protein and is required to generate a homotetrameric complex that binds to the p53 responsive elements [202]. Finally, a recent study has shown that the regulatory domain is involved in stabilizing p53 by an inter-monomer interaction with the DBD of another subunit in the tetramer leading to an additional connection of all subunits in the tetramer [203]. With the enormous variety of functions that p53 holds, a strict regulatory and communication system is in place using post translational

modifications (PTMs). At different locations on its protein sequence, p53 can receive phosphorylation, acetylation, methylation, ubiquitination, SUMOylation, or glycosylation [204]. Together, the location, type of modification and occasionally protein modifiers or cofactors convey one message that results in a specific p53 pathway activation [205].

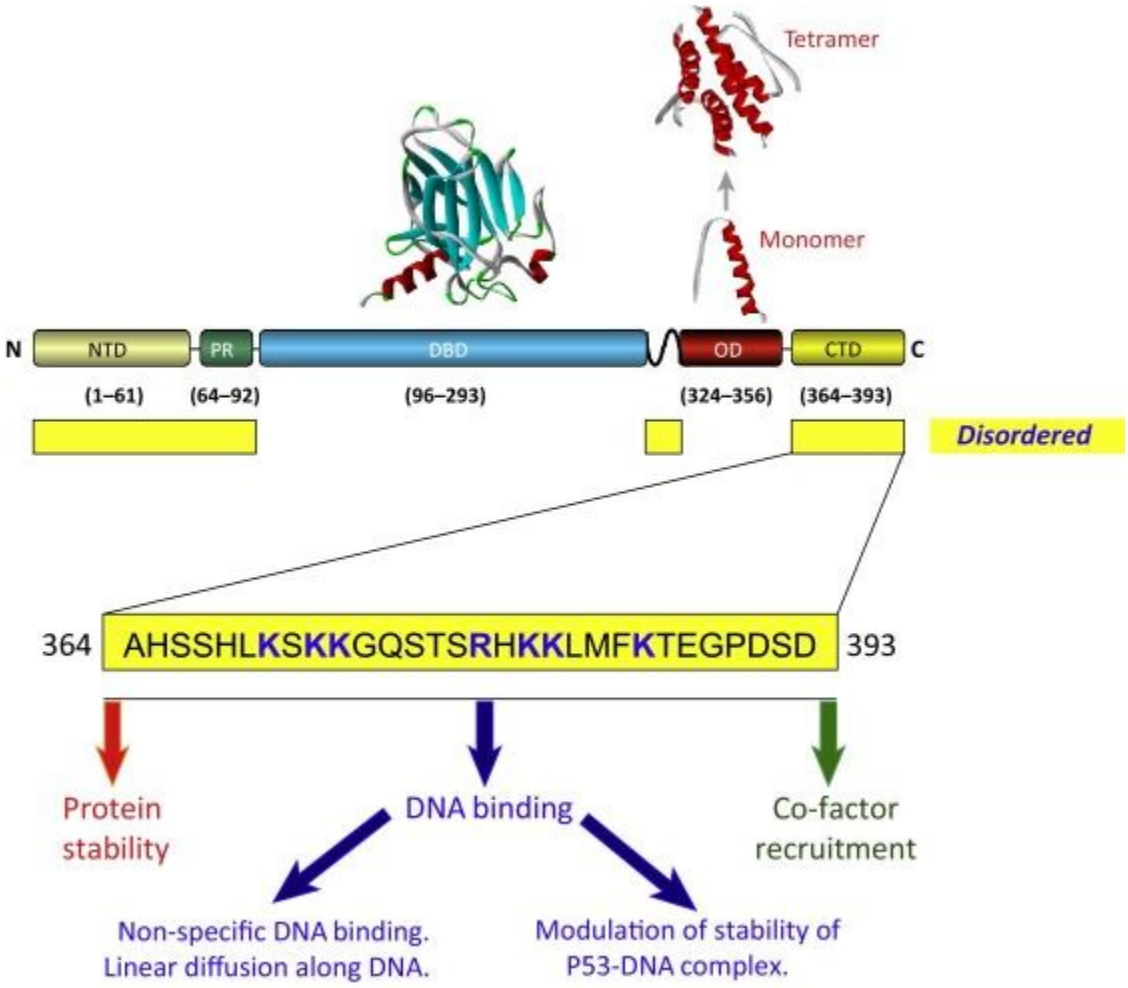

Figure 13: The structure of the p53 protein from n-terminal to c-terminal.

The 5 domains range from n-terminal transactivation domain (NTD), proline-rich domain (PR), DBD, oligomerization domain (OD) to the c-terminal domain (CTD). Below represents the amino acid sequence of human p53 at the CTD with its function in protein stability DNA binding and co-factor recruitment [206].

9.2. The power of p53 within the cell

Nicknamed the guardian of the genome, p53 is involved in many mechanisms throughout the cell. External stress signals including, irradiation, ultraviolet (UV), genotoxic drugs, nutrition deprivation, heat or cold shock or internal stress including replication or translation stress, metabolic changes or oncogene activation including MYC, E2F1, Ras or BCR-ABL gene expression results in the activation of p53. Irradiation, UV, and genotoxic drugs result in DNA damage, recognised by ATM or ATR, phosphorylating, and activating Checkpoint kinase 1 (Chk1) or Checkpoint kinase 2 (Chk2), resulting in p53 phosphorylation. Additionally, proto-oncogenes converted to oncogenes by mutations or accidental activation are detected by p14ARF [207]. This protein inhibits MDM2 resulting in release and activation of p53. Activation of the target genes including p21, p53 upregulated modulator of apoptosis (PUMA), Phosphatase and tensin homolog (PTEN), plasminogen activator inhibitor (PAI) and tumour suppressor activated pathway-6 (TSAP6) result in cell cycle arrest with possible cellular senescence, apoptosis, angiogenesis, and metastasis inhibition, mammalian target of rapamycin (mTOR) pathway inhibition, exosome mediated secretion or the activation of a negative p53 feedback signal (Figure 14).

Phosphorylation has been mainly linked to the transcriptional activation of the p53 proteins. For example, the phosphorylation of Thr18 results in increased interaction between p53 and the transcription factor p300 and decreases the p53-MDM2 interaction, promoting the release and activation of p53 [208], [209]. Moreover, phosphorylation of Ser20 in response to DNA damage results in the transcription activation of p21 while the phosphorylation of Ser15 by Ataxia-telangiectasia mutated (ATM) or Ataxia telangiectasia and Rad3 related (ATR) promotes p53 stabilization and phosphorylation of Ser46 revealed to contribute to apoptosis induction [210]–[213]. The acetylation of p53 has been linked to apoptosis and cell cycle arrest in response to genotoxic stress [214]. C-terminus acetylation protects the protein from ubiquitination and degradation, acetylation of K382 by p300 promotes oligomerization and acetylation of K120 after DNA damage results in the transcription of apoptosis genes [215]. The ubiquitination PTM is required for returning to cell homeostasis after a stress event has been resolved. Monoubiquitination of p53 transports the protein from the nucleus into the cytoplasm. Here, polyubiquitination occurs, labelling the protein for degradation by proteases [216]. Although relatively less known, methylation on arginine or lysine residues and

SUMOylation on lysine residues has been linked to both p53 inhibition and activation following cellular stress [216]–[219].

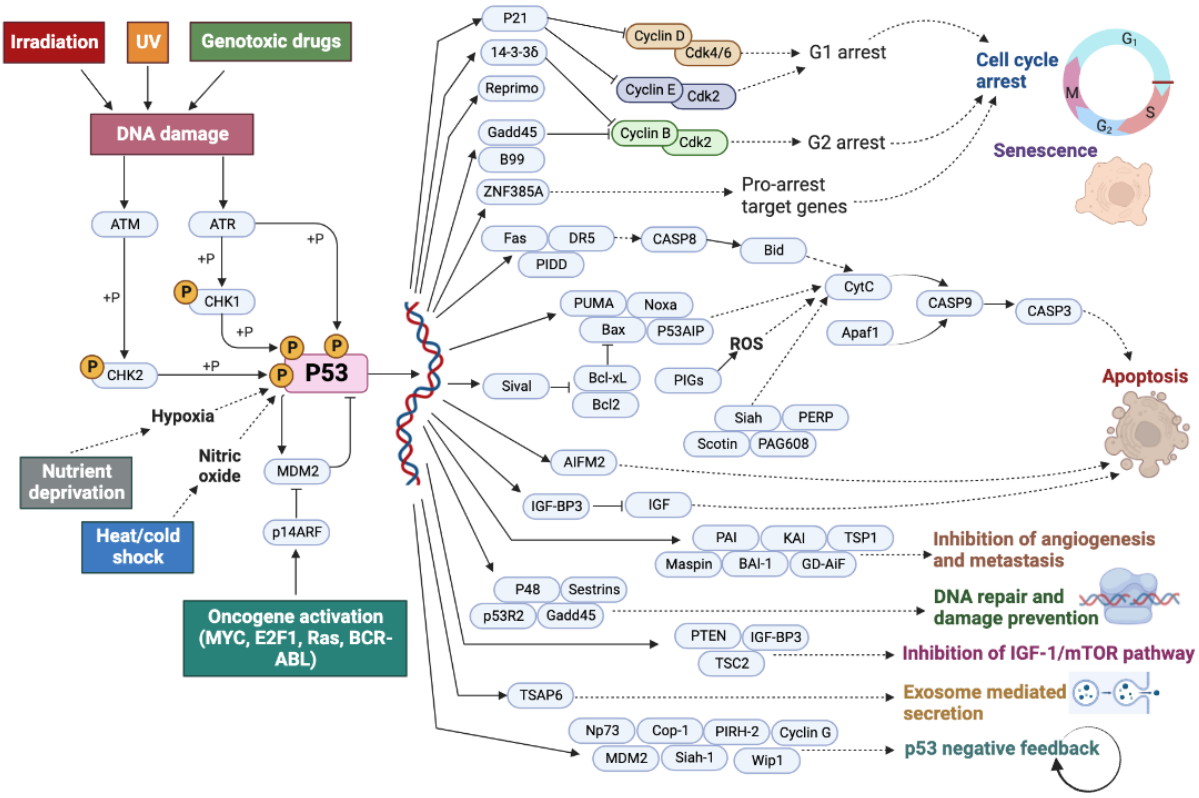

Figure 14: p53 activation and its downstream effects.

External factors can result in DNA damage or are promoted through hypoxia and nitric oxide, results in the phosphorylation and activation of p53. MDM2 can inhibit the activity of p53 by binding and inactivating the protein. Oncogene activation results in the release of p53 from MDM2 by inhibiting MDM2. Following phosphorylation, p53 is activated and can induce gene transcription of proteins driving cell cycle arrest, senescence, apoptosis, inhibition of angiogenesis and metastasis, DNA repair and damage prevention, inhibition of IGF-1/mTOR pathways, exosome mediated secretion and its own p53 negative feedback signalling. (Adapted from Kaneshia laboratories, created with BioRender.com)

9.3. The function of p53 in cell cycle arrest

During cell cycle progression multiple checkpoints are in place to ensure faithful DNA replication and proper chromosome segregation, and cell cycle arrest is among p53 proteins many pathway functions. Upon damage, the DNA damage response (DDR) is activated, which is controlled by three related kinases: ATM, ATR and DNA-PK [220]. Recruitment of those kinases at the chromatin depends on the nature of the damage and the phase of the cell cycle. The ATM-dependent pathway is essentially involved for the repair of DSBs, while the ATR-

dependent pathway is activated in response to replication stress generating single-stranded DNA (ssDNA) regions. Nevertheless, the roles of ATM and ATR are heavily intertwined in response to DSBs [221]. The third component, DNA-PK, is also recruited at sites of DSBs and its major role is to promote non-homologous end-joining (NHEJ) [220]. It is to note that most (≈ 80%) IR-induced DSBs outside of S-phase are repaired by NHEJ independently of ATM. Once activated, these 3 kinases can phosphorylate a variety of substrates, among them p53 and the histone variant H2AX, a marker of DNA damage and further explained in section Biomarkers of AsiDNA™ activity and sensitivity.

Activation of p53 in response to DNA damage is associated with a rapid increase in its levels and ability of p53 to bind DNA and mediate transcriptional activation. This activation is primarily mediated by several PTMs, among them phosphorylation essentially in the N-terminal domain of p53 [222]. Phosphorylation at ser15 and 20 disrupt the interaction of p53 with MDM2, prolonging the half-life of p53 through the incapability of degradation in a MDM2-dependent manner. In vivo, both ATM and ATR can phosphorylate p53 on ser15 in response to IR and UV, while p53 phosphorylation on ser20 is also dependent on two checkpoint kinases 1 and 2 (Chk1 and Chk2), acting downstream of ATM and ATR, respectively [222]. Although in vitro studies have shown that DNA-PK can phosphorylate p53 on ser15 and ser37, which disrupts the interaction of p53 with MDM2, this was not proven to occur in vivo [222], [223].

P53 transcribes the CDKN1A gene encoding for the Cdk inhibitor 1 p21 protein, that can inhibit and inactivate cyclin D-Cdk4/6 and cyclin E-Cdk2 complexes. The protein interferes with the phosphorylation of the Rb protein ensuring the prevention of E2F release for continued transcriptions of cell cycle progression genes, resulting in a G1/S cell cycle arrest [224], [225]. Research has furthermore identified that senescence is dependent on the p53 cell cycle arrest as knock out of p21 resulted in a loss of senescence capabilities [226]. Although lower in affinity, p21 can also induce a G2/M arrest by inhibition of the cyclin B-Cd1 complex [227]. Additional less explored p53 driven cell cycle arrests are the interaction with proliferating cell nuclear antigen (PCNA) and 14-3-3δ, blocking DNA replication and inducing a G2/M arrest and the transcription of target gene GADD45. This induces a G1/S or G2/M arrest through the interaction with CR6-CRIF1 inhibiting Chk1 and Chk2, or by direct inhibition of Chk1 [228], [229]. If the damage repair was unsuccessful, p53 will induce premature senescence or apoptosis [230], [231]. Interestingly, research of Li et al. (2012) revealed that mice bearing

mutations on the p53 acetylation sites responsible for p21 and PUMA activation, driving cell cycle arrest and apoptosis, did not result in spontaneous tumour development [232]. The mutations maintained the ability of p53 to control antioxidant response and regulate energy metabolism, identifying unique mechanisms of p53 outside of the cell cycle control and apoptosis induction to ensure tumour repression [232].

9.4. P53 activation following radiation exposure

DNA damage introduced by ionizing radiation results in increased translation of the p53 protein and the inhibition of the proteins degradation followed by the activation of various downstream pathways, including apoptosis and senescence [233]–[236]. The complexity of an organism results in p53 responses that vary between normal tissues. Within the following chapter, the contribution of p53 to tissue specific radiation toxicity responses are explored.

9.4.1. Vascular endothelial cells

The radiation induced damage to vascular endothelial cells is a contributor to the development of both early and late toxicities. Cell death occurs similarly as in other cell types through mitotic catastrophe, senescence, or apoptosis [237], [238]. Radiation exposure results in endothelial degeneration and decrease in the density of micro vessels within the myocardium. The p53 status of endothelial cells plays a crucial role in reducing radiation induced cardiac injury. The study of lee et al (2012) and reconfirmed by Kuo et al. (2022) revealed that the loss of p53 function by mutation of the TAD1 domain, complete loss of p53 or p21 in endothelial cells increased radiation-induced cardiac injury, accompanied with systolic dysfunction, cardiac hypertrophy, myocardial necrosis, and fibrosis [239], [240]. In addition, the loss of p53 resulted in increased hypoxia and disorganisation of the vasculature of the heart. The research revealed that the presence of p53 in endothelial cells protects the cell from radiation-induced mitotic catastrophe.

9.4.2. The hematopoietic system

Cells within the hematopoietic systems, including both differentiated and progenitor cells, are sensitive to radiotherapy treatment, where exposure results in anaemia and leukopenia [241]–[243]. The acute toxicity revealed to be induced by increased apoptosis. Mice with a deficiency in p53 downstream proteins PUMA or BAX, responsible in the p53 mediated apoptosis activation, displayed increased progenitor cells with resistance against acute radiation-induced

hematopoietic toxicity [244]–[246]. In contrary, late radiation-induced hematopoietic toxicity is associated with senescence induced in hematopoietic stem cells, independent of apoptosis. Various studies have examined the p53 dependency on late radiation induced hematopoietic toxicity by depletion of p53 pathways, resulting in senescence. The depletion of CDK inhibitor 2A gene, responsible for the transcription of p16INK4a and p19ARF, resulted in increased progenitor and hematopoietic stem cell division, leading to a decrease in senescence [247]. However, within the same population of progenitor and stem cells, the depletion of downstream p53 protein p21 resulted in increased stem cell toxicity, losing the capacity of p21 to reduce p53 activation in hematopoietic stem cells, promoting apoptosis [248]. This is in correlation with the results obtained by Mohrin et al (2010) where hematopoietic stem cells have increased resistance to p53 mediated apoptosis by promoting increased NHEJ to repair DSBs [249]. Blocking of p53 has been proposed as a tool to reduce normal tissue toxicity. However, this needs to be approached with caution as for some tissues it can further enhance the sensitivity of the tissue to radiation-induced toxicities.

9.4.3. The gastrointestinal system

As described earlier in chapter 4 intestine toxicity, the sensitivity against radiation damage varies per cell type throughout the intestinal crypt. Overall, the dependency of p53 activity to radiation-induced GI toxicity is contradictory to the hematopoietic system. Following abdominal irradiations in p53 knock out mice, increased radiation-induced GI toxicities was observed [246]. Stem cells in the crypt first respond with a delayed progression and late S-phase arrest and mitotic arrest together with epithelial cell migration along the crypt axis and exiting from the tip of the villus resulting in severe shrinking of the intestinal crypts [250]–[252]. The release back into the cell cycle results in hyperproliferation of the stem cells and eventually results in death by mitotic catastrophe [251]. In addition, radiotherapy can activate apoptosis in the radiosensitive GI epithelial cells 4 hours following radiation exposure that is dependent on active p53. A decrease in apoptosis and increased resistance to radiation-induced apoptosis was observed in epithelial cells within p53 knock out mice [253]. However, this resistance to apoptosis does not result in a decrease of cell death. Radiation exposure following the loss of p53 activity results in a delay in the cell death of epithelial cells from 4h to 24h post exposure resulting in death by mitotic catastrophe [254], [255]. In addition, the study of Kirsch et al. (2010) displayed that the loss of apoptosis, through knock out of BAX,

did not result in an impact on radiation induced GI toxicity. In addition, loss of p53 resulted in increased GI damage while overactivation of p53 had the capacity to protect against radiation induced toxicity [246]. Although the depletion of Bax did not impact the GI toxicity, the depletion of upstream protein PUMA did result in decreased GI toxicity correlated to increased p21 activity [256], [257]. In correlation, the depletion of p21 resulted in increased radiation induced GI toxicity [256]. Interestingly, p53 also has a contributed factor in late toxicity within the intestine following radiotherapy. The study of Lee et al. (2019) revealed that the loss of p53 in vascular endothelial cells did not impact acute radiation-induced GI toxicity but did greatly contribute to late radiation-induced enteropathy. The study revealed in p53 deficient vascular endothelial cells following abdominal irradiation increased intestinal injury occurring at late timepoints, accompanied with increased microvessel damage and hypoxia [258]. Finally, the preprint publication of Morral et al. (2023) revealed that the recently discovered de-differentiation of CBC daughter cells to Lgr5+ CBCs is dependent on p53 activity. The research identified the need of p53 activation to promote the de-differentiation of revival stem cells through Yap-dependent reprogramming with its main contributor of Clu+ cells as revival stem cells. The study furthermore identified that p53 inhibition impairs the de-differentiation. Similarly, continues p53 activation following the inhibition of mdm2 resulted again in impaired de-differentiation, striking an important feedback loop of p53-mdm2 to maintain homeostasis for de-differentiation following GI toxicity. Surprisingly, the study of Plant et al. (2019) did identify that the loss of MDM2 increased p53 activity, resulting in decreased radiation-induced GI toxicity [257]. These results provide evidence that the regulation of the radiation-induced GI toxicity is independent of apoptosis but dependent on functioning p53 and p21. The presence of the MDM2 feedback mechanism appears to be important in maintaining de-differentiation but its loss does not enhance radiation-induced GI toxicity if p53 remains functional.

10. Radioprotectors to reduce radiation induced toxicities

The development of the first radiosensitizer was pioneered by Patt. et al. in 1949 [259]. His research identified that mice receiving cysteine displayed a significant increase in survival following total body irradiation. Cysteine was identified to contain a sulfhydryl (SH) group, that can donate a hydrogen atom to a radicalized DNA molecule, resulting in chemical DNA repair, or donate a hydrogen atom to oxygen-based radicals, eliminating the oxygen based radical [260]. The identification of the radioprotective capacities of cysteine sparked interest at the U.S. army. With the chance of possible nuclear attacks and the visible damage inflicted in Japan at the end of the second world war, the U.S. introduced a drug development program to screen the capacity of substances to protect the healthy tissue against radiation-induced toxicity. Over 4000 chemical substances were screened within this program and gave rise to the first FDA approved radioprotection drug, amifosine, also known as WR-2721 [261].

10.1. FDA approved radioprotectors

The radiation protection of compounds containing the SH group is enhanced by adding phosphate to the SH group, creating a prodrug. The phosphate group ensures less toxicity and is stripped off the prodrug in the blood by alkaline phosphatase, exposing the drug with the SH group for diffusion into the cells. The chemical radioprotector amifosine as prodrug WR-1065, contains a phosphate group [262]. Several animal studies revealed a rapid increase of amifosine in normal tissue compared to tumour cells caused by the poor vasculature in tumours and less availability of enzyme alkaline phosphatase [263]. With the aim of reducing radiation-induced toxicity, amifosine treatment resulted in radioprotection in numerous normal tissues when combined to radiotherapy together with maintaining equal tumour control [264]. However, its application is limited due to the common occurrence of severe side effects including hypotension, fatigue, and somnolence in up to 20% of patients [265]. The drug received FDA approval only for its application in preventing xerostoma in head and neck cancers.

The keratinocyte growth factor (KGF) resides in the family of fibroblast growth factor (FGF). The drug palifermin is a human truncated and recombinant form of KGF. Palifermin can activate the KFG receptors on epithelial cells stimulating survival, division, and differentiation of the cells. The KFG receptor activation results in Th2 cytokinesis, reorganization of the tissue,

decrease in induced DNA damage and inhibition of cell apoptosis [266]. Although tumour cells contain KFG receptors and treatment could enhance tumour growth or secondary malignancies, long term observations of patients receiving Palifermin did not result in increase of secondary malignancies [267]. The drug is furthermore well tolerated with limited adverse effects. However, the drug received FDA approval only for its application in reducing radio- or chemotherapy induced mucositis in patients undergoing bone marrow transplantation [268], [269]. However, chemically derived radioprotectors, including amifostine, are accompanied with severe side effects and complexity in its delivery route.

10.2. Radioprotectors and the DNA damage repair

An interesting finding identified in various preclinical and clinical radioprotectors, is the capacity to enhance the DNA repair machinery, reducing radiation-induced damage and radiation-induced toxicity. Among these radioprotectors are ferulic acid, Genistein, tyrosine kinase inhibitors, sesamol, troxerutin, quercetin, parathyroid hormone, and the previously described Palifermin [270]–[277]. The combination of radiotherapy with ferulic acid [270], sesamol [272], [278], troxerutin [273], [279] or quercetin [274], [280], displayed a decrease in damaged DNA fragments and y-H2AX foci, compared to standalone radiotherapy. In addition, various radioprotectors displayed an upregulation of repair proteins such as ATM [281], 53BP1 [281], ATR signalling [275], Ku70 [276], or DNA-PK [277] in response to combined treatment with radiotherapy, displaying a direct enhancement of the DNA repair mechanisms. Corresponding, no research has identified DNA repair inhibitors to function in radioprotection. However, DNA repair inhibitors function as suitable radiosensitizers. The next chapter will explore the different methods of radio sensitization and radiosensitizers, including the unique radiosensitizer AsiDNA™.

11. Enhance tumour radiosensitivity with radiosensitizers

To enhance curing chances, research has been focusing on the development of compounds that, once combined with radiotherapy, can increase tumour control.

11.1. The use of nanoparticles

One approach to sensitize tumours is by using nanoparticles. The particles can have central elements containing noble metals, heavy metals, or non-metallic as functioning units. Examples that have been implemented in nanoparticles include gold, AGulX, Hafnium or Nano-C60 [282]–[285]. The high Z number of the particles absorb energy from the x ray and can locally emit various electron types, creating a local irradiation. Its specificity for tumours is solidary based on the lack of a complete vasculature system. Nanoparticles get stuck and accumulate therefore in tumour areas [286]. The local tumour irradiation deposits its energy to the nanoparticles, causing the main dose and radio sensitizing properties of these noble or metal nanoparticles to be allocated to the tumour [287], [288]. Additionally, research is ongoing examining the use of nanomaterials to transport radioactive or chemotherapeutic content. Materials including silica have been indicated to function as successful vessels for the transport and accumulation of chemotherapeutic tirapazimine in tumours [289]. Although promising, the adverse effects of nanoparticles need to be determined and will vary depending on their structure and implemented functioning unit.

11.2. Targeting of hypoxia

A more familiar approach of enhancing tumours radiosensitivity is by affecting the hypoxic tumour core. Many tumours experience chronic and acute lesions of hypoxia. Due to the absence of oxygen, hydrolysis following radiation creates less ROS, resulting in less damage, depending on the radiation modality. This results in an increase up to 3-fold in tumour survival following radiotherapy known as the Oxygen Enhancement Ratio (OER). Removal of the hypoxic margins from tumours will decrease tumour cell survival. Interesting research replaced air with 100% oxygen known as hyperbaric oxygen, resulting in a saturation of oxygen availability, and reducing the hypoxic core [290]. However, the treatment can be accompanied by complications and is impractical as optimum conditions require the implementation of hyperbaric oxygen during irradiation. Another promising approach is the use of oxygen

mimetics. These compounds are presented with equal properties of oxygen in the radiation hydrolysis and chemical fixation of DNA damage, but have better diffusion rates and often contain nitrogen or nitric oxide (NO) components [291]–[293]. First generation oxygen mimetic drugs have been accompanied with moderate toxicity; however, progress was achieved in the second-generation oxygen mimetic drugs. The second generation nimorazole has been confirmed successfully in clinical trials and is currently included in the standard of care and administered prior to each radiotherapy session of head and neck squamous cell carcinoma in Denmark [294]–[296]. Additional promising research was obtained by Coates et al. (2020), revealing the unique properties of malaria drug atovaquone in eliminating hypoxia cores [297]. Atovaquone enables the overall decrease of oxygen consumption by targeting of the tumour mitochondrial metabolism within oxygen rich layers. This results in increased oxygen availability, further diffusion of oxygen into the tumours, and reducing the hypoxic core. Patients bearing NSCLC tumours received treatment with atovaquone which resulted in the increase in tumour oxygenation and decrease of hypoxic tumour areas [298]. Interestingly, upon combined treatment of carboplatin or cisplatin with atovaquone, a significant decrease in cell and spheroid survival was observed in vitro [297]. The efficacy and adverse effects of combined treatment of atovaquone and radiotherapy in patients with NSCLC is currently being explored in an ongoing phase I clinical trial (OCTO_088).

11.3. Targeted radio sensitization by pathway inhibition

The use of inhibitors targeting pathways of proliferation, division, migration, and DNA repair has been widely explored to enhance tumour radiosensitivity. The inhibition of the Wnt pathway, important in cell migration and proliferation, has revealed in several studies to increase antitumour efficacy by improved the immune response in tumour microenvironment together with increasing radiation induced complex lesions on the DNA [299], [300]. Similarly, inhibition of the Mitogen-activated protein kinases (MAPK) or P13K-Akt-mTOR pathway, important in cell proliferation and differentiation, resulted in increased antitumour efficacy resulting in increased apoptosis and inhibition of DSB repair following radiotherapy [301], [302]. The increased genomic instability in tumour cells or its dependency on specific repair mechanisms can be used as a target for reducing tumour resistance. A possible target is repair protein ATM, important for the detection of the initial DSB and introducing the signalling to activate DNA repair. The research of Durant et al. (2018) revealed that inhibition of ATM by

AZD1390 resulted in hypersensitivity of tumours following radiotherapy in vitro and in vivo [303]. The ATM inhibition resulted in a decrease of ATM activity, changes in DNA damage repair (DDR) that ultimately resulted in increased radiosensitivity. The presence of a mutation in p53, causing improper cell cycle arrest after treatment, resulted in synergy in decreased cell survival following AZD1390 treatment. Similar promising results are obtained by Fok et al. (2019) where DNA-PK inhibition resulted in increased antitumour efficacy [304]. DNA-PK inhibitor AZD7648 significantly decreased cell survival fractions in vitro, and increased in tumour control in vivo, following combined AZD7648 and radiotherapy treatment compared to irradiation standalone [304]. DNA-PK is an important participant in DNA repair through non-homologous end joining (NHEJ), binding to the DSB ends using Ku70/Ku80, recruiting and activating additional repair proteins. Its inhibition results in a severe decrease in NHEJ activity resulting in inefficient DNA repair following radiotherapy and ultimately, cell death. Conversely, the developed inhibitors are not tumour specific, and the proteins remain of utmost importance to normal cells which can result in adverse effects. In addition, the inhibition of a single protein has resulted in vast resistance mechanism development in the past. Parallel pathway targeting as revealed by the radiosensitizer AsiDNA™, might resolve this issue.

11.4. AsiDNA™, a unique radiosensitizer mimicking a double stranded break

The effectiveness of a single protein inhibition in cancer treatment is often short-lived as cancer cells can develop resistance through the development of mutations within the protein target that disrupt protein-drug interaction [305], the gained ability to transport drugs out of cells [306], and utilization of additional repair or signalling routes that remain functional and are not inhibited using the drug treatment [307]. In addition, the activity of inhibitors is unspecific to cell types and can therefore cause major complications in healthy cells. The development of new agents, interacting and interfering with cellular mechanisms that have not been exploited before, could be a suitable direction for future treatment modalities. Targeted DNA repair proteins has gained particular interest as cancer cells are more susceptible to DNA damage than normal cells, and they rely on specific functional repair pathways to survive [308]. The laboratory of Marie Dutreix has successfully developed a new

class of DNA repair inhibitors, Dbait, able to simultaneously interfere with numerous DNA repair pathways.

11.4.1. Dbait mimics a double stranded break

The Dbait molecule was primarily designed to mimic a DSB. DSBs are considered as the most toxic lesion on the DNA and will result in cell death if repair is unsuccessful. By designing a novel agent mimicking a DSB, both DSB repair pathways, NHEJ and HR, can be affected, rendering the cells more sensitive to physical and chemical agents producing DSBs. In detail, Dbait consists of two complementary DNA sequences of 32 nucleotides that are connected through a 1,19-bis (phosphor)-8-hydraza-2-hydroxy-4-oxa-9-oxo-nonadecane linker [309], [310]. The blunt end was protected from exonuclease attack by substituting the three 3′ and 5′ terminal nucleotide residues with phosphorothioate nucleotides. The base-pair sequence revealed to have no beneficial impact on the drug's activity and currently consists of 5′-GsCsTs GTG CCC ACA ACC CAG CAA ACA AGC CTA GA -H- TCT AGG CTT GTT TGC TGG GTT GTG GGC AC sAsGsC -3′ where H is the hexaethylene glycol linker, and s the phosphorothioate linkages [311]. Dbait binds and activates DNA-PK and poly(ADP-ribose) polymerase (PARP) [309], [311], [312] which leads to γH2AX and heat shock protein 90 (HSP90-p) [311], [313], [314] and to parylation [309] in cells. In fact, Dbait revealed to activate a pan-nuclear yH2AX signal resulting from an overactivation of DNA-PK and confirmed to disorganize the repair mechanisms by additional ATM phosphorylation and KU protein activation. Phosphorylation of Chk2, Chk1, Rpa32, Nbs1 and p53 appeared to also occur upon Dbait treatment [311], [313]. Continued research revealed that Dbait treatment increases foci formation of X-ray repair cross-complementing protein (XRCC) 1 and PCNA after standalone treatment, but prevented Rad51, XRCC1 and PCNA foci formation at laser-induced damage sites following Dbait treatment [309].

11.4.2. From Dbait to AsiDNA™, the molecular design and function

One of the major limitations of the use of Dbait in pre-clinical studies arose from the fact that Dbait cannot diffuse into the cells without the help of a transfection agent. Therefore, for transition to clinical applications, an additional linker containing a cholesteryl tetraethyleneglycol group was added at the 5′-end to Dbait, creating AsiDNA™ (Figure 15) [310], [312], [315]. The uptake of AsiDNA™ has been linked to low-density lipoprotein receptor

(LDL-R) activation and is completely independent of transfection agents. Evaluation of cell membrane LDL-R concentration revealed a correlation between LDL-R concentration and intracellular AsiDNA™ levels without any correlation to cellular resistance to AsiDNA™ [316].

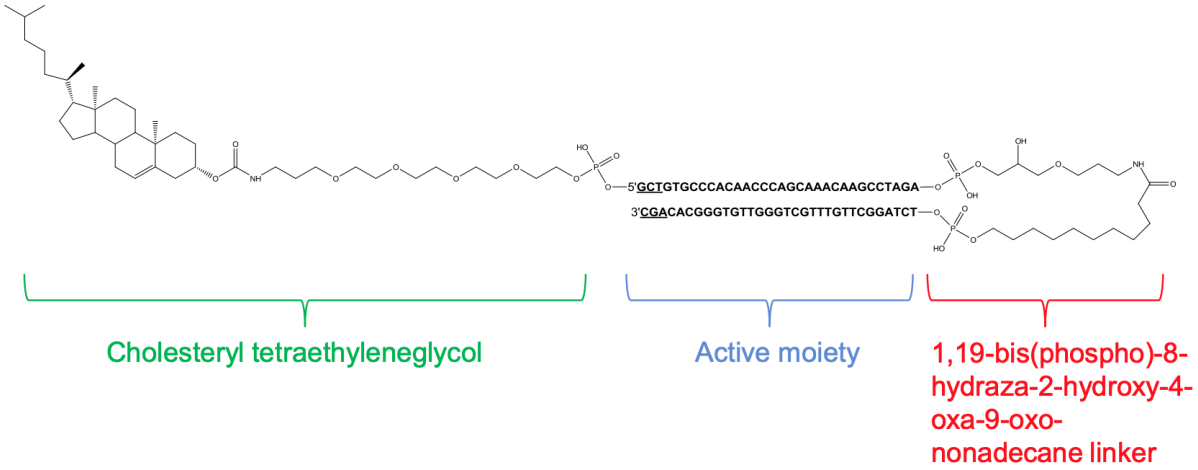

Figure 15: Chemical structure of AsiDNA™.

The molecule consists of two complementary DNA sequences of 32 nucleotides that are connected through a 1,19-bis (phosphor)-8-hydraza-2-hydroxy-4-oxa-9-oxo-nonadecane linker containing a cholesterol at the 5'-end together with three phosphorothioate nucleotides at both 3' and 5' terminal [317].

11.4.3. The AsiDNA™ molecule, DSB decoy with unique properties

Identical to Dbait, AsiDNA™ activity results in the inappropriate activation of ATM, PARP and DNA-PK. The phosphorylation of ATM appears within an hour upon AsiDNA™ treatment and resolves within 10 hours while DNA-PK induced γH2AX displays maximum signal at 24h of AsiDNA™ treatment. Strikingly, PARylation displays a maximum level at 48h of AsiDNA™ treatment and remains consistently high for days [318]. The hyperactivation of these proteins results in pan-nuclear γH2AX and HSP90-p, and finally generate a false DNA damage signal [318], [319]. Consequently, the activated and modified repair proteins are unable to produce foci at the initial site of damage on the genomic DNA and the induction of pan-nuclear γH2AX further encourages the disorganization of the repair signals. The interference of the various repair proteins results in both the impairment of homologous recombination [319] as well as non-homologous end joining [318]. As PARP is a key protein in base excision repair and single-stranded break repair, the autoPARylation by PARP1 upon AsiDNA™ activity impairs likewise these repair mechanisms [318]. Overall, numerous repair factors have been examined that revealed a dysregulation or complete absents of IR- or laser-induced foci formation in the

presence of AsiDNA™ including NHEJ and homologous recombination (HR) proteins ATM, NBS1, RAD51, DNA-PK, BRCA1, XRCC4, RPA and 53BP1, and repair proteins functioning in single-stand break repair (SSBR) including PARP [315], [319]. Tumour cells will expectantly undergo mitotic catastrophe after damage accumulation.

11.4.4. Biomarkers of AsiDNA™ activity and sensitivity

The pan-nuclear γH2AX staining induced by DNA-PK upon AsiDNA™ treatment has been clearly observed in all cell lines including healthy and tumour cell lines, with the only exception of DNA-PK deficient cells. The AsiDNA™-induced DNA-PK activity furthermore results in a pan-nuclear HSP90-p staining and forms, together with the phosphorylation of histone 2AX at serine 139 and PARylation, simple biomarkers of AsiDNA™ activity in cells (Figure 16) [318], [319]. The γH2AX is primarily mediated by ATM in response to DSBs, and ATR-dependent in responsγγe to ssDNA generated by replication stress or UV radiation [220], [320], [321]. In addition, IR-induced H2AX phosphorylation can be conducted by ATM and DNA-PK in a redundant, overlapping manner [322]–[324]. DNA-PK is solely responsible for H2AX phosphorylation during apoptosis while ATM is dispensable for the process [325]. Furthermore, H2AX phosphorylation is only dependent on DNA-PK activity in response to AsiDNA™ treatment (Figure 16C) [318]. γH2AX forms discrete nuclear foci in response to IR, which is indicative of DSBs [326]. However, in response to replicative stress [327], UV radiation [328], clustered DNA lesions [322], AsiDNA™ [318], and in cells undergoing apoptosis [329], γH2AX has a pan-nuclear staining. The activity of these biomarkers represented by pan-nuclear staining's have been shown after AsiDNA™ treatment compared to various DNA repair inhibitors and chemotherapeutics [319]. The capacity of AsiDNA™ to cause cell toxicity standalone can be evaluated by micronuclei formation and large genome rearrangements, depending on the endogenous level of genomic instability of the tumour cells. Increased micronuclei formation upon AsiDNA™ treatment signifies increased toxicity and can therefore function as biomarker for AsiDNA™ sensitivity [317].

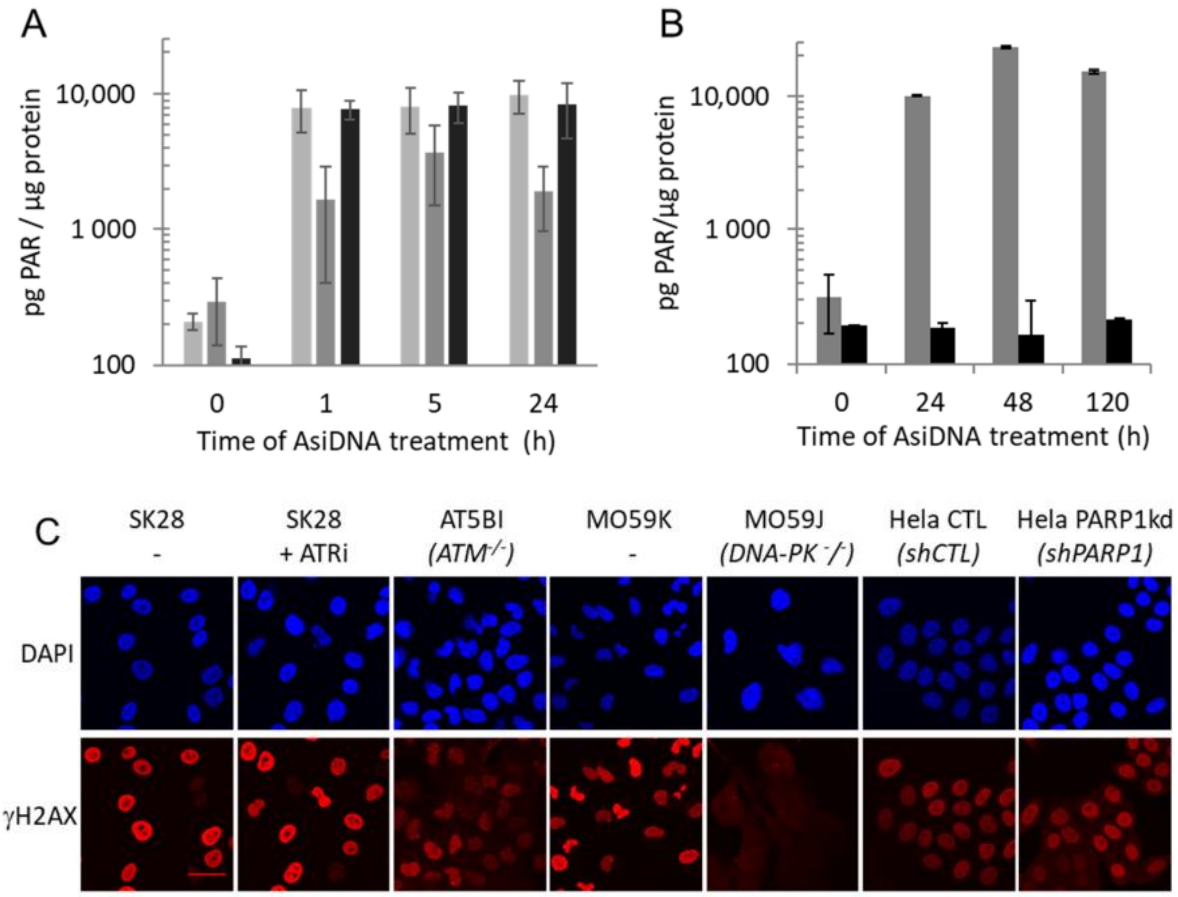

Figure 16: Biomarkers of AsiDNA™ activity.

(A) PARP activation following AsiDNA™ treatment on SK28 tumour cells detected in the nucleus (dark gray), cytoplasm (black) and total PARylation (light gray). (B) Kinetics of PARP activation following AsiDNA™ treatment with (black) or without (grey) 1h pre-treatment of Olaparib on SK28 tumour cells. (C) Immunofluorescence staining of γH2AX following 24h of AsiDNA™ treatment in tumour cell lines SK28, AT5BI, MO59K, MO59J, Hela with or without inhibition of ATR, ATM, DNA-PK or PARP1. Represented scale bar of 30 µm [318].

11.4.5. Lack of tumour resistance

Recent studies have examined the impact of repeatable AsiDNA™ treatment in a broad variety of cell lines and demonstrated a complete absence of any resistance development against AsiDNA™ treatment. Likewise, the cyclic treatment identified sensitive cell lines that were unable to recover and resistant cell lines that represented an increase in sensitization up to a minimum survival threshold. This increase in sensitivity was correlated with the downregulation of genes coded for proteins in the DNA-PK pathway. Interestingly, treatment of KMB7 tumour cells with PARP inhibitors Imatinib, Olaparib or chemokinetic 6-thioguanine, all displayed a rise

of tumour resistant clones whereas AsiDNA™ treatment displayed a complete absence of AsiDNA™ resistance clones [330]. AsiDNA™'s unique ability to impact numerous repair pathways in parallel results in the complete lack of any possible flexibility of tumour cells to develop any resistance mechanism.

11.4.6. Pharmacokinetics of AsiDNA™

Pharmacokinetics of AsiDNA™ revealed a severe reduction of AsiDNA™ in mouse plasma within 2 hours following AsiDNA™ administration with both intraperitoneal and intravenous injection. Moreover, an accumulation of AsiDNA™ was observed in liver, intestines, and kidneys with a vast increase in γH2AX, explicitly in liver tumours. AsiDNA™ significantly chemo sensitized liver metastasis in the colorectal cancer model, represented by a shrinkage in tumour volume and increase in necrosis [331], [332]. Likewise, preclinical toxicology studies of AsiDNA™ performed in wistar rats and cynomolgus monkeys' solitary revealed a maximum plasma concentration between 2 and 4 hours after administration together with a reversible inflammatory response at the site of injection and no observed adverse effects, providing evidence of the safety of AsiDNA™ [332], [333]. Within the conducted first phase I dose escalation study (DRIIM), patients received intratumoral and peritumoral injections ranging between 16 and 96 mg AsiDNA™, three times a week over 2 weeks, 3-5h prior to radiotherapy of 30 Gy delivered in 10 fractions over 2 weeks. The half-life of AsiDNA™ detected within the serum of patients ranged from 2.4 to 4.9 hours and no dose-limiting toxicity was observed [334]. During the second phase I dose escalation study (DRIIV-1), patients received intravenous injections to reach deep seeded tumours with concentrations ranging between 200 and 1800 mg AsiDNA™ [335]. The drug was administered daily for 3 days within the first week, followed by weekly treatment thereafter, with treatment cycles of 21 days per cycle. Treatment cycles were continued up to disease progression or unacceptable toxicity. The half-life of AsiDNA™ detected within the serum of patients ranged from 3 to 5 hours with increased dose proportional and consistent to the AsiDNA™ dose delivered. Dose-limiting toxicity was observed in only 2 patients receiving AsiDNA™ doses above 900mg.

11.4.7. The additive or synergistic effect of combined treatment with AsiDNA™ and additional therapies

Deliberately induced DNA damage by chemo- or radiotherapy can result in tumour cell death. AsiDNA™ does not induce damage standalone and is therefore dependent on endogenous damage arising from genomic instability or damage induced by an additional therapy [317], [319].

11.4.7.1. Combined AsiDNA™ chemotherapy treatment

The study of Jdey et al. (2017) [319] revealed that the combination of AsiDNA™ treatment with PARP inhibitor, Olaparib, influences the DNA repair by independent pathways, resulting in a supra-additive effect. Indeed, the inhibition of PARP by Olaparib inhibits base excision repair, represented by a decrease of XRCC1 recruitment upon treatment, whereas AsiDNA™ interferes with homologous recombination repair, characterised by a decrease in Rad51 and 53BP1 recruitment. The combination of AsiDNA™ and Olaparib therefore caused a proliferated accumulation of damage [319]. Similar results can be obtained by exploiting synthetic lethality dependencies, including the well-known BRCA deficiency [319].

Likewise, the publication of Herath *et al.* (2017) combined trans arterial chemoembolization (TACE) using doxorubicin with AsiDNA™ treatment, in a liver tumour model [336]. AsiDNA™ enhanced the efficacy of TACE in the treatment of human hepatocellular carcinoma (HCC) observed by a compelling increase in necrosis and decrease in proliferation and tumour growth reduction. Moreover, the results displayed an inhibition of neo-angiogenesis by specific Vascular endothelial growth factor receptor 2 (VEGFR2) suppression, reduced tumour volume together with histological changes, in the primary hepatocellular carcinoma model [336].

11.4.7.2. Combined AsiDNA™ radiotherapy treatment

The capacity of Dbait molecules to radio sensitize tumour cells in mouse models was initially established by Quanz et al. (2009) where the survival fraction of tumour cells decreased upon combined Dbait and radiotherapy treatment [311]. Implementing in vitro and in vivo combined therapy on melanoma models revealed similar capacities of Dbait (in vitro) / AsiDNA™ (in vivo) to radio sensitize tumours. The research displayed an additive effect on survival reduction of SK28 and 501mel tumour cells upon the combined radiotherapy AsiDNA™ treatment. The

introduction of AsiDNA™, priorly known as DT01, appeared in vivo where every other day AsiDNA™ administration was combined with fractionated radiotherapy consisting of 10 times 3 Gy daily fractions. The combined therapy revealed a significant decrease in tumour growth together with increased survival (Figure 17) [332].

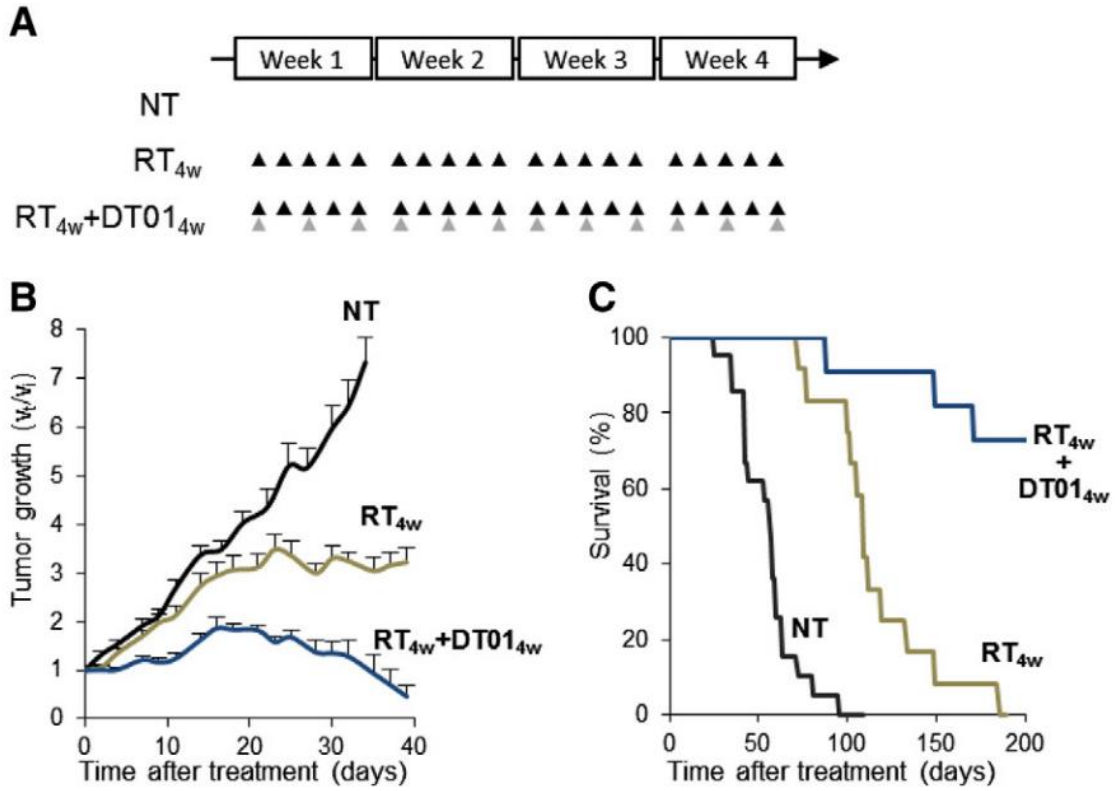

Figure 17: AsiDNA™ (DT01) radiosensitizes SK28 tumours in vivo.

Mice bearing SK28 tumours received no treatment (NT), 10 fractions of 3 Gy divided over 4 weeks (RT_{4w}), or AsiDNA™ combined with fractionated radiotherapy (RT_{4w} + $DT01_{4w}$). (A) Treatment schedule of 4 weeks with black triangles representing a 3 Gy radiation fraction and gray triangles representing an AsiDNA™ treatment. (B) Tumour growth curve in days after treatment completion. (C) Percentage of surviving mice in in days after treatment completion. Endpoint of 1500mm^3 tumour size [332].

A major obstacle in drug delivery is the ability of the supplemented agents to reach and infiltrate in tumours. With respect to brain tumours, an additional line of defence, the blood brain barrier (BBB), results in the inaccessibility of many drugs to reach the region of interest. Promising results obtained by Coquery *et al.* (2012) revealed the ability of AsiDNA™ to cross the BBB, infiltrate within glioma tumours. AsiDNA™ was administered, combined with radiotherapy, resulting in an increase in tumour response, increase inflammation, and destabilization of the microenvironment without changes in angiogenesis in rats with RG2-

glioma [315]. Identical results were obtained recently by the research of Ferreira et al. (2020) revealing AsiDNA™ infiltration within medulloblastoma tumours and radio sensitization of the tumours upon single and fractionated radiotherapy [337]. Strikingly, AsiDNA™ treatment did not introduce an added toxicity and upon combined AsiDNA™ treatment with brain irradiation, there was an increase in survival compared to standalone radiotherapy. The absence of added toxicity to normal tissues has been reported priorly with combined Dbait and oxaliplatin, 5-fluorouracil [338] or radiotherapy [332] treatment along with combined AsiDNA™ and radiotherapy [315], doxorubicin [336], [339] or carboplatin [340]. However, a reduction of normal tissue toxicity has not been formerly reported in those studies.

11.4.8. AsiDNA™ in clinical applications

The first phase 1 trial (DRIIM) was performed on patients with skin metastasis from melanoma. Patients were treated with radiotherapy in combination with intra- and peri-tumoral AsiDNA™ injections, 3 times a week. The results reported no dose-limiting toxicities, and the maximum-tolerated dose was not reached. Antitumour activity was similarly observed in non-injected tumours and is expected to be caused by a systemic distribution of AsiDNA™ after local injection or an activation of the immune response, indicating a form of abscopal effect [334]. The second phase 1 trial dose escalation study (DRIIV-1) was performed on patients with a variety of solid tumour. Patients were treated for three consecutive days with IV administration of AsiDNA™ and continued treatment once a week in the following weeks. Tumour biopsies revealed increased AsiDNA™ activity in the tumour as revealed by the biomarkers γH2AX and HSP90 phosphorylation (Figure 18).

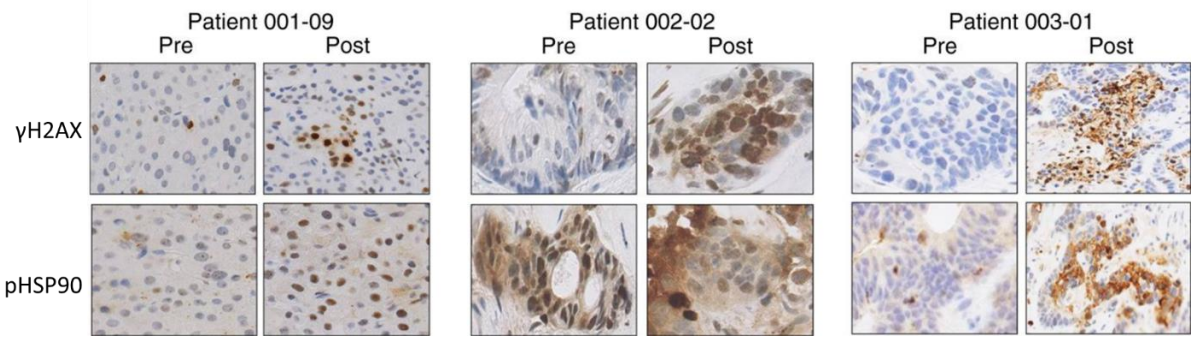

Figure 18: AsiDNA™ biomarker detection in patients' biopsies.

Tumour biopsies from patients pre- and post- treatment with AsiDNA™ with immunohistochemistry detection of AsiDNA™ biomarkers γH2AX and pHSP90 [335].

Remarkably, the optimum tolerated dose was concluded at 600mg while no AsiDNA™-induced toxicity limiting the dose was observed, and the maximum tolerated dose was not reached [335]. In recent case studies the lack of toxicity was not only reconfirmed, but AsiDNA™ treatment enabled a vast increase in the total of endured cycles of carboplatin -/+ paclitaxel, by delay of the chemotherapy-induced treatment toxicities, in the majority of patients [341].

Collectively, the phase 1 clinical trials together with the case studies and the pre-clinical research of Ferreira et al. (2020) revealed an entirely unexplored abundant impact of AsiDNA™ on normal tissue toxicity, paving the way to examine the molecular and cellular impact of AsiDNA™ treatment on normal cells.

II. THESIS PROJECT

The DNA repair inhibitor AsiDNA™ has been designed and developed within Institut Curie to widen the therapeutic window of both radiotherapy treatments and chemotherapeutic treatments. The AsiDNA™ molecule was identified in various studies to radio- and chemo-sensitize tumours, in vitro and in vivo, following combined treatment [319], [332], [336]. In addition, AsiDNA™ revealed no increase in toxicity to normal cells or tissue in vitro, in vivo, in phase I clinical trials and in case reports [334], [335], [341]. Remarkably, case reports revealed a strong delay in the onset of chemotherapeutic toxicities while maintaining tumour control once patients received AsiDNA™ treatment in combination with the allocated chemotherapeutics [341]. Collectively, these observations sparked the interest to examine the impact of AsiDNA™ treatment on normal cells by identifying, in greater detail, the mechanism driving the lack of AsiDNA™ toxicity in normal cells.

The aim of the work presented in this thesis will reveal a novel mechanism of AsiDNA™ explicitly in normal cells and normal tissue. In addition, the research revealed a possible utilization of this novel AsiDNA™-induced mechanisms to protect normal tissue against radiation induced toxicity, expanding the therapeutic window. In the following chapters, the novel research we have conducted on exploring the behaviour of AsiDNA™ in normal cells, the mechanisms involved in normal cells and its capacity to protect against normal tissue toxicity will be further discussed.

III. RESULTS

12. Article I:

The following research is of both fundamental and translational nature. In this study we examined and identified the impact of AsiDNA™ treatment on normal epithelial cells and fibroblasts and its impact on reducing radiation toxicities to the normal tissue of the lung and intestine. We have identified the capabilities of AsiDNA™ treatment to explicitly activate cellular pathways in normal cells, translatable to preclinical models of radiation-induced toxicity in which AsiDNA™ treatment impacts the severity of the induced toxicity. The preclinical experiments conducted within this study (early radiation-induced intestine toxicity and late radiation-induced lung fibrosis) can be translated to other models of radio- or chemo-induced toxicities and furthermore can be utilized to examine the mechanisms driving radiation responses in the normal tissue. Here we present the work in the form of an article that was submitted to NAR cancer (Manuscript ID NARC-2023-079) and received revisions of which responses to the revisions are currently ongoing.

MANUSCRIPT TITLE

The AsiDNA™ decoy mimicking DSBs protects the normal tissue from radiation toxicity through a DNA-PK/p53/p21-dependent G1/S arrest.

AUTHORS

Anouk Sesink[1,2], Margaux Becerra[1,2], Jia-Ling Ruan[3], Sophie Leboucher[1,4], Maxime Dubail[1,2], Sophie Heinrich[1,2], Wael Jdey[5], Kristoffer Petersson[3,6], Charles Fouillade[1,2], Marie Dutreix[1,2], and Pierre-Marie Girard[1,2,*]

[1] Institut Curie, PSL Research University, CNRS, INSERM, UMR 3347, F-91405, Orsay, France

[2] Université Paris Sud, Université Paris-Saclay, CNRS, UMR 3347, F-91405 Orsay, France

[3] Oxford Institute for Radiation Oncology, Department of Oncology, University of Oxford, Old Road Campus Research Building, Roosevelt Drive, Oxford, United Kingdom

[4] Université Paris Sud, Université Paris-Saclay, CNRS, UMR 3348, F-91405 Orsay, France

[5] Valerio Therapeutics, Bd du Général Martial Valin, F-75015 Paris, France

[6] Radiation Physics, Department of Hematology, Oncology and Radiation Physics, Skåne University Hospital, and Lund University, Lund, Sweden.

[*] To whom correspondence should be addressed: Tel: +33 (0)1 69 86 31 31; email: pierre-marie.girard@curie.fr

ABSTRACT

AsiDNA™, a cholesterol-coupled oligonucleotide mimicking double-stranded DNA breaks, was developed to sensitize tumour cells to radio- and chemotherapy. This drug acts as a decoy hijacking the DNA damage response. Previous studies have demonstrated that standalone AsiDNA™ administration is well tolerated with no additional adverse effects when combined with chemo- and/or radiotherapy. This lack of normal tissue complication encouraged further examination into the role of AsiDNA™ in normal cells. This research demonstrates the radioprotective properties of AsiDNA™. In vitro, AsiDNA™ induces a DNA-PK/p53/p21-dependent G1/S arrest in normal epithelial cells and fibroblasts that is absent in tumour cells. This cell cycle arrest improved survival after irradiation or pharmacological drug treatment, only in p53 proficient epithelial cells. Combined administration of AsiDNA™ with conventional radiotherapy in mouse models of late and early radiation toxicity resulted in decreased onset of lung fibrosis and increased crypt survival in the intestine. Similar results were observed following FLASH radiotherapy in standalone or combined with AsiDNA™. Furthermore, mechanisms comparable to those identified in vitro were detected both in vivo, in the intestine and ex vivo, in precision cut lung slices. Collectively, the results suggest that AsiDNA™, can partially protect healthy tissues from radiation toxicity by triggering a G1/S arrest in normal epithelial cells and fibroblasts.

INTRODUCTION

Radiotherapy and chemotherapy are customarily implemented in cancer treatments with curative intent; however, these therapies are often accompanied by the development of moderate to high levels of treatment-related toxicity. Radiotherapy frequently results in loss of epithelial integrity, tissue senescence, and cell death. Fibrosis formation, vascular damage with the potential development of secondary malignancies, and cardiac arrhythmia can all develop in the long term (1,2). Toxicities correlated to chemotherapy depend on the type of chemotherapeutic administered. These injuries range from anorexia, vomiting, and gastrointestinal toxicities to neurotoxicity (3). Consequently, treatment-induced toxicities often interfere with the completion of the initial treatment plan. To enhance treatment effect, it is crucial to alleviate treatment-related toxicities to both improve post-treatment outcomes

and advance patients' welfare. This can be achieved by expanding the therapeutic index using sensitizers or protective treatment modalities to shift the normal tissue complication probability or the tumour control probability (4). The DNA repair inhibitor AsiDNA™ has previously been validated as a suitable treatment agent to enhance this index. The active part of the molecule consists of two complementary oligonucleotides of 32 bases stabilized at one blunt end by a hexaethyleneglycol linker (5). The functionalization of a cholesterol group at the other blunt-end of the molecule allows its cellular uptake via LDL receptors expressed at the cell membrane both in vitro and in vivo. (6,7). AsiDNA was designed to mimic double-stranded breaks, triggering deceptive signalling of DNA damage and impairing DNA repair of chromosomes damaged by radiation or chemical treatments (8,9). Indeed, AsiDNA™ binds both DNA-dependent protein kinase (DNA-PK) and PARP enzymes, activating their kinase and polymerase activity, respectively, and consequently leading to modification of numerous proteins in the cell [see (10) and references therein]. The characteristic substrates phosphorylated by AsiDNA™-dependent DNA-PK activation are, histone H2AX and heat shock protein 90 (HSP90) (6,9,11,12).

Several preclinical studies have demonstrated an additive or synergistic tumour control effect of AsiDNA™ combined with radiotherapy or chemotherapy, without any added toxicity. (10,13-17). These observations are further supported by in vitro data, revealing no additional toxicity after continuous or cycling treatment of AsiDNA™ on normal cell models, while simultaneously increasing tumour cell sensitivity with no acquired resistance (7,8,18). In addition, human clinical trials have failed to show any dose-limiting toxicity, with none reaching the maximum-tolerated dose (19,20). Recently, AsiDNA™ treatment in combination with carboplatin +/- paclitaxel was tested in patients bearing solid tumours (21). These case reports showed no increased toxicity of combined carboplatin and AsiDNA™ treatment. Moreover, combined treatment allowed the dose delivery times of carboplatin to be exceeded before the occurrence of toxicities (21). Taken together, these pre-clinical and clinical studies suggest that AsiDNA™ can increase the therapeutic window by radio- or chemo-sensitizing tumour cells upon treatment, while minimizing normal tissue injuries. However, the mechanism of normal tissue resistance remains still poorly understood.

To address this knowledge gap, in the present study, we aimed to characterize the molecular mechanism underlying the potential normal tissue protection capacities of AsiDNA™ and to demonstrate its radioprotective potential in vivo. To evaluate if the radioprotection property of AsiDNA™ is retained or enhanced with different modes of radiation, we combined AsiDNA™ with conventional radiotherapy (CONV-RT) or FLASH radiotherapy (FLASH-RT). FLASH-RT is based on dose rates delivery over 1000 times higher (≥ 40 Gy/s) compared to CONV-RT (22). Numerous studies have demonstrated that FLASH-RT diminishes the severity of radiation-induced toxicities in normal tissues that remains present in CONV-RT, while maintaining an equivalent anti-tumour response (23-29).

Herein, we report that AsiDNA™ induces a DNA-PK/p53/p21-dependent G1/S arrest specifically in normal epithelial cells and fibroblasts, referred to as normal cells, resulting in improved survival following ionizing radiation and treatment with pharmacologic drugs. This research provides evidence that this mechanism could account in mouse models for reduced early toxicity in the small intestine and reduced late toxicity in lung, demonstrating the potential benefit of the association of AsiDNA™ to standard radiotherapy in cancer treatment.

MATERIAL AND METHODS

Cell culture and transfection

Immortalized retinal pigment epithelial cell line hTERT (RPE-hTERT, kindly provided by A. Londono, Institut Curie, France), RPE-hTERT with shp53 (kindly provided by D. Fachinetti, Institut Curie, France), primary human skin fibroblasts (NHSF: BJ, ATCC CRL-2522), primary human lung fibroblasts (MRC-5, kindly provided by P. Jeggo, GDSC, Brighton, U.K.), and SV40-transformed MRC-5 fibroblasts (MRC-5v1, kindly provided by P. Jeggo, GDSC, Brighton, U.K.) were cultured in DMEM/F12 glutamax™ supplement medium (Thermo Fisher Scientific, France) supplemented with 10% fetal calf serum (FCS, Eurobio, France) and 100U/ml penicillin 100 µg/ml streptomycin (P/S, Thermo Fisher Scientific, France). A549 lung carcinoma cells (ATCC CCL-185), HCT116 colon carcinoma cells (ATCC CCL-247) and U-2 OS

osteosarcoma cells (ATCC HTB-96) were cultured in DMEM/F12 glutamax™ supplement medium supplemented with 10% FCS, P/S and 1x Non-Essential Amino Acids (MEM NEAA 100X, Thermo Fisher Scientific, France). All cell lines were maintained in a humidified atmosphere at 37°C with 5% CO_2. The absence of Mycoplasma contamination was determined in-house by using LookOut Mycoplasma PCR (Sigma-Aldrich). Transfection of cell lines are described in the Supplementary Materials and Methods.

Molecules

AsiDNA™ (MW = 20931.4 g/mol) is a 64-nucleotide (nt) oligodeoxyribonucleotide consisting of two 32 nt strands of complementary sequence connected through a 1.19bis (phospho)-8-hydraza-2-hydroxy-4-oxa-9-oxo-nonadecane linker with cholesterol at the 5′-end and three phosphorothioate internucleotide linkages at each of the 5′ and the 3′ ends. The sequence is: 5′-X GsCsTs GTG CCC ACA ACC CAG CAA ACA AGC CTA GA L-CL TC TAG GCT TGT TTG CTG GGT TGT GGG CAC sAsGsC-3′, where L is an amino linker, X a cholesteryl tetraethylene glycol, CL a carboxylic (hydroxyundecanoic) acid linker, and s is a phosphorothioate linkage. AsiDNA™ was synthesized and purified by LGC (U.K) and kindly provided by Wael Jdey (Valerio Therapeutics). The stock concentration of AsiDNA™ dissolved in water was at 40 mg/mL. Nol8 (MW = 6005.8 g/mol) has the same chemical structure as AsiDNA™ with the exception that it consists of two 8 nt strands of complementary sequence and was synthesized and purified by Eurogentec (Belgium). The stock concentration of Nol8 dissolved in water was at 61 mg/mL.

In vitro treatments

Cell culture medium was supplemented with AsiDNA™ at concentrations of 5, 10, 20 or 40 µmol/L 24 or 48 h prior to drug or IR treatment. In vitro irradiation was conducted using the GSR D1 (GSM) ^{137}Cs unit with the dose rate of 0.8-1.1 Gy/min, or the ElectronFLASH (S.I.T., Vicenza, Italy) at a dose rate of 0.4 Gy/sec.

Cell cycle analysis

Complete medium with total 10 µmol/L BrdU (Merck, France) was added to cells for a 40 min incubation either pre- or post-AsiDNA™ treatment, under standard culture conditions. For

drug treatment, cells were exposed to 1 µM Olaparib (AZD-2281, Roowin chemicals), 10 µM NU7026 (Merck, France), and 1µM p21 inhibitor UC2288 (Merck, France) 1 h prior to AsiDNA™ treatment. Cells were harvested, fixed in cold 70% EtOH, and permeabilised in 1x PBS / 0.5% BSA / 0.1% Tween-20. BrdU detection was performed using FITC mouse anti-BrdU antibody (BD biosciences, France, #51-33284X). Following 1 h incubation, the cells were centrifuged and resuspended in 1x PBS containing 0.5% BSA, 10 µg/mL propidium iodide (Merck, France) and 0.5 mg/mL RNAse A (Merck, France). FACS analysis was performed using the LSRFortessa™ X-20 Cell Analyzer (BD biosciences, France).

ATP based cell viability assay

Cell viability was measured using the CellTiter-Glo® luminescent assay (Promega, France), which assesses the relative mitochondrial capacity of surviving cells. Cells were treated for 24 h with 20 µmol/L AsiDNA™ followed by chemotherapy treatment of Carboplatin (10 mg/mL, Accord), Olaparib, or Etoposide (20 mg/mL, Accord) at increasing doses of 0, 1, 10 and 100 µmol/L, or irradiated with doses of 0, 2, 4, 6, 8, and 10 Gy. The cell culture medium was removed 24 h post co-treatment and replaced by drug-free medium, and the mitochondrial capacity of surviving cells was measured 6 days post chemotherapeutic exposure, following the manufacturer's instructions.

Western blot analysis

Cell pellets were lysed in lysis buffer [10 mM Hepes, pH 7.5, 100 mM NaCl, 300 mM sucrose, 3 mM $MgCl_2$, 1 mM EGTA, 50 mM NaF, 20 mM ß-glycerophosphate, 0.3% Triton X-100, 0.1 mM sodium orthovanadate, and complete mini EDTA-free protease inhibitors (Roche Diagnosis)] on ice for 5 min. Following centrifugation at 240 rcf 4°C, supernatants were transferred into 1.5 mL Eppendorf tubes and protein concentration determined using Bradford assay (Bio-Rad). Twenty to thirty micrograms of protein extracts were separated on 4–15% Mini-PROTEAN® TGX™ Precast Protein Gels (Bio-Rad) and transferred onto PROTRAN® nitrocellulose membrane (Whatman) using a Mini Trans-Blot Cell (Bio-Rad). Membranes were probed overnight at 4°C with the following primary antibodies diluted in Intercept blocking buffer (LI-COR Biosciences – GmbH): anti-p53 (R&D systems, AF1355-sp, dil. 1:500), anti-p21 (Waf/Cip (12D1), Cell Signaling Technologies, 2947s, dil. 1:1000), anti-

hsp90-p (T5/7, Cell Signaling Technologies, 3488s, dil. 1:1000), anti-DNA-PK (Thr2609, Novus Biologicals, dil. 1:1000), and anti-β-actin (Signa, A1978, dil. 1:2000). The membranes were probed with the appropriate secondary antibodies diluted in Intercept blocking buffer: IRDye 800CW goat anti rabbit (LI-COR 926-32211, dil. 1:15000), IRDye 680RD goat anti mouse (LI-COR 926-32220, dil. 1:5000), IRDye 800CW goat anti mouse (LI-COR 926-32210, dil. 1:5000), IRDye 800CW donkey anti goat (LICOR 926-32214, dil. 1:5000). Direct infrared fluorescence was detected on the Odyssey Infrared Imaging System (LI-COR Biosciences – GmbH).

Ex vivo and In vivo experimentation

Studies were performed in accordance with the recommendations of the European Community (2010/63/UE) or UK Home Office guideline for the care and use of laboratory animals. Experimental procedures were explicitly approved by the ethics committee of Institut Curie CEEA-IC #118 (Authorization numberAPAFIS#5479-201605271 0291841 given by National Authority), or by the University of Oxford's Animal Welfare and Ethical Review Body (under project licenses PP8415318), in compliance with the international guidelines. All animals used within this research were acclimated for at least 1 week prior to experimentation. Mice were housed under pathogen-free conditions in cages containing sawdust with a maximum of six animals per cage, under a controlled 12 h light/dark cycle, a relative humidity of 55%, and a controlled temperature of 21°C. Food and sterile water were provided *ad libitum*. All experiments were conducted on C57BL/6J mice (Charles River, France) at 8-9 weeks of age, unless otherwise indicated in the corresponding materials and methods.

Precision-cut lung slices (PCLS)

PCLS were obtained from the lungs of female C57BL/6J mice (Charles River, France) or male and female C57BL/6J p53 Knock-out mice (Curie collection), at 4-6 months old, as described in the Supplementary Materials and Methods. AsiDNA™ or Nol8 treatment of 5 µmol/L was performed for 48 h in 24-well plates, followed by a 24 h co-incubation with 10 µmol/L EdU. EdU positive cells were revealed using EdU DetectPro Imaging kit Imaging (647 nm, BCK-EdUPro-IM647/BCK488-IV-IM-S, Baseclick), and visualized with the Inverted spinning disk-TIRF-FRAP (Nikon) with a 300 ms emission and 30% laser, DAPI (405 nm), 400 ms emission

and 70% laser, 10X objective with 50 stacks of 3 µm. Data analysis was performed using IMARIS with spot function and PRISM software.

Animal irradiation and fibrosis analysis

The female C57BL6/J mice model of radiation induced lung fibrosis was used (23,30). Mice were irradiated after 2 consecutive days of intraperitoneal AsiDNA™ injections (100 mg/kg), followed by a third day with intraperitoneal AsiDNA™ injection (200 mg/kg) and FLASH/CONV irradiation. Bilateral thorax irradiation of 13 Gy was performed using the ElectronFLASH (S.I.T., Vicenza, Italy), including a CONV dose rate of 0.4 Gy/sec and a FLASH dose rate of >100 Gy/s (beam parameters are described in Supplementary data Table 1). Animals were immobilized under anaesthesia (2.5% Isoflurane in air) and positioned vertically with lead shielding designed to protect the entire body excluding the thorax. GAFchromic™ EBT-XD film (Ashland Inc., Wayne, NJ, USA) was used for the dosimetry of entrance and exit dose at each irradiation. Animals were examined for weight loss and respiratory distress daily post IR. High resolution Micro-CT imaging (Molecubes), 100 µm FDK reconstruction, was performed to examine lung fibrosis development each month from 4 months post irradiation. The 3D lung reconstruction and fibrosis classification (24) were performed using VivoQuant 2021 (VivoQuant) and ImageJ/FIJI (ImageJ) software. For the 3D lung reconstruction, connected Hounsfield Units between -800 and -100 (bottom), detection of the lung volumes, were detected. Upon reaching the ethical endpoint, mice were anesthetized (2.5% Isoflurane in air) and underwent CT scanning prior to euthanasia by cervical dislocation. Lungs were isolated and histology was performed to detect areas of affected lung by pulmonary fibrosis.

Single cell RNA sequencing

Single cell RNA sequencing was performed on 3 controls provided by Curras et al. (31), 1 CONV, 1 CONV AsiDNA™, and 1 FLASH female C57BL6/J mice 5 months post 13 Gy thorax irradiation. The protocol and data processing procedures were performed as previously described (31). In brief, following lung tissue dissociation, single cell samples for RNA sequencing were prepared using the droplet based scRNA-seq system (10x GENOMICS) followed by lysis of encapsulated single cells, RNA capturing, cDNA production,

amplification, purification, library preparation, and sequencing. scRNA-seq data analysis was processed through the creation of a count matrix table suitable for R (4.0.5) and analysed using Seurat package (v4.0.1.).

Histology

For histological analysis, the lungs were removed, and gently inflated in 4% paraformaldehyde (PFA) under mild vacuum pressure (25 Torr, 1 h at room temperature). Lungs were fixed for 24 h at RT, after which they were embedded in paraffin and cut into 7-mm thick slices. The preparations were stained with hematoxylin–eosin or Masson trichrome (R.A.L Diagnostics, #361350).

Animal irradiation and intestine analysis

Female C57BL6/J mice were irradiated and treated as previously described (29). Lower body irradiation of 10 Gy was performed using the linear accelerator described in Ruan J. *et al.* (2021), including CONV dose rate of 0.1 Gy/min and FLASH dose rate of 3000 Gy/s with beam parameters described in Supplementary data Table 2. Animals were immobilized under anaesthesia in a cradle exposing the lower body. Brass shielding was used to protect the entire animal's body excluding the abdominal region. GAFchromic™ EBT-XD film was used for the dosimetry of the exit dose for each irradiation. Animals were examined for weight loss with the endpoint set at 4 days post IR. The jejunum of the small intestine was isolated using the swiss roll technique followed by intestine histology with haematoxylin and Eosin staining as previously described (32). The count of intestinal crypts was performed over a length of 3mm for each sample and conducted twice by independent researchers.

In vivo detection of EdU, Ki67 and p21

Female C57BL6/J mice received intraperitoneal AsiDNA™ injections (100 mg/kg) for 2 consecutive days, followed by a third day with intraperitoneal AsiDNA™ injection (200 mg/kg). EdU (100 mg/kg) was injected 4 h prior to euthanasia at 0, 24, 48, and 72 h post AsiDNA™ injection. The small intestine was isolated from 3 cm after the stomach, with a total length of 10 cm intestine isolated overall, using the swiss roll technique (33). Samples were fixed in 4% PFA for 36 h, embedded in parafilm, and cut into 4 µm thick slices. These slices

were then deparaffinized and hydrated following a standard protocol. DAPI (0.5 µg/mL) staining and EdU detection were performed using BaseClick EdU IV Imaging kit 488 M in accordance with the manufacturer's protocol. EdU positive cells were detected using the 3D SIM Upright Widefield microscope (Leica), and quantified using a nuclear segmentation algorithm (Cellpose) and MIC-MAQ macro (supplementary Materials and methods), applied on nuclear DAPI signal and the individual EdU cell signal. Furthermore, standard immunofluorescence was conducted to detect Ki-67 (FISHER, MA5-14520, 1:200) and immunohistochemistry staining to detect p21 (Tebu-Bio, E-AB-70068, 1:200).

Statistical analysis

All statistical analyses were performed using GraphPad Prism (v 7.03). Statistical significance was set at * < 0.05, ** < 0.01, *** < 0.001 and, **** < 0.0001. All statistical information is presented in the figures and figure legends.

RESULTS

AsiDNA™ induces a G1/S arrest in normal proliferating epithelial cells and fibroblasts

The adverse side effects induced by radio- and chemo-therapies are derived from damage to dividing normal cells, resulting in cell death within the healthy tissue (34,35). Cell cycle arrest has previously been demonstrated to protect normal cells against cytotoxic radio- and chemo-therapies (36,37). Consequently, in the present study, we assessed cell cycle progression in a panel of normal human cells treated with AsiDNA™. For this, primary fibroblasts (NHSF and MRC5), and immortalized normal epithelial cells (RPE-hTERT) were exposed to 20 and 40 µM of AsiDNA™ for 24 and 48 h, followed by cell cycle analysis using PI-BrdU bivariate flow cytometric dot plots (**Figure 1A and 1B, Supplementary Figure 1SA**). The corresponding histograms showing cell cycle analysis (**Figure 1C and 1D**) allow quantification of the number of cells in each cell cycle phase (**Figure 1E and 1F**). Analysis of these results indicated significant cell cycle arrest at the G1/S boundary, which implies an accumulation of cells in G1 and a strong decrease of S-phase cells (**Figure 1E and 1F, Supplementary Figure S1B**). In contrast, MRC-5V1 cells (MRC-5 SV40-transformed cells),

which are p53-defective, do not arrest at the G1/S boundary upon AsiDNA™ treatment (**Supplementary Figure S1C,D**).

A functional DNA-PK/p53/p21 pathway is required to promote AsiDNA™-induced G1/S arrest in normal proliferating epithelial cells and fibroblasts

Nol8, which is structurally similar to AsiDNA™ but with an 8 bp instead of 32 bp nucleotide strand, showed no capacity to activate PARP and DNA-PK (**Supplementary Figures S2A and S2B**). Furthermore, treatment with Nol8 induced only a moderate G1/S arrest, although not significant, with no p21 induction (**Supplementary Figures S2C-E**). These results prompted us to investigate the role of PARP and DNA-PK in AsiDNA-induced cell cycle arrest. PARP and DNA-PKcs activity were inhibited using olaparib (38), and NU7026 (39), respectively, and cell cycle progression was examined upon combined treatment with AsiDNA™. The inhibition of DNA-PK activity, but not of PARP, was able to prevent AsiDNA™-induced G1/S arrest in RPE-hTERT and NHSF (**Figure 2A and Supplementary Figure S3A**). This dependency on DNA-PK activation was further confirmed using cells in which the expression of DNA-PK was down-regulated (**Figure 2B and Supplementary Figure S3B**). In support of this, previous research has shown that the p53-p21 axis is an important pathway controlling G1/S arrest upon activation of the DNA damage response (40). Comparable results were obtained following the downregulation of p21 expression (**Figures 2B**) in RPE-hTERT cells. Efficient down-regulation of DNA-PKcs, p53, and p21 expression was confirmed by western blot analysis (**Supplementary Figure S3C**). In addition, the expression level of p53 and p21 in response to 24h and 48h of AsiDNA™ treatment was examined by western blot analysis in RPE-hTERT, RPE-hTERT shp53, and RPE-hTERT cells treated with NU7026. These results revealed that AsiDNA™ exposure triggered p21 induction in RPE-hTERT, but not in RPE-hTERT shp53 (**Supplementary S3E**) or RPE-hTERT cells treated with NU7026 (**Supplementary Figure S3D**). Collectively, these results demonstrate that DNA-PK activity is required to promote the p53-dependent transcriptional activation of p21 which leads to the G1/S arrest induced by AsiDNA™. Furthermore, AsiDNA™-induced G1/S arrest was reversible. Following the removal of AsiDNA™ treatment, cells restarted their cell cycle, and p21 expression returned to basal level (**Supplementary Figure S4**).

P53-proficient tumour cells show no G1/S arrest upon AsiDNA™ treatment

Standalone AsiDNA™ treatment has previously been demonstrated to cause toxicity in malignant cells, irrespective of their p53 status, and exerted no toxicity against normal cells (7,8,18,41). As such, we subsequently investigated AsiDNA™-induced cell cycle arrest in p53 proficient tumour cells (U2OS, A549, and HCT116). All assessed tumour cells within this study displayed no G1/S arrest after AsiDNA™ treatment, suggesting that this only occurs in normal cells (**Figure 3**). This was confirmed with the absence of p21 induction upon AsiDNA™ treatment in the tumour cell lines (**Supplementary Figure S5**)

AsiDNA™-induces G1/S arrest promotes cell survival in response to ionizing radiation and chemotherapies in normal cells

The G1/S cell cycle checkpoint primarily prevents damaged DNA from being replicated during the S phase, which can be either mutagenic or lethal for cells. It is therefore hypothesized that AsiDNA™-dependent G1/S arrest could protect healthy cells from chemo- or radio-induced toxicity. To test this hypothesis, normal human cell lines (NHSF and RPE-hTERT) were treated with AsiDNA™ prior to radiation or chemotherapy (olaparib, carboplatin, etoposide) exposure. An increase in cell survival of AsiDNA™-treated normal cells upon combined treatment with genotoxic agents or radiation was compared to AsiDNA™-free cells (**Figure 4A, and Supplementary Figure S6A**). Importantly, there was no protection from these genotoxic agents in cells lacking AsiDNA™-induced G1/S arrest such as in RPE-hTERT shp53 cells or in tumour cells (A549 and HCT116) (**Figure 4B, and Supplementary Figure S6B-C**). These in vitro results demonstrate the crucial role of AsiDNA™-induced G1/S arrest in protecting cells against the cytotoxicity and radiotoxicity of DNA damaging treatments.

AsiDNA™ alleviates radiation-induced lung fibrosis in mice

To demonstrate that AsiDNA™ is similarly able to induce normal tissue protection against radiation-induced toxicity in vivo, radiation-induced lung fibrosis in C57BL/6J mice, a well-established model of late-responding radiation toxicity, was used (42). As using FLASH-RT instead of CONV-RT similarly alleviates radiation-induced lung fibrosis in mice (23,24), we

examined the possible gain of combined AsiDNA™ and FLASH-RT treatment on the protection of healthy tissue. Thirty mice were equally divided into 5 groups (n = 6), sham-irradiated or exposed to 13 Gy CONV +/- AsiDNA™ or 13 Gy FLASH +/- AsiDNA™, through bilateral thorax irradiation. Lung fibrosis was evaluated using computed tomography (CT) from 4 months post-irradiation. Each lobe of the lung was collected for histopathological analysis and single cell RNA sequencing, immediately after euthanasia (**Figure 5A**).

CT scans taken five months post irradiation revealed increased levels of fibrosis in the CONV-RT treated group, while fibrosis was absent in the mock-treated group and much less pronounced in the CONV-RT + AsiDNA™ treated group (**Figure 5B**). As expected, FLASH-RT also reduced the occurrence of lung fibrosis, while combined treatment with AsiDNA™ appears to further reduce the development of fibrosis (**Figure 5B**). Long-term follow-up of survival post irradiation demonstrated that AsiDNA™ delayed the onset of lethal lung fibrosis when combined with CONV-RT (**Figure 5C**). We also confirmed the FLASH effect as previously reported (23). However, AsiDNA™ combined with FLASH-RT did not seem to further improve survival (**Figure 5C**). Histopathological analyses of the lobes collected at the day of euthanasia confirmed the onset of lung fibrosis by detection of fibrotic masses, indicated with black arrows (**Figure 5D and Supplementary Table 3**).

A decreased myofibroblast gene profile is observed in fibroblasts upon AsiDNA™ treatment

To characterize the similarity in cellular changes and expression signatures in lungs 5 months post CONV-RT, FLASH-RT, AsiDNA™ + CONV-RT or non-irradiated (Control) treatment, single cell suspensions were created and analysed using scRNA sequencing. By exploiting previously published single-cell datasets and known identifying markers (31), the identity of the various cell clusters was determined (**Figure 6A**). This analysis detected 21 distinct clusters: alveolar macrophages (AM), proliferating AM, AT1, AT2, B-cells, basophils, ciliated cells, ciliated club cells, club cells, dendritic cells (DC), endothelial cells (EC), fibroblasts, interstitial macrophages (IM), mesitheliocytes, monocytes, neutrophils, natural killer cells (NK cells), NK-T-cells, smooth muscle cells (SMC), T-cells and proliferating T-cells (**Figure 6B-D**). All cell types were identified independently of the received treatment modality but a

radiation-induced cell proportion shift was detected in the AT2, B-cells, IM, and NK-T cells (**Figure 6D**). Additionally, the AM, DC, Monocytes and NK-cells populations displayed altered cell proportions following CONV-RT compared to the other conditions (**figure 6D**). Recent findings by Curras et al. (2023) (31) have identified a unique fibroblast subcluster exclusively present in irradiated mice lungs. In response to irradiation, fibroblasts can transition into myofibroblasts which are known to secrete and modify the extracellular matrix (ECM), including altering the collagen production, which in turn contributes to pulmonary fibrosis formation (43). To identify the contribution of fibroblasts in the development of, or the lack of, pulmonary fibrosis formation after CONV-RT, CONV AsiDNA™ treatment and FLASH-RT, myofibroblast markers expression, collagen homeostasis, fibroblast activation and EMC remodelling markers were examined within the fibroblast cell cluster. Clustering of the fibroblast resulted in the detection of a total of 891 cells, divided over the different treatment conditions (**Figure 6E**). Myofibroblast markers Hp and Pla1a, previously identified in Curras et al. (2023) (31), revealed to be substantially increased after CONV-RT standalone (**Figure 6F-G**). Remarkably, Nr1d1 gene expression, linked to healthy collagen homeostasis (44), was found to be significantly decreased in CONV-RT compared to the control or FLASH-RT (**Figure 6H**).

These results reveal an increase in fibroblast activation and myofibroblast transition together with an impact on the ECM, including collagen homeostasis, in the fibroblast cell cluster following CONV-RT standalone. This observed altered gene expression in CONV-RT exposed fibroblast was decreased or absent in fibroblasts exposed to CONV AsiDNA™ or FLASH-RT, and supports the increased pathway activation known to play an essential role in the development of pulmonary fibrosis.

AsiDNA™ induces cell cycle arrest in ex vivo precision cut lung slices involving DNA-PK and p53

To investigate AsiDNA™-induced cell cycle arrest in the lung, ex vivo precision cut lung slices (PCLS) were used. Untreated C57BL6/J mice were sacrificed, and agarose inflated lungs were isolated and cut. The PCLS were treated for 24h with AsiDNA™ or Nol8, and EdU (a marker of replicative cell division) was co-incubated for an additional 24h. Cell nuclei were then stained for EdU incorporation **(Figure 7A)**. There was a significant loss of EdU positive cells following AsiDNA™ treatment compared to both untreated and Nol8 treated PCLS **(Figure 7B)** suggesting that DNA-PK activation by AsiDNA™ also triggered cell cycle arrest, likely at the G1/S border, in PCLS. To further support this conclusion, PCLS were derived from wild-type C57BL6/J mice and p53 knock out (p53-/-) mice. Upon AsiDNA™ treatment in wild-type (WT) mice, a significant decrease in EdU positive cells was detected compared to the untreated conditions **(Figures 7C and 7D).** Additionally, the incorporated EdU positive cells of untreated PCLS in WT and in KO were similar. Strikingly, p53 KO PCLS treated with AsiDNA™ resulted in no significant decrease in the EdU incorporation **(Figure 7D)**. Collectively, these results strongly support the activation of G1/S arrest induced by AsiDNA™ treatment in PCLS requiring the activation of DNA-PK and p53.

AsiDNA™ alleviates radiation-induced intestine toxicity in mice

To study the capacity of AsiDNA™ to protect normal tissue from early responding radiation toxicity, a model of acute intestinal toxicity after whole abdominal irradiation in mice was used (29). The possible gain-of-protection by AsiDNA™ was examined in combination with CONV-RT and FLASH-RT (**Figure 8A**). For crypts analysis, intestine was isolated at 4 days post treatment, and the jejunum was further processed for histochemistry analyses **(Figure 8B)**. The number of damaged crypts in each condition was normalized to the number of crypts present in the non-irradiated mice. More crypts remained after CONV-RT combined with AsiDNA™ compared with CONV-RT alone ($P < 0.0018$) (**Figure 8C**). Similarly, FLASH-RT resulted in less toxicity, preserving more of the intestinal crypts than CONV-RT ($P < 0.006$). Additionally, there was no difference detected in the percentage of remaining crypts

between FLASH-RT and FLASH-RT combined with AsiDNA™ **(Figure 8C)**. Collectively, these results showed a gain-of-protection for AsiDNA™ only when combined with CONV-RT.

AsiDNA™ induces a reversible cell cycle arrest in vivo

To demonstrate the capacity of AsiDNA™ treatment to arrest normal cell division in vivo, we used a well-established intestine model which exhibits a high rate of cell proliferation within the small intestinal crypts (45,46). EdU incorporation in intestine crypt cells of C57BL6/J mice was examined at 0, 24, 48 and 72h post AsiDNA™ treatment, and the small intestine was isolated for immunohistochemistry analyses 4h after EdU incorporation (**Figure 9A**). A significant loss of EdU positive cells without any decrease in Ki67 was observed immediately following the final AsiDNA™ injection, compared to the untreated group at time 0 h or 72h (**Figures 9B and 9C, Supplementary Figure S7**). However, this reduction was only transient, as the level of EdU positive cells has recovered at 24h, 48h and 72h post AsiDNA™ treatment. Strikingly, this level exceeds that of the control groups suggesting a boost of cell proliferation upon release from AsiDNA™ (**Figure 9C**). As the reported in vitro G1/S arrest relies on p21 induction, p21 initiation in the small intestinal crypts in response to AsiDNA™ treatment was monitored. The number of p21 positive ($p21^+$) cells was reduced in untreated groups (average of 8 and 13 $p21^+$ cells per 100 cells at 0h and 72h, respectively) but significantly increased upon AsiDNA™ treatment (average of 64 $p21^+$ cells per 100 cells, 0h post AsiDNA™) (**Figures 9D and 9E**). Most importantly, the number of p21 positive cells decreased rapidly at 24h post treatment (average of 20 $p21^+$ cells per 100 cells, 24h post AsiDNA™) reaching a basal level at 48h and 72h post treatment (average of 13 $p21^+$ cells per 100 cells, 48h and 72h post AsiDNA™) (**Figure 9D**). Taken together, these results demonstrated that the loss of DNA replication following AsiDNA™ treatment, as revealed by the decline of EdU incorporation, correlates with p21 induction, while recovery of EdU incorporation post-treatment correlates with a decrease in p21 initiation.

DISCUSSION

The capacity of radiotherapy to damage and eradicate tumour cells comes at the expense of toxicity to the normal tissue, causing severe patient distress and leads to critical conditions in the treatment delivery. One approach to reduce or mitigate these toxic side-effects is to utilise chemical or biological agents as radioprotectors, administered in parallel to radiotherapy delivery (47). The ideal radioprotector exhibits low toxicity and exclusive protection of normal cells against the harmful effects of radiation, without compromising the cytotoxic effects on cancer cells. In recent years, our laboratory has developed a new class of drugs mimicking DNA DSBs that can disrupt the DNA repair machinery of cancer cells, thereby enhancing the antitumoral action of radiation (9,48). The leading molecule used in pre-clinical and clinical studies, termed AsiDNA™, is well tolerated, does not induce normal tissue toxicity, and allows increased treatment duration, (17,19-21) all indicating its suitability as a radioprotector. AsiDNA™ was designed based on its ability to bind and activate PARP and DNA-PK, with the aim of destabilizing the DNA repair machinery (9). Although activation of DNA-PK occurs in tumours as well as in normal cells, only tumour cells are sensitive to AsiDNA™ treatment (7,49).

The G1/S cell cycle checkpoint is responsible for ensuring that the optimum conditions are reached for a cell to undergo successful cell division, through the sensing of both mitogens and DNA damage (50). One of the key players of this checkpoint is the transcription factor p53 (51). p53 transactivates numerous target genes involved in the induction of cell cycle arrest and/or apoptosis (52). In the present study, we demonstrated that in p53 proficient normal cells, AsiDNA™ treatment results in p53 activation, leading to p21 induction which, in turn, initiates a reversible G1/S cell cycle arrest. Normal cells deficient in either DNA-PK, p53, or p21 are unable to arrest at the G1/S boundary following AsiDNA™ treatment. Pull-down experiments with biotinylated AsiDNA™ have revealed that DNA-PK binds to AsiDNA™ in cellulo (M. Dutreix, unpublished results). Several studies have shown that structured DNA, single-stranded DNA, and damaged DNA promote the interaction of DNA-PK with p53 (53-55). We propose that AsiDNA™ can serve as a platform to connect DNA-PK and p53, resulting in p53 activation. In line with this assumption, our results revealed that MRC-5

primary cells can arrest at the G1/S boundary in response to AsiDNA™ treatment, while MRC-5V1 cells failed to do so. MRC-5V1 are SV40-transformed cells instigating p53 protein blockage by the SV40 large T antigen (56), which abrogates the DNA binding activity and transcriptional activity of p53. These results are in agreement with a previous report showing the absence of p21 induction and G1/S arrest in MRC-5V1, that was present in MRC-5 primary cells, in response to ionizing radiation (57).

The p53 proficient tumour cell lines used within this study (A549, U-2 OS, and HCT116) did not arrest at the G1/S boundary upon AsiDNA™ treatment, correlated with a lack of p21 induction. However, a p53- and p21-dependent G1/S arrest in tumour cells has been observed in the past, in response to chemical compounds (58-60) and ionizing radiation (61-63). Regardless, a radiation-induced G1/S arrest is ATM/Chk2/p53/p21-dependent (64) whereas the AsiDNA™-induced G1/S arrest, identified within this study, revealed its dependency on DNA-PK/p53/p21. As outlined in (65), in order for p53 to accumulate in cells and to transactivate target genes, the degradation of p53 must be inhibited, the p53 protein must accumulate in the nucleus and the sequence-specific binding activity must be induced. As DNA-PK is recruited, and consequently activated, in response to AsiDNA™ in all cell lines examined so far, revealed by phosphorylation of H2AX ((7,9)}, and unpublished data), it suggests that the recruitment of p53 to the AsiDNA™/DNA-PK complex and downstream transactivation of p21 is impaired in p53 proficient tumour cells, unlike p53 proficient normal cells. Normal and cancer cells differ by several phenotypic and genotypic modifications very well documented in ((66) and references therein). Among them, it is well described that the metabolism of cancer cells differs from that of normal cells (67). We have previously demonstrated that PARP is another important protein that is activated by AsiDNA™ (9). High PARP activity leads to energy exhaustion in part due to NAD depletion (68). Notably, p53 is not only a key metabolic regulator, including NAD metabolism (69), but there is a cross-talk between p53, NAD homeostasis and PARP (70). Whether there is a competition between p53 recruitment at AsiDNA™/DNA-PK complex involving its role in NAD homeostasis in tumour and not normal cells, remains to be demonstrated.

In the present study, we confirmed the presence of the activated G1/S checkpoint in complex ex vivo and in vivo biological models. The ex vivo PCLS model retains comparable viability and tissue homeostasis during a cultivation period of 1 to 3 days (71), and can be used to monitor cell proliferation using EdU incorporation (M. Dubail and C. Fouillade, submitted manuscript). AsiDNA™-treated PCLS derived from p53 WT mice revealed a severe decrease of EdU positive cells, while this decrease was absent in PCLS derived from p53 knock-out mice, or in PCLS p53 WT treated with Nol8, an AsiDNA™-like molecule unable to activate DNA-PK (5). This provides further evidence that AsiDNA™ treatment in PCLS results in DNA-PK/p53-dependent G1/S arrest. Additional conformation was observed in vivo where the capacity of AsiDNA™ to induce the G1/S arrest in the intestine was demonstrated with a severe decrease of EdU incorporation in the intestinal crypts of mice directly after AsiDNA™ treatment. It furthermore disclosed a full recovery of crypt division 24-48h post-AsiDNA™ treatment, verifying the reversibility of the G1/S arrest. Remarkably, the decrease of EdU incorporation immediately after AsiDNA™ and its recovery post treatment, were both concomitantly associated with an increase of p21 expression, followed by its decrease. This provides further evidence that AsiDNA™ can activate a reversible G1/S checkpoint in PCLS. Moreover, the recovery of cell division in the crypt is associated to an excess in EdU-positive dividing cells from 24h post AsiDNA™ treatment. This boost in normal cell proliferation post drug treatment is a phenomenon that has been previously identified (72,73). As AsiDNA™ has widely been identified to not result in toxicity, this compensation occurrence might accompany the contribution to improved tissue recovery.

In response to DNA damaging agents, dividing cells stall or arrest their cell cycle progression to detect and repair DNA damage before they can resume the cell cycle (64). This contributes to the maintenance of both genome integrity, and overall survival. The results within this research revealed a significant increase of in vitro cell survival, in normal cells upon chemo- or radiotherapy combined with AsiDNA™, compared to standalone treatment. This increase in cell survival was absent in tumour cells, independent of the p53 status, as well as in normal cells with a p53 deficient status. This confirms the necessity of an active and intact DNA-PK/p53/p21 cascade to exploit the normal tissue protection properties of AsiDNA™. The protective capacities of AsiDNA™ were similarly identified in vivo in the intestine crypt

survival, as early model of radiation induced toxicity (29), and in the radiation-induced lung fibrosis, as late model of radiation induced toxicity (23). CONV-RT + AsiDNA™ resulted in an increase in crypt survival, compared to CONV-RT standalone, confirming the capacity of AsiDNA™ to protect against radiation induced toxicity in vivo. The intestinal epithelium regenerates itself through the proliferation and differentiation of stem cells (74). The intestine can therefore fully regenerate from any type of damage if the stem cells remain functional, revealing the capacity of AsiDNA™ to protect the stem cells in the crypts by acting at the G1/S transition. Remarkably, pharmacologic inhibition of the G1/S transition by CDK4/6 inhibitors prior to radiation (75), or by UCN-01 prior to chemotherapy (37) also protect the gastrointestinal epithelium in mice. The protective capacities of AsiDNA™ treatment were confirmed in vivo, with similar results obtained on the late radiotoxicity model of radiation-induced pulmonary fibrosis. Here, once again, AsiDNA™ combined with CONV-RT revealed increased protection of the lung to radiation toxicity presented by a delay in the onset of radiation induced fibrosis, compared to CONV-RT standalone.

Finally, the combination of AsiDNA™ with FLASH-RT, a RT modality that has been shown to alleviate radiation-induced toxicity (23,29), was explored. In one respect, FLASH-RT was shown to be less toxic, with decreased early (intestine model) and late (lung model) toxicity compared with CONV-RT, thereby reconfirming the FLASH effect. However, AsiDNA™ combined with CONV-RT did not result in the same delay in the onset of fibrosis compared to FLASH radiotherapy standalone, while AsiDNA™ CONV-RT was as efficient as FLASH-RT at protecting intestinal crypts. This may be explained by the possible limitations in the capacity of AsiDNA™ to interfere with the complex, and still relatively unknown, mechanism driving fibrosis in late responding tissues (76). Moreover, AsiDNA™ combined with FLASH-RT treatment did not result in any additive effect on the protection of toxicity in the intestinal crypts nor the lung, compared to FLASH-RT as standalone treatment. Interestingly, single cell RNA sequencing of irradiated lungs revealed a closer resemblance between CONV AsiDNA™ and FLASH-RT in profibrotic gene signatures within the fibroblast population, in comparison to CONV-RT standalone. Similar results on profibrotic gene signatures were observed in the alveolar macrophages population (A. Sesink, and P-M. Girard, unpublished results). Collectively, all results indicate that the activity of AsiDNA™ and FLASH-RT could draw upon

identical mechanism interference to result in the protective capacities within the normal tissue. Currently, additional research is in progress to explore the spatio-temporal dynamics of mechanisms leading to radiation-induced pulmonary fibrosis (31).

In summary, we have identified an AsiDNA™-induced reversible G1/S-arrest dependent on the DNA-PK/p53/p21 activation cascade exclusively in healthy normal cells. The activation cascade can be exploited to protect the normal tissue against radiation induced toxicity while maintaining tumour control, thereby acting as a unique bilateral agent.

AUTHOR CONTRIBUTIONS

Anouk Sesink and Pierre-Marie Girard designed and conceptualized the research; Anouk Sesink, Margaux Becerra, Jia-Ling Ruan, and Sophie Leboucher performed experiments and analyzed, validated, and visualized the results; Sophie Heinrich and Kristoffer Peterson analyzed and validated the results; Maxime Dubail and Charles Fouillade developed ex vivo models; Anouk Sesink and Pierre-Marie Girard wrote the original manuscript draft. Marie Dutreix, and Pierre-Marie Girard supervised the work; Kristoffer Peterson, Wael Jdey, Marie Dutreix and Pierre-Marie Girard acquired the fundings. All authors critically revised, edited, and approved the final version of the manuscript.

ACKNOWLEDGEMENTS

AsiDNA™ molecules were kindly provided by Wael Jdey. We would like to acknowledge L. Besse and M-N. Soler for their helpful advice on image processing and the accessibility of the microscopy platform (Institut Curie, Orsay). We would further like to express out significant gratitude to V. Favaudon for his support throughout the work. We acknowledge L. Portier, and J. Soulier for their excellent technical support, and the Pathex platform (Institut Curie, Paris) for their aid in the assessment of pulmonary fibrosis in lung histology samples.

FUNDING

The work was supported by grants to PMG from European Union's Framework Program for Research and Innovation Horizon 2020 (ITN THERADNET) [under the Marie Skłodowska-Curie Grant Agreements n° 860245], and from Valerio Therapeutics (Paris, France) [Grant Agreement CT10605]. The work was also supported by a grant to MD from S.I.T. Sordina IORT Technologies S.p.A. (Vicenza, Italy) [Grant Agreement CT9792]. AS is the recipient of a PhD fellowship from ITN THERADNET [Grant Agreements No. 860245] and from Fondation pour la Recherche sur le Cancer (ARC, Villejuif, France). MD and PMG wish to thank the Centre National de la Recherche Scientifique (CNRS), Institut Curie and Université Paris-Saclay for their financial and technical support.

CONFLICT OF INTEREST

Wael Jdey is employed by Valerio Therapeutics (former ONXEO)

REFERENCES

1. Barnett, G.C., West, C.M., Dunning, A.M., Elliott, R.M., Coles, C.E., Pharoah, P.D. and Burnet, N.G. (2009) Normal tissue reactions to radiotherapy: towards tailoring treatment dose by genotype. *Nat Rev Cancer*, **9**, 134-142.
2. De Ruysscher, D., Niedermann, G., Burnet, N.G., Siva, S., Lee, A.W.M. and Hegi-Johnson, F. (2019) Radiotherapy toxicity. *Nat Rev Dis Primers*, **5**, 13.
3. Al-Mahayri, Z.N., Patrinos, G.P. and Ali, B.R. (2020) Toxicity and Pharmacogenomic Biomarkers in Breast Cancer Chemotherapy. *Front Pharmacol*, **11**, 445.
4. Hellman, S. (1980) Improving the therapeutic index in breast cancer treatment: the Richard and Hinda Rosenthal Foundation Award lecture. *Cancer Res*, **40**, 4335-4342.
5. Quanz, M., Berthault, N., Roulin, C., Roy, M., Herbette, A., Agrario, C., Alberti, C., Josserand, V., Coll, J.L., Sastre-Garau, X. *et al.* (2009) Small-molecule drugs mimicking DNA damage: a new strategy for sensitizing tumors to radiotherapy. *Clin Cancer Res*, **15**, 1308-1316.
6. Berthault, N., Maury, B., Agrario, C., Herbette, A., Sun, J.S., Peyrieras, N. and Dutreix, M. (2011) Comparison of distribution and activity of nanoparticles with short interfering DNA (Dbait) in various living systems. *Cancer Gene Ther*, **18**, 695-706.
7. Thierry, S., Jdey, W., Alculumbre, S., Soumelis, V., Noguiez-Hellin, P. and Dutreix, M. (2017) The DNA Repair Inhibitor Dbait Is Specific for Malignant Hematologic Cells in Blood. *Mol Cancer Ther*, **16**, 2817-2827.
8. Jdey, W., Thierry, S., Russo, C., Devun, F., Al Abo, M., Noguiez-Hellin, P., Sun, J.S., Barillot, E., Zinovyev, A., Kuperstein, I. *et al.* (2017) Drug-Driven Synthetic Lethality: Bypassing Tumor Cell Genetics with a Combination of AsiDNA and PARP Inhibitors. *Clin Cancer Res*, **23**, 1001-1011.
9. Berthault, N., Bergam, P., Pereira, F., Girard, P.M. and Dutreix, M. (2022) Inhibition of DNA Repair by Inappropriate Activation of ATM, PARP, and DNA-PK with the Drug Agonist AsiDNA. *Cells*, **11**.
10. Herath, N.I., Berthault, N., Thierry, S., Jdey, W., Lienafa, M.C., Bono, F., Noguiez-Hellin, P., Sun, J.S. and Dutreix, M. (2019) Preclinical Studies Comparing Efficacy and Toxicity of DNA Repair Inhibitors, Olaparib, and AsiDNA, in the Treatment of Carboplatin-Resistant Tumors. *Front Oncol*, **9**, 1097.
11. Quanz, M., Herbette, A., Sayarath, M., de Koning, L., Dubois, T., Sun, J.S. and Dutreix, M. (2012) Heat shock protein 90alpha (Hsp90alpha) is phosphorylated in response to DNA damage and accumulates in repair foci. *J Biol Chem*, **287**, 8803-8815.

12. Kotula, E., Faigle, W., Berthault, N., Dingli, F., Loew, D., Sun, J.S., Dutreix, M. and Quanz, M. (2013) DNA-PK target identification reveals novel links between DNA repair signaling and cytoskeletal regulation. *PLoS One*, **8**, e80313.
13. Coquery, N., Pannetier, N., Farion, R., Herbette, A., Azurmendi, L., Clarencon, D., Bauge, S., Josserand, V., Rome, C., Coll, J.L. *et al.* (2012) Distribution and radiosensitizing effect of cholesterol-coupled Dbait molecule in rat model of glioblastoma. *PLoS One*, **7**, e40567.
14. Biau, J., Devun, F., Jdey, W., Kotula, E., Quanz, M., Chautard, E., Sayarath, M., Sun, J.S., Verrelle, P. and Dutreix, M. (2014) A preclinical study combining the DNA repair inhibitor Dbait with radiotherapy for the treatment of melanoma. *Neoplasia*, **16**, 835-844.
15. Herath, N.I., Devun, F., Lienafa, M.C., Herbette, A., Denys, A., Sun, J.S. and Dutreix, M. (2016) The DNA Repair Inhibitor DT01 as a Novel Therapeutic Strategy for Chemosensitization of Colorectal Liver Metastasis. *Mol Cancer Ther*, **15**, 15-22.
16. Herath, N.I., Devun, F., Herbette, A., Lienafa, M.C., Chouteau, P., Sun, J.S., Dutreix, M. and Denys, A. (2017) Potentiation of doxorubicin efficacy in hepatocellular carcinoma by the DNA repair inhibitor DT01 in preclinical models. *Eur Radiol*, **27**, 4435-4444.
17. Ferreira, S., Foray, C., Gatto, A., Larcher, M., Heinrich, S., Lupu, M., Mispelter, J., Boussin, F.D., Pouponnot, C. and Dutreix, M. (2020) AsiDNA Is a Radiosensitizer with no Added Toxicity in Medulloblastoma Pediatric Models. *Clin Cancer Res*, **26**, 5735-5746.
18. Jdey, W., Kozlak, M., Alekseev, S., Thierry, S., Lascaux, P., Girard, P.M., Bono, F. and Dutreix, M. (2019) AsiDNA Treatment Induces Cumulative Antitumor Efficacy with a Low Probability of Acquired Resistance. *Neoplasia*, **21**, 863-871.
19. Le Tourneau, C., Dreno, B., Kirova, Y., Grob, J.J., Jouary, T., Dutriaux, C., Thomas, L., Lebbe, C., Mortier, L., Saiag, P. *et al.* (2016) First-in-human phase I study of the DNA-repair inhibitor DT01 in combination with radiotherapy in patients with skin metastases from melanoma. *Br J Cancer*, **114**, 1199-1205.
20. Le Tourneau, C., Delord, J.P., Kotecki, N., Borcoman, E., Gomez-Roca, C., Hescot, S., Jungels, C., Vincent-Salomon, A., Cockenpot, V., Eberst, L. *et al.* (2020) A Phase 1 dose-escalation study to evaluate safety, pharmacokinetics and pharmacodynamics of AsiDNA, a first-in-class DNA repair inhibitor, administered intravenously in patients with advanced solid tumours. *Br J Cancer*, **123**, 1481-1489.
21. Kotecki, N., Jungels, C., Hoerner, F., Canon, J., Colinet, B. and De Beaumont, O. (2021) Long stabilization and disease control with AsiDNATM, a first-in-class DNA Repair Inhibitor in combination with carboplatin with or without paclitaxel in patients with advanced solid tumors: A case report. *Oncology & Cancer Case Reports*, **07**, 001-007.

22. Esplen, N., Mendonca, M.S. and Bazalova-Carter, M. (2020) Physics and biology of ultrahigh dose-rate (FLASH) radiotherapy: a topical review. *Phys Med Biol*, **65**, 23TR03.
23. Favaudon, V., Caplier, L., Monceau, V., Pouzoulet, F., Sayarath, M., Fouillade, C., Poupon, M.F., Brito, I., Hupe, P., Bourhis, J. *et al.* (2014) Ultrahigh dose-rate FLASH irradiation increases the differential response between normal and tumor tissue in mice. *Sci Transl Med*, **6**, 245ra293.
24. Fouillade, C., Curras-Alonso, S., Giuranno, L., Quelennec, E., Heinrich, S., Bonnet-Boissinot, S., Beddok, A., Leboucher, S., Karakurt, H.U., Bohec, M. *et al.* (2020) FLASH Irradiation Spares Lung Progenitor Cells and Limits the Incidence of Radio-induced Senescence. *Clin Cancer Res*, **26**, 1497-1506.
25. Simmons, D.A., Lartey, F.M., Schuler, E., Rafat, M., King, G., Kim, A., Ko, R., Semaan, S., Gonzalez, S., Jenkins, M. *et al.* (2019) Reduced cognitive deficits after FLASH irradiation of whole mouse brain are associated with less hippocampal dendritic spine loss and neuroinflammation. *Radiother Oncol*, **139**, 4-10.
26. Velalopoulou, A., Karagounis, I.V., Verginadis, I.I., Goia, D., Kim, M., Shoniyozov, K., Cengel, K., Diffenderfer, E., Dong, L., Metz, J. *et al.* (2020) Proton FLASH radiation spares normal skin and soft tissues of the murine leg from radiation-induced damage while being equipotent with standard proton radiation in controlling sarcoma growth. *Cancer Research*, **80**.
27. Velalopoulou, A., Karagounis, I.V., Cramer, G.M., Kim, M.M., Skoufos, G., Goia, D., Hagan, S., Verginadis, II, Shoniyozov, K., Chiango, J. *et al.* (2021) FLASH Proton Radiotherapy Spares Normal Epithelial and Mesenchymal Tissues While Preserving Sarcoma Response. *Cancer Res*, **81**, 4808-4821.
28. Diffenderfer, E.S., Verginadis, I.I., Kim, M.M., Shoniyozov, K., Velalopoulou, A., Goia, D., Putt, M., Hagan, S., Avery, S., Teo, K. *et al.* (2020) Design, Implementation, and in Vivo Validation of a Novel Proton FLASH Radiation Therapy System. *Int J Radiat Oncol*, **106**, 440-448.
29. Ruan, J.L., Lee, C., Wouters, S., Tullis, I.D.C., Verslegers, M., Mysara, M., Then, C.K., Smart, S.C., Hill, M.A., Muschel, R.J. *et al.* (2021) Irradiation at Ultra-High (FLASH) Dose Rates Reduces Acute Normal Tissue Toxicity in the Mouse Gastrointestinal System. *International journal of radiation oncology, biology, physics*, **111**, 1250-1261.
30. Jin, H., Yoo, Y., Kim, Y., Kim, Y., Cho, J. and Lee, Y.S. (2020) Radiation-Induced Lung Fibrosis: Preclinical Animal Models and Therapeutic Strategies. *Cancers (Basel)*, **12**.
31. Curras-Alonso, S., Soulier, J., Defard, T., Weber, C., Heinrich, S., Laporte, H., Leboucher, S., Lameiras, S., Dutreix, M., Favaudon, V. *et al.* (2023) An interactive murine single-cell atlas of the lung responses to radiation injury. *Nat Commun*, **14**, 2445.

32. Groselj, B., Ruan, J.L., Scott, H., Gorrill, J., Nicholson, J., Kelly, J., Anbalagan, S., Thompson, J., Stratford, M.R.L., Jevons, S.J. *et al.* (2018) Radiosensitization In Vivo by Histone Deacetylase Inhibition with No Increase in Early Normal Tissue Radiation Toxicity. *Mol Cancer Ther*, **17**, 381-392.
33. He, X.Y., Xiang, C., Zhang, C.X., Xie, Y.Y., Chen, L., Zhang, G.X., Lu, Y. and Liu, G. (2015) p53 in the Myeloid Lineage Modulates an Inflammatory Microenvironment Limiting Initiation and Invasion of Intestinal Tumors. *Cell Rep*, **13**, 888-897.
34. Wang, K. and Tepper, J.E. (2021) Radiation therapy-associated toxicity: Etiology, management, and prevention. *CA Cancer J Clin*, **71**, 437-454.
35. Prieto-Callejero, B., Rivera, F., Fagundo-Rivera, J., Romero, A., Romero-Martin, M., Gomez-Salgado, J. and Ruiz-Frutos, C. (2020) Relationship between chemotherapy-induced adverse reactions and health-related quality of life in patients with breast cancer. *Medicine (Baltimore)*, **99**, e21695.
36. Tian, J., Doi, H., Saar, M., Santos, J., Li, X., Peehl, D.M. and Knox, S.J. (2013) Radioprotection and cell cycle arrest of intestinal epithelial cells by darinaparsin, a tumor radiosensitizer. *International journal of radiation oncology, biology, physics*, **87**, 1179-1185.
37. Mull, B.B., Livingston, J.A., Patel, N., Bui, T., Hunt, K.K. and Keyomarsi, K. (2020) Specific, reversible G1 arrest by UCN-01 in vivo provides cytostatic protection of normal cells against cytotoxic chemotherapy in breast cancer. *Br J Cancer*, **122**, 812-822.
38. Gunderson, C.C. and Moore, K.N. (2015) Olaparib: an oral PARP-1 and PARP-2 inhibitor with promising activity in ovarian cancer. *Future Oncol*, **11**, 747-757.
39. Veuger, S.J., Curtin, N.J., Richardson, C.J., Smith, G.C. and Durkacz, B.W. (2003) Radiosensitization and DNA repair inhibition by the combined use of novel inhibitors of DNA-dependent protein kinase and poly(ADP-ribose) polymerase-1. *Cancer Res*, **63**, 6008-6015.
40. Bartek, J. and Lukas, J. (2001) Pathways governing G1/S transition and their response to DNA damage. *FEBS Lett*, **490**, 117-122.
41. Ferreira, S. and Dutreix, M. (2019) DNA repair inhibitors to enhance radiotherapy: Progresses and limitations. *Cancer Radiother*, **23**, 883-890.
42. Jackson, I.L., Vujaskovic, Z. and Down, J.D. (2010) Revisiting strain-related differences in radiation sensitivity of the mouse lung: recognizing and avoiding the confounding effects of pleural effusions. *Radiat Res*, **173**, 10-20.
43. Crosby, L.M. and Waters, C.M. (2010) Epithelial repair mechanisms in the lung. *Am J Physiol Lung Cell Mol Physiol*, **298**, L715-731.

44. Chang, J., Garva, R., Pickard, A., Yeung, C.C., Mallikarjun, V., Swift, J., Holmes, D.F., Calverley, B., Lu, Y., Adamson, A. *et al.* (2020) Circadian control of the secretory pathway maintains collagen homeostasis. *Nat Cell Biol*, **22**, 74-86.
45. Marshman, E., Booth, C. and Potten, C.S. (2002) The intestinal epithelial stem cell. *Bioessays*, **24**, 91-98.
46. Parker, A., Maclaren, O.J., Fletcher, A.G., Muraro, D., Kreuzaler, P.A., Byrne, H.M., Maini, P.K., Watson, A.J. and Pin, C. (2017) Cell proliferation within small intestinal crypts is the principal driving force for cell migration on villi. *FASEB J*, **31**, 636-649.
47. Checker, R., Patwardhan, R.S., Jayakumar, S., Maurya, D.K., Bandekar, M., Sharma, D. and Sandur, S.K. (2021) Chemical and biological basis for development of novel radioprotective drugs for cancer therapy. *Free Radic Res*, **55**, 595-625.
48. Biau, J., Chautard, E., Verrelle, P. and Dutreix, M. (2019) Altering DNA Repair to Improve Radiation Therapy: Specific and Multiple Pathway Targeting. *Front Oncol*, **9**, 1009.
49. Jdey, W., Thierry, S., Popova, T., Stern, M.H. and Dutreix, M. (2017) Micronuclei Frequency in Tumors Is a Predictive Biomarker for Genetic Instability and Sensitivity to the DNA Repair Inhibitor AsiDNA. *Cancer Res*, **77**, 4207-4216.
50. Hume, S., Dianov, G.L. and Ramadan, K. (2020) A unified model for the G1/S cell cycle transition. *Nucleic Acids Res*, **48**, 12483-12501.
51. Engeland, K. (2022) Cell cycle regulation: p53-p21-RB signaling. *Cell Death Differ*, **29**, 946-960.
52. Ozaki, T. and Nakagawara, A. (2011) Role of p53 in Cell Death and Human Cancers. *Cancers (Basel)*, **3**, 994-1013.
53. Soubeyrand, S., Schild-Poulter, C. and Hache, R.J. (2004) Structured DNA promotes phosphorylation of p53 by DNA-dependent protein kinase at serine 9 and threonine 18. *Eur J Biochem*, **271**, 3776-3784.
54. Achanta, G., Pelicano, H., Feng, L., Plunkett, W. and Huang, P. (2001) Interaction of p53 and DNA-PK in response to nucleoside analogues: potential role as a sensor complex for DNA damage. *Cancer Res*, **61**, 8723-8729.
55. Shieh, S.Y., Ikeda, M., Taya, Y. and Prives, C. (1997) DNA damage-induced phosphorylation of p53 alleviates inhibition by MDM2. *Cell*, **91**, 325-334.
56. Ahuja, D., Saenz-Robles, M.T. and Pipas, J.M. (2005) SV40 large T antigen targets multiple cellular pathways to elicit cellular transformation. *Oncogene*, **24**, 7729-7745.
57. Kohli, M. and Jorgensen, T.J. (1999) The influence of SV40 immortalization of human fibroblasts on p53-dependent radiation responses. *Biochem Biophys Res Commun*, **257**, 168-176.

58. Shin, S.Y., Yoon, H., Ahn, S., Kim, D.W., Bae, D.H., Koh, D., Lee, Y.H. and Lim, Y. (2013) Structural properties of polyphenols causing cell cycle arrest at G1 phase in HCT116 human colorectal cancer cell lines. *Int J Mol Sci*, **14**, 16970-16985.
59. Yun, H.J., Jeoung, D.J., Jin, S., Park, J.H., Lee, E.W., Lee, H.T., Choi, Y.H., Kim, B.W. and Kwon, H.J. (2022) Induction of Cell Cycle Arrest, Apoptosis, and Reducing the Expression of MCM Proteins in Human Lung Carcinoma A549 Cells by Cedrol, Isolated from Juniperus chinensis. *J Microbiol Biotechnol*, **32**, 918-926.
60. Liu, Z., Liu, Q., Xu, B., Wu, J., Guo, C., Zhu, F., Yang, Q., Gao, G., Gong, Y. and Shao, C. (2009) Berberine induces p53-dependent cell cycle arrest and apoptosis of human osteosarcoma cells by inflicting DNA damage. *Mutat Res*, **662**, 75-83.
61. Wang, Z., Zhao, Z., Lu, J., Chen, Z., Mao, A., Teng, G. and Liu, F. (2015) A comparison of the biological effects of 125I seeds continuous low-dose-rate radiation and 60Co high-dose-rate gamma radiation on non-small cell lung cancer cells. *PLoS One*, **10**, e0133728.
62. Halacli, S.O., Canpinar, H., Cimen, E. and Sunguroglu, A. (2013) Effects of gamma irradiation on cell cycle, apoptosis and telomerase activity in p53 wild-type and deficient HCT116 colon cancer cell lines. *Oncol Lett*, **6**, 807-810.
63. Shen, H. and Maki, C.G. (2010) p53 and p21(Waf1) are recruited to distinct PML-containing nuclear foci in irradiated and Nutlin-3a-treated U2OS cells. *J Cell Biochem*, **111**, 1280-1290.
64. Shaltiel, I.A., Krenning, L., Bruinsma, W. and Medema, R.H. (2015) The same, only different - DNA damage checkpoints and their reversal throughout the cell cycle. *J Cell Sci*, **128**, 607-620.
65. Ljungman, M. (2000) Dial 9-1-1 for p53: mechanisms of p53 activation by cellular stress. *Neoplasia*, **2**, 208-225.
66. Hanahan, D. (2022) Hallmarks of Cancer: New Dimensions. *Cancer Discov*, **12**, 31-46.
67. Amoedo, N.D., Valencia, J.P., Rodrigues, M.F., Galina, A. and Rumjanek, F.D. (2013) How does the metabolism of tumour cells differ from that of normal cells. *Biosci Rep*, **33**.
68. Girard, P.M., Berthault, N., Kozlac, M., Ferreira, S., Jdey, W., Bhaskara, S., Alekseev, S., Thomas, F. and Dutreix, M. (2020) Evolution of tumor cells during AsiDNA treatment results in energy exhaustion, decrease in responsiveness to signal, and higher sensitivity to the drug. *Evol Appl*, **13**, 1673-1680.
69. Lacroix, M., Riscal, R., Arena, G., Linares, L.K. and Le Cam, L. (2020) Metabolic functions of the tumor suppressor p53: Implications in normal physiology, metabolic disorders, and cancer. *Mol Metab*, **33**, 2-22.
70. Pfister, N.T., Yoh, K.E. and Prives, C. (2014) p53, DNA damage, and NAD+ homeostasis. *Cell Cycle*, **13**, 1661-1662.

71. Liu, G., Betts, C., Cunoosamy, D.M., Aberg, P.M., Hornberg, J.J., Sivars, K.B. and Cohen, T.S. (2019) Use of precision cut lung slices as a translational model for the study of lung biology. *Respir Res*, **20**, 162.

72. Hietanen, K.E., Jarvinen, T.A., Huhtala, H., Tolonen, T.T., Kuokkanen, H.O. and Kaartinen, I.S. (2019) Treatment of keloid scars with intralesional triamcinolone and 5-fluorouracil injections - a randomized controlled trial. *J Plast Reconstr Aesthet Surg*, **72**, 4-11.

73. He, S., Roberts, P.J., Sorrentino, J.A., Bisi, J.E., Storrie-White, H., Tiessen, R.G., Makhuli, K.M., Wargin, W.A., Tadema, H., van Hoogdalem, E.J. *et al.* (2017) Transient CDK4/6 inhibition protects hematopoietic stem cells from chemotherapy-induced exhaustion. *Sci Transl Med*, **9**.

74. Noah, T.K., Donahue, B. and Shroyer, N.F. (2011) Intestinal development and differentiation. *Exp Cell Res*, **317**, 2702-2710.

75. Wei, L., Leibowitz, B.J., Wang, X., Epperly, M., Greenberger, J., Zhang, L. and Yu, J. (2016) Inhibition of CDK4/6 protects against radiation-induced intestinal injury in mice. *J Clin Invest*, **126**, 4076-4087.

76. Arroyo-Hernandez, M., Maldonado, F., Lozano-Ruiz, F., Munoz-Montano, W., Nunez-Baez, M. and Arrieta, O. (2021) Radiation-induced lung injury: current evidence. *BMC Pulm Med*, **21**, 9.

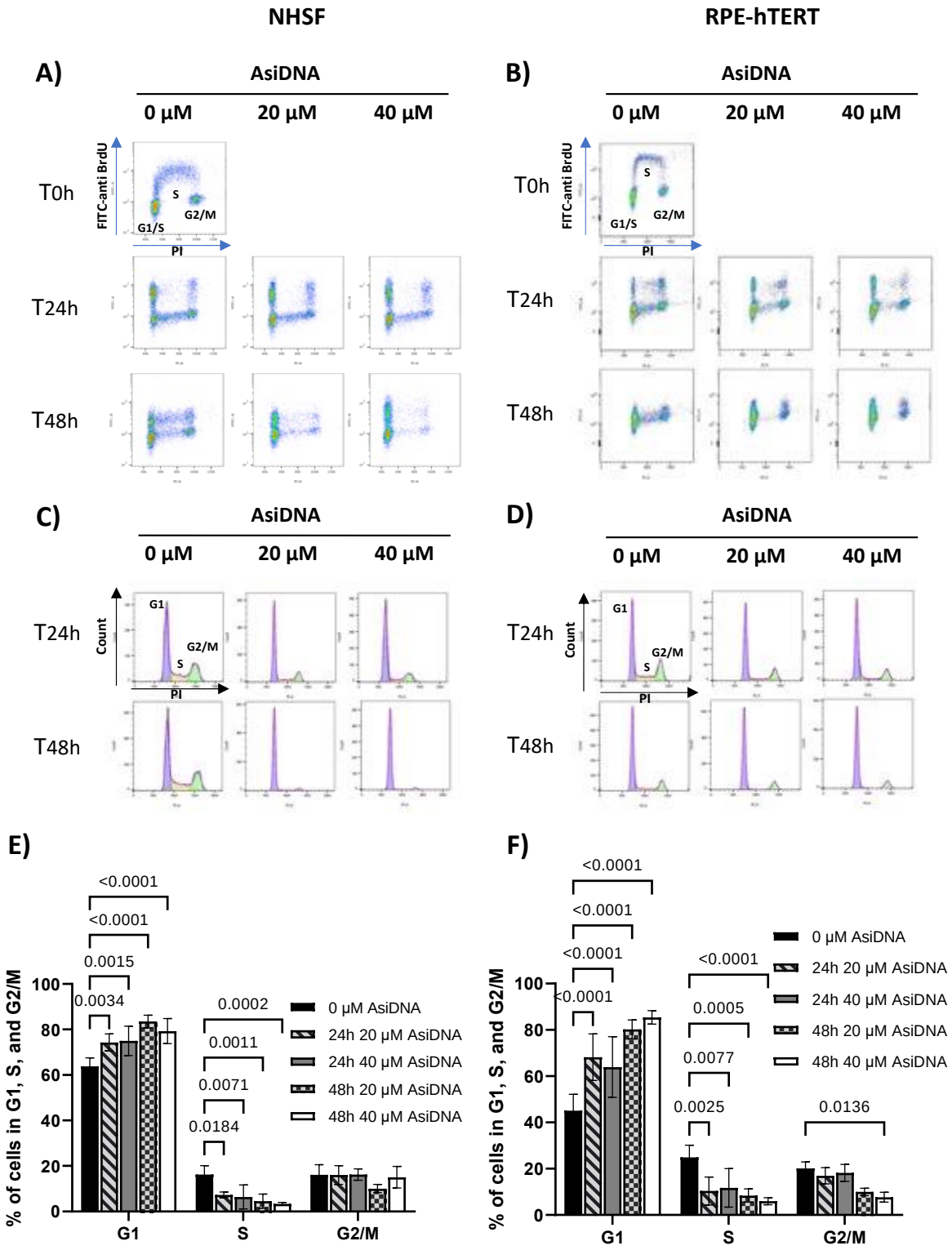
NHSF
RPE-hTERT
A)
B)
C)
D)
E)
F)
AsiDNA
0 µM
20 µM
40 µM
T0h
T24h
T48h
FITC-anti BrdU
PI
G1/S
S
G2/M
Count
G1
% of cells in G1, S, and G2/M
0 µM AsiDNA
24h 20 µM AsiDNA
24h 40 µM AsiDNA
48h 20 µM AsiDNA
48h 40 µM AsiDNA
<0.0001
0.0015
0.0034
0.0002
0.0011
0.0071
0.0184
0.0005
0.0077
0.0025
0.0136
G1
S
G2/M

Figure 1

Figure 1. AsiDNA™ induces G1/S arrest in healthy cells in vitro. Cells were pulse-labelled with BrdU following incubation with 20 µM and 40 µM of AsiDNA™ for 24h and 48h. Representative images of the bivariate analysis by flow cytometry of BrdU incorporation versus DNA content (PI) in (**A**) NHSF and (**B**) RPE-hTERT cells. The deconvolution of the cellular DNA content frequency histograms allows the identification of G1 phase (purple), S-phase (orange), and G2/M-phase (green) in (**C**) NHSF, and (**D**) RPE-hTERT cells. The percentage of cells in G1, S, and G2/M is shown in (**E**) for NHSF, and in (**F**) for RPE-hTERT cells. Data are expressed as mean ± standard deviation (n=3-5) with significance given by two-way ANOVA, Tukey's multiple comparison tests, and represented above the bar plots.

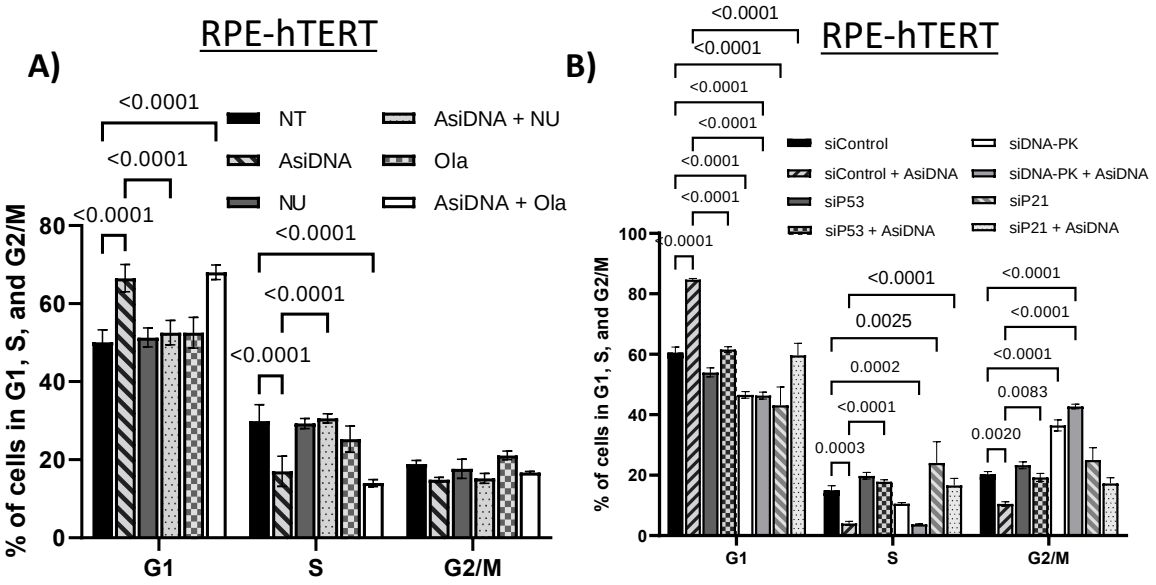
A)
RPE-hTERT
NT
AsiDNA
NU
AsiDNA + NU
Ola
AsiDNA + Ola
% of cells in G1, S, and G2/M
G1
S
G2/M
<0.0001
B)
RPE-hTERT
siControl
siControl + AsiDNA
siP53
siP53 + AsiDNA
siDNA-PK
siDNA-PK + AsiDNA
siP21
siP21 + AsiDNA
0.0025
0.0002
0.0003
0.0020
0.0083

Figure 2

Figure 2. AsiDNA™-induced G1/S arrest in vitro is dependent on DNA-PK, p53, and p21. (**A**) RPE-hTERT cells were pre-treated with olaparib (Ola) or NU7026 (NU) for 1h before addition of 20 µM AsiDNA™. The percentage of cells in G1, S, and G2/M was analysed by flow cytometry 48h post-AsiDNA™ treatment based on PI staining. (**B**) RPE-hTERT cells were transiently transfected with small inhibitory RNA (siRNA) silencing DNA-PKcs, p53, or p21 before being exposed to AsiDNA™ for 48h. The percentage of cells in G1, S, and G2/M was analysed by flow cytometry at the end of AsiDNA™ treatment based on PI staining. The data are expressed as mean ± standard deviation (n=3-5) with significance given by two-way ANOVA, Tukey's multiple comparison tests, and represented above the bar plots.

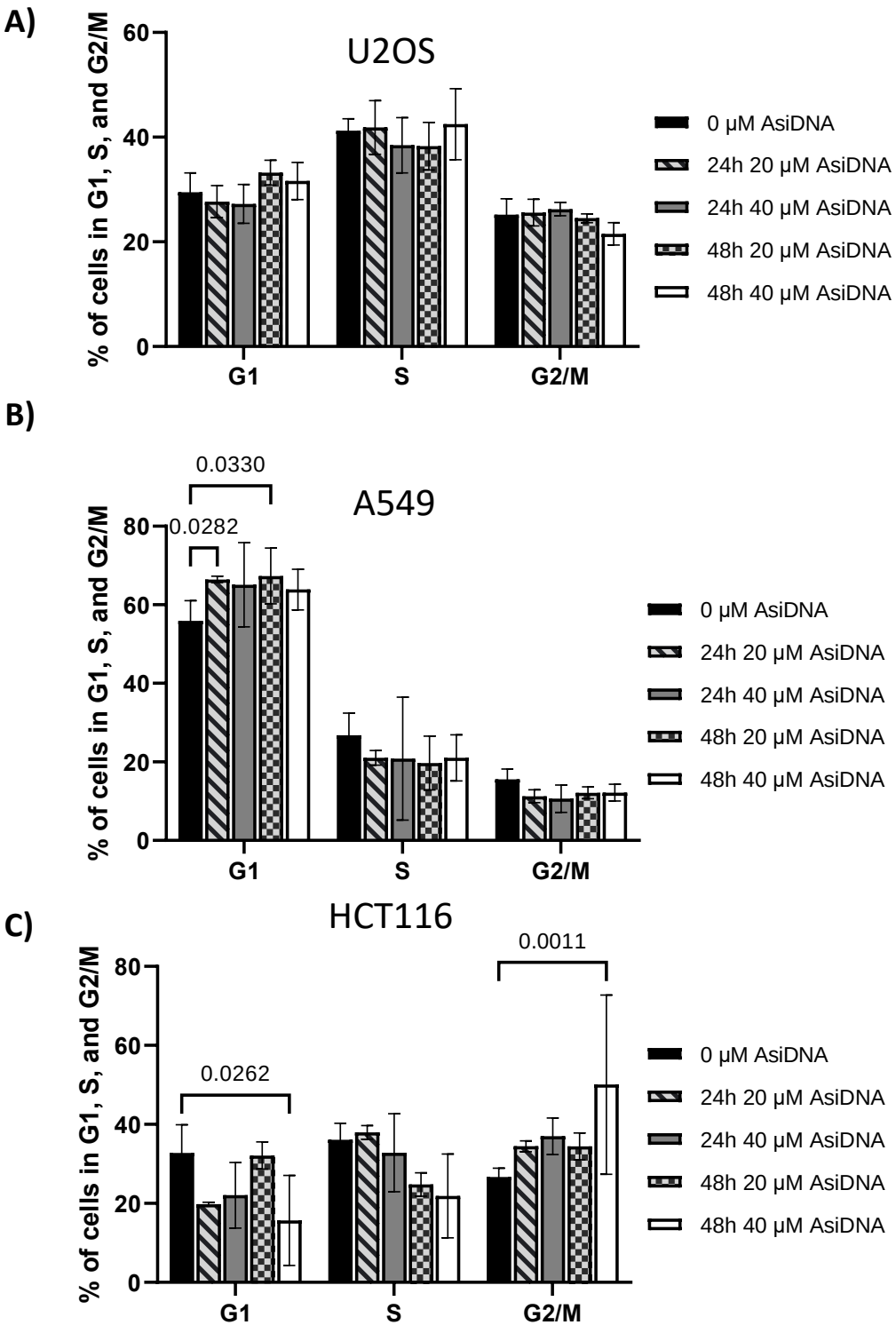
A)
U2OS
% of cells in G1, S, and G2/M
60
40
20
0
G1
S
G2/M
0 µM AsiDNA
24h 20 µM AsiDNA
24h 40 µM AsiDNA
48h 20 µM AsiDNA
48h 40 µM AsiDNA
B)
A549
0.0330
0.0282
80
60
40
20
0
C)
HCT116
0.0011
0.0262

Figure 3

Figure 3. No effect of AsiDNA™ on cell cycle progression in p53 proficient tumour cells in vitro. (**A**) U2OS, (**B**) A549 and (**C**) HCT116 tumour cells were exposed to 20 µM and 40 µM of AsiDNA™ for 24h and 48h. The percentage of cells in G1, S, and G2/M was analysed by flow cytometry 48h post-AsiDNA™ treatment based on PI staining. Data are expressed as mean ± standard deviation (n=3) with significance given by two-way ANOVA, Tukey's multiple comparison tests, and represented above the bar plots.

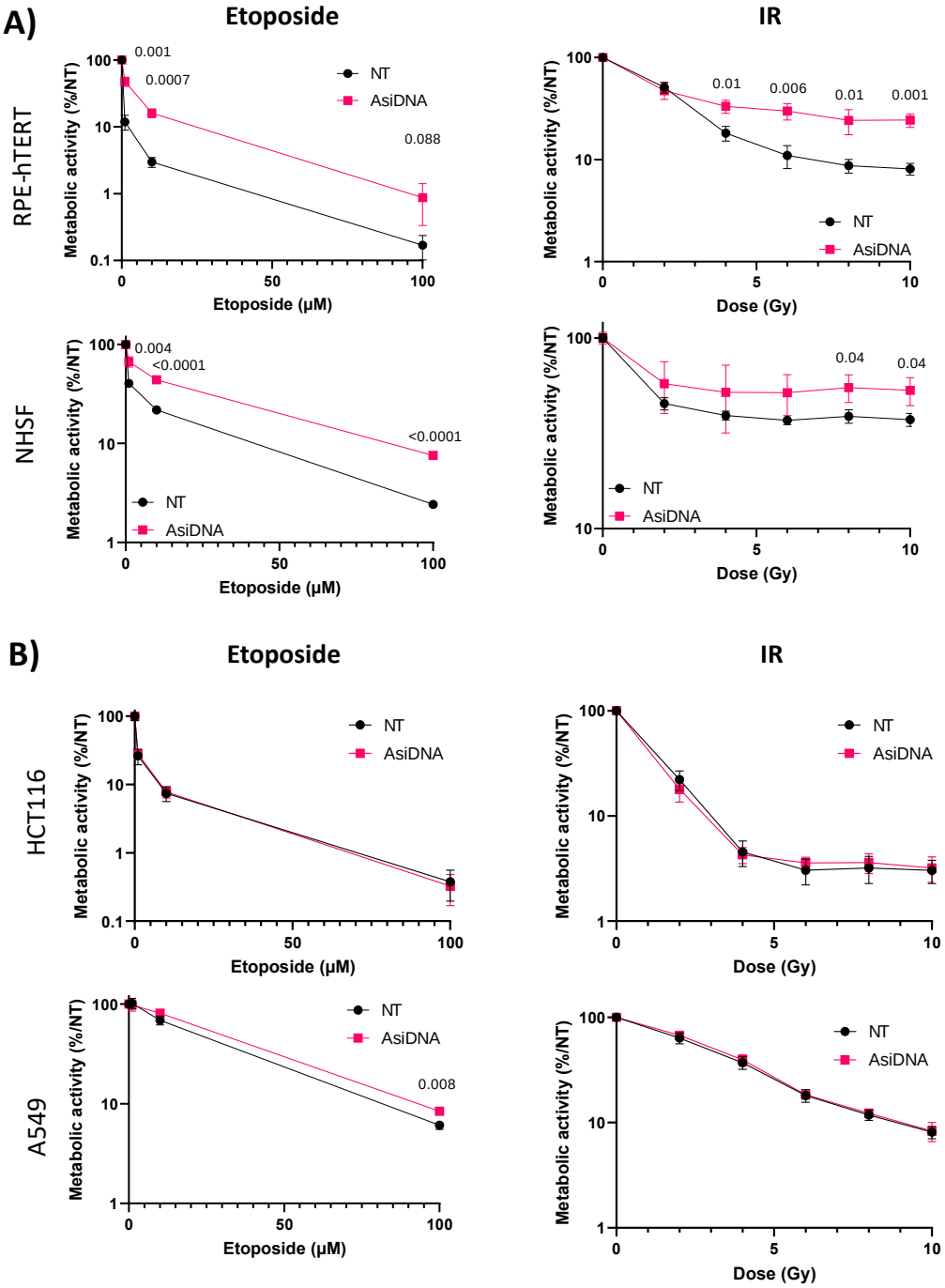
A)
Etoposide
IR
RPE-hTERT
NHSF
Metabolic activity (%/NT)
Etoposide (μM)
Dose (Gy)
NT
AsiDNA
0.001
0.0007
0.088
0.01
0.006
0.01
0.001
0.004
<0.0001
<0.0001
0.04
0.04
B)
Etoposide
IR
HCT116
A549
Metabolic activity (%/NT)
Etoposide (μM)
Dose (Gy)
NT
AsiDNA
0.008

Figure 4

Figure 4. AsiDNA™ treatment protects p53-proficient normal cells from chemo- and radio-therapy toxicity in vitro, with absence in tumour cells. (**A**) Normal (RPE-hTERT and NHSF) and (**B**) tumour (HCT116 and A549) cells were pre-treated with AsiDNA™ 24h before being co-exposed to various concentrations of etoposide (0-100 µM) or various doses of ionizing radiation (0-10 Gy). Cell viability was determined 6 days post-treatment using an ATP-based assay. Data are expressed as mean ± standard deviation (n=3) with significance given by unpaired T-test.

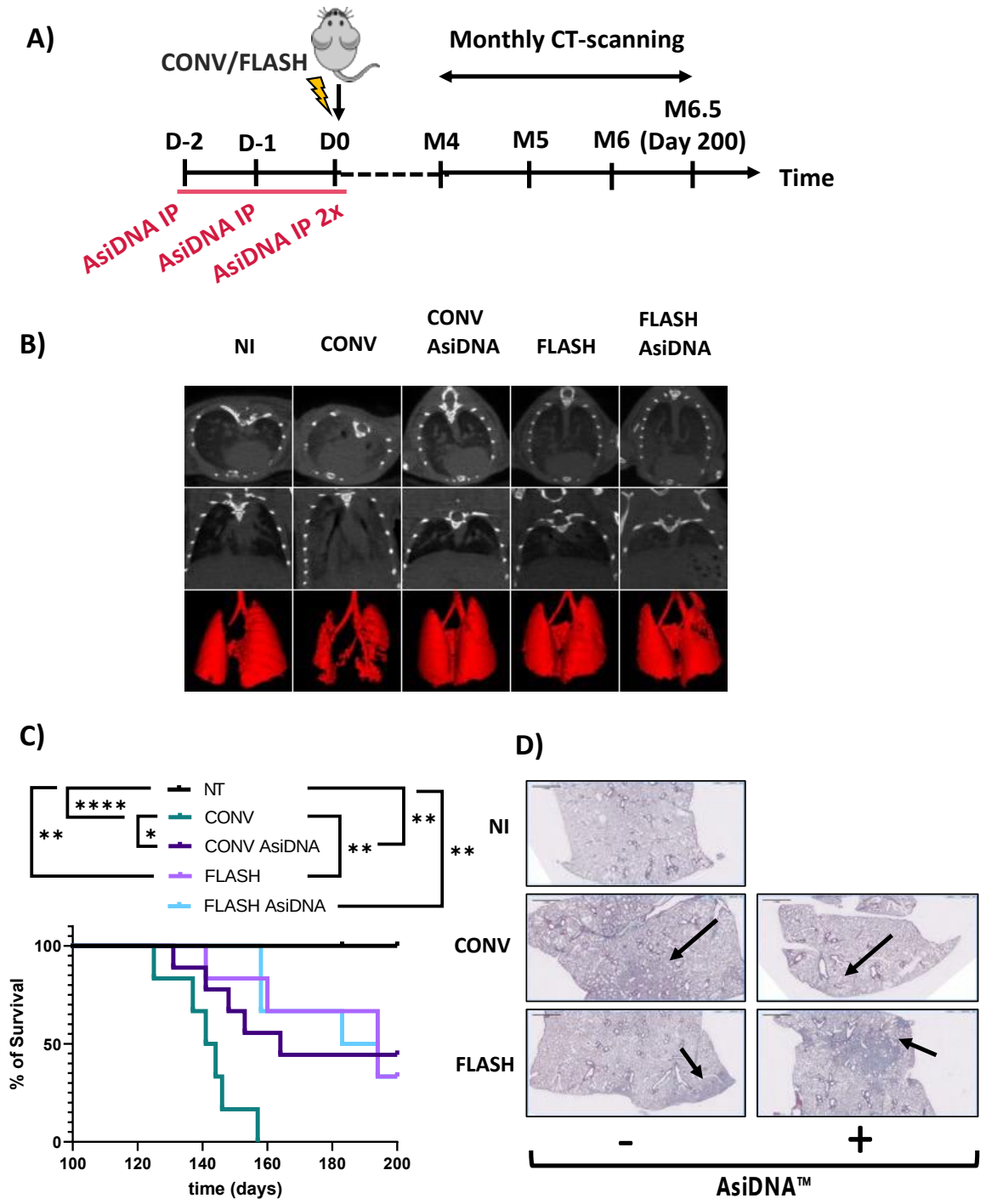
A)
CONV/FLASH
Monthly CT-scanning
M6.5
D-2
D-1
D0
M4
M5
M6
(Day 200)
Time
AsiDNA IP
AsiDNA IP
AsiDNA IP 2x
B)
NI
CONV
CONV AsiDNA
FLASH
FLASH AsiDNA
C)
NT
CONV
CONV AsiDNA
FLASH
FLASH AsiDNA
****
**
*
**
**
**
100
50
0
% of Survival
100
120
140
160
180
200
time (days)
D)
NI
CONV
FLASH
-
+
AsiDNA™

Figure 5

Figure 5. AsiDNA™ delayed the onset of radiation-induced pulmonary fibrosis in vivo. (**A**) Scheme of the experimental protocol. C57BL6/J mice were treated for 3 consecutive days with AsiDNA™ followed by 13 Gy CONV or FLASH irradiation of the thorax on the final day. Retro-orbital blood sampling was performed from 1 week up to 5 months post-treatment. CT scans were recorded from 4 to 6.5 months (sacrifice) post-treatment, and lobes of the lung were collected at the day of sacrifice (day 200) for histologic analysis. (**B**) Representative CT scans of lung from untreated mice (NI) or 5 months post-irradiation at 13 Gy CONV or FLASH radiotherapy alone or combined with AsiDNA™. Images are obtained using micro-CT imaging, high resolution, and 100 µm reconstruction by Molecubes software (Molecubes, Belgium). Representative images are shown with the CT axial slice (top), CT coronal slice (middle), and 3D lung reconstruction of connected Hounsfield Units -800 to -100 (bottom). Images were obtained using VivoQuant software (Konica Minolta Company, Japan). (**C**) Kaplan-Meier representation of animal surviving fraction displayed in days post-treatment. Data are expressed with significance given by survival, curve comparison, and Logrank test. Significance: not significant, ns; * $p<0.05$; ** $p<0.01$, *** $p<0.001$, **** $p<0.0001$. (**D**) Representative images of lung fibrosis stained with H&E, and Masson staining from each treatment group of experiment. Arrows indicate visible grade 5 Ashcroft fibrosis score. Scale bar = 200 µm.

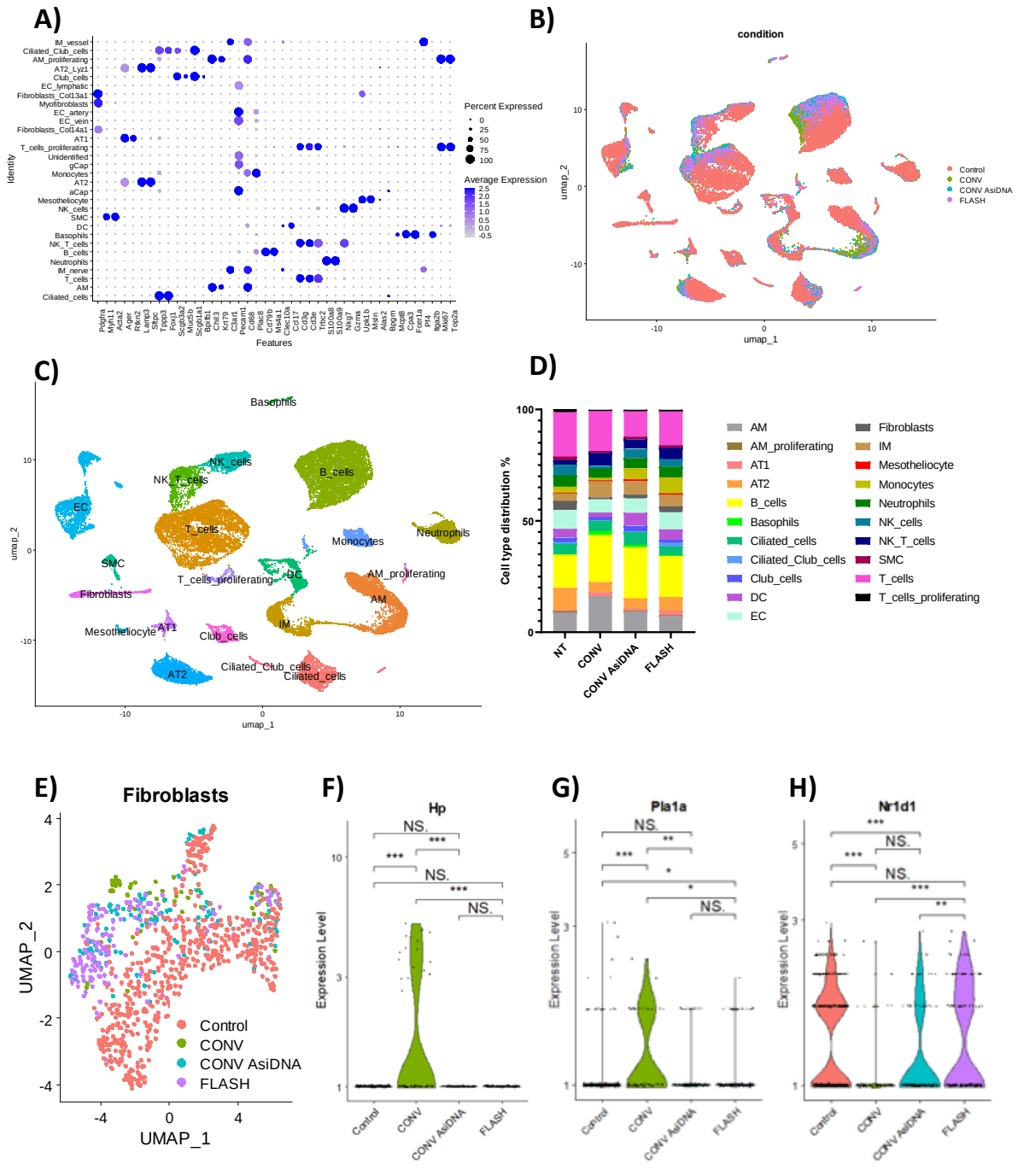
A)
B)
condition
Control
CONV
CONV AsiDNA
FLASH
umap_1
umap_2
C)
Basophils
NK_cells
NK_T_cells
B_cells
EC
T_cells
Monocytes
Neutrophils
SMC
T_cells_proliferating
DC
AM_proliferating
Fibroblasts
AM
IM
Mesothelicyte
AT1
Club_cells
AT2
Ciliated_Club_cells
Ciliated_cells
D)
Cell type distribution %
NT
CONV
CONV AsiDNA
FLASH
AM
AM_proliferating
AT1
AT2
B_cells
Basophils
Ciliated_cells
Ciliated_Club_cells
Club_cells
DC
EC
Fibroblasts
IM
Mesothelicyte
Monocytes
Neutrophils
NK_cells
NK_T_cells
SMC
T_cells
T_cells_proliferating
E)
Fibroblasts
UMAP_1
UMAP_2
F)
Hp
G)
Pla1a
H)
Nr1d1
Expression Level
NS.

Figure 6

Figure 6. **Single-cell RNA sequencing after irradiation and AsiDNA™ treatment**. Identification of cell populations represented by (**A**) Dot plot of marker expression utilized for cell population identification. (**B**) UMAP visualizing the identified cell clusters separating representation of the Control (red), CONV (green), AsiDNA™ + CONV (blue), and FLASH (purple) treated samples. (**C**) UMAP visualizing the identified cell types in all samples. The individual dots signify single cells. Additionally, the created clusters are established on transcriptome resemblances. (**D**) Cell population proportions after Control, CONV, AsiDNA™ + CONV and FLASH treatment. Fibroblast populations represented by (**E**) UMAP visualizing the identified fibroblast cluster separating representation of the Control (red), CONV (green), AsiDNA™ CONV (blue) and FLASH (purple) treated samples. Pro-fibrotic markers were examined using Violin plots with myofibroblast signature genes Hp (**F**) and Pla1a (**G**), and healthy collagen homeostasis Nr1d1 (**H**). CONV irradiation upregulates the expression of Hp and Pla1a and decreases the expression of Nr1d1 compared to FLASH, CONV + AsiDNA™, and NI control, significance given by Wilcox test. (NS, p-value > 0.05; *, p-value < 0.05; **, p-value < 0.01; ***, p-value < 0.001; ****, p-value < 0.0001).

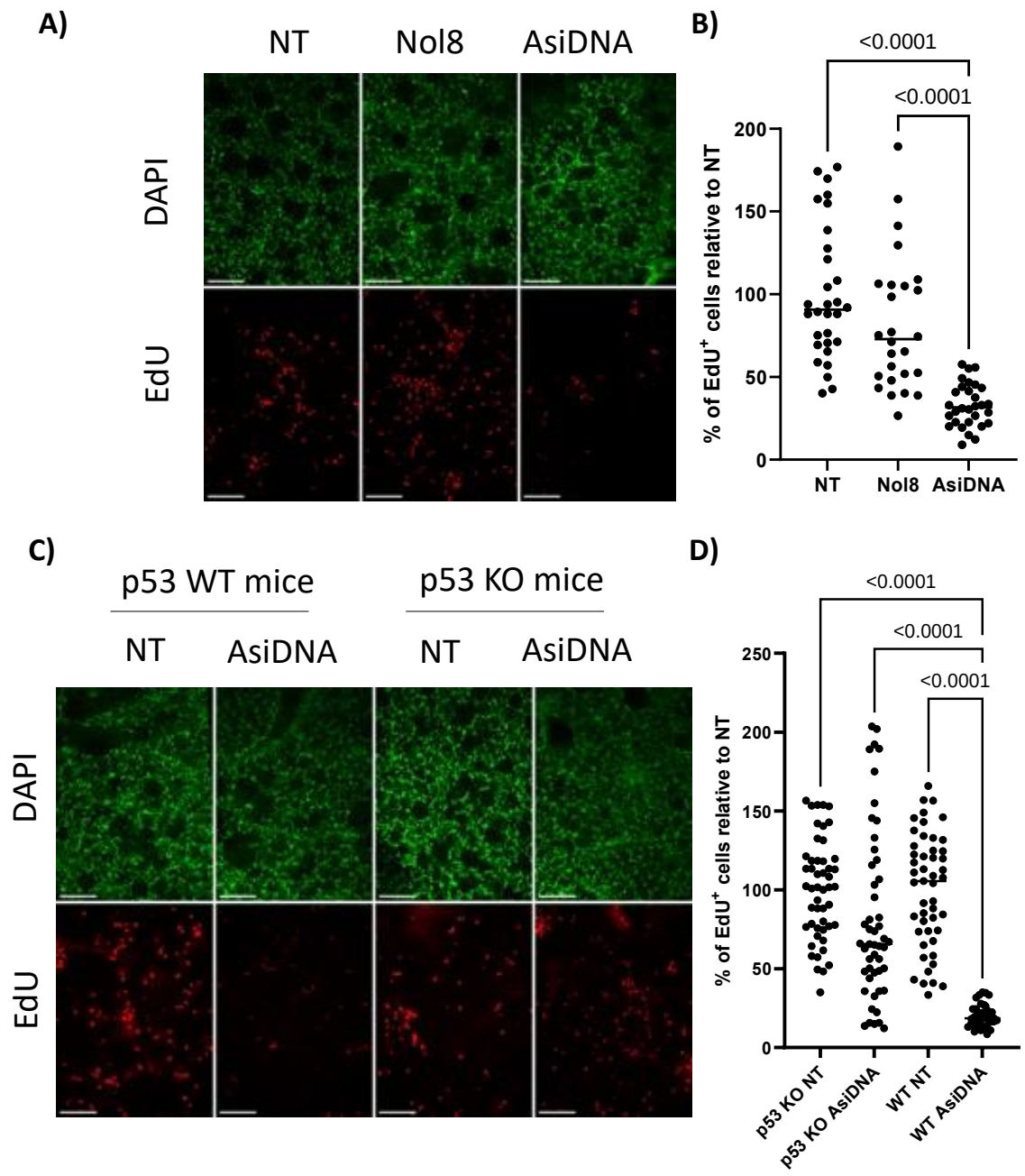
A)
NT
Nol8
AsiDNA
DAPI
EdU
B)
<0.0001
<0.0001
% of EdU+ cells relative to NT
200
150
100
50
0
NT
Nol8
AsiDNA
C)
p53 WT mice
p53 KO mice
NT
AsiDNA
NT
AsiDNA
DAPI
EdU
D)
<0.0001
<0.0001
<0.0001
% of EdU+ cells relative to NT
250
200
150
100
50
0
p53 KO NT
p53 KO AsiDNA
WT NT
WT AsiDNA

Figure 7

Figure 7. AsiDNA™ induces a DNA-PK and p53-dependent cell cycle arrest in the ex vivo model of precision cut lung slices. Precision cut lung slices (PCLS) were derived from C57BL6/J WT or p53 knock-out mice and treated with EdU upon 24h of AsiDNA™ or Nol8 treatment. (**A**) Representative images of PCLS derived from WT mice (N=2) with DAPI and EdU detection after AsiDNA™ or Nol8 treatment. (**B**) EdU positive cells detected after AsiDNA™ or Nol8 treatment (N=2). EdU was detected in 6 slices per condition with 5 readouts per slice. (**C**) Representative Images of PCLS derived from WT (N=2) and p53 knock-out mice (N=2) with DAPI and EdU detection after AsiDNA™ treatment. (**D**) EdU positive cells detected after AsiDNA™ or Nol8 treatment of two WT mice. EdU was detected in 8-10 slices per condition with 5 readouts per slice. Data are expressed as mean ± standard deviation with significance given by two-way ANOVA, Tukey's multiple comparison test and represented above the bar plots. Arrows point to the intestinal crypts. Scale bar = 100 µm.

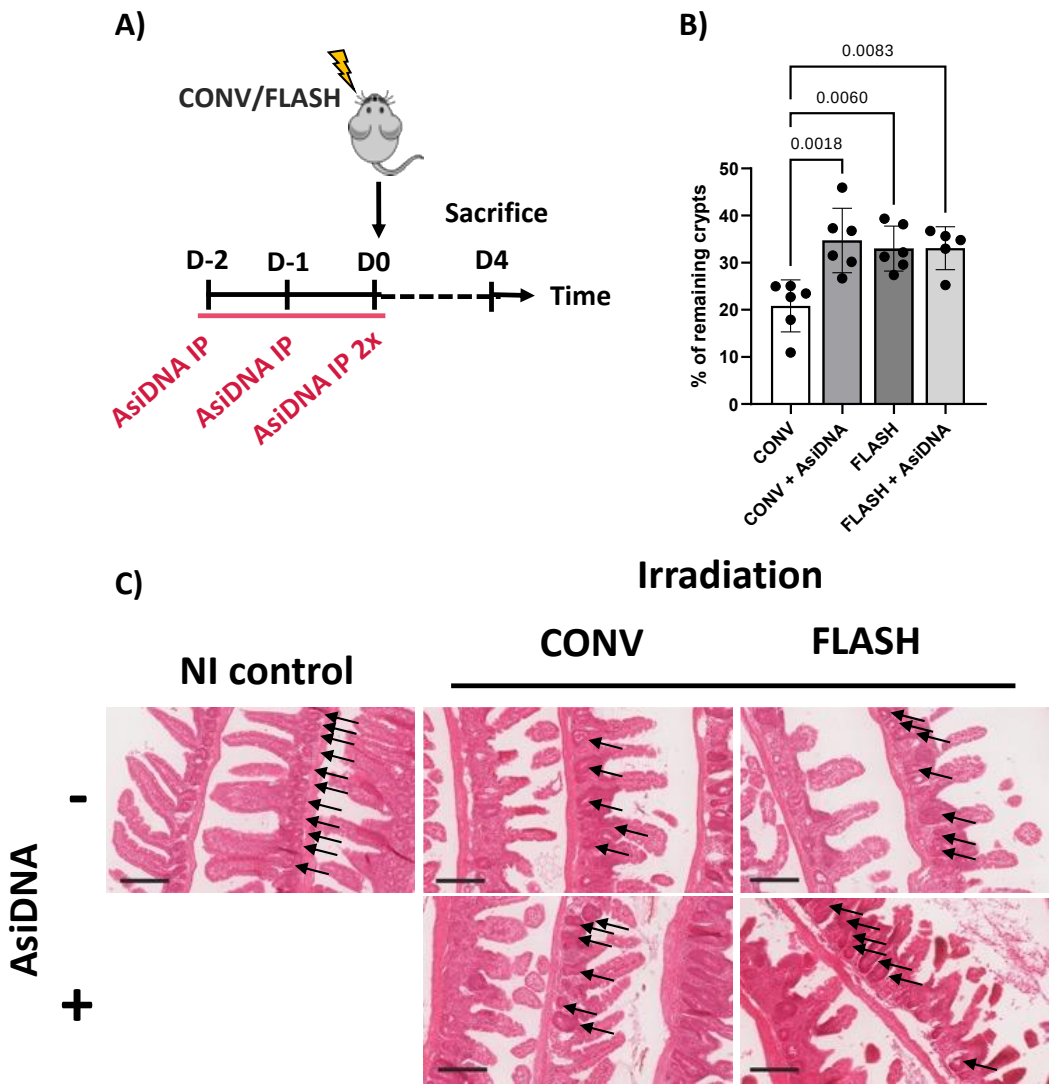
A)
CONV/FLASH
Sacrifice
D-2
D-1
D0
D4
Time
AsiDNA IP
AsiDNA IP
AsiDNA IP 2x
B)
0.0083
0.0060
0.0018
% of remaining crypts
50
40
30
20
10
0
CONV
CONV + AsiDNA
FLASH
FLASH + AsiDNA
C)
Irradiation
NI control
CONV
FLASH
AsiDNA
-
+

Figure 8

Figure 8. AsiDNA™ protects intestinal crypts from radiation toxicity. (**A**) Scheme of the experimental treatment timeline. C57BL6/J mice were treated for 3 consecutive days with AsiDNA™ followed by 10 Gy CONV or FLASH irradiation of the abdomen on the final day. (**B**) Small intestinal crypt survival of C57BL6/J mice 4 days after abdominal radiation, normalised to non-irradiated control mice. Data are expressed as mean ± standard deviation (n=5-6) with significance given by one-way ANOVA, Tukey's multiple comparison test and represented above the bar plots. (**C**) Representative images of intestinal rolls stained with H&E from each treatment group. Scale bar = 200 µm.

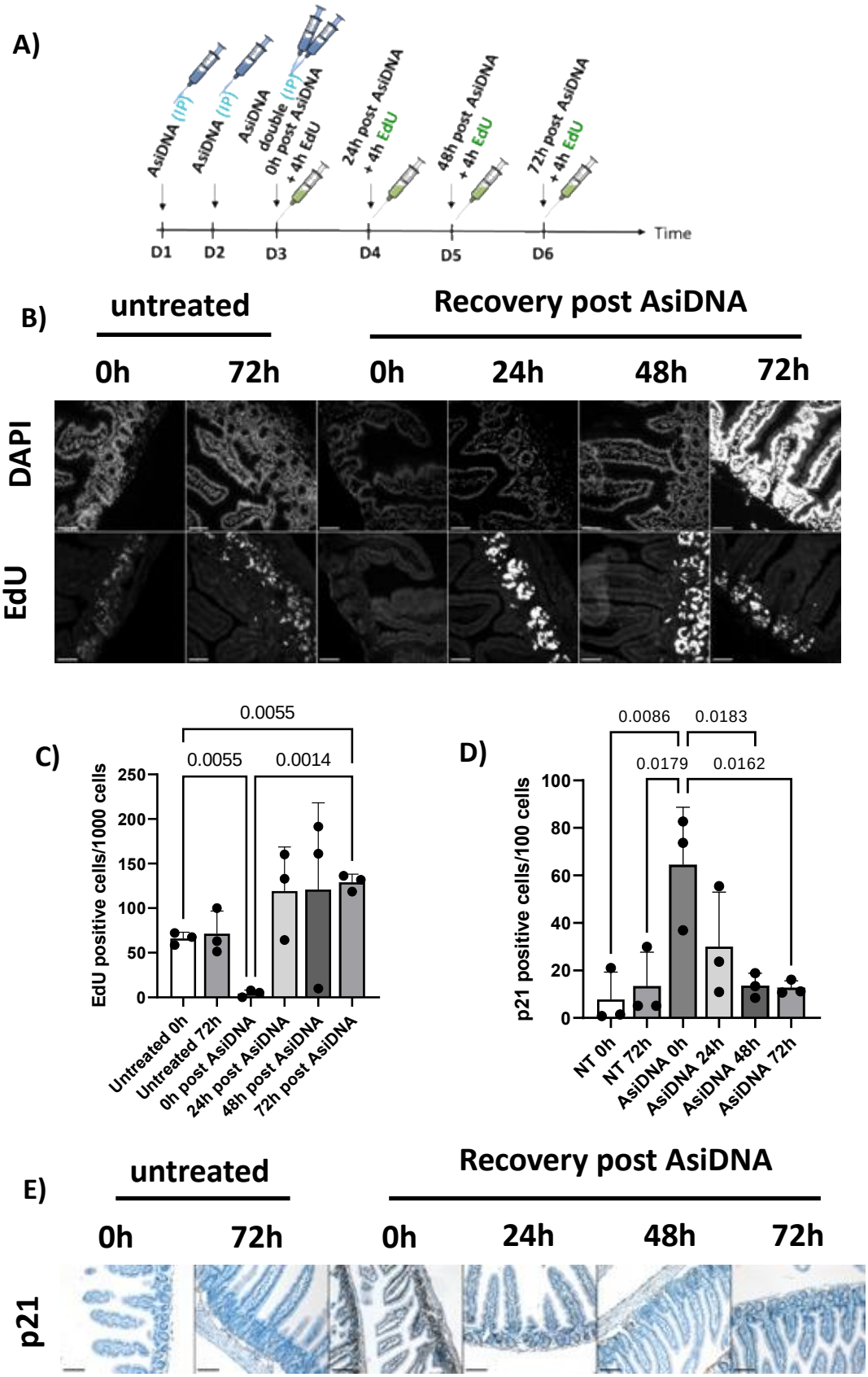
A)
AsiDNA (IP)
AsiDNA (IP)
AsiDNA double (IP) 0h post AsiDNA + 4h EdU
24h post AsiDNA + 4h EdU
48h post AsiDNA + 4h EdU
72h post AsiDNA + 4h EdU
Time
D1
D2
D3
D4
D5
D6
B)
untreated
Recovery post AsiDNA
0h
72h
0h
24h
48h
72h
DAPI
EdU
C)
0.0055
0.0055
0.0014
EdU positive cells/1000 cells
250
200
150
100
50
0
Untreated 0h
Untreated 72h
0h post AsiDNA
24h post AsiDNA
48h post AsiDNA
72h post AsiDNA
D)
0.0086
0.0183
0.0179
0.0162
p21 positive cells/100 cells
100
80
60
40
20
0
NT 0h
NT 72h
AsiDNA 0h
AsiDNA 24h
AsiDNA 48h
AsiDNA 72h
E)
untreated
Recovery post AsiDNA
0h
72h
0h
24h
48h
72h
p21

Figure 9

Figure 9. AsiDNA™-induced cell cycle arrest is reversible upon release of AsiDNA™ in intestinal normal tissue. (**A**) Scheme of the experimental treatment timeline. C57BL6/J mice were treated for 3 consecutive days with AsiDNA™ followed by 0h-72h of recovery. Thereafter, mice received EdU for 4h prior to sacrifice. (**B**) Representative images of intestinal rolls stained with DAPI and Click-iT™ EdU AlexaFluor™ 488 for each treatment group. (**C**) EdU positive cells per 1000 detected cells in small intestinal crypts after AsiDNA™ treatment. A total number of 14000-16000 cells per mouse were scored. Data are expressed as mean ± standard deviation (n=3) with significance given by one-way ANOVA, Brown-Forsythe and Welch tests. Scale bar = 50 µm. (**D**) p21 positive cells per 100 detected cells in small intestinal crypts after AsiDNA™ treatment. A total number of 6000-11000 cells per mouse were scored. Data are expressed as mean ± standard deviation (n=3) with significance given by one-way ANOVA, Tukey's multiple comparison test and represented above the bar plots. (**E**) Representative images of intestinal rolls stained by immunohistochemistry to detect p21 expression in each treatment group. Scale bar = 200 µm.

SUPPLEMENTARY MATERIALS AND METHODS

Transfection

Prior to RNA interference, cells were attached overnight in 6-well plates for RPE-hTERT cells with or without shp53 and in 60mm2 dishes for NHSF. P53 siRNA low GC; GAG UGG AAG GAA AUU UGC UGG A (20 nM, TP53HSS186390, Invitrogen) GAACUUCGACUUUGUCACCGAGACA (40 nM, CDKNIAVHS40209, Invitrogen) or DNA-PK siRNA mix (PRKDC, 18 nM s773 GCGUUGGAGUGCUACAACATT, 18 nM s774 GCGCUUUUCUGGGUGAACUTT, Thermofisher Scientific) were supplemented to Opti-MeM serum free medium (Gibco). RNA interference was performed following manufacturer's instructions for INTERFERin (Polyplus transfection) with medium replacement 7h post transfection. AsiDNA™ treatment on transfected cells was performed for 48h starting at 24h post transfection.

PCLS collection

The PCLS were obtained from the lungs of female C57BL/6J mice or male and female C57BL/6J p53 Knock-out mice. Mice were sacrificed by cervical dislocation. Low-melting agarose/medium solution (Invitrogen) of 2,5% was injected into the trachea and the lung lobes were isolated followed by the generation of equal tissue pieces using the surgical punch (8 mm). The isolated tissue is placed in plastic moulds, containing 5% agarose solution. PCLS were generated in DMEM/F-12 medium supplemented with 1% P/S, 1% SVF, 1% L-glutamine and 1% NEAA, using Leica VT 1000 S vibrating blade microtome (Leica Biosystems B.V., Amsterdam, the Netherlands) with a cutting frequency of 90 Hz at position 9 and sectioning speed of 2.25 mm/s at position 9 creating 300 µm-thick lung slices. The slices were placed at 37°C for 30 minutes (to eliminate agarose around the slice) and washed with fresh medium before being transferred to clean culture medium and maintained up to 48h in a humidified incubator in an atmosphere of 5% CO2 at 37°C. AsiDNA™ or Nol8 treatment with 5µM was performed after the additional wash with fresh medium, followed by the supplementation of 10µM EdU 24h post the start of the AsiDNA™ treatment. The slices are fixed with 4% PFA (Electron Microscopy Sciences) at RT overnight in the dark and permeabilized with Saponin. The EdU detection protocol (647nm) and

using EdU DetectPro Imaging kit Imaging (488 or 647nm, BCK-EdUPro-IM647/BCK488-IV-IM-S, Baseclick) and viewed with the Inverted spinning disk-TIRF-FRAP (Nikon) using 300 ms emission and 30 % laser, DAPI (405 nm), 400 ms emission and 70 % laser, x10 objective with 50 stacks of 3 µm. Data analysis was performed using IMARIS with spot function and PRISM software.

MIC-MAQ macro

EdU intestine images were generated using 3D SIM microscopy, 40x magnification. Images were processed in Image J with subtraction of background noise. The masks were generated and established on DAPI-positive cells. Nuclei parameters: cellpose model cyto2, cellpose cell diameter 80, exclude on edges yes, SPOT EdU Parameters, background reduction of 40 pixels, cellpose segmentation on and pixel diameter of 80. Total detected nuclei and EdU-positive nuclei were calculated. Ki67 intestine images were generated and processed as described above. P21 intestine images were generated using a Zeiss microscope, 20x magnification. Images were processed in Image J by image colour deconvolution, separating nuclei and p21 staining, and image inverting. Additional processing occurred as described above.

Supplementary data Table 1: Information in vivo thorax irradiation setup parameters

Mode	**CONV**	**FLASH**
Energy (MeV)	5	5
Applicator type (mm diameter)	50	50
Collimator type	Graphite	Graphite
Field dimension (mm^2)	18x26	18x26
Detector type	Gafchromic EBT-XD	Gafchromic EBT-XD
Skin-collimator Distance (mm)	35	35
Depth of measured dose (mm)	0	0

Frequency (Hz)	**10**	**100**
Dose rate (Gy/s)	0.12-0.13	399-498
Dose/pulse (Gy/p)	0.0117-0.0130	3.0-3.7
Pulse length measured (µs)	-	2.78-3.25
No. of pulses	1080-1296	4
Treatment time (s)	107.9-129.4	0.03

Supplementary data Table 2: Information in vivo intestine irradiation setup parameters

Mode	**CONV**	**FLASH**
Energy (MeV)	6	6
Applicator type (mm diameter)	50	50
Collimator type	Brass	Brass
Field dimension (mm^2)	30x33	30x33
Detector type	Gafchromic EBT-XD	Gafchromic EBT-XD
Skin-collimator Distance (mm)	0	0
Depth of measured dose (mm)	15	15
Given dose (Gy)	10	10
Frequency (Hz)	25	300
Dose rate (Gy/s)	0.11-0.14	3000
Dose/pulse (Gy/p)	4-6 x 10^{-3}	5
Pulse length measured (µs)	3.5	3.5
No. of pulses	1750-2250	2

Supplementary data Table 3: Ashcroft fibrosis scoring after thorax irradiation in mice

Mice ID (LL= Left lobe, SL= Superior lobe)	Treatment	Ashcroft fibrosis score	Additional observations	Day of sacrifice	Average day of sacrifice post-treatment
3293 SL	NT	0		158	
3294 LL	NT	0		158	
3295 LL	NT	0		158	
3341 SL	NT	0		200	
3342 LL	NT	0		200	
3343 LL	NT	0		200	
4103 LL	NT	0		200	
4104 LL	NT	0		200	
4105 LL	NT	0		200	
3305 LL	CONV 13 Gy	4-5		142	
3306 LL	CONV 13 Gy	5	ossification	147	
3307 LL	CONV 13 Gy	5		145	143 ± 11
3308 SL	CONV 13 Gy	5		126	
3309 LL	CONV 13 Gy	4-5		158	
3310 LL	CONV 13 Gy	5		138	
3317 LL	CONV 13 Gy AsiDNA	4-5		165	
3318 LL	CONV 13 Gy AsiDNA	5		154	

3319 LL	**CONV 13 Gy AsiDNA**	**4**		**200**	**171 ± 34**
3320 LL	CONV 13 Gy AsiDNA	5		132	
3321 LL	CONV 13 Gy AsiDNA	5		142	
3322 LL	CONV 13 Gy AsiDNA	5		149	
3306 LL	CONV 13 Gy AsiDNA	2		200	
3307 LL	CONV 13 Gy AsiDNA	5		200	
3308 LL	CONV 13 Gy AsiDNA	4		200	
3353 LL	FLASH 13 Gy	5		194	
3354 LL	FLASH 13 Gy	5-6		141	
3356 LL	FLASH 13 Gy	5		200	186 ± 25
3357 LL	FLASH 13 Gy	5		200	
3358 LL	FLASH 13 Gy	5-6		194	
3365 LL	FLASH 13 Gy AsiDNA	5	many macrophages	183	
3366 LL	FLASH 13 Gy AsiDNA	6		200	
3367 LL	FLASH 13 Gy AsiDNA	6		194	182 ± 20
3368 LL	FLASH 13 Gy AsiDNA	5-6		158	

Ashcroft fibrosis score

- Grade 0: normal lung
- Grade 1: small fibrous changes in the alveoli of the lung
- Grade 2: presence of some fibrous changes
- Grade 3: contiguous fibrous modification
- Grade 4: small masses of fibrosis
- Grade 5: confluent fibrotic masses
- Grade 6: large contiguous masses of fibrosis
- Grade 7: confluent masses of fibrosis extending into almost all the parenchyma
- Grade 8: complete obliteration by fibrosis

MRC5 primary cells

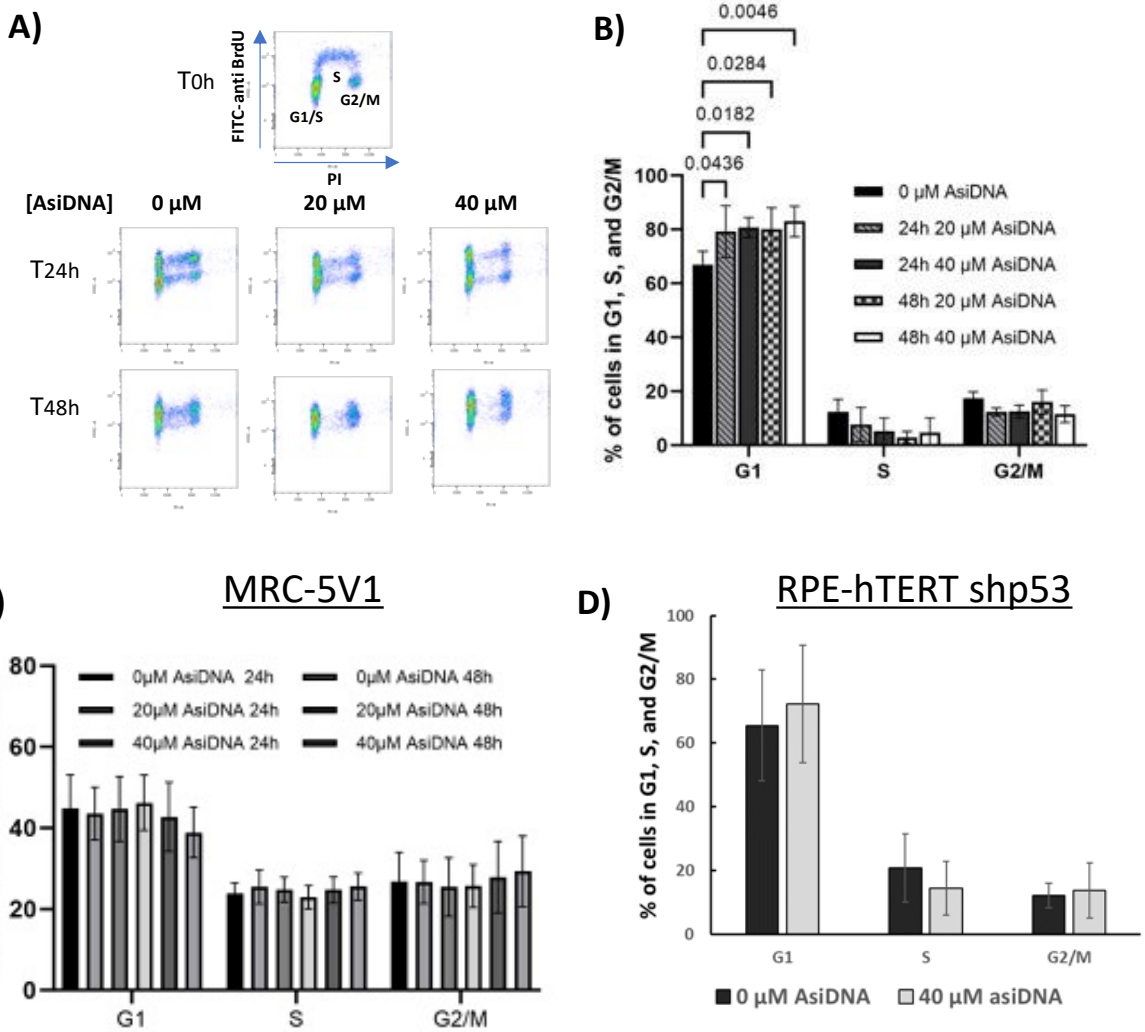

Supplementary Figure S1

Supplementary Figure 1. Effect of AsiDNA™ on MRC5 primary and MRC-5V1 cell cycle progression. Cells were pulse-labeled with BrdU following incubation with 20 µM and 40 µM of AsiDNA™ for 24h and 48h. Representative images of the bivariate analysis by flow cytometry of BrdU incorporation versus DNA content (PI) in (**A**) MRC5 primary. The percentage of cells in G1, S, and G2/M is shown in (**B**) MRC5 primary cells, (**C**) MRC5-V1 cells and (**D**) RPE-hTERT shp53 cells. Data are expressed as mean ± standard deviation (n=3) with significance given by two-way ANOVA, Tukey's multiple comparison test, and represented above the bar plots.

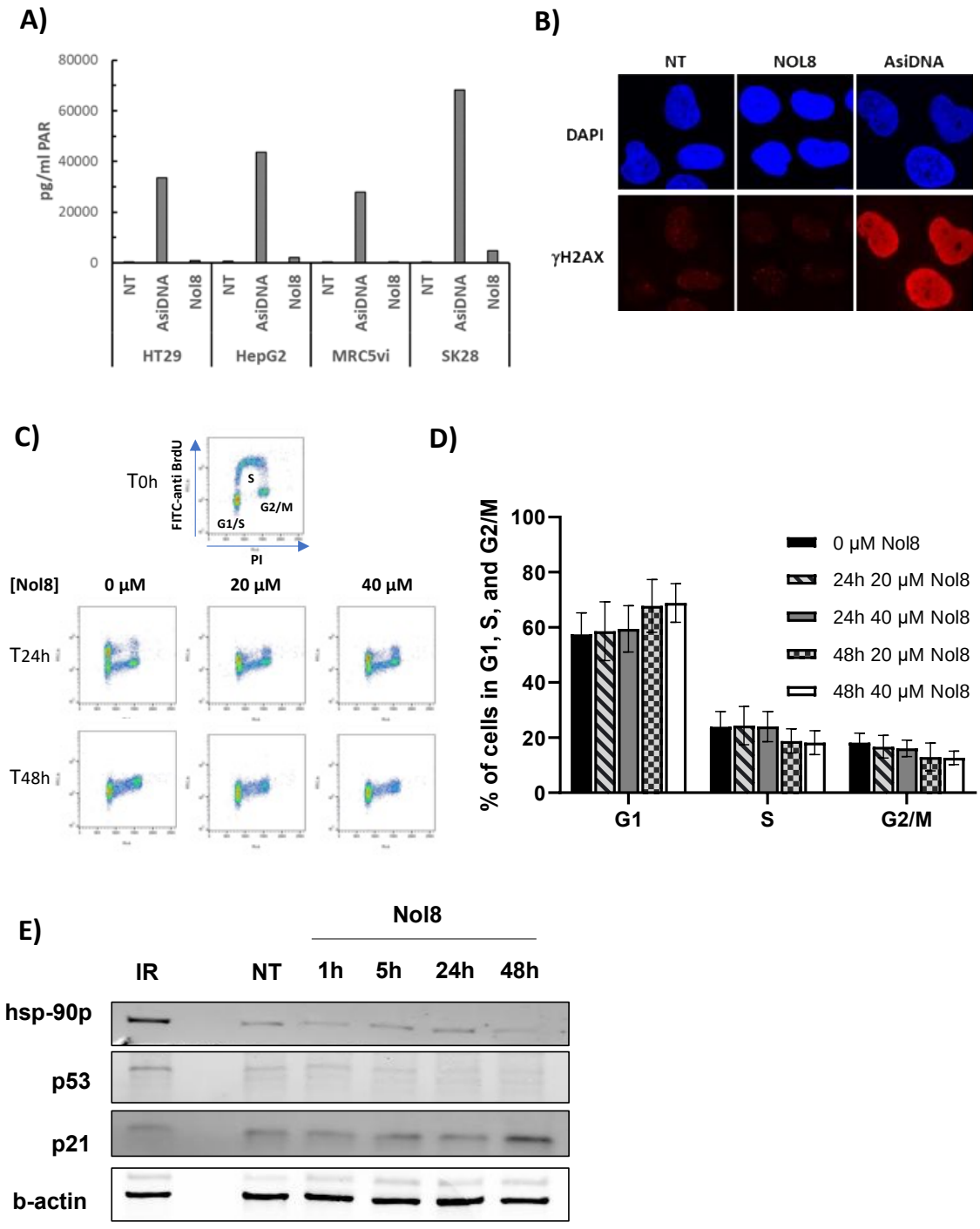

Supplementary Figure S2

Supplementary Figure 2. No effect of Nol8 treatment on RPE-hTERT cell cycle progression. (**A**) PARylation after AsiDNA™ and Nol8 treatment in various cell lines. (**B**) Gamma-H2AX immunofluorescence post AsiDNA™ or Nol8 treatment. (**C**) Representative images of the bivariate analysis by flow cytometry of BrdU incorporation versus DNA content (PI) in RPE-hTERT cells upon Nol8 treatment. (**D**) The percentage of cells in G1, S, and G2/M is shown in RPE-hTERT cells upon Nol8 treatment. Data are expressed as mean ± standard deviation (n=3) with significance given by two-way ANOVA, Tukey's multiple comparison test, and represented above the bar plots. (**E**) Western blot analysis of RPE-hTERT cells upon Nol8 treatment.

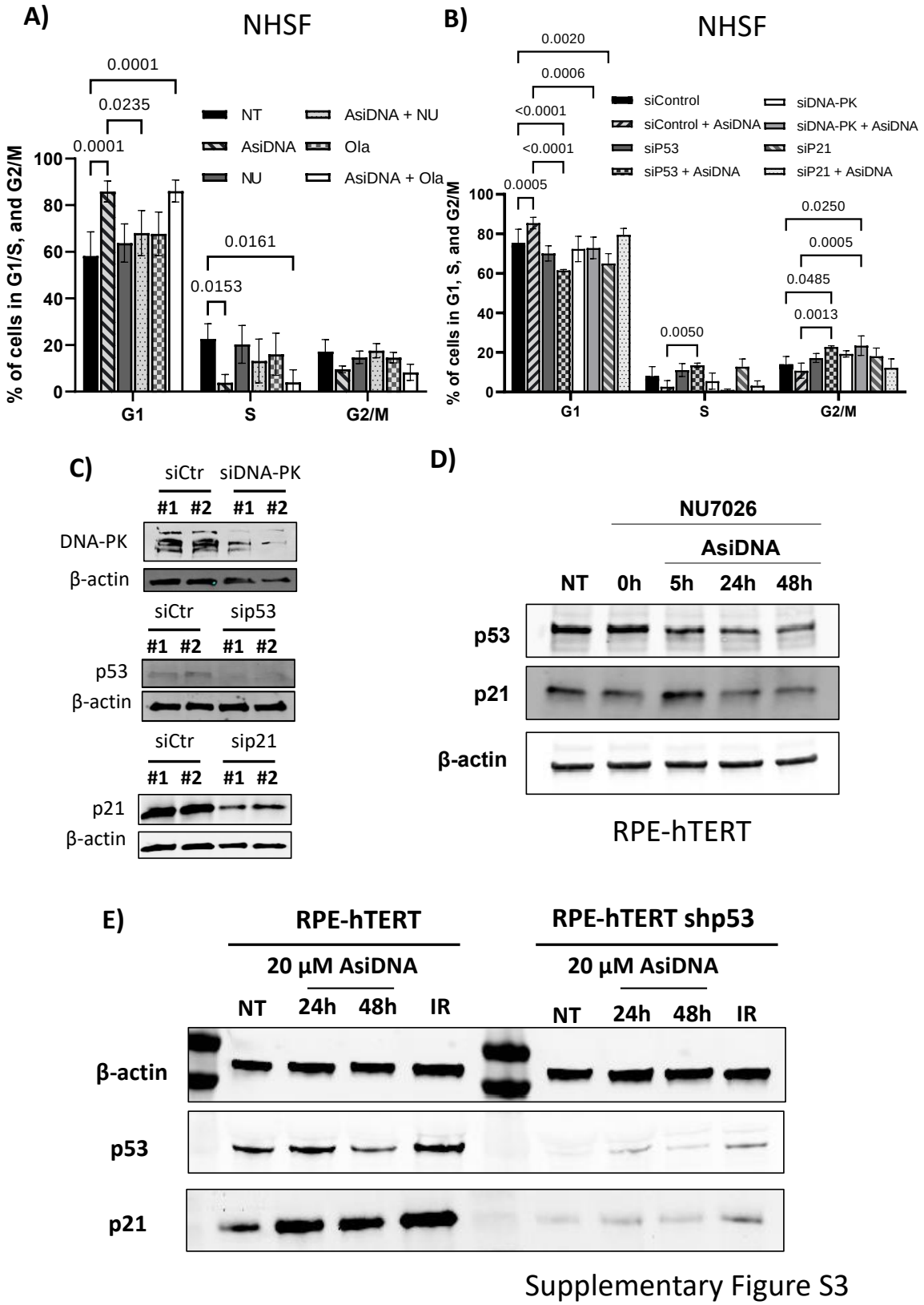

Supplementary Figure S3

Supplementary Figure 3. AsiDNA™ induced cell cycle arrest is dependent on DNA-PK and p53. Mean percentage of NHSF cells per cell cycle phase with combined (**A**) AsiDNA™/NU or AsiDNA™/Olaparib, and (**B**) AsiDNA™/sip53 or AsiDNA™/sip21 or AsiDNA™/siDNA-PK were measured by PI staining and analysed by FACS. (**C**) Mean percentage of RPE-hTERT shp53 cells per cell cycle phase after AsiDNA™ treatment. Data are expressed as mean ± standard deviation (n=3-4) with significance given by two-way ANOVA, Tukey's multiple comparison test, and represented above the bar plots. (**C**) Western blot analysis of the down expression of DNA-PKcs, p53, and p21 expression following transfection of siRNA DNA-PKcs, siRNA p53, and siRNA p21 in RPE-hTERT. #1 and #2 represent independent replicates. (**D**) Western blot analysis of p53 and p21 expression levels in RPE-hTERT cells upon combined AsiDNA™ with NU7026 for 5h, 24h and 48h. (**E**) Western blot analysis of p53 and p21 expression level in RPE-hTERT cells proficient and deficient for p53 in response to AsiDNA™ for 24h and 48h. In (**C**), (**D**) and (**E**), β-actin was used as a loading control. Gels are representatives of at least 2 independent experiments. NT: no treatment

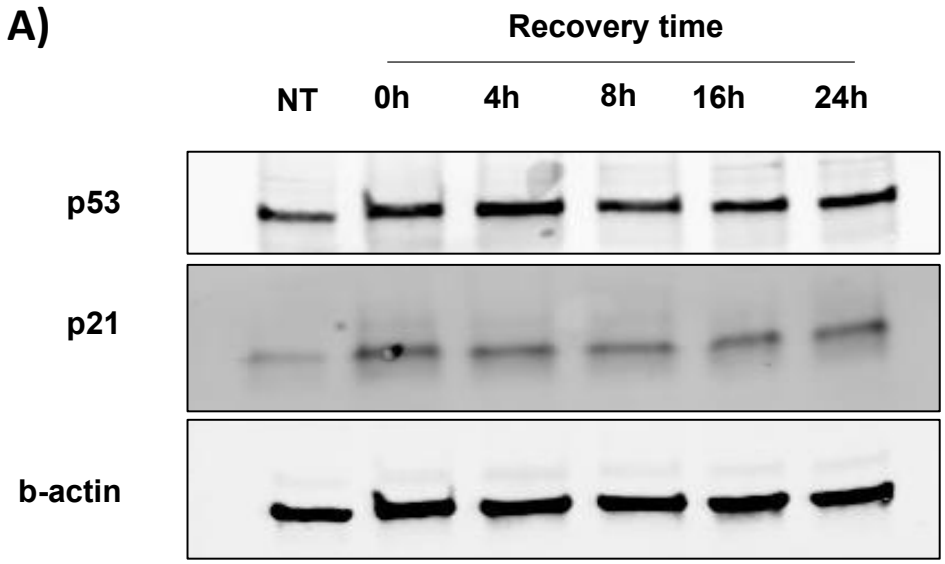

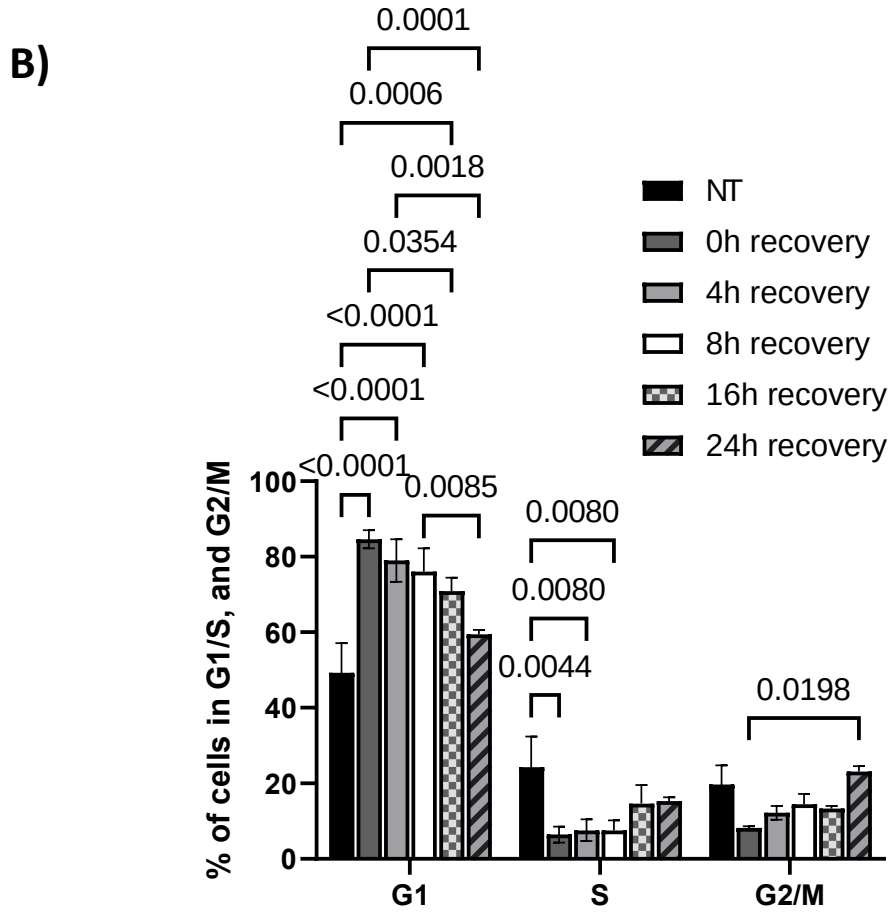

Supplementary Figure S4

Supplementary Figure 4. Recovery of cell cycle progression after AsiDNA™ treatment. RPE-hTERT cells received increased recovery times post AsiDNA™ treatment. (**A**) Western blot analysis of RPE-hTERT cells of p53 and p21 expression levels. (**B**) Mean percentage of RPE-hTERT cells per cell cycle phase measured by PI staining and analysed by FACS. Data are expressed as mean ± standard deviation (n=3) with significance given by two-way ANOVA, Tukey's multiple comparison test, and represented above the bar plots.

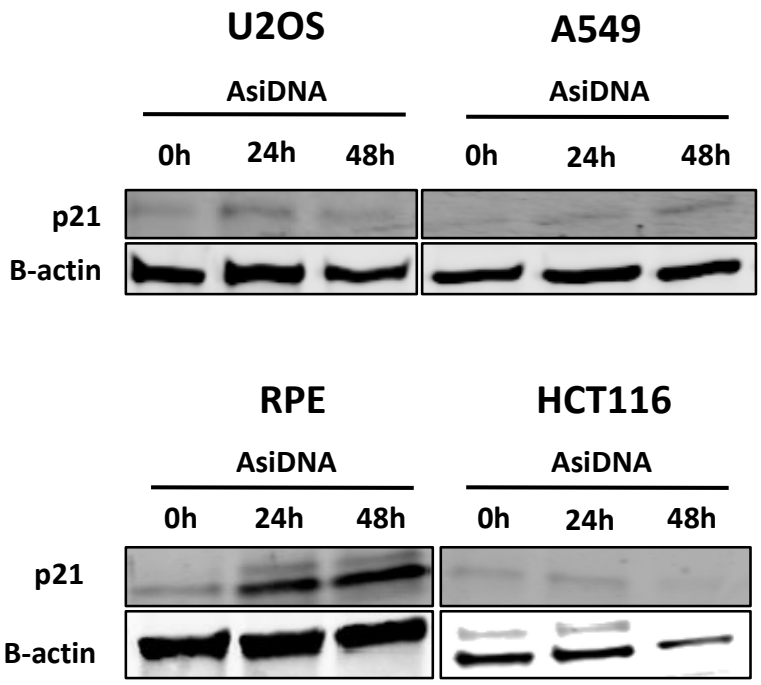

Supplementary Figure S5

Supplementary Figure 5. No p21 induction in AsiDNA™-treated p53 proficient tumour cells. Western blot analysis of A549, HCT116, U-2OS, and RPE-hTERT cells treated with 20 μM AsiDNA for 24h and 48h. Detection of p21 induction with β-actin was used as loading control.

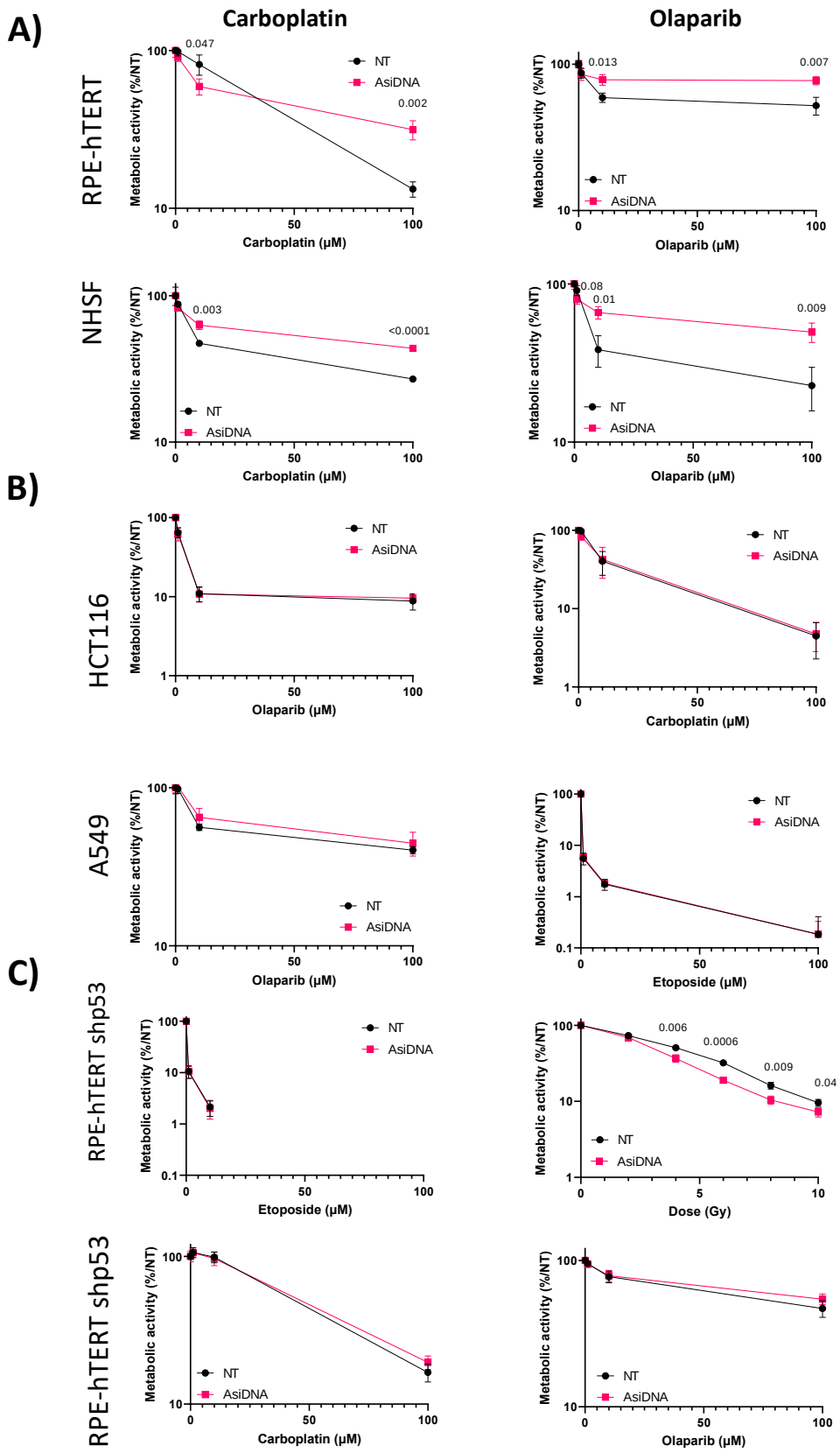

Supplementary Figure S6

Supplementary Figure 6. AsiDNA™ treatment protects p53-proficient normal cells from chemo- and radio-therapy toxicity in vitro, with absence in tumour cells. (**A**) Normal (RPE-hTERT and NHSF) and (**B**) tumour (HCT116 and A549) cells were pre-treated with AsiDNA™ 24h before being co-exposed to various concentrations of carboplatin (0-100 µM) or olaparib (0-100 µM). (**C**) RPE-hTERT hsp53 cells were pre-treated with AsiDNA™ 24h before being co-exposed to various concentrations of etoposide (0-100 µM), various doses of ionizing radiation (0-10 Gy), carboplatin (0-100 µM) or Olaparib (0-100 µM). Cell viability was determined 6 days post-treatment using an ATP-based assay. Data are expressed as mean ± standard deviation (n=3) with significance given by unpaired T-test.

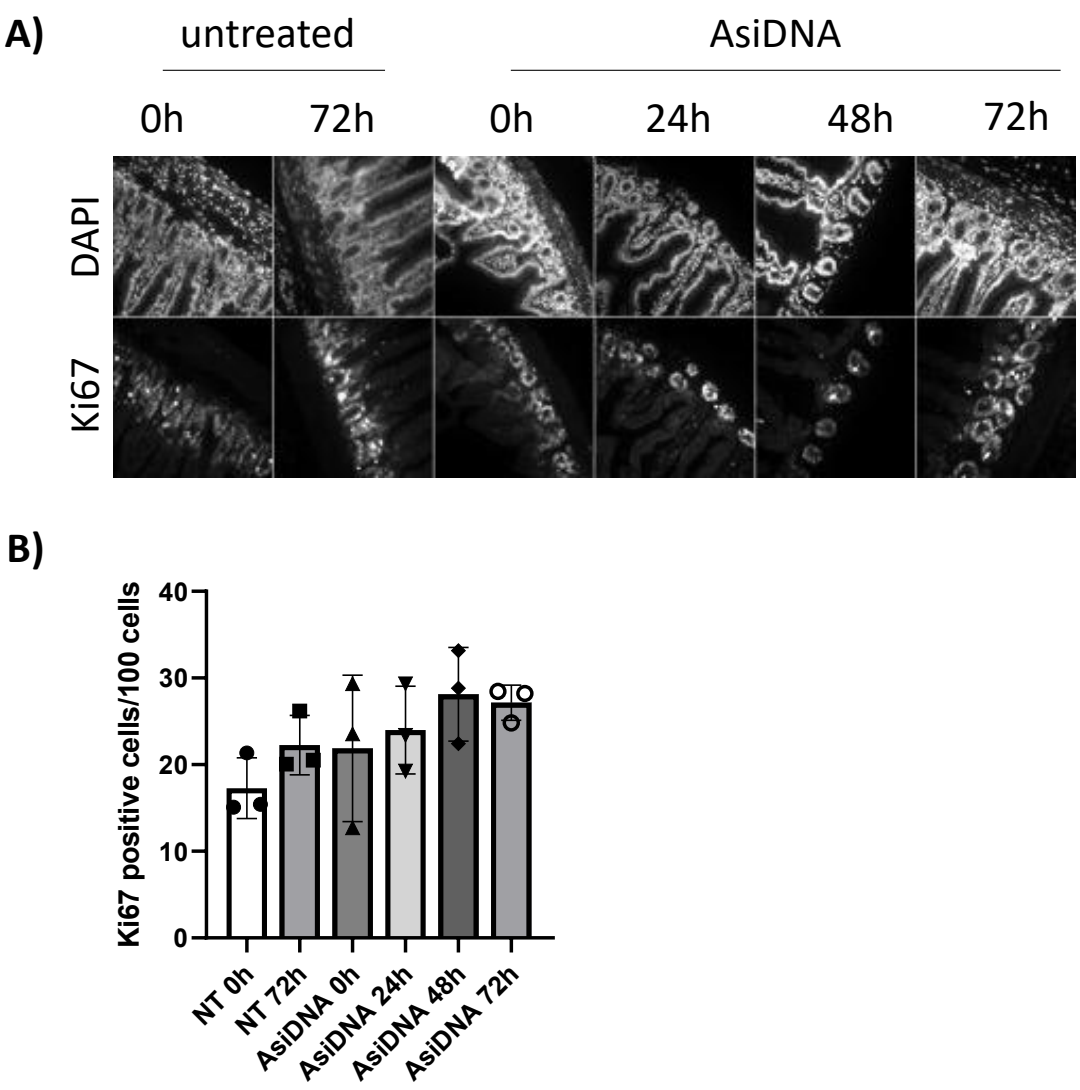

Supplementary Figure S7

Supplementary Figure 7. AsiDNA™ treatment did not result in decreased Ki67 signal in intestinal crypts. (**A**) Representative images of intestinal rolls stained with DAPI and Ki67 for each treatment group. (**B**) Ki67 positive cells per 100 detected cells in small intestinal crypts after AsiDNA™ treatment. A total number of 14000-16000 cells per mouse were scored. Scale bar = 50 µm.

13. Additional results

The following research is ongoing work that resulted from observations made during the conducted study described in paper 1. Here, we aim to further identify the impact of AsiDNA™ treatment combined with radiotherapy in correlation with radiation-induced late toxicity at a cellular level, by examining the lung cell populations, and at a systemic level, by examining inflammatory markers. In addition, we further examined the behaviour of AsiDNA™ within normal cells, in particular its behaviour within dividing and non-dividing normal cells. Additional results I describes changes in gene transcription in fibrosis associated cell types of fibroblasts and alveolar macrophages after AsiDNA™ and radiotherapy exposure. Followed by additional results II, describing the increase in inflammatory cytokine activity following AsiDNA™ treatment and thorax irradiation. Finally, additional results III will further explore the mechanism of action of AsiDNA™ in normal cells and provide preliminary results in an ongoing study. The materials and methods utilized throughout the additional results are combinedly described in the methods section below.

13.1. Methods

In vitro cell culture

Normal tissue cell lines, hTERT-immortalized retinal pigment epithelial cell line (RPE-hTERT), RPE-hTERT with shp53 (Curie collection) and normal human skin fibroblasts (NHSF) were cultured in DMEM/F12 medium (Gibco) supplemented with 10% fetal calf serum (FCS, Eurobio), 100U/ml penicillin/100 µg/ml streptomycin (P/S, Gibco). All cell lines were maintained in a humidified atmosphere at 37°C with 5% CO_2. The absence of mycoplasma contamination was determined in-house by using LookOut Mycoplasma PCR (Sigma-Aldrich).

In vitro treatments

AsiDNA™ molecules concentrated at 10 or 20 µmol/L were supplemented to the medium 24 or 48 hours prior to drug treatment.

FACS analysis

Cells were harvested following AsiDNA™ treatment, fixed in 70% EtOH, and suspended in 1 x PBS-BSA 0.5%-Tween-20 0.1%. γH2AX-PI detection was performed using AlexaFluor647 Mouse anti-H2AXpS139 (BD Pharmingen cat° 560447), 10 µg/ml propidium iodide (Sigma Aldrich) and 0.5 mg/ml RNAse A (Merck-Sigma Aldrich). FACS analysis occurred using Analyzer LSR Fortessa X-20 (BD biosciences).

Pan-nuclear detection assay

Dividing and confluent cells were fixed and preparation for immunofluorescence (IF) were performed as described in Ferreira et. al. 2020 [337]. Antibodies used were: γH2AX (Millipore, 05-636, 1:500) and HSP90 phosphorylation (cell signalling, 3488s, 1:1000) together with DAPI staining (0.5 µg/ml in PBS 1x, F6057, Sigma-Aldrich). Positive pan-nuclear cells were detected on the 3D SIM Upright Widefield microscope (Leica) and compared to overall detected cell number.

ELISA PARylation measurement

The detection of Poly (ADP-Ribose) (PAR) polymers was performed on dividing and confluent cells using a sandwich ELISA as described in Berthault et al. 2022 [318]. Antibodies used were capture antibody (mouse anti-PAR at 4 µg/ml, Trevigen 4335 1:1000), detection antibody (Poly/Mono-ADP Ribose (E6F6A) Rabbit mAb, Cell signaling, 83732, 1:1000) and secondary antibody HRP-conjugated anti-rabbit (Abcam, ab97085, 1:5000).

Quantitative Image-Based Cytometry (QIBC) analysis

Cell culture medium, containing or not 10% FCS, with total 10 µmol/L BrdU (Invitrogen) was prepared and supplemented to the dividing and serum starved cells for 40 min of incubation prior to AsiDNA™ or AsiDNA™-Cya5.5 treatment, under culturing conditions. QIBC experiments were conducted and analysed following the protocol described in Besse et al. 2023 [342]. In short, cells were fixed, permeabilizated, EdU positive cells revealed using EdU DetectPro Imaging kit Imaging (488nm EdU kit, BCK-EdUPro-IM488, Baseclick) and γH2AX visualized using anti-phospho-Histone H2AX (S139) (JBW301 05-636, Merck, 1:40) followed by secondary antibody Donkey Alexa Fluor mouse (594nm, A-21203, Thermofisher Scientific, 1:500). Nuclei were stained with DAPI. Images were obtained using a DMi6000B inverted widefield Microscope (Leica) using a x 40 Plan Apochromat dry objective (Leica, NA: 0.95). Fluorescence signal was documented using two fast filter wheels (Lambda 10-3, Sutter Instrument ®). The nD-SCAN module (Gataca Systems®) was implemented for automatic acquirement of fields for the coverage of at least 5000 nuclei.

In vivo experimentation

Studies were performed in accordance with the recommendations of the European Community (2010/63/UE) for the care and use of laboratory animals as previously described in III. Results, 12. Article 1. In short, experimental procedures were approved by the ethics committee of Institut Curie CEEA-IC #118 (Authorization number APAFIS#5479-201605271 0291841 given by National Authority), in compliance with the international guidelines. All animals used within this research were acclimated for at least 1 week prior to experimentation, housed under pathogen-free conditions, under a controlled 12h light/dark cycle, a relative humidity of 55%,

and a controlled temperature of 21°C. Food and sterile water were provided ad libitum. All experiments were conducted on C57BL/6J mice (Charles River, France) at 8-9 weeks of age.

Animal irradiation

The female C57BL6/J mice model of radiation-induced lung fibrosis was used as previously described in III. Results, 12. Article 1. In short, mice were irradiated after 2 consecutive days of AsiDNA™ or Nol8 injections (100mg/kg), followed by a third day with AsiDNA™ or Nol8 injection (200mg/kg) and 13 Gy of bilateral thorax irradiation FLASH/CONV irradiation. Animals were immobilized under anaesthesia and positioned vertically. GAFchromic™ EBT-XD film were used for the dosimetry of entrance and exit dose at each irradiation.

Single cell RNA sequencing (scRNA-seq)

ScRNA-seq was performed on 3 controls provided by Curras et al. [343], 1 CONV, 1 CONV AsiDNA™, and 1 FLASH female C57BL6/J mice, 5 months post 13 Gy thorax irradiation as described in III. Results, 12. Article 1. The protocol and data processing procedures were performed as previously described [343]. In short, single cell samples for RNA sequencing were prepared using the droplet based scRNA-seq system (10x GENOMICS) following lung tissue dissociation and lysis of encapsulated single cells, RNA capturing, cDNA production, amplification, purification, library preparation, and sequencing. ScRNA-seq data analysis was processed through the creation of a count matrix table suitable for R (4.0.5) and analysed using Seurat package (v4.0.1.). Cell-type markers for each identified cluster were explored by using FindAllMarkers of Seurat followed by naming of cell clusters by utilizing previous published data [112], [344], [345]. Violin plots were generated using Seurat for significant differentially expressed genes of significance to fibrosis development.

Inflammatory marker detection

Serum for cytokine detection were obtained from female C57BL/6J mice 2 weeks post thorax irradiation, as described under animal irradiation, followed by collection every month up to the ethical endpoint. Blood samples were obtained by retro-orbital blood sampling and recovered in Eppendorf tubes. Serum was recovered through centrifugation at RT and stored at -80°C. Cytokine detection was performed using the LEGENDplex Mouse inflammation Panel

(Biolegend) following manufacturer's instructions. LEGENDplex bead analysis was performed using the LSRFortessa™ X-20 Cell Analyzer (BD biosciences) followed by concentration calculations using LEGENDplex FlowVigene™ V10 software.

13.2. Additional results I: Changes in gene transcription in fibrosis-associated cell types may reveal signature for maintaining of healthy lung following CONV-RT and AsiDNA™ exposure.

The delayed development of pulmonary fibrosis after FLASH-RT compared to CONV-RT might be a known phenomenon but the complexity behind this specific tissue response is completely unidentified. Radiation has been shown to impact various cell types present in the lung, resulting in changes in cellular activity and numerous pathway activations [343]. Current unpublished data from the laboratory suggest a clear variety between the CONV and FLASH-RT gene signatures examined using scRNA-seq. As the combined treatment of AsiDNA™ with CONV-RT resulted in a delay in radiation induced lung fibrosis compared to CONV-RT standalone, it is to be questioned if the signature of combined AsiDNA™ CONV-RT treatment is rather similar to FLASH-RT or CONV-RT. To characterize the similarity in cellular changes and expression signatures in lungs 5 months post CONV-RT, FLASH-RT, combined AsiDNA™ CONV-RT or non-irradiated (Control) treatments, single cell suspensions were created followed by scRNA-seq using the 10x Genomic platform. The results displayed below are an extension of the briefly described scRNA-seq results described in III. Results, 12. Article 1.

The identification of 21 main cell populations using scRNA-seq.

By exploiting previously published single-cell datasets and known identifying markers [343], the identity of the various cell clusters was determined (figure 19A). The identification resulted in the detection of 21 distinct clusters: alveolar macrophages (AM), proliferating AM, AT1, AT2, B-cells, basophils, ciliated cells, ciliated club cells, club cells, dendritic cells (DC), endothelial cells (EC), fibroblasts, interstitial macrophages (IM), mesotheliocyetes, monocytes, neutrophils, natural killer cells (NK cells), NK-t-cells, smooth muscle cells (SMC), t-cells and proliferating t-cells (figure 19B-D). All cell types were identified independently of the received treatment modality but in the AT2, B-cells, IM and NK-t cells, a shift in the radiation-induced cell proportion was detected (figure 19D). Additionally, the AM, DC, monocytes, and NK-cells populations displayed altered cell proportion post CONV-RT in comparison to the additional conditions (figure 19D).

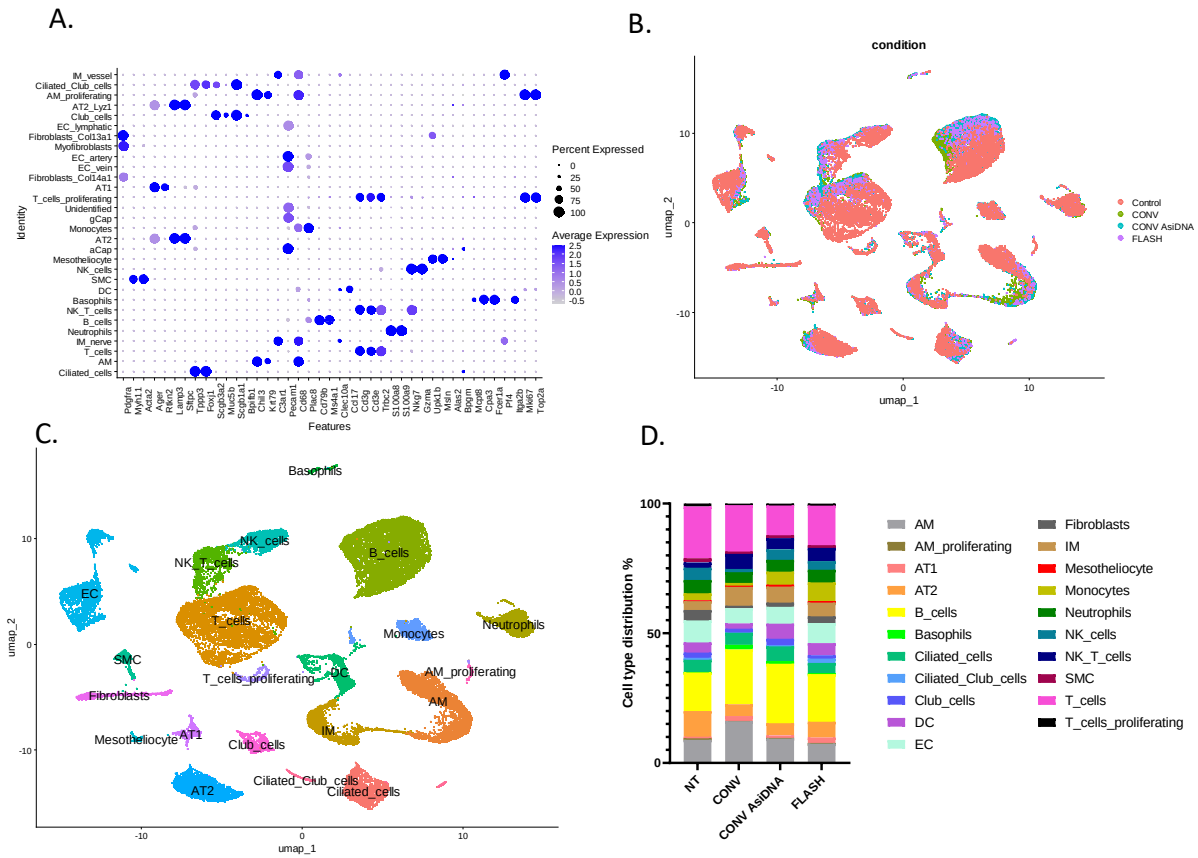

Figure 19: Identification of cell populations.

(A) Dot plot of marker expression utilized for cell populations identification. (B) UMAP visualizing the identified cell clusters separating representation of the Control (red), CONV (green), AsiDNA™ CONV (blue) and FLASH (purple) treated samples. (C) UMAP visualizing the identified cell types in all samples. The individual dots signify single cells, additionally the created clusters are established on transcriptome resemblances. (D) Cell population proportions after Control, CONV, AsiDNA™ CONV and FLASH treatment.

The identification of reduced radiation-induced toxicity at the cellular level

Fibroblasts

Fibroblast can transition into myofibroblast in response to radiation. Myofibroblasts are known to secrete and modify the ECM, including changing the collagen production, which in turn results in the contribution to pulmonary fibrosis formation [346]. To investigate the contribution of this cell type in the development of pulmonary fibrosis formation after CONV-RT, combined AsiDNA™ CONV-RT treatment, and FLASH-RT, myofibroblast marker expression, collagen homeostasis, fibroblast activation and EMC remodelling markers were examined within the fibroblast cell cluster.

Clustering of the fibroblasts resulted in the detection of a total of 891 cells, divided over the different treatment conditions (Figure 20A). Myofibroblast markers Hp, Pla1a and Ltbp2, previously identified in Curras et al. (2023) [343], revealed to be substantially increased after CONV-RT standalone (Figure 20B-D). Fibroblast activation marker Fn1 [347], and ECM remodelling marker Tnc [347], [348], revealed a similar exclusive increase in gene expression only after CONV-RT standalone compared to the additional treatment groups (Figure 20E-F). Remarkably, Nr1d1 gene expression, linked to healthy collagen homeostasis [349], revealed to be significantly decreased in CONV-RT compared to the control or FLASH-RT, further supporting the loss of healthy and gain of damaged profile (Figure 20G).

These results reveal an increase in fibroblast activation, increased myofibroblast transition together with an impact on the ECM, including collagen homeostasis, in the fibroblast cell cluster after CONV-RT standalone. This observed altered gene expression was decreased or absent in fibroblasts exposed to combined AsiDNA™ CONV-RT or FLASH-RT treatments and supports an essential role of this pathway activation in the development of pulmonary fibrosis.

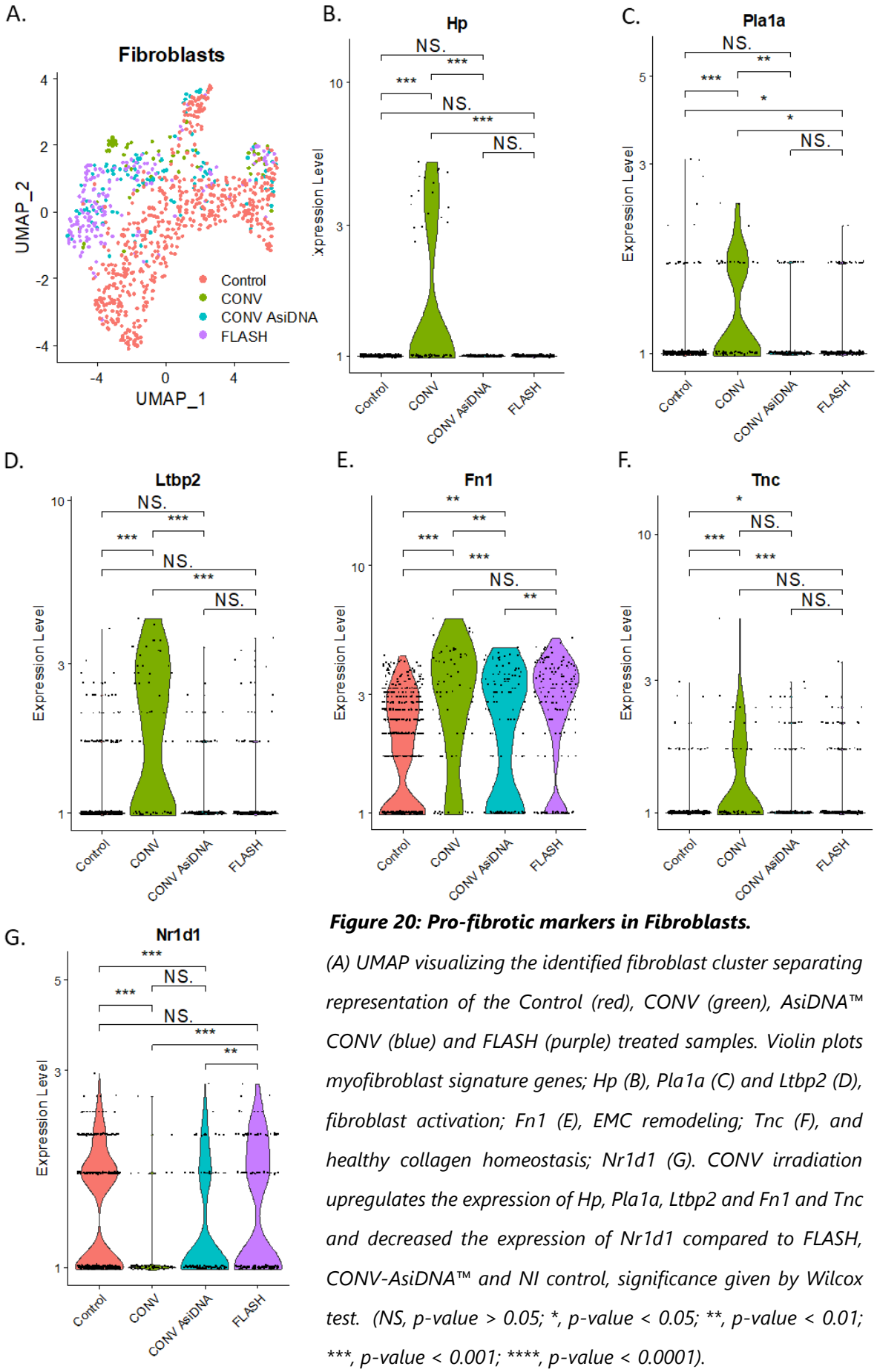

Figure 20: Pro-fibrotic markers in Fibroblasts.

*(A) UMAP visualizing the identified fibroblast cluster separating representation of the Control (red), CONV (green), AsiDNA™ CONV (blue) and FLASH (purple) treated samples. Violin plots myofibroblast signature genes; Hp (B), Pla1a (C) and Ltbp2 (D), fibroblast activation; Fn1 (E), EMC remodeling; Tnc (F), and healthy collagen homeostasis; Nr1d1 (G). CONV irradiation upregulates the expression of Hp, Pla1a, Ltbp2 and Fn1 and Tnc and decreased the expression of Nr1d1 compared to FLASH, CONV-AsiDNA™ and NI control, significance given by Wilcox test. (NS, p-value > 0.05; *, p-value < 0.05; **, p-value < 0.01; ***, p-value < 0.001; ****, p-value < 0.0001).*

Alveolar macrophages (AM)

In the complexity of radiation-induced lung injury, various cell types, including alveolar macrophages (AM), have revealed to contribute to its development and severity. Several previous research has observed an accumulation of AM cells in the lung following irradiation together with increased Th2-related cytokine expression, the promotion of wound healing and tissue regeneration. This increase in pro-fibrotic factors by AM cells, ultimately, greatly contributes to fibrosis formation [350]–[352].

Clustering of the AM resulted in the detection of a total of 3381 cells, divided over the different treatment conditions (Figure 21A). To identify an indication of any profibrotic contribution of AM to the development of pulmonary fibrosis, previous discovered profibrotic markers and Th2 cytokine receptor markers were examined. Profibrotic genes Lipa, Lpl and Spp1 have been priorly linked to pulmonary fibrosis formation [343], [353]–[358] and revealed a significant upregulation after CONV-RT standalone compared to the additional conditions (Figure 21B-D). Additionally, Th2 cytokine reception markers, linked to increased inflammation and fibrosis development [359]–[361], revealed significant gene upregulation of Il10rb, but not Il4ra, after CONV-RT compared to the additional conditions (Figure 21E-G). Strikingly, the upregulation of Il13ra1 was observed in all irradiated conditions equally (Figure 21F).

These results revealed a compelling increased pro-fibrotic gene signature and response of AM after CONV-RT, that was decreased or completely absent in the control group, after AsiDNA™ CONV-RT treatment or after FLASH-RT. Strikingly, AsiDNA™ CONV-RT treatment and FLASH-RT revealed similar levels of profibrotic signatures in the AM cell cluster. The results insinuate an AM response between the combined AsiDNA™ CONV-RT and FLASH-RT treated groups, resulting in decreased pro-fibrosis signalling and, possibly, decreased normal tissue toxicity after radiotherapy, that was maintained upon CONV-RT.

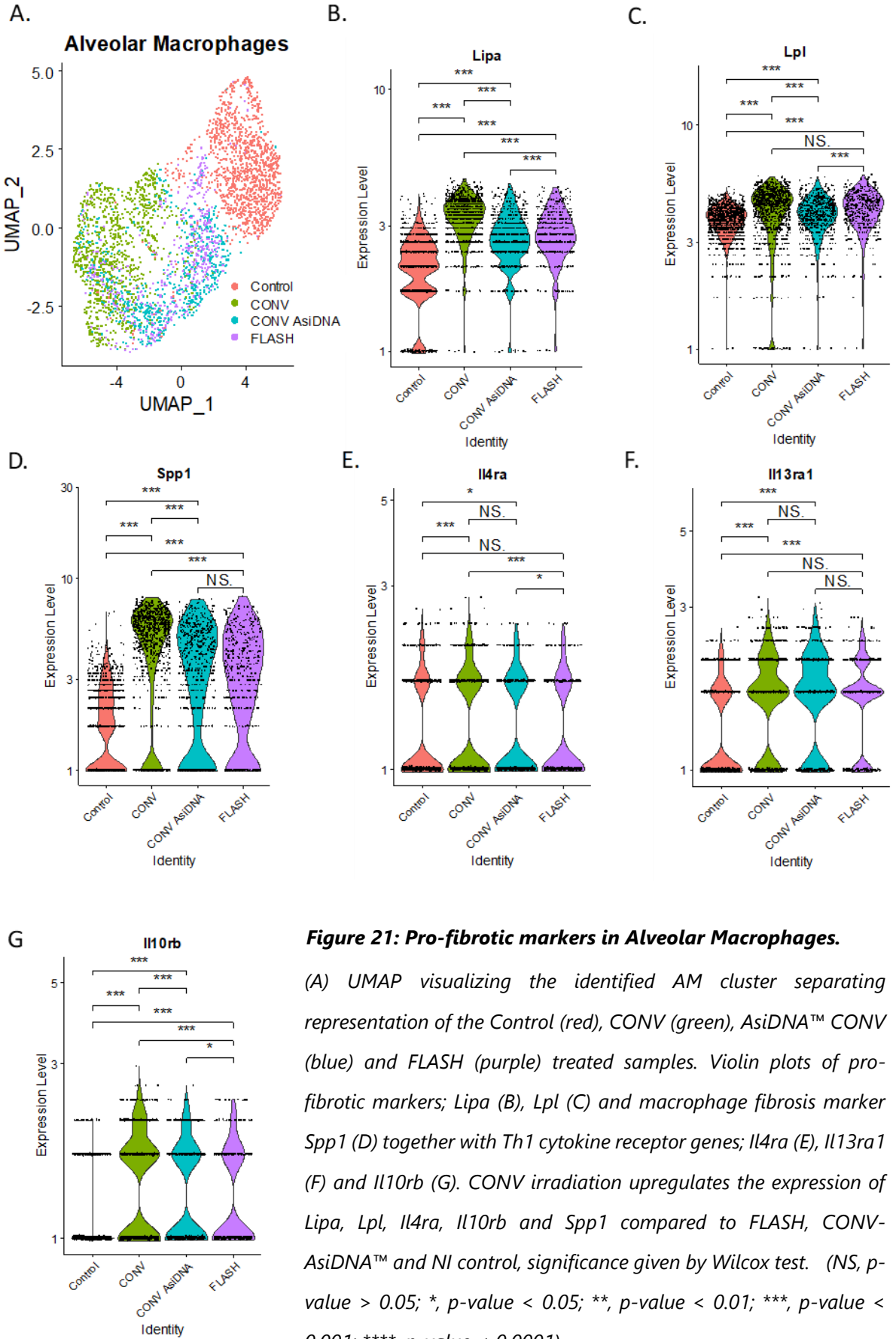

Figure 21: Pro-fibrotic markers in Alveolar Macrophages.

*(A) UMAP visualizing the identified AM cluster separating representation of the Control (red), CONV (green), AsiDNA™ CONV (blue) and FLASH (purple) treated samples. Violin plots of pro-fibrotic markers; Lipa (B), Lpl (C) and macrophage fibrosis marker Spp1 (D) together with Th1 cytokine receptor genes; Il4ra (E), Il13ra1 (F) and Il10rb (G). CONV irradiation upregulates the expression of Lipa, Lpl, Il4ra, Il10rb and Spp1 compared to FLASH, CONV-AsiDNA™ and NI control, significance given by Wilcox test. (NS, p-value > 0.05; *, p-value < 0.05; **, p-value < 0.01; ***, p-value < 0.001; ****, p-value < 0.0001).*

13.3. Additional results II: Unique increase in inflammatory cytokine activity post combined AsiDNA™ treatment and thorax irradiation

Cytokines are important contributors to numerous functions within the body including maintaining homeostasis, promoting development, nociception, cell activation and immune activation. Modified levels of inflammatory markers participate greatly in the development of lung fibrosis through the regulation of inflammation and response, inducing senescence, changes of the EMT and inhibiting autophagy [362]. To unravel the complexity of the delay in the onset of radiation-induced lung fibrosis observed after combined AsiDNA™ CONV-RT treatment, the impact of the various treatments upon inflammatory cytokine homeostasis was examined. Additionally, it enabled to examine if cytokine concentration could be used to function as biomarkers for treatment activity. For this, a panel of inflammatory cytokines were examined monthly following irradiation. Blood sampling was conducted at 0.5, 1, 2, 3, 4 and 5 months on mice receiving three consecutive days of AsiDNA™ treatment with or without 13 Gy thorax CONV/FLASH irradiation. Note that in these experiments, Nol8 was used as negative control (with a similar chemical structure as AsiDNA™ however, with lack of PARP and DNA-PK activation) to identify the specific capacity of AsiDNA™ to trigger a biological response.

Following AsiDNA™ combined with CONV- or FLASH-RT treatments, a clear increase from 1-month following treatment of inflammatory cytokines Granulocyte-macrophage colony-stimulating factor (GM-CSF), TNF-α and IFN-γ was observed (Figure 22). This synergistic effect was stable up to 5 months following treatment, and peaks at 1 month following treatment. AsiDNA™ treatment, CONV-RT or FLASH-RT standalone resulted in no increase of GM-CSF, TNF-α and IFN-γ inflammatory cytokines (Figure 22).

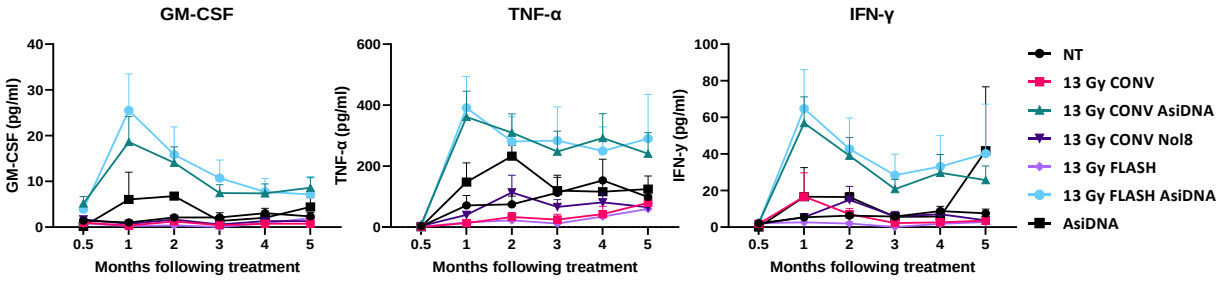

Figure 22: Cytokine GM-CSF, TNF-α and IFN-γ serum analysis.

Mice administered with Saline (NT, black dot), 13 Gy CONV (pink square), 13 Gy CONV with AsiDNA™ treatment (green triangle), 13 Gy CONV with Nol8 treatment (purple triangle), 13 Gy FLASH (violet

diamond), 13 Gy FLASH with AsiDNA™ treatment (blue diamond) and AsiDNA™ treatment standalone (black square), underwent blood collection 0.5-, 1-, 2-, 3-, 4- and 5-months post treatment. Data is expressed in pg/ml of cytokines to months following irradiation (IR). 1-3 months N=6, 4-5 months N=1-6, representing the mean ± SEM.

The inflammatory cytokines IFN-β, IL-12p70, IL-1β, IL-17α and IL-27 revealed to be activated following AsiDNA™ treatment standalone and in combination with CONV- or FLASH-RT (Figure 23). This AsiDNA™-dependent cytokine activation was induced from 1-month following treatment. This was sustained up to 5 months following treatment only for the combined treatment conditions, with its peak of cytokine production at 1- and 2-months following treatment. Radiotherapy standalone did not reveal any changes in IFN-β, IL-12p70, IL-1β, IL-17α or IL-27 cytokine production (Figure 23).

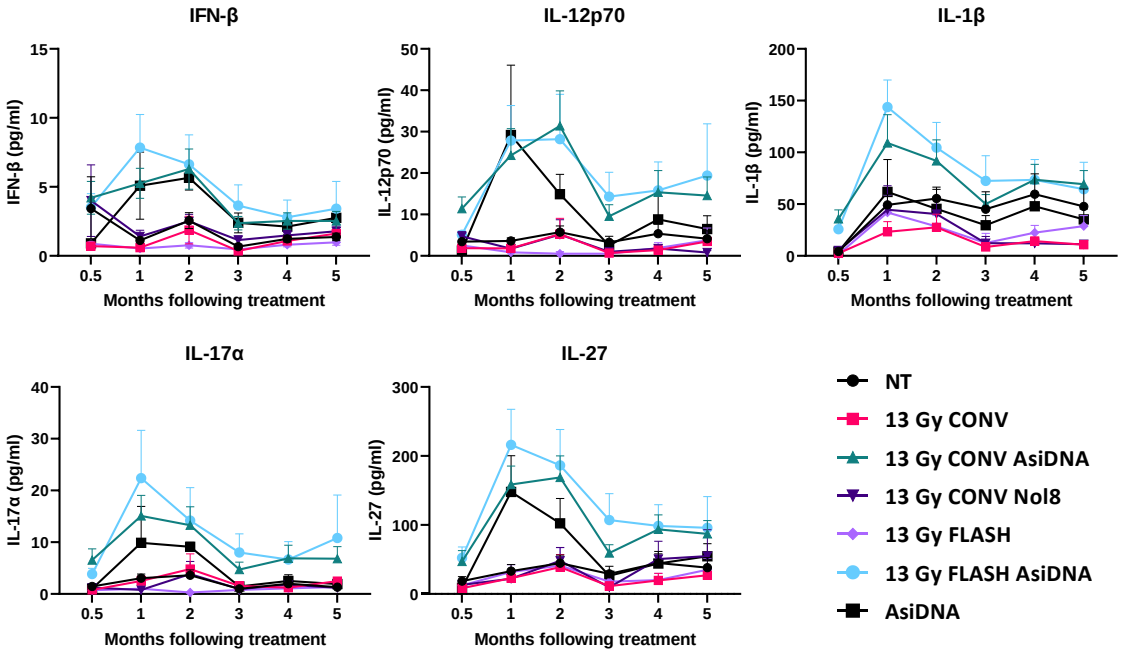

Figure 23: Cytokine IFN-β, IL-12p70, IL-1β, IL-17α and IL-27 serum

Mice administered with Saline (NT, black dot), 13 Gy CONV (pink square), 13 Gy CONV with AsiDNA™ treatment (green triangle), 13 Gy CONV with Nol8 treatment (purple triangle), 13 Gy FLASH (violet diamond), 13 Gy FLASH with AsiDNA™ treatment (blue diamond) and AsiDNA™ treatment standalone (black square), underwent blood collection 0.5-, 1-, 2-, 3-, 4- and 5-months post treatment. Data is expressed in pg/ml of cytokines to months following irradiation (IR). 1-3 months N=6, 4-5 months N=1-6, representing the mean ± SEM.

Notably, for cytokines IL-10, IL-6, MCP-1, IL-1α and IL-23 no clear interpretation can be driven from the shape of the curves (Figure 24). A minor increase at 1- and 2-months following treatment is observed in cytokine expression of IL-6 in AsiDNA™ standalone or AsiDNA™ combined with CONV- or FLASH-RT treatments, IL-10 at 1- and 2-months following AsiDNA™ combined with CONV- or FLASH-RT treatments, and for IL-1α at 1- and 2-months following AsiDNA™ standalone treatment (Figure 24). Additionally, MCP-1 and IL-23 exhibit a peak of production at 0.5 months only following AsiDNA™ CONV-RT treatment (Figure 24).

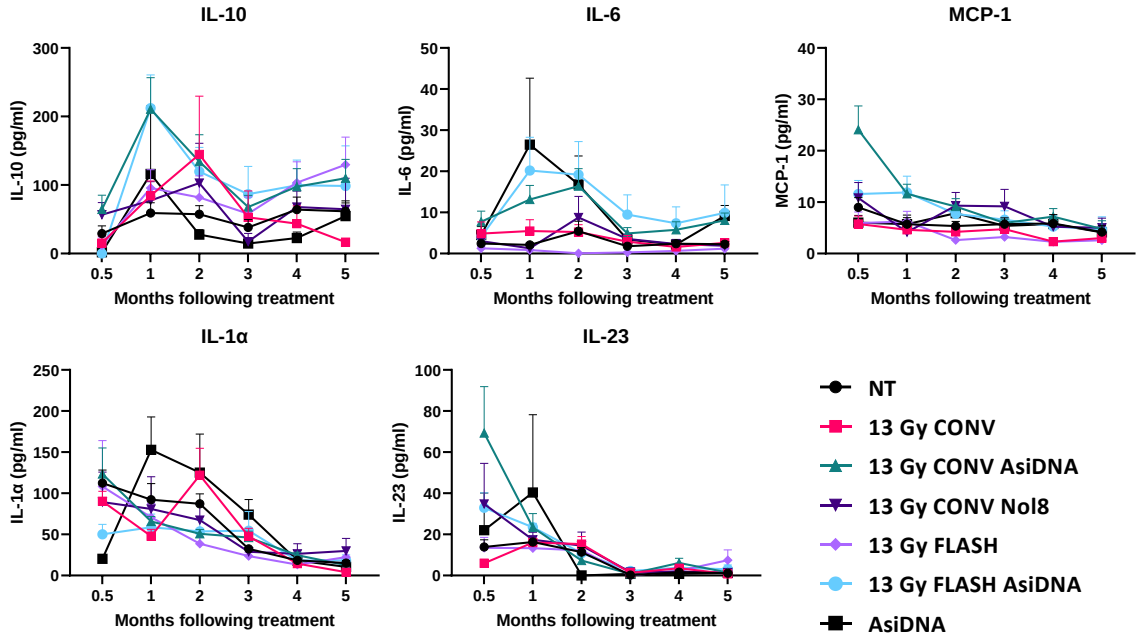

Figure 24: Cytokine IL-10, IL-6, MCP-1, IL-1α and IL-23 serum analysis.

Mice administered with Saline (NT, black dot), 13 Gy CONV (pink square), 13 Gy CONV with AsiDNA™ treatment (green triangle), 13 Gy CONV with Nol8 treatment (purple triangle), 13 Gy FLASH (violet diamond), 13 Gy FLASH with AsiDNA™ treatment (blue diamond) and AsiDNA™ treatment standalone (black square), underwent blood collection 0.5-, 1-, 2-, 3-, 4- and 5-months post treatment. Data is expressed in pg/ml of cytokines to months following irradiation (IR). 1-3 months N=6, 4-5 months N=1-6, representing the mean ± SEM.

These results disclose a synergistic effect in inflammatory cytokine activation following AsiDNA™ combined with CONV- or FLASH-RT treatments, with a possible impact on the development of pulmonary fibrosis through increased IFN-γ. It furthermore revealed a set of inflammatory cytokines singly activated upon AsiDNA™ treatment that persist up to 5 months post treatment, qualifying it to possibly function as biomarkers for AsiDNA™ activity in vivo.

13.4. Additional results III: Exploring the mechanism of action of AsiDNA™ in normal epithelial cells and fibroblasts

The anti-cancer drug AsiDNA™, mimicking a double stranded break, has been identified as a chemo- and radiosensitizer with no impact to the normal tissue. The previous study, found in III. Results, 12. Article 1, revealed that AsiDNA™ treatment results in a DNA-PK/p53/p21 dependent G1/S arrest, explicitly in epithelial cells and fibroblasts, characterised in this chapter as normal cells. The study furthermore revealed that the AsiDNA™-induced G1/S arrest in normal cells is accompanied with the induction of normal tissue protection against radiation-induced toxicity. In this study, we aim to further identify the normal cell response to AsiDNA™ treatment and examine the distinctive response of dividing and non-dividing healthy cells in response to AsiDNA™ treatment.

Loss of DNA-PK-induced markers post AsiDNA™ activity in normal non-dividing epithelial cells and fibroblasts

The characteristic markers of AsiDNA™ activity that have been identified in dividing normal cells and tumour cells, linked to DNA-PK activation, are the phosphorylation of HSP90 and the phosphorylation of H2AX, represented as a pan-nuclear signal. In vivo, the pan-nuclear staining of γH2AX following AsiDNA™ treatment was present in tumours and severely decreased or completely absent in the normal tissue [331], [337]. This initiated the question of differential AsiDNA™ activity in dividing compared to non-dividing healthy cells. NHSF and RPE-hTERT cells were treated in dividing and non-dividing confluent state for 24 and 48h with 20 μM AsiDNA™ followed by the examination of pan-nuclear yH2AX and HSP90-p. Pan-nuclear staining of yH2AX and HSP90-p was detected in both cell lines post AsiDNA™ treatment with a peak at 24h of AsiDNA™ treatment (Figure 25A,C). Both biomarkers revealed a significant decrease once the normal cells reached confluency and stalled its capacity to divide (Figure 25B-D). The significant decrease in pan-nuclear yH2AX following AsiDNA™ treatment in confluent normal cells was confirmed using flow cytometry analysis (Figure 25E-F).

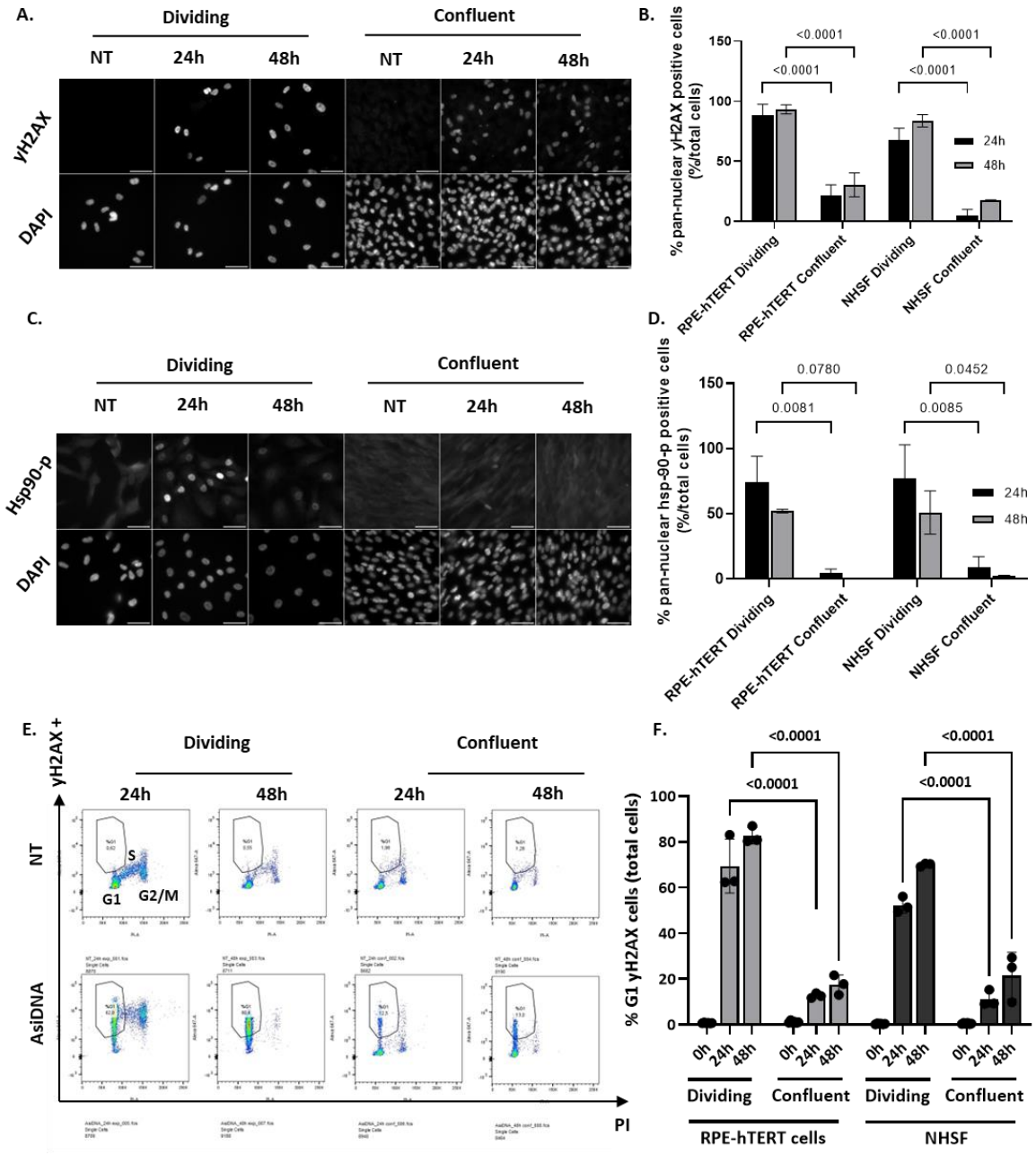

Figure 25: Loss of AsiDNA™ activation markers in non-dividing normal cells.

Representative immunofluorescence imaging of (A) pan-nuclear γH2AX or (C) HSP90-p in dividing and non-dividing RPE-hTERT cells. Quantitative histogram representing the percentages of immunofluorescence detected (B) pan-nuclear γH2AX positive cells or (D) HSP90-p positive cells in RPE-hTERT cells and NHSF in dividing and non-dividing state. (E) Representative flow cytometry imaging of pan-nuclear γH2AX and PI staining in dividing and non-dividing RPE-hTERT cells. (F) Quantitative histogram representing the percentages of flow cytometry detected pan-nuclear γH2AX positive cells in RPE-hTERT cells and NHSF in dividing and non-dividing state. Data are expressed as mean ± standard deviation (n=2-3) with significance given by two-way ANOVA, Tukey's multiple comparison tests, and represented above the bar plots.

AsiDNA™ can enter healthy epithelial cells and fibroblasts, independent on the state of cell division

To determine if AsiDNA™ is unable to enter non-dividing normal cells or unable to enter the nucleus to activate DNA-PK, AsiDNA™-induced PARP activation was examined. PARP activation upon AsiDNA™ treatment have been identified to occur mainly in the cytoplasm [318]. NHSF and RPE-hTERT cells were treated in a dividing and non-dividing confluent state with 20μM of AsiDNA™ for 24 and 48h followed by PARylation ELISA. Both cell lines revealed a strong PARylation after both 24 and 48h of AsiDNA™ treatment. The increase in PARylation was present in both dividing and non-dividing normal cells, independent on the status of the cell division (Figure 26A). The presence of AsiDNA™ was confirmed in RPE cells treated for 12h with AsiDNA™-Cy5.5 followed by QIBC single cell analysis. A severe decrease of yH2AX was reconfirmed after the cells lost its dividing state (Figure 26B-C) However, the presence of AsiDNA™-Cy5.5 in the nucleus was present in both dividing and non-dividing cells with measured AsiCy5.5 intensities of 1200 a.u. in dividing cells and 1205 a.u. in non-dividing cells. Remarkably, the AsiDNA™-induced yH2AX is explicitly occurring in the G1 phase (Figure 26B). Similar pattern of γH2AX was also observed using p53 proficient and deficient tumour cells (data not shown).

Currently, research is ongoing in examining the mechanism driving the G1 specific yH2AX following AsiDNA™ treatment and the strong reduction of γH2AX staining in non-dividing cells.

A.

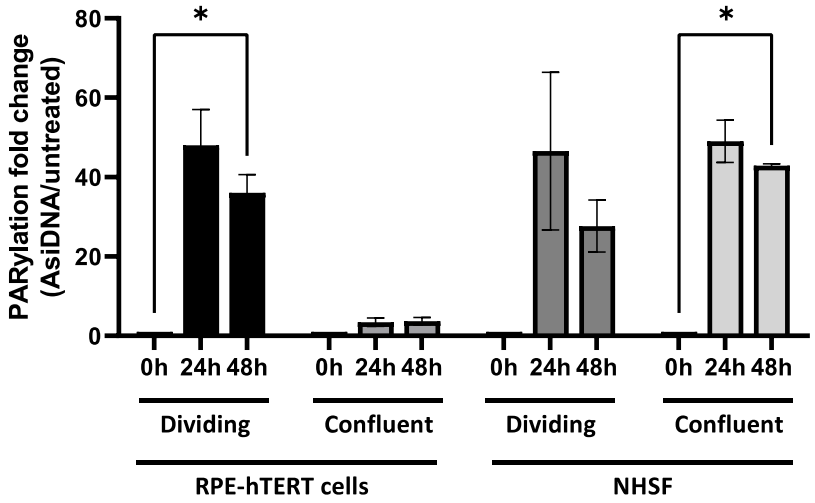

B.

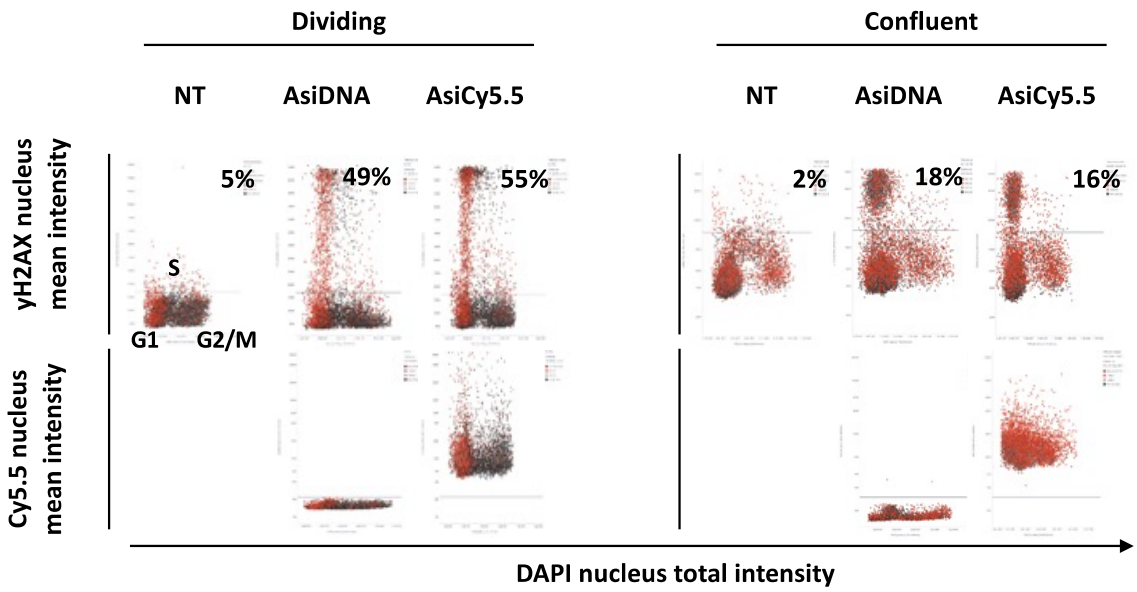

C.

	NT γH2AX positive signal	AsiDNA γH2AX positive signal	AsiCy5.5 γH2AX positive signal	Cy5.5 intensity
Dividing	5%	48%	56%	1200 a.u.
Confluent	2%	18%	18%	1205 a.u.

Figure 26: Dividing and non-dividing normal cells have similar AsiDNA™ uptake.

(A) Quantitative histogram representing the percentage of PARylation activity of RPE-hTERT and NHSF following AsiDNA™ treatment in dividing and non-dividing state. Data are expressed as mean ± standard deviation (n=2-3) with significance given by two-way ANOVA, Tukey's multiple comparison tests, and represented above the bar plots. (B) QIBC representation of RPE-hTERT cells following AsiDNA™ or AsiCy5.5 treatment for the detection of γH2AX and Cy5.5 nuclear intensity with values represented in table (C).

IV. FINAL DISCUSSION

Discussion

Unravelling the cellular and molecular consequences of AsiDNA™ treatment to the normal tissue exposed unique capacities of AsiDNA™ to the normal tissue that have never been identified in prior research. In the discussion below, the various results that are described in the result section will be discussed.

The AsiDNA™ decoy mimicking DSBs protects the normal tissue from radiation toxicity through a DNA-PK/p53/p21-dependent G1/S arrest: a summary.

To reduce toxic side-effects, chemical or biological agents can be implemented as radioprotectors, administered in parallel to radiotherapy delivery [363]. AsiDNA™ is a drug mimicking DNA DSBs and can disrupt the DNA repair machinery of cancer cells, thereby enhancing the antitumoral action of radiation [318], [364]. The leading molecule used in pre-clinical and clinical studies, termed AsiDNA™, is well tolerated indicating its suitability as a radioprotector [334], [335], [337], [341]. Although activation of AsiDNA™ occurs in both tumour and normal cells, only tumour cells are sensitive to the treatment [316], [317]. The G1/S cell cycle checkpoint is responsible for ensuring that the optimum conditions are reached for a cell to undergo successful cell division, by sensing of both mitogens and DNA damage, using key player protein p53 [365]. We demonstrated that explicitly in p53 proficient normal cells, AsiDNA™ treatment results in p53 activation, leading to p21 induction, and initiation of a reversible G1/S cell cycle arrest. Normal cells deficient in either DNA-PK, p53, or p21 are unable to arrest at the G1/S boundary following AsiDNA™ treatment. We propose that AsiDNA™ can serve as a platform to connect DNA-PK and p53, resulting in p21 activation.

We confirmed the presence of the activated G1/S checkpoint in complex ex vivo and in vivo biological models. AsiDNA™-treated PCLS derived from p53 WT mice revealed a decrease of EdU positive cells, that was absent in PCLS derived from p53 knock-out mice, or in PCLS p53 WT treated with Nol8, an AsiDNA™-like molecule unable to activate DNA-PK [311].

This supports that AsiDNA™ treatment in PCLS results in DNA-PK/p53-dependent G1/S arrest. In addition, the capacity of AsiDNA™ to induce the G1/S arrest was observed in vivo in the intestine, demonstrated with a severe decrease of EdU incorporation in the intestinal crypts of mice directly after AsiDNA™ treatment. This was accompanied with a full recovery of crypt

division 24-48h post-AsiDNA™ treatment, and increased p21 expression following AsiDNA™ treatment that decreased similarly with the recovery of crypt proliferation.

The results within this research revealed a significant increase of in vitro cell survival, in normal cells upon chemo- or radiotherapy combined with AsiDNA™, compared to standalone treatment. This increase in cell survival was absent in tumour cells, independent of the p53 status, as well as in normal cells with a p53 deficient status. This confirms the necessity of an active and intact DNA-PK/p53/p21 cascade to exploit the normal tissue protection properties of AsiDNA™. The protective capacities of AsiDNA™ were similarly identified in vivo in the intestine crypt survival, and in the radiation-induced lung fibrosis when combining CONV-RT with AsiDNA™ treatment compared to CONV-RT standalone. The intestine can fully regenerate from any type of damage if the stem cells remain functional [366], revealing the capacity of AsiDNA™ to protect the stem cells in the crypts by acting at the G1/S transition. Remarkably, inhibition of the G1/S transition prior to radiation or chemotherapy also protect the GI epithelium in mice [187], [367]. Similar results obtained in radiation-induced pulmonary fibrosis where AsiDNA™ combined with CONV-RT revealed increased protection of the lung to radiation toxicity, presented by a delay in the onset of radiation-induced fibrosis, compared to CONV-RT standalone.

Finally, the combination of AsiDNA™ with FLASH-RT, a RT modality that has been shown to alleviate radiation-induced toxicity [54], [60], was explored. FLASH-RT was less toxic in vivo compared with CONV-RT, reconfirming the FLASH effect. However, AsiDNA™ combined with CONV-RT did not result in the same delay in the onset of fibrosis compared to FLASH radiotherapy standalone, while AsiDNA™ CONV-RT was as efficient as FLASH-RT at protecting intestinal crypts. This may be explained by the possible limitations in the capacity of AsiDNA™ to interfere with the complex mechanism driving fibrosis in late responding tissues [368]. Moreover, AsiDNA™ combined with FLASH-RT treatment did not result in any additive effect in vivo compared to FLASH-RT as standalone treatment. Collectively, all results indicate that the activity of AsiDNA™ and FLASH-RT could draw upon identical mechanism interference or epistatic interaction, to result in the protective capacities within the normal tissue.

The full discussion of the AsiDNA™ decoy mimicking DSBs protects the normal tissue from radiation toxicity through a DNA-PK/p53/p21-dependent G1/S arrest can be found in III. Results, 12. Article 1.

Enhanced DNA repair and de-differentiation as possible hypothesis for normal tissue protection

The introduction of a G1/S cell cycle arrest has been indicated priorly to protect normal cells in vivo against chemotherapeutic-induced toxicity [187] and has been observed to go through the identical p53 dependent route [257]. However, one aspect that was not discussed before is the explanation why AsiDNA™ treatment is explicitly able to protect normal cells against toxicities. One hypothesis is that the AsiDNA™-induced cell cycle arrest increases the DNA repair capacities of normal cells. The intestine can fully regenerate from damage if the stem cells survive or the possibility of de-differentiation remains [155], [257], [366]. Remarkably, previous research by Hua et al. (2012) revealed that the stem cell population, at position +1-3 within the crypts, have the capability to increase their DNA repair capacities to survive genotoxicity induced by chemotherapeutics or radiation [153]. In addition, mice with a DNA-PK or p53 deficiency displayed an increase in radiation induced GI toxicity [246], [369]. Similarly, enhancing p53 activity by the addition of extra p53 gene copies resulted in a significant decrease in GI injury and enhanced DNA damage response with increased p21 expression following radiotherapy, compared to p53 wild-type mice [246]. In addition, the inhibition of the G1/S transition, prior to radiation or chemotherapy, has indicated to reduce the GI toxicity in mice and enhancing Lgr5+ stem cell survival with dependency on active p53 and p21 and increased repair capacities [187], [367]. These findings suggest that the capacity of AsiDNA™ to activate the DNA-PK, p53 and p21 cascade to induce the G1/S transition, enhances the DNA damage response, boosting crypt cell regeneration and supports de-differentiation, resulting in enhancing the intestinal stem cell survival and decreasing radiation induced toxicity.

Changes in gene transcription in fibrosis-correlated cell types may reveal similar decreased fibrosis signature after combined AsiDNA™ CONV-RT and FLASH-RT exposure.

The delayed development of pulmonary fibrosis after FLASH-RT compared to CONV-RT might be a known phenomenon but the complexity behind this specific tissue response is completely unidentified. Radiation has been shown to impact various cell types present in the lung, resulting in changes in cellular activity and numerous pathway activations [343]. As the combined treatment of AsiDNA™ with CONV-RT resulted in a delay in radiation-induced lung fibrosis compared to CONV-RT standalone, it is to be questioned if the signature of combined AsiDNA™ CONV-RT treatment is similar to FLASH-RT or CONV-RT standalone treatment. By exploiting previously published single-cell datasets [343], cell populations within the lung were clearly detected and fibroblasts and AM clusters were identified.

Fibroblast can transition into myofibroblast in response to radiation, modifying the ECM, increasing collagen production, which in turn results in the contribution to pulmonary fibrosis formation, and has recently been identified as the main effector cells of pulmonary fibrosis [346], [370]. Our research revealed similar results with gene expression of myofibroblast markers previously identified in Curras et al. (2023) [343], increased fibroblast activation marker [347], and increased ECM marker [347], [348] after CONV-RT standalone. In addition, the gene expression of healthy collagen homeostasis [349], revealed to be significantly decreased in CONV-RT standalone compared to the control or FLASH-RT standalone. The difference between the gene expression profiles of CONV-RT standalone compared to the control condition, FLASH-RT standalone or combined CONV-RT with AsiDNA™ treatment, suggests that AsiDNA™ treatment could have an adverse impact on myofibroblast formation following radiotherapy, decreasing the onset of pulmonary fibrosis formation.

Comparable to fibroblasts, accumulation of AM cells in the lung following irradiation has been linked to an increase in pro-fibrotic factors generated by AM cells that contribute to fibrosis formation [350]–[352]. Within the AM population, profibrotic genes revealed to be significantly upregulated after CONV-RT standalone compared to the additional conditions. However, this increase was absent in some of the examined Th2 cytokine reception markers, priorly identified to enhanced inflammation and fibrosis development [359]–[361]. The results highlight the complexity of radiation-induced lung fibrosis and could explain the observed survival of mice

following CONV-RT standalone, combined AsiDNA™ with CONV-RT and FLASH-RT standalone treatments. Here, AsiDNA™ treatment combined with CONV-RT revealed a delay in the onset of lung fibrosis compared to CONV-RT standalone but not as significant as FLASH-RT standalone.

Notably, during the obtaining of gene expression results in both the fibroblasts and the AM, no sub clustering was performed of these cell populations. Prior scRNA-seq research of mice lungs following radiotherapy revealed a myofibroblast subcluster within the fibroblast population. This subcluster was present only following radiotherapy treatment and absent in control mice [343]. Furthermore, additional AM subclusters were identified that underwent a significant shift following radiotherapy treatment. Future sub-clustering of the fibroblast and AM populations can provide a stronger view of the impact of AsiDNA™ treatment and FLASH-RT on its difference compared to CONV-RT standalone, and perhaps provides more explanation on the mechanism behind both AsiDNA™-and FLASH-RT-induced delay of radiation-induced lung fibrosis.

Inflammatory cytokines in response to AsiDNA™ treatment

Changes in inflammatory cytokines that lead to macrophage activation and changes in immune cell activity, contribute to pulmonary fibrosis formation in the lung and is hypothesized as the phago-cytosis-secretion immunity network. The pro- and anti-inflammatory cytokines function in an equilibrium and issues are developed once this equilibrium is disturbed [362]. At a first glance, this equilibrium appears to be disturbed within mice receiving AsiDNA™ treatment. However, the inflammatory cytokines that are exclusively activated post AsiDNA™ treatment (IFN-β, IL-12p70, IL-1β, IL-17α and IL-27) cover both pro and anti-inflammatory cytokines, suggesting that the equilibrium might be maintained. Nonetheless, AsiDNA™ standalone treatment resulted in an increase in IL-12. This cytokine is known to activate Th1 cells, leading to the production of IFN-γ, GM-CSF and TNF-α [362]. Surprisingly IFN-γ, GM-CSF or TNF-α activation was not detected following AsiDNA™ standalone treatment, indicated that Th1 cells are likely not activated in this condition. It is important to note that AsiDNA™ standalone treatment does not induce lung fibrosis. Consequently, any change observed in the cytokine's expression in response to AsiDNA™ treatment standalone likely reflects a physiological response to a non-damaging stress. In contrast, following combined AsiDNA™ with CONV-RT or FLASH-RT treatment, a severe

increase in all IFN-γ, GM-CSF and TNF-α was detected. The AsiDNA™-induced IL-12 accompanied by radiotherapy damage resulted in the activation of Th1 cells and the production of IFN-γ, GM-CSF and TNF-α. Increased IFN-γ revealed to significantly inhibit the collagen production in fibroblasts, inhibiting fibrosis formation [371]. The IFN-γ cytokine increase only upon combined AsiDNA™ with radiotherapy treatments and could therefore function as a contributor to the delay in the onset of radiation-induced lung fibrosis observed following combined AsiDNA™ with CONV-RT treatment. Additionally, both TNF-α and IFN-γ have been identified as players in anti-cancer mechanisms. Studies revealed that TNF-α can damage neovascular endothelia, inducing broad scale cancer apoptosis signalling, impacting sites of metastasis, and combined TNF-α chemotherapy treatment can induce a synergy in tumour control [372], [373]. Additionally, IFN-γ can reduce tumour angiogenesis by inhibition of VEGF expression in the tumour microenvironment, and directly activate arrest of cell growth and apoptosis in ovarian cancer [374], [375]. It is to be speculated that this unique activation can, therefore, not only contribute to decreasing fibrosis formation, but also increasing tumour control, supporting the unique bilateral capacities of AsiDNA™.

Exploring the mechanism of action of AsiDNA™ in normal cells

The unique characteristics of AsiDNA™ activity have been used in vitro and in vivo for the identification and activation of AsiDNA™ in tumours and normal cells. There is however a distinct difference that appeared in previous conducted research of AsiDNA™ activity in normal cell. In vitro, normal cell lines that underwent treatment of AsiDNA™ exhibit the characteristic AsiDNA™ activity markers of pan nuclear γH2AX and HSP90-p equally to tumour treated cells [319]. Nevertheless, in vivo a clear difference appeared where AsiDNA™ activity detected through the pan-nuclear γH2AX staining revealed to be highly detectable in pre-clinical tumours and even in clinical tumours of patients receiving IV treatments of AsiDNA™ [335], [337]. In parallel, the detection of pan-nuclear γH2AX in normal tissue is severely decreased. The conducted research identified that normal cells respond differently to AsiDNA™ exposure depending on the division state of the cell. Our research revealed that non-dividing cells have a severe decrease of the standard AsiDNA™ activation markers γH2AX and HSP90-p that are activated following the inappropriate activation of DNA-PK by AsiDNA™, occurring in the nucleus. Our results furthermore illustrated that AsiDNA™ can enter both epithelial cells and fibroblasts, independent of their division state, evidenced by PARylation

following AsiDNA™ treatment in a dividing and quiescent cell state. AsiDNA is therefore In addition, AsiCy5.5 was detected in the nucleus of non-dividing and dividing cells, indicating that AsiDNA™ can enter the nucleus of both dividing and non-dividing cells. However, AsiDNA™ is unable to activate DNA-PK explicitly in the nucleus of non-dividing cells (G0/G1-phase cells). A possible explanation for this is the need for the cells to go through the cell cycle for AsiDNA™ to be activated. More evidence for this can be found in the appearance of the AsiDNA™ induced pan-nuclear staining explicitly in the G1-phase following M-phase progression. This appeared to be present in both normal and tumour cells (data not shown). More strikingly, γH2AX appears in G1 cells within hours post AsiDNA™ treatment, and the signal progressively increases with the incubation time, while AsiDNA™ can enter irrespectively of the phase of the cell cycle. One hypothesis that could explicitly link the pan-nuclear activation in G1-phase, is AsiDNA™'s dependency for cells to progress through cytokinesis allowing it to activate DNA-PK. It can be speculated that, in interphase and before cytokinesis, AsiDNA™ is not able to bind and activate DNA-PK or is able to bind and activate DNA-PK, but the latter cannot phosphorylate its substrates (H2AX and HSP90). During mitosis, the genome is tightly packed to facilitate smooth division of the chromosomes into the daughter cells and the nuclear membrane dissembled [376]. These structural changes may be required to form an AsiDNA™/DNA-PK complex which becomes fully active, after division, within the daughter cells. Future research is allocated to identify the mechanism driving the specific AsiDNA™-induced G1 phase pan-nuclear γH2AX.

In summary, the conducted research within this thesis has identified an AsiDNA™-induced reversible G1/S-arrest dependent on the DNA-PK/p53/p21 activation cascade exclusively in normal epithelial cells, fibroblasts, and intestinal crypt cells. The activation cascade can be exploited to protect intestine and lung against radiation-induced toxicity while maintaining tumour control, thereby acting as a unique bilateral agent. Additional studies revealed the possibility of the impact of AsiDNA™ treatment on tumour control through changes in inflammatory cytokine expression and the potential to exploit alterations in inflammatory cytokine expression for late responding biomarkers of AsiDNA™ activity. Finally, combined treatment of AsiDNA™ and FLASH radiotherapy indicate a potential similar mechanism through which the treatment modalities protect the normal tissue, uncovering a possible novel biological contributor to the FLASH effect.

V. BIBLIOGRAPHY

[1] H. Sung *et al.*, "Global Cancer Statistics 2020: GLOBOCAN Estimates of Incidence and Mortality Worldwide for 36 Cancers in 185 Countries," *CA Cancer J Clin*, vol. 71, no. 3, 2021, doi: 10.3322/caac.21660.

[2] C. M. Tilsed, S. A. Fisher, A. K. Nowak, R. A. Lake, and W. J. Lesterhuis, "Cancer chemotherapy: insights into cellular and tumor microenvironmental mechanisms of action," *Frontiers in Oncology*, vol. 12. 2022. doi: 10.3389/fonc.2022.960317.

[3] R. Sullivan *et al.*, "Global cancer surgery: Delivering safe, affordable, and timely cancer surgery," *The Lancet Oncology*, vol. 16, no. 11. 2015. doi: 10.1016/S1470-2045(15)00223-5.

[4] N. Kokudo *et al.*, "Genetic and histological assessment of surgical margins in resected liver metastases from colorectal carcinoma: Minimum surgical margins for successful resection," *Archives of Surgery*, vol. 137, no. 7, 2002.

[5] G. Delaney, S. Jacob, C. Featherstone, and M. Barton, "The role of radiotherapy in cancer treatment: Estimating optimal utilization from a review of evidence-based clinical guidelines," *Cancer*, vol. 104, no. 6. 2005. doi: 10.1002/cncr.21324.

[6] E. J. Hall and A. J. Giaccia, *Radiobiology for the Radiologist*, 8th edition. Lippincott Williams & Wilkins (LWW), 2018.

[7] D. T. Goodhead, "Spatial and temporal distribution of energy," *Health Phys*, vol. 55, no. 2, 1988, doi: 10.1097/00004032-198808000-00015.

[8] S. Le Caër, "Water radiolysis: Influence of oxide surfaces on H2 production under ionizing radiation," *Water (Switzerland)*, vol. 3, no. 1. 2011. doi: 10.3390/w3010235.

[9] R. Labarbe, L. Hotoiu, J. Barbier, and V. Favaudon, "A physicochemical model of reaction kinetics supports peroxyl radical recombination as the main determinant of the FLASH effect," *Radiotherapy and Oncology*, vol. 153, 2020, doi: 10.1016/j.radonc.2020.06.001.

[10] J. F. Ward, "DNA Damage Produced by Ionizing Radiation in Mammalian Cells: Identities, Mechanisms of Formation, and Reparability," *Prog Nucleic Acid Res Mol Biol*, vol. 35, no. C, 1988, doi: 10.1016/S0079-6603(08)60611-X.

[11] D. R. Boreham, K. L. Gale, S. R. Maves, J. A. Walker, and D. P. Morrison, "Radiation-induced apoptosis in human lymphocytes: Potential as a biological dosimeter," *Health Phys*, vol. 71, no. 5, 1996, doi: 10.1097/00004032-199611000-00007.

[12] A. Das *et al.*, "RIP1 and RIP3 complex regulates radiation-induced programmed necrosis in glioblastoma," *Tumor Biology*, vol. 37, no. 6, 2016, doi: 10.1007/s13277-015-4621-6.

[13] T. Juretschke and P. Beli, "Causes and consequences of DNA damage-induced autophagy," *Matrix Biology*, vol. 100–101, 2021, doi: 10.1016/j.matbio.2021.02.004.

[14] E. A. McCart *et al.*, "Accelerated senescence in skin in a murine model of radiation-induced multi-organ injury," *J Radiat Res*, vol. 58, no. 5, 2017, doi: 10.1093/jrr/rrx008.

[15] M. Fujimoto, T. Bo, K. Yamamoto, H. Yasui, T. Yamamori, and O. Inanami, "Radiation-induced abnormal centrosome amplification and mitotic catastrophe in human cervical tumor HeLa cells and murine mammary tumor EMT6 cells," *J Clin Biochem Nutr*, vol. 67, no. 3, 2020, doi: 10.3164/jcbn.19-80.

[16] E. I. Azzam, S. M. De Toledo, and J. B. Little, "Direct evidence for the participation of gap junction-mediated intercellular communication in the transmission of damage signals from α-particle irradiated to nonirradiated cells," *Proc Natl Acad Sci U S A*, vol. 98, no. 2, 2001, doi: 10.1073/pnas.011417098.

[17] H. Nagasawa and J. B. Little, "Induction of Sister Chromatid Exchanges by Extremely Low Doses of a-Particles," *Cancer Res*, vol. 52, no. 22, 1992.
[18] T. K. Hei *et al.*, "Mechanism of radiation-induced bystander effects: a unifying model," *Journal of Pharmacy and Pharmacology*, vol. 60, no. 8, 2010, doi: 10.1211/jpp.60.8.0001.
[19] S. J. McMahon and K. M. Prise, "Mechanistic modelling of radiation responses," *Cancers*, vol. 11, no. 2. 2019. doi: 10.3390/cancers11020205.
[20] R. M. Tuttle, "Controversial issues in thyroid cancer management," *Journal of Nuclear Medicine*, vol. 59, no. 8, 2018, doi: 10.2967/jnumed.117.192559.
[21] G. Marwaha, R. Macklis, A. D. Singh, and A. Wilkinson, "Brachytherapy," *Developments in Ophthalmology*, vol. 52. 2013. doi: 10.1159/000351053.
[22] A. Kaiser *et al.*, "Proton Therapy Delivery and Its Clinical Application in Select Solid Tumor Malignancies," *Journal of Visualized Experiments*, vol. 2019, no. 144, 2019, doi: 10.3791/58372.
[23] L. Faillace *et al.*, "Perspectives in linear accelerator for FLASH VHEE: Study of a compact C-band system," *Physica Medica*, vol. 104, 2022, doi: 10.1016/j.ejmp.2022.10.018.
[24] M. V. Graham, J. W. Matthews, W. B. Harms, B. Emami, H. S. Glazer, and J. A. Purdy, "Three-dimensional radiation treatment planning study for patients with carcinoma of the lung," *Int J Radiat Oncol Biol Phys*, vol. 29, no. 5, 1994, doi: 10.1016/0360-3016(94)90407-3.
[25] L. Begnozzi *et al.*, "Quality assurance of 3D-CRT: Indications and difficulties in their applications," *Critical Reviews in Oncology/Hematology*, vol. 70, no. 1. 2009. doi: 10.1016/j.critrevonc.2008.07.016.
[26] S. Webb, "The physical basis of IMRT and inverse planning," *British Journal of Radiology*, vol. 76, no. 910. 2003. doi: 10.1259/bjr/65676879.
[27] S. Derycke, W. R. T. De Gersem, B. B. R. Van Duyse, and W. C. J. De Neve, "Conformal radiotherapy of stage III non-small cell lung cancer: A class solution involving non-coplanar intensity-modulated beams," *Int J Radiat Oncol Biol Phys*, vol. 41, no. 4, 1998, doi: 10.1016/S0360-3016(98)00114-X.
[28] S. G. Chun *et al.*, "Impact of intensity-modulated radiation therapy technique for locally advanced non-small-cell lung cancer: A secondary analysis of the NRG oncology RTOG 0617 randomized clinical trial," *Journal of Clinical Oncology*, vol. 35, no. 1, 2017, doi: 10.1200/JCO.2016.69.1378.
[29] C. Lin *et al.*, "Effect of radiotherapy techniques (IMRT vs. 3D-CRT) on outcome in patients with intermediate-risk rhabdomyosarcoma enrolled in COG D9803 - A report from the children's oncology group," *Int J Radiat Oncol Biol Phys*, vol. 82, no. 5, 2012, doi: 10.1016/j.ijrobp.2011.01.036.
[30] J. Fleckenstein, K. Kremp, S. Kremp, J. Palm, and C. Rübe, "IMRT and 3D conformal radiotherapy with or without elective nodal irradiation in locally advanced NSCLC: A direct comparison of pet-based treatment planning," *Strahlentherapie und Onkologie*, vol. 192, no. 2, 2015, doi: 10.1007/s00066-015-0900-9.
[31] I. de Bree, M. G. E. van Hinsberg, and L. R. van Veelen, "High-dose radiotherapy in inoperable nonsmall cell lung cancer: Comparison of volumetric modulated arc therapy, dynamic IMRT and 3D conformal radiotherapy," *Medical Dosimetry*, vol. 37, no. 4, 2012, doi: 10.1016/j.meddos.2011.12.002.
[32] A. R. Yeung *et al.*, "Intensity-Modulated Radiation Therapy Reduces Patient-Reported Chronic Toxicity Compared with Conventional Pelvic Radiation Therapy: Updated

Results of a Phase III Trial," in *Journal of Clinical Oncology*, 2022. doi: 10.1200/JCO.21.02831.
[33] Y. Rong and J. S. Welsh, "Dosimetric and clinical review of helical tomotherapy," *Expert Review of Anticancer Therapy*, vol. 11, no. 2. 2011. doi: 10.1586/era.10.175.
[34] K. Otto, "Volumetric modulated arc therapy: IMRT in a single gantry arc," *Med Phys*, vol. 35, no. 1, 2008, doi: 10.1118/1.2818738.
[35] J. C. Marsh, G. E. Ziel, A. Z. Diaz, J. A. Wendt, R. Gobole, and J. V. Turian, "Integral dose delivered to normal brain with conventional intensity-modulated radiotherapy (IMRT) and helical tomotherapy IMRT during partial brain radiotherapy for high-grade gliomas with and without selective sparing of the hippocampus, limbic circuit and neural stem cell compartment," *J Med Imaging Radiat Oncol*, vol. 57, no. 3, 2013, doi: 10.1111/1754-9485.12048.
[36] H. H. Lee *et al.*, "Five-year survival outcomes of intensity-modulated radiotherapy with simultaneous integrated boost (IMRT-SIB) using forward IMRT or Tomotherapy for breast cancer," *Sci Rep*, vol. 10, no. 1, 2020, doi: 10.1038/s41598-020-61403-6.
[37] J. D. Ruben *et al.*, "The Effect of Intensity-Modulated Radiotherapy on Radiation-Induced Second Malignancies," *Int J Radiat Oncol Biol Phys*, vol. 70, no. 5, 2008, doi: 10.1016/j.ijrobp.2007.08.046.
[38] R. A. Scrimger, W. A. Tomé, G. H. Olivera, P. J. Reckwerdt, M. P. Mehta, and J. F. Fowler, "Reduction in radiation dose to lung and other normal tissues using helical tomotherapy to treat lung cancer, in comparison to conventional field arrangements," *American Journal of Clinical Oncology: Cancer Clinical Trials*, vol. 26, no. 1, 2003, doi: 10.1097/00000421-200302000-00014.
[39] W. P. Levin, H. Kooy, J. S. Loeffler, and T. F. DeLaney, "Proton beam therapy," *British Journal of Cancer*, vol. 93, no. 8. 2005. doi: 10.1038/sj.bjc.6602754.
[40] N. Y. Yu *et al.*, "Cardiopulmonary Toxicity Following Intensity-Modulated Proton Therapy (IMPT) Versus Intensity-Modulated Radiation Therapy (IMRT) for Stage III Non-Small Cell Lung Cancer," *Clin Lung Cancer*, vol. 23, no. 8, 2022, doi: 10.1016/j.cllc.2022.07.017.
[41] J. Y. Chang *et al.*, "Significant reduction of normal tissue dose by proton radiotherapy compared with three-dimensional conformal or intensity-modulated radiation therapy in Stage I or Stage III non-small-cell lung cancer," *Int J Radiat Oncol Biol Phys*, vol. 65, no. 4, 2006, doi: 10.1016/j.ijrobp.2006.01.052.
[42] D. N. Slatkin *et al.*, "Design of a multislit, variable width collimator for microplanar beam radiotherapy," *Review of Scientific Instruments*, vol. 66, no. 2, 1995, doi: 10.1063/1.1145940.
[43] F. A. Dilmanian *et al.*, "Interlaced x-ray microplanar beams: A radiosurgery approach with clinical potential," *Proc Natl Acad Sci U S A*, vol. 103, no. 25, 2006, doi: 10.1073/pnas.0603567103.
[44] Y. Prezado *et al.*, "Proton minibeam radiation therapy widens the therapeutic index for high-grade gliomas," *Sci Rep*, vol. 8, no. 1, 2018, doi: 10.1038/s41598-018-34796-8.
[45] Y. Prezado, S. Sarun, S. Gil, P. Deman, A. Bouchet, and G. Le Duc, "Increase of lifespan for glioma-bearing rats by using minibeam radiation therapy," *J Synchrotron Radiat*, vol. 19, no. 1, 2012, doi: 10.1107/S0909049511047042.
[46] Y. Prezado *et al.*, "Proton minibeam radiation therapy spares normal rat brain: Long-Term Clinical, Radiological and Histopathological Analysis," *Sci Rep*, vol. 7, no. 1, 2017, doi: 10.1038/s41598-017-14786-y.

[47] Y. Prezado *et al.*, "Tumor Control in RG2 Glioma-Bearing Rats: A Comparison Between Proton Minibeam Therapy and Standard Proton Therapy," *Int J Radiat Oncol Biol Phys*, vol. 104, no. 2, 2019, doi: 10.1016/j.ijrobp.2019.01.080.
[48] J. W. Hopewell and K. R. Trott, "Volume effects in radiobiology as applied to radiotherapy," *Radiotherapy and Oncology*, vol. 56, no. 3. 2000. doi: 10.1016/S0167-8140(00)00236-X.
[49] R. Asur, K. T. Butterworth, J. A. Penagaricano, K. M. Prise, and R. J. Griffin, "High dose bystander effects in spatially fractionated radiation therapy," *Cancer Letters*, vol. 356, no. 1. 2015. doi: 10.1016/j.canlet.2013.10.032.
[50] B. J. Blyth and P. J. Sykes, "Radiation-induced bystander effects: What are they, and how relevant are they to human radiation exposures?," *Radiation Research*, vol. 176, no. 2. 2011. doi: 10.1667/RR2548.1.
[51] A. Bertho *et al.*, "Evaluation of the Role of the Immune System Response After Minibeam Radiation Therapy," *Int J Radiat Oncol Biol Phys*, vol. 115, no. 2, 2023, doi: 10.1016/j.ijrobp.2022.08.011.
[52] A. Bouchet, R. Serduc, J. A. Laissue, and V. Djonov, "Effects of microbeam radiation therapy on normal and tumoral blood vessels," *Physica Medica*, vol. 31, no. 6, 2015, doi: 10.1016/j.ejmp.2015.04.014.
[53] A. A. Friedl, K. M. Prise, K. T. Butterworth, P. Montay-Gruel, and V. Favaudon, "Radiobiology of the FLASH effect," in *Medical Physics*, 2021. doi: 10.1002/mp.15184.
[54] V. Favaudon *et al.*, "Ultrahigh dose-rate FLASH irradiation increases the differential response between normal and tumor tissue in mice," *Sci Transl Med*, 2014, doi: 10.1126/scitranslmed.3008973.
[55] P. Montay-Gruel *et al.*, "Irradiation in a flash: Unique sparing of memory in mice after whole brain irradiation with dose rates above 100 Gy/s," *Radiotherapy and Oncology*, 2017, doi: 10.1016/j.radonc.2017.05.003.
[56] P. Montay-Gruel *et al.*, "X-rays can trigger the FLASH effect: Ultra-high dose-rate synchrotron light source prevents normal brain injury after whole brain irradiation in mice," *Radiotherapy and Oncology*, 2018, doi: 10.1016/j.radonc.2018.08.016.
[57] L. A. Soto *et al.*, "Flash irradiation results in reduced severe skin toxicity compared to conventional-dose-rate irradiation," *Radiat Res*, vol. 194, no. 6, 2020, doi: 10.1667/RADE-20-00090.
[58] A. Velalopoulou *et al.*, "Flash proton radiotherapy spares normal epithelial and mesenchymal tissues while preserving sarcoma response," *Cancer Res*, vol. 81, no. 18, 2021, doi: 10.1158/0008-5472.CAN-21-1500.
[59] K. Levy *et al.*, "Abdominal FLASH irradiation reduces radiation-induced gastrointestinal toxicity for the treatment of ovarian cancer in mice," *Sci Rep*, vol. 10, no. 1, 2020, doi: 10.1038/s41598-020-78017-7.
[60] J. L. Ruan *et al.*, "Irradiation at Ultra-High (FLASH) Dose Rates Reduces Acute Normal Tissue Toxicity in the Mouse Gastrointestinal System," *Int J Radiat Oncol Biol Phys*, vol. 111, no. 5, 2021, doi: 10.1016/j.ijrobp.2021.08.004.
[61] B. Singers Sørensen *et al.*, "In vivo validation and tissue sparing factor for acute damage of pencil beam scanning proton FLASH," *Radiotherapy and Oncology*, vol. 167, 2022, doi: 10.1016/j.radonc.2021.12.022.
[62] M. M. Kim *et al.*, "Comparison of flash proton entrance and the spread-out bragg peak dose regions in the sparing of mouse intestinal crypts and in a pancreatic tumor model," *Cancers (Basel)*, vol. 13, no. 16, 2021, doi: 10.3390/cancers13164244.

[63] E. S. Diffenderfer *et al.*, "Design, Implementation, and in Vivo Validation of a Novel Proton FLASH Radiation Therapy System," *Int J Radiat Oncol Biol Phys*, vol. 106, no. 2, 2020, doi: 10.1016/j.ijrobp.2019.10.049.
[64] M. C. Vozenin *et al.*, "The Advantage of FLASH Radiotherapy Confirmed in Mini-pig and Cat-cancer Patients," *Clinical Cancer Research*, 2019, doi: 10.1158/1078-0432.CCR-17-3375.
[65] P. Montay-Gruel *et al.*, "Long-term neurocognitive benefits of FLASH radiotherapy driven by reduced reactive oxygen species," *Proc Natl Acad Sci U S A*, 2019, doi: 10.1073/pnas.1901777116.
[66] X. Cao *et al.*, "Quantification of Oxygen Depletion During FLASH Irradiation In Vitro and In Vivo," *Int J Radiat Oncol Biol Phys*, vol. 111, no. 1, 2021, doi: 10.1016/j.ijrobp.2021.03.056.
[67] H. Kacem *et al.*, "Comparing radiolytic production of H2O2 and development of Zebrafish embryos after ultra high dose rate exposure with electron and transmission proton beams," *Radiotherapy and Oncology*, vol. 175, 2022, doi: 10.1016/j.radonc.2022.07.011.
[68] S. Cunningham *et al.*, "Flash proton pencil beam scanning irradiation minimizes radiation-induced leg contracture and skin toxicity in mice," *Cancers (Basel)*, vol. 13, no. 5, 2021, doi: 10.3390/cancers13051012.
[69] C. L. Limoli and M. C. Vozenin, "Reinventing Radiobiology in the Light of FLASH Radiotherapy," *Annual Review of Cancer Biology*, vol. 7. 2023. doi: 10.1146/annurev-cancerbio-061421-022217.
[70] P. Montay-Gruel *et al.*, "Hypofractionated FLASH-RT as an effective treatment against glioblastoma that reduces neurocognitive side effects in mice," *Clinical Cancer Research*, vol. 27, no. 3, 2021, doi: 10.1158/1078-0432.CCR-20-0894.
[71] H. Zhu *et al.*, "Comparison of intratumor and local immune response between MV X-ray FLASH and conventional radiotherapies," *Clin Transl Radiat Oncol*, vol. 38, 2023, doi: 10.1016/j.ctro.2022.11.005.
[72] L. Iturri *et al.*, "Proton FLASH Radiation Therapy and Immune Infiltration: Evaluation in an Orthotopic Glioma Rat Model," *Int J Radiat Oncol Biol Phys*, vol. 116, no. 3, 2023, doi: 10.1016/j.ijrobp.2022.12.018.
[73] S. Shukla *et al.*, "Ultra-high dose-rate proton FLASH improves tumor control," *Radiotherapy and Oncology*, vol. 186, p. 109741, Sep. 2023, doi: 10.1016/j.radonc.2023.109741.
[74] J. T. Eggold *et al.*, "Abdominopelvic FLASH Irradiation Improves PD-1 Immune Checkpoint Inhibition in Preclinical Models of Ovarian Cancer," *Mol Cancer Ther*, vol. 21, no. 2, 2022, doi: 10.1158/1535-7163.MCT-21-0358.
[75] J. Bourhis *et al.*, "Treatment of a first patient with FLASH-radiotherapy," *Radiotherapy and Oncology*, 2019, doi: 10.1016/j.radonc.2019.06.019.
[76] A. E. Mascia *et al.*, "Proton FLASH Radiotherapy for the Treatment of Symptomatic Bone Metastases: The FAST-01 Nonrandomized Trial," *JAMA Oncol*, vol. 9, no. 1, 2023, doi: 10.1001/jamaoncol.2022.5843.
[77] Y. Alaghband *et al.*, "Uncovering the Protective Neurologic Mechanisms of Hypofractionated FLASH Radiotherapy," *Cancer Research Communications*, vol. 3, no. 4, pp. 725–737, Apr. 2023, doi: 10.1158/2767-9764.crc-23-0117.

[78] C. L. Limoli *et al.*, "The sparing effect of FLASH-RT on synaptic plasticity is maintained in mice with standard fractionation," *Radiotherapy and Oncology*, p. 109767, Sep. 2023, doi: 10.1016/j.radonc.2023.109767.
[79] F. E. Van Leeuwen and A. K. Ng, "Long-term risk of second malignancy and cardiovascular disease after Hodgkin lymphoma treatment," *Hematology*, vol. 2016, no. 1, 2016, doi: 10.1182/asheducation-2016.1.323.
[80] D. De Ruysscher, G. Niedermann, N. G. Burnet, S. Siva, A. W. M. Lee, and F. Hegi-Johnson, "Radiotherapy toxicity," *Nat Rev Dis Primers*, 2019, doi: 10.1038/s41572-019-0064-5.
[81] B. Emami *et al.*, "Tolerance of normal tissue to therapeutic irradiation," *Int J Radiat Oncol Biol Phys*, vol. 21, no. 1, 1991, doi: 10.1016/0360-3016(91)90171-Y.
[82] R. Mir *et al.*, "Organ at risk delineation for radiation therapy clinical trials: Global Harmonization Group consensus guidelines: GHG OAR consensus contouring guidance," *Radiotherapy and Oncology*, vol. 150, 2020, doi: 10.1016/j.radonc.2020.05.038.
[83] T. S. Kehwar, "Analytical approach to estimate normal tissue complication probability using best fit of normal tissue tolerance doses into the NTCP equation of the linear quadratic model," *J Cancer Res Ther*, vol. 1, no. 3, 2005, doi: 10.4103/0973-1482.19597.
[84] H. Rodney Withers, J. M. G. Taylor, and B. Maciejewski, "Treatment volume and tissue tolerance," *Int J Radiat Oncol Biol Phys*, vol. 14, no. 4, 1988, doi: 10.1016/0360-3016(88)90098-3.
[85] M. Ruiz-Ortega, S. Rayego-Mateos, S. Lamas, A. Ortiz, and R. R. Rodrigues-Diez, "Targeting the progression of chronic kidney disease," *Nature Reviews Nephrology*, vol. 16, no. 5. 2020. doi: 10.1038/s41581-019-0248-y.
[86] C. Wilke, D. Grosshans, J. Duman, P. Brown, and J. Li, "Radiation-induced cognitive toxicity: Pathophysiology and interventions to reduce toxicity in adults," *Neuro Oncol*, vol. 20, no. 5, 2018, doi: 10.1093/neuonc/nox195.
[87] M. E. Nader and P. W. Gidley, "Challenges of Hearing Rehabilitation after Radiation and Chemotherapy," *Journal of Neurological Surgery, Part B: Skull Base*, vol. 80, no. 2. 2019. doi: 10.1055/s-0039-1677865.
[88] S. J. Ahn *et al.*, "Dosimetric and clinical predictors for radiation-induced esophageal injury," *Int J Radiat Oncol Biol Phys*, vol. 61, no. 2, 2005, doi: 10.1016/j.ijrobp.2004.06.014.
[89] E. Donnellan, D. Phelan, C. P. Mccarthy, P. Collier, M. Desai, and B. Griffin, "Radiation-induced heart disease: A practical guide to diagnosis and management," *Cleveland Clinic Journal of Medicine*, vol. 83, no. 12. 2016. doi: 10.3949/ccjm.83a.15104.
[90] S. Zuppone *et al.*, "Pre-clinical Research on Bladder Toxicity After Radiotherapy for Pelvic Cancers: State-of-the Art and Challenges," *Frontiers in Oncology*, vol. 10. 2020. doi: 10.3389/fonc.2020.527121.
[91] T. Rancati *et al.*, "Radiation Dose-Volume Effects in the Larynx and Pharynx," *Int J Radiat Oncol Biol Phys*, vol. 76, no. 3 SUPPL., 2010, doi: 10.1016/j.ijrobp.2009.03.079.
[92] L. A. Dawson, D. Normolle, J. M. Balter, C. J. McGinn, T. S. Lawrence, and R. K. Ten Haken, "Analysis of radiation-induced liver disease using the Lyman NTCP model," *Int J Radiat Oncol Biol Phys*, vol. 53, no. 4, 2002, doi: 10.1016/S0360-3016(02)02846-8.
[93] A. N. Hanania, W. Mainwaring, Y. T. Ghebre, N. A. Hanania, and M. Ludwig, "Radiation-Induced Lung Injury: Assessment and Management," *Chest*, vol. 156, no. 1. 2019. doi: 10.1016/j.chest.2019.03.033.

[94] A. L. Dicarlo *et al.*, "Cutaneous Radiation Injuries: Models, Assessment and Treatments1," in *Radiation Research*, 2020. doi: 10.1667/RADE-20-00120.1.
[95] A. K. Shadad, F. J. Sullivan, J. D. Martin, and L. J. Egan, "Gastrointestinal radiation injury: symptoms, risk factors and mechanisms.," *World journal of gastroenterology : WJG*, vol. 19, no. 2. 2013. doi: 10.3748/wjg.v19.i2.185.
[96] C. S. Wong, M. G. Fehlings, and A. Sahgal, "Pathobiology of radiation myelopathy and strategies to mitigate injury," *Spinal Cord*, vol. 53, no. 8. 2015. doi: 10.1038/sc.2015.43.
[97] R. Nuzzi *et al.*, "Ocular complications after radiation therapy: An observational study," *Clinical Ophthalmology*, vol. 14, 2020, doi: 10.2147/OPTH.S263291.
[98] J. O. Deasy, V. Moiseenko, L. Marks, K. S. C. Chao, J. Nam, and A. Eisbruch, "Radiotherapy Dose-Volume Effects on Salivary Gland Function," *Int J Radiat Oncol Biol Phys*, vol. 76, no. 3 SUPPL., 2010, doi: 10.1016/j.ijrobp.2009.06.090.
[99] R. ping Zhai, F. fang Kong, C. run Du, C. su Hu, and H. mei Ying, "Radiation-induced hypothyroidism after IMRT for nasopharyngeal carcinoma: Clinical and dosimetric predictors in a prospective cohort study," *Oral Oncol*, vol. 68, 2017, doi: 10.1016/j.oraloncology.2017.03.005.
[100] M. K. Farris *et al.*, "Bench to bedside: Animal models of radiation induced musculoskeletal toxicity," *Cancers*, vol. 12, no. 2. 2020. doi: 10.3390/cancers12020427.
[101] Z. Huang *et al.*, "Dimethyl Sulfoxide Attenuates Radiation-Induced Testicular Injury through Facilitating DNA Double-Strand Break Repair," *Oxid Med Cell Longev*, vol. 2022, 2022, doi: 10.1155/2022/9137812.
[102] R. C. Reulen *et al.*, "Pregnancy and Labor Complications in Female Survivors of Childhood Cancer: The British Childhood Cancer Survivor Study," *J Natl Cancer Inst*, vol. 109, no. 11, 2017, doi: 10.1093/jnci/djx056.
[103] D. Meirow, H. Biederman, R. A. Anderson, and W. H. B. Wallace, "Toxicity of chemotherapy and radiation on female reproduction," *Clinical Obstetrics and Gynecology*, vol. 53, no. 4. 2010. doi: 10.1097/GRF.0b013e3181f96b54.
[104] N. S. Bese, A. Iribas, A. Dirican, D. Oksuz, G. Atkovar, and A. Ober, "Ovarian ablation by radiation therapy: Is it still an option for the ablation of ovarian function in endocrine responsive premenopausal breast cancer patients?," *Breast*, vol. 18, no. 5, 2009, doi: 10.1016/j.breast.2009.09.005.
[105] P. Gehr, M. Bachofen, and E. R. Weibel, "The normal human lung: ultrastructure and morphometric estimation of diffusion capacity," *Respir Physiol*, vol. 32, no. 2, 1978, doi: 10.1016/0034-5687(78)90104-4.
[106] J. D. Crapo, B. E. Barry, P. Gehr, M. Bachofen, and E. R. Weibel, "Cell number and cell characteristics of the normal human lung," *American Review of Respiratory Disease*, vol. 126, no. 2, 1982, doi: 10.1164/arrd.1982.126.2.332.
[107] M. R. Knowles and R. C. Boucher, "Mucus clearance as a primary innate defense mechanism for mammalian airways," *Journal of Clinical Investigation*, vol. 109, no. 5. 2002. doi: 10.1172/JCI0215217.
[108] L.-C. Chen, Z. Zhang, A. C. Myers, and S.-K. Huang, "Cutting Edge: Altered Pulmonary Eosinophilic Inflammation in Mice Deficient for Clara Cell Secretory 10-kDa Protein," *The Journal of Immunology*, vol. 167, no. 6, 2001, doi: 10.4049/jimmunol.167.6.3025.
[109] A. J. Booth *et al.*, "Acellular normal and fibrotic human lung matrices as a culture system for in vitro investigation," *Am J Respir Crit Care Med*, vol. 186, no. 9, 2012, doi: 10.1164/rccm.201204-0754OC.

[110] J. Xue *et al.*, "Transcriptome-Based Network Analysis Reveals a Spectrum Model of Human Macrophage Activation," *Immunity*, vol. 40, no. 2, 2014, doi: 10.1016/j.immuni.2014.01.006.
[111] J. A. Zepp *et al.*, "Distinct Mesenchymal Lineages and Niches Promote Epithelial Self-Renewal and Myofibrogenesis in the Lung," *Cell*, vol. 170, no. 6, 2017, doi: 10.1016/j.cell.2017.07.034.
[112] K. J. Travaglini *et al.*, "A molecular cell atlas of the human lung from single-cell RNA sequencing," *Nature*, vol. 587, no. 7835, 2020, doi: 10.1038/s41586-020-2922-4.
[113] J. A. Zepp and E. E. Morrisey, "Cellular crosstalk in the development and regeneration of the respiratory system," *Nature Reviews Molecular Cell Biology*, vol. 20, no. 9. 2019. doi: 10.1038/s41580-019-0141-3.
[114] PDQ Pediatric Treatment Editorial Board, *Unusual Cancers of Childhood Treatment (PDQ®): Patient Version*. 2002.
[115] R. P. Abratt, G. W. Morgan, G. Silvestri, and P. Willcox, "Pulmonary complications of radiation therapy," *Clinics in Chest Medicine*, vol. 25, no. 1. 2004. doi: 10.1016/S0272-5231(03)00126-6.
[116] R. P. Hill, A. Zaidi, J. Mahmood, and S. Jelveh, "Investigations into the role of inflammation in normal tissue response to irradiation," *Radiotherapy and Oncology*, vol. 101, no. 1, 2011, doi: 10.1016/j.radonc.2011.06.017.
[117] R. Perez-Alvarez *et al.*, "Interstitial Lung Disease Induced or Exacerbated by TNF-Targeted Therapies: Analysis of 122 Cases," *Semin Arthritis Rheum*, vol. 41, no. 2, 2011, doi: 10.1016/j.semarthrit.2010.11.002.
[118] G. W. Morgan, B. Pharm, and S. N. Breit, "Radiation and the lung: A reevaluation of the mechanisms mediating pulmonary injury," *Int J Radiat Oncol Biol Phys*, vol. 31, no. 2, 1995, doi: 10.1016/0360-3016(94)00477-3.
[119] G. C. Barnett *et al.*, "Normal tissue reactions to radiotherapy: Towards tailoring treatment dose by genotype," *Nature Reviews Cancer*, vol. 9, no. 2. 2009. doi: 10.1038/nrc2587.
[120] P. Rubin, C. J. Johnston, J. P. Williams, S. McDonald, and J. N. Finkelstein, "A perpetual cascade of cytokines postirradiation leads to pulmonary fibrosis," *Int J Radiat Oncol Biol Phys*, vol. 33, no. 1, 1995, doi: 10.1016/0360-3016(95)00095-G.
[121] Z. Vujaskovic, L. B. Marks, and M. S. Anscher, "The physical parameters and molecular events associated with radiation-induced lung toxicity," *Semin Radiat Oncol*, vol. 10, no. 4, 2000, doi: 10.1053/srao.2000.9424.
[122] K. Fleckenstein *et al.*, "Temporal Onset of Hypoxia and Oxidative Stress After Pulmonary Irradiation," *Int J Radiat Oncol Biol Phys*, vol. 68, no. 1, 2007, doi: 10.1016/j.ijrobp.2006.12.056.
[123] A. Andersson-Sjöland, K. Nihlberg, L. Eriksson, L. Bjermer, and G. Westergren-Thorsson, "Fibrocytes and the tissue niche in lung repair," *Respiratory Research*, vol. 12, no. 1. 2011. doi: 10.1186/1465-9921-12-76.
[124] M. Okubo *et al.*, "Predicting risk factors for radiation pneumonitis after stereotactic body radiation therapy for primary or metastatic lung tumours," *British Journal of Radiology*, vol. 90, no. 1073, 2017, doi: 10.1259/bjr.20160508.
[125] T. J. Bledsoe, S. K. Nath, and R. H. Decker, "Radiation Pneumonitis," *Clinics in Chest Medicine*, vol. 38, no. 2. W.B. Saunders, pp. 201–208, Jun. 01, 2017. doi: 10.1016/j.ccm.2016.12.004.

[126] C. K. Chan, "Corticosteroids and azathioprine do not prevent radiation-induced lung injury," *Can Respir J*, vol. 5, no. 3, 1998, doi: 10.1155/1998/896131.
[127] C. E. Rübe *et al.*, "Dose-dependent induction of transforming growth factor β (TGF-β) in the lung tissue of fibrosis-prone mice after thoracic irradiation," *Int J Radiat Oncol Biol Phys*, vol. 47, no. 4, 2000, doi: 10.1016/S0360-3016(00)00482-X.
[128] F. H. Epstein, W. A. Border, and N. A. Noble, "Transforming Growth Factor β in Tissue Fibrosis," *New England Journal of Medicine*, vol. 331, no. 19, pp. 1286–1292, Nov. 1994, doi: 10.1056/nejm199411103311907.
[129] X. Xu, P. Hong, Z. Wang, Z. Tang, and K. Li, "MicroRNAs in Transforming Growth Factor-Beta Signaling Pathway Associated With Fibrosis Involving Different Systems of the Human Body," *Frontiers in Molecular Biosciences*, vol. 8. 2021. doi: 10.3389/fmolb.2021.707461.
[130] X. Wu *et al.*, "Rho-Kinase 1/2 Inhibition Prevents Transforming Growth Factor-β-Induced Effects on Pulmonary Remodeling and Repair," *Front Pharmacol*, vol. 11, 2021, doi: 10.3389/fphar.2020.609509.
[131] K. C. Flanders *et al.*, "Mice lacking Smad3 are protected against cutaneous injury induced by ionizing radiation," *American Journal of Pathology*, vol. 160, no. 3, 2002, doi: 10.1016/S0002-9440(10)64926-7.
[132] S. A. Park *et al.*, "EW-7197 inhibits hepatic, renal, and pulmonary fibrosis by blocking TGF-β/Smad and ROS signaling," *Cellular and Molecular Life Sciences*, vol. 72, no. 10, 2015, doi: 10.1007/s00018-014-1798-6.
[133] J. Kharofa, E. P. Cohen, R. Tomic, Q. Xiang, and E. Gore, "Decreased risk of radiation pneumonitis with incidental concurrent use of angiotensin-converting enzyme inhibitors and thoracic radiation therapy," *Int J Radiat Oncol Biol Phys*, vol. 84, no. 1, 2012, doi: 10.1016/j.ijrobp.2011.11.013.
[134] D. H. Xia *et al.*, "The protective effects of ambroxol on radiation lung injury and influence on production of transforming growth factor β1 and tumor necrosis factor α," *Medical Oncology*, vol. 27, no. 3, 2010, doi: 10.1007/s12032-009-9271-3.
[135] D. Kenchegowda, D. L. Bolduc, L. Kurada, and W. F. Blakely, "Severity scoring systems for radiation-induced GI injury–prioritization for use of GI-ARS medical countermeasures," *International Journal of Radiation Biology*. Taylor and Francis Ltd., 2023. doi: 10.1080/09553002.2023.2210669.
[136] C. Atuma, V. Strugala, A. Allen, and L. Holm, "The adherent gastrointestinal mucus gel layer: Thickness and physical state in vivo," *Am J Physiol Gastrointest Liver Physiol*, vol. 280, no. 5 43-5, 2001, doi: 10.1152/ajpgi.2001.280.5.g922.
[137] H. Clevers, "XThe intestinal crypt, a prototype stem cell compartment," *Cell*, vol. 154, no. 2. 2013. doi: 10.1016/j.cell.2013.07.004.
[138] K. S. Yan *et al.*, "The intestinal stem cell markers Bmi1 and Lgr5 identify two functionally distinct populations," *Proc Natl Acad Sci U S A*, vol. 109, no. 2, 2012, doi: 10.1073/pnas.1118857109.
[139] N. Barker *et al.*, "Identification of stem cells in small intestine and colon by marker gene Lgr5," *Nature*, vol. 449, no. 7165, 2007, doi: 10.1038/nature06196.
[140] L. Ma *et al.*, "Effects of Immune Cells on Intestinal Stem Cells: Prospects for Therapeutic Targets," *Stem Cell Reviews and Reports*, vol. 18, no. 7. 2022. doi: 10.1007/s12015-022-10347-7.

[141] M. Hauer-Jensen, "Late radiation injury of the small intestine clinical, pathophysiologic and radiobiologic aspects: A review," *Acta Oncologica*, vol. 29, no. 4. 1990. doi: 10.3109/02841869009090022.
[142] M. Hauer-Jensen, J. W. Denham, and H. J. N. Andreyev, "Radiation enteropathy-Pathogenesis, treatment and prevention," *Nature Reviews Gastroenterology and Hepatology*, vol. 11, no. 8. 2014. doi: 10.1038/nrgastro.2014.46.
[143] H. J. N. Andreyev, "Gastrointestinal Problems after Pelvic Radiotherapy: the Past, the Present and the Future," *Clin Oncol*, vol. 19, no. 10, 2007, doi: 10.1016/j.clon.2007.08.011.
[144] F. A. Olopade *et al.*, "A modified Inflammatory Bowel Disease questionnaire and the Vaizey incontinence questionnaire are simple ways to identify patients with significant gastrointestinal symptoms after pelvic radiotherapy," *Br J Cancer*, vol. 92, no. 9, 2005, doi: 10.1038/sj.bjc.6602552.
[145] H. Li *et al.*, "Radiation-induced gastrointestinal (GI) syndrome as a function of age," *Cell Death Discov*, vol. 9, no. 1, 2023, doi: 10.1038/s41420-023-01298-0.
[146] A. Trotti *et al.*, "CTCAE v3.0: Development of a comprehensive grading system for the adverse effects of cancer treatment," in *Seminars in Radiation Oncology*, 2003. doi: 10.1016/S1053-4296(03)00031-6.
[147] F. Rieder, J. Brenmoehl, S. Leeb, J. Schölmerich, and G. Rogler, "Wound healing and fibrosis in intestinal disease," *Gut*, vol. 56, no. 1. 2007. doi: 10.1136/gut.2006.090456.
[148] J. Wei, H. Xu, Y. Liu, B. Li, and F. Zhou, "Effect of captopril on radiation-induced TGF-β1 secretion in EA.Hy926 human umbilical vein endothelial cells," *Oncotarget*, vol. 8, no. 13, 2017, doi: 10.18632/oncotarget.15356.
[149] S. Sathishkumar *et al.*, "Elevated sphingomyelinase activity and ceramide concentration in serum of patients undergoing high dose spatially fractionated radiation treatment. Implications for endothelial apoptosis," *Cancer Biol Ther*, vol. 4, no. 9, 2005, doi: 10.4161/cbt.4.9.1915.
[150] J. Kountouras and C. Zavos, "Recent advances in the management of radiation colitis," *World J Gastroenterol*, vol. 14, no. 48, 2008, doi: 10.3748/wjg.14.7289.
[151] L. Lu *et al.*, "Radiation-induced intestinal damage: Latest molecular and clinical developments," *Future Oncology*, vol. 15, no. 35. 2019. doi: 10.2217/fon-2019-0416.
[152] C. S. Potten, R. Gandara, Y. R. Mahida, M. Loeffler, and N. A. Wright, "The stem cells of small intestinal crypts: Where are they?," *Cell Proliferation*, vol. 42, no. 6. 2009. doi: 10.1111/j.1365-2184.2009.00642.x.
[153] G. Hua *et al.*, "Crypt base columnar stem cells in small intestines of mice are radioresistant," *Gastroenterology*, vol. 143, no. 5, 2012, doi: 10.1053/j.gastro.2012.07.106.
[154] C. S. Potten, "Radiation, the Ideal Cytotoxic Agent for Studying the Cell Biology of Tissues such as the Small Intestine," in *Radiation Research*, 2004. doi: 10.1667/RR3104.
[155] A. Ayyaz *et al.*, "Single-cell transcriptomes of the regenerating intestine reveal a revival stem cell," *Nature*, vol. 569, no. 7754, 2019, doi: 10.1038/s41586-019-1154-y.
[156] R. A. Shivdasani, H. Clevers, and F. J. de Sauvage, "Tissue regeneration: Reserve or reverse?," *Science (1979)*, vol. 371, no. 6531, 2021, doi: 10.1126/science.abb6848.
[157] B. J. Sheahan *et al.*, "Epithelial Regeneration After Doxorubicin Arises Primarily From Early Progeny of Active Intestinal Stem Cells," *CMGH*, vol. 12, no. 1, 2021, doi: 10.1016/j.jcmgh.2021.01.015.

[158] C. Linard, A. Ropenga, M. C. Vozenin-Brotons, A. Chapel, and D. Mathe, "Abdominal irradiation increases inflammatory cytokine expression and activates NF-κB in rat ileal muscularis layer," *Am J Physiol Gastrointest Liver Physiol*, vol. 285, no. 3 48-3, 2003, doi: 10.1152/ajpgi.00094.2003.
[159] V. S. Theis, R. Sripadam, V. Ramani, and S. Lal, "Chronic Radiation Enteritis," *Clin Oncol*, vol. 22, no. 1, 2010, doi: 10.1016/j.clon.2009.10.003.
[160] M. Hauer-Jensen, J. Wang, M. Boerma, Q. Fu, and J. W. Denham, "Radiation damage to the gastrointestinal tract: mechanisms, diagnosis, and management.," *Current opinion in supportive and palliative care*, vol. 1, no. 1. 2007. doi: 10.1097/spc.0b013e3281108014.
[161] V. Haydont, B. L. Riser, J. Aigueperse, and M. C. Vozenin-Brotons, "Specific signals involved in the long-term maintenance of radiation-induced fibrogenic differentiation: A role for CCN2 and low concentration of TGF-β1," *Am J Physiol Cell Physiol*, vol. 294, no. 6, 2008, doi: 10.1152/ajpcell.90626.2007.
[162] L. J. Wedlake *et al.*, "Evaluating the efficacy of statins and ACE-inhibitors in reducing gastrointestinal toxicity in patients receiving radiotherapy for pelvic malignancies," *Eur J Cancer*, vol. 48, no. 14, 2012, doi: 10.1016/j.ejca.2011.12.034.
[163] F. Ye, J. Ning, Z. Fardous, T. Katsube, Q. Li, and B. Wang, "Citrulline, A Potential Biomarker of Radiation-Induced Small Intestine Damage," *Dose-Response*, vol. 18, no. 3. 2020. doi: 10.1177/1559325820962341.
[164] A. M. Decker, Y. Jung, F. C. Cackowski, K. Yumoto, J. Wang, and R. S. Taichman, "Sympathetic signaling reactivates quiescent disseminated prostate cancer cells in the bone marrow," *Molecular Cancer Research*, vol. 15, no. 12, 2017, doi: 10.1158/1541-7786.MCR-17-0132.
[165] A. Koff *et al.*, "Human cyclin E, a new cyclin that interacts with two members of the CDC2 gene family," *Cell*, vol. 66, no. 6, 1991, doi: 10.1016/0092-8674(91)90044-Y.
[166] S. Ortega, M. Malumbres, and M. Barbacid, "Cyclin D-dependent kinases, INK4 inhibitors and cancer," *Biochimica et Biophysica Acta - Reviews on Cancer*, vol. 1602, no. 1. 2002. doi: 10.1016/S0304-419X(02)00037-9.
[167] S. W. Blain, "Switching cyclin D-Cdk4 kinase activity on and off," *Cell Cycle*, vol. 7, no. 7. 2008. doi: 10.4161/cc.7.7.5637.
[168] I. H. Lee *et al.*, "Atg7 modulates p53 activity to regulate cell cycle and survival during metabolic stress (Science (2012) (225-258))," *Science*, vol. 341, no. 6145. 2013. doi: 10.1126/science.341.6145.457-b.
[169] M. Malumbres and M. Barbacid, "Mammalian cyclin-dependent kinases," *Trends in Biochemical Sciences*, vol. 30, no. 11. 2005. doi: 10.1016/j.tibs.2005.09.005.
[170] D. R. Iyer and N. Rhind, "The intra-S checkpoint responses to DNA damage," *Genes*, vol. 8, no. 2. 2017. doi: 10.3390/genes8020074.
[171] D. Ciardo, A. Goldar, and K. Marheineke, "On the interplay of the DNA replication program and the Intra-S phase checkpoint pathway," *Genes*, vol. 10, no. 2. 2019. doi: 10.3390/genes10020094.
[172] L. H. Tsai, E. Harlow, and M. Meyerson, "Isolation of the human cdk2 gene that encodes the cyclin A- and adenovirus E1A-associated p33 kinase," *Nature*, vol. 353, no. 6340, 1991, doi: 10.1038/353174a0.
[173] M. Malumbres, "Physiological relevance of cell cycle kinases," *Physiological Reviews*, vol. 91, no. 3. 2011. doi: 10.1152/physrev.00025.2010.

[174] B. Xu, S.-T. Kim, D.-S. Lim, and M. B. Kastan, " Two Molecularly Distinct G 2 /M Checkpoints Are Induced by Ionizing Irradiation ," *Mol Cell Biol*, vol. 22, no. 4, 2002, doi: 10.1128/mcb.22.4.1049-1059.2002.
[175] N. Pavin and I. M. Tolić, "Mechanobiology of the Mitotic Spindle," *Developmental Cell*, vol. 56, no. 2. 2021. doi: 10.1016/j.devcel.2020.11.003.
[176] M. Sun *et al.*, "NuMA regulates mitotic spindle assembly, structural dynamics and function via phase separation," *Nat Commun*, vol. 12, no. 1, 2021, doi: 10.1038/s41467-021-27528-6.
[177] S. Jensen and L. H. Johnston, "Complexity of mitotic exit.," *Cell cycle (Georgetown, Tex.)*, vol. 1, no. 5. 2002. doi: 10.4161/cc.1.5.142.
[178] C. Norden, M. Mendoza, J. Dobbelaere, C. V. Kotwaliwale, S. Biggins, and Y. Barral, "The NoCut Pathway Links Completion of Cytokinesis to Spindle Midzone Function to Prevent Chromosome Breakage," *Cell*, vol. 125, no. 1, 2006, doi: 10.1016/j.cell.2006.01.045.
[179] D. J. Gordon, B. Resio, and D. Pellman, "Causes and consequences of aneuploidy in cancer," *Nature Reviews Genetics*, vol. 13, no. 3. 2012. doi: 10.1038/nrg3123.
[180] R. Bhowmick *et al.*, "The RIF1-PP1 Axis Controls Abscission Timing in Human Cells," *Current Biology*, vol. 29, no. 7, 2019, doi: 10.1016/j.cub.2019.02.037.
[181] W. K. Sinclair, "Cyclic X-ray responses in mammalian cells in vitro," *Radiat Res*, vol. 33, no. 3, pp. 620–643, Aug. 1968, doi: 10.1667/RRAV09.1.
[182] W. K. Sinclair and R. A. Morton, "X-ray sensitivity during the cell generation cycle of cultured Chinese hamster cells.," *Radiat Res*, vol. 29, no. 3, 1966, doi: 10.2307/3572025.
[183] W. K. Sinclair and R. A. Morton, "X-Ray and Ultraviolet Sensitivity of Synchronized Chinese Hamster Cells at Various Stages of the Cell Cycle," *Biophys J*, vol. 5, no. 1, 1965, doi: 10.1016/S0006-3495(65)86700-5.
[184] O. Vos, H. A. E. M. Schenk, and D. Bootsma, "Survival of excess thymidine synchronized cell populations in vitro after x-irradiation in various phases of the cell cycle," *Int J Radiat Biol*, vol. 11, no. 5, pp. 495–503, 1966, doi: 10.1080/09553006614551281.
[185] X. Chen *et al.*, "Protection of normal proliferating cells against chemotherapy by staurosporine-mediated, selective, and reversible G1 arrest," *J Natl Cancer Inst*, vol. 92, no. 24, 2000, doi: 10.1093/jnci/92.24.1999.
[186] P. M. Price, R. L. Safirstein, and J. Megyesi, "Protection of renal cells from cisplatin toxicity by cell cycle inhibitors," *Am J Physiol Renal Physiol*, vol. 286, no. 2 55-2, 2004, doi: 10.1152/ajprenal.00192.2003.
[187] B. B. Mull, J. A. Livingston, N. Patel, T. Bui, K. K. Hunt, and K. Keyomarsi, "Specific, reversible G1 arrest by UCN-01 in vivo provides cytostatic protection of normal cells against cytotoxic chemotherapy in breast cancer," *Br J Cancer*, vol. 122, no. 6, 2020, doi: 10.1038/s41416-019-0707-z.
[188] B. Rao *et al.*, "Evaluation of an Actinomycin D/VX-680 aurora kinase inhibitor combination in p53-based cyclotherapy.," *Oncotarget*, vol. 1, no. 7, 2010, doi: 10.18632/oncotarget.198.
[189] J. E. Bisi, J. A. Sorrentino, P. J. Roberts, F. X. Tavares, and J. C. Strum, "Preclinical characterization of G1T28: A novel CDK4/6 inhibitor for reduction of chemotherapy-induced myelosuppression," *Mol Cancer Ther*, vol. 15, no. 5, 2016, doi: 10.1158/1535-7163.MCT-15-0775.

[190] J. Tian *et al.*, "Radioprotection and cell cycle arrest of intestinal epithelial cells by darinaparsin, a tumor radiosensitizer," *Int J Radiat Oncol Biol Phys*, vol. 87, no. 5, 2013, doi: 10.1016/j.ijrobp.2013.08.051.
[191] S. M. Johnson *et al.*, "Mitigation of hematologic radiation toxicity in mice through pharmacological quiescence induced by CDK4/6 inhibition," *Journal of Clinical Investigation*, vol. 120, no. 7, 2010, doi: 10.1172/JCI41402.
[192] D. I. H. Linzer and A. J. Levine, "Characterization of a 54K Dalton cellular SV40 tumor antigen present in SV40-transformed cells and uninfected embryonal carcinoma cells," *Cell*, vol. 17, no. 1, 1979, doi: 10.1016/0092-8674(79)90293-9.
[193] D. P. Lane and L. V. Crawford, "T antigen is bound to a host protein in SY40-transformed cells [19]," *Nature*, vol. 278, no. 5701. 1979. doi: 10.1038/278261a0.
[194] L. A. Donehower *et al.*, "Mice deficient for p53 are developmentally normal but susceptible to spontaneous tumours," *Nature*, vol. 356, no. 6366, 1992, doi: 10.1038/356215a0.
[195] S. Lain and D. Lane, "Improving cancer therapy by non-genotoxic activation of p53," *European Journal of Cancer*, vol. 39, no. 8. 2003. doi: 10.1016/S0959-8049(03)00063-7.
[196] V. L. Buchman, P. M. Chumakov, N. N. Ninkina, O. P. Samarina, and G. P. Georgiev, "A variation in the structure of the protein-coding region of the human p53 gene," *Gene*, vol. 70, no. 2, 1988, doi: 10.1016/0378-1119(88)90196-5.
[197] S. J. Baker *et al.*, "Chromosome 17 deletions and p53 gene mutations in colorectal carcinomas," *Science (1979)*, vol. 244, no. 4901, 1989, doi: 10.1126/science.2649981.
[198] C. C. Harris, "Structure and function of the p53 tumor suppressor gene: Clues for rational cancer therapeutic strategies," *J Natl Cancer Inst*, vol. 88, no. 20, pp. 1442–1455, 1996, doi: 10.1093/jnci/88.20.1442.
[199] C. A. Brady *et al.*, "Distinct p53 transcriptional programs dictate acute DNA-damage responses and tumor suppression," *Cell*, vol. 145, no. 4, 2011, doi: 10.1016/j.cell.2011.03.035.
[200] M. Berger, R. V. Sionov, A. J. Levine, and Y. Haupt, "A Role for the Polyproline Domain of p53 in Its Regulation by Mdm2," *Journal of Biological Chemistry*, vol. 276, no. 6, 2001, doi: 10.1074/jbc.M008879200.
[201] W. S. El-Deiry, S. E. Kern, J. A. Pietenpol, K. W. Kinzler, and B. Vogelstein, "Definition of a consensus binding site for p53," *Nat Genet*, vol. 1, no. 1, 1992, doi: 10.1038/ng0492-45.
[202] T. D. Halazonetis and A. N. Kandil, "Conformational shifts propagate from the oligomerization domain of p53 to its tetrameric DNA binding domain and restore DNA binding to select p53 mutants.," *EMBO J*, vol. 12, no. 13, 1993, doi: 10.1002/j.1460-2075.1993.tb06199.x.
[203] M. Retzlaff *et al.*, "The regulatory domain stabilizes the p53 tetramer by intersubunit contacts with the DNA binding domain," *J Mol Biol*, vol. 425, no. 1, 2013, doi: 10.1016/j.jmb.2012.10.015.
[204] D. W. Meek and C. W. Anderson, "Posttranslational modification of p53: cooperative integrators of function.," *Cold Spring Harbor perspectives in biology*, vol. 1, no. 6. 2009. doi: 10.1101/cshperspect.a000950.
[205] K. D. Sullivan, M. D. Galbraith, Z. Andrysik, and J. M. Espinosa, "Mechanisms of transcriptional regulation by p53," *Cell Death and Differentiation*, vol. 25, no. 1. 2018. doi: 10.1038/cdd.2017.174.

[206] O. Laptenko, D. R. Tong, J. Manfredi, and C. Prives, "The Tail That Wags the Dog: How the Disordered C-Terminal Domain Controls the Transcriptional Activities of the p53 Tumor-Suppressor Protein," *Trends in Biochemical Sciences*, vol. 41, no. 12. 2016. doi: 10.1016/j.tibs.2016.08.011.
[207] A. M. Bode and Z. Dong, "Post-translational modification of p53 in tumorigenesis," *Nature Reviews Cancer*, vol. 4, no. 10. 2004. doi: 10.1038/nrc1455.
[208] D. P. Teufel, M. Bycroft, and A. R. Fersht, "Regulation by phosphorylation of the relative affinities of the N-terminal transactivation domains of p53 for p300 domains and Mdm2," *Oncogene*, vol. 28, no. 20, 2009, doi: 10.1038/onc.2009.71.
[209] H. Feng *et al.*, "Structural Basis for p300 Taz2-p53 TAD1 Binding and Modulation by Phosphorylation," *Structure*, vol. 17, no. 2, 2009, doi: 10.1016/j.str.2008.12.009.
[210] J. R. Jabbur, P. Huang, and W. Zhang, "DNA damage-induced phosphorylation of p53 at serine 20 correlates with p21 and Mdm-2 induction in vivo," *Oncogene*, vol. 19, no. 54, 2000, doi: 10.1038/sj.onc.1204017.
[211] R. S. Tibbetts *et al.*, "A role for ATR in the DNA damage-induced phosphorylation of p53," *Genes Dev*, vol. 13, no. 2, 1999, doi: 10.1101/gad.13.2.152.
[212] L. Feng, M. Hollstein, and Y. Xu, "Ser46 phosphorylation regulates p53-dependent apoptosis and replicative senescence," *Cell Cycle*, vol. 5, no. 23, 2006, doi: 10.4161/cc.5.23.3526.
[213] K. Oda *et al.*, "p53AIP1, a potential mediator of p53-dependent apoptosis, and its regulation by ser-46-phosphorylated p53," *Cell*, vol. 102, no. 6, 2000, doi: 10.1016/S0092-8674(00)00073-8.
[214] Y. Tang, W. Zhao, Y. Chen, Y. Zhao, and W. Gu, "Acetylation Is Indispensable for p53 Activation," *Cell*, vol. 133, no. 4, 2008, doi: 10.1016/j.cell.2008.03.025.
[215] S. M. Sykes *et al.*, "Acetylation of the p53 DNA-Binding Domain Regulates Apoptosis Induction," *Mol Cell*, vol. 24, no. 6, 2006, doi: 10.1016/j.molcel.2006.11.026.
[216] M. Li, C. L. Brooks, F. Wu-Baer, D. Chen, R. Baer, and W. Gu, "Mono- Versus Polyubiquitination: Differential Control of p53 Fate by Mdm2," *Science (1979)*, vol. 302, no. 5652, 2003, doi: 10.1126/science.1091362.
[217] M. S. Rodriguez, J. M. P. Desterro, S. Lain, C. A. Midgley, D. P. Lane, and R. T. Hay, "SUMO-1 modification activates the transcriptional response of p53," *EMBO Journal*, vol. 18, no. 22, 1999, doi: 10.1093/emboj/18.22.6455.
[218] L. Chen and J. Chen, "MDM2-ARF complex regulates p53 sumoylation," *Oncogene*, vol. 22, no. 34, 2003, doi: 10.1038/sj.onc.1206851.
[219] D. P. Xirodimas, M. K. Saville, J. C. Bourdon, R. T. Hay, and D. P. Lane, "Mdm2-mediated NEDD8 conjugation of p53 inhibits its transcriptional activity," *Cell*, vol. 118, no. 1, 2004, doi: 10.1016/j.cell.2004.06.016.
[220] A. N. Blackford and S. P. Jackson, "ATM, ATR, and DNA-PK: The Trinity at the Heart of the DNA Damage Response," *Molecular Cell*, vol. 66, no. 6. 2017. doi: 10.1016/j.molcel.2017.05.015.
[221] R. M. Williams and X. Zhang, "Roles of ATM and ATR in DNA double strand breaks and replication stress," *Prog Biophys Mol Biol*, vol. 161, 2021, doi: 10.1016/j.pbiomolbio.2020.11.005.
[222] E. Appella and C. W. Anderson, "Post-translational modifications and activation of p53 by genotoxic stresses," *European Journal of Biochemistry*, vol. 268, no. 10. 2001. doi: 10.1046/j.1432-1327.2001.02225.x.

[223] N. D. Lakin and S. P. Jackson, "Regulation of p53 in response to DNA damage," *Oncogene*, vol. 18, no. 53. 1999. doi: 10.1038/sj.onc.1203015.
[224] J. W. Harper *et al.*, "Inhibition of cyclin-dependent kinases by p21," *Mol Biol Cell*, vol. 6, no. 4, 1995, doi: 10.1091/mbc.6.4.387.
[225] K. Engeland, "Cell cycle regulation: p53-p21-RB signaling," *Cell Death and Differentiation*, vol. 29, no. 5. 2022. doi: 10.1038/s41418-022-00988-z.
[226] J. P. Brown, W. Wei, and J. M. Sedivy, "Bypass of senescenoe after disruption of p21(CIP1)/(WAF1) gene in normal diploid human fibroblasts," *Science (1979)*, vol. 277, no. 5327, pp. 831–834, 1997, doi: 10.1126/science.277.5327.831.
[227] B. C. Dash and W. S. El-Deiry, " Phosphorylation of p21 in G 2 /M Promotes Cyclin B-Cdc2 Kinase Activity ," *Mol Cell Biol*, vol. 25, no. 8, pp. 3364–3387, 2005, doi: 10.1128/mcb.25.8.3364-3387.2005.
[228] H. Hermeking *et al.*, "14-3-3σ is a p53-regulated inhibitor of G2/M progression," *Mol Cell*, vol. 1, no. 1, 1997, doi: 10.1016/S1097-2765(00)80002-7.
[229] S. Jin *et al.*, "GADD45-induced cell cycle G2-M arrest associates with altered subcellular distribution of cyclin B1 and is independent of p38 kinase activity," *Oncogene*, vol. 21, no. 57, 2002, doi: 10.1038/sj.onc.1206034.
[230] M. Fischer, P. Grossmann, M. Padi, and J. A. DeCaprio, "Integration of TP53, DREAM, MMB-FOXM1 and RB-E2F target gene analyses identifies cell cycle gene regulatory networks," *Nucleic Acids Res*, vol. 44, no. 13, 2016, doi: 10.1093/nar/gkw523.
[231] J. Campisi, "Senescent cells, tumor suppression, and organismal aging: Good citizens, bad neighbors," *Cell*, vol. 120, no. 4. 2005. doi: 10.1016/j.cell.2005.02.003.
[232] T. Li *et al.*, "Tumor suppression in the absence of p53-mediated cell-cycle arrest, apoptosis, and senescence," *Cell*, vol. 149, no. 6, 2012, doi: 10.1016/j.cell.2012.04.026.
[233] M. Takagi, M. J. Absalon, K. G. McLure, and M. B. Kastan, "Regulation of p53 translation and induction after DNA damage by ribosomal protein L26 and nucleolin," *Cell*, vol. 123, no. 1, 2005, doi: 10.1016/j.cell.2005.07.034.
[234] C. L. Brooks and W. Gu, "p53 ubiquitination: Mdm2 and beyond," *Molecular Cell*, vol. 21, no. 3. 2006. doi: 10.1016/j.molcel.2006.01.020.
[235] K. Schlereth, J. P. Charles, A. C. Bretz, and T. Stiewe, "Life or death: p53-induced apoptosis requires DNA binding cooperativity," *Cell Cycle*, vol. 9, no. 20. 2010. doi: 10.4161/cc.9.20.13595.
[236] F. Murray-Zmijewski, E. A. Slee, and X. Lu, "A complex barcode underlies the heterogeneous response of p53 to stress," *Nature Reviews Molecular Cell Biology*, vol. 9, no. 9. 2008. doi: 10.1038/nrm2451.
[237] F. Paris *et al.*, "Endothelial apoptosis as the primary lesion initiating intestinal radiation damage in mice," *Science (1979)*, vol. 293, no. 5528, 2001, doi: 10.1126/science.1060191.
[238] M. S. Mendonca, H. Chin-Sinex, R. Dhaemers, L. E. Mead, M. C. Yoder, and D. A. Ingram, "Differential mechanisms of X-ray-induced cell death in human endothelial progenitor cells Isolated from cord blood and adults," *Radiat Res*, vol. 176, no. 2, 2011, doi: 10.1667/RR2427.1.
[239] H. C. Kuo *et al.*, "The p53 Transactivation Domain 1-Dependent Response to Acute DNA Damage in Endothelial Cells Protects against Radiation-Induced Cardiac Injury," *Radiat Res*, vol. 198, no. 2, 2022, doi: 10.1667/RADE-22-00001.1.

[240] C. L. Lee *et al.*, "p53 functions in endothelial cells to prevent radiation-induced myocardial injury in mice," *Sci Signal*, vol. 5, no. 234, 2012, doi: 10.1126/scisignal.2002918.
[241] N. Dainiak, "Hematologic consequences of exposure to ionizing radiation," *Experimental Hematology*, vol. 30, no. 6. 2002. doi: 10.1016/S0301-472X(02)00802-0.
[242] P. Mauch *et al.*, "Hematopoietic stem cell compartment: Acute and late effects of radiation therapy and chemotherapy," *Int J Radiat Oncol Biol Phys*, vol. 31, no. 5, 1995, doi: 10.1016/0360-3016(94)00430-S.
[243] J. P. Williams *et al.*, "Animal models for medical countermeasures to radiation exposure," *Radiation Research*, vol. 173, no. 4. 2010. doi: 10.1667/RR1880.1.
[244] H. Yu *et al.*, "Deletion of Puma protects hematopoietic stem cells and confers long-term survival in response to high-dose γ-irradiation," *Blood*, vol. 115, no. 17, 2010, doi: 10.1182/blood-2009-10-248278.
[245] L. Shao *et al.*, "Deletion of proapoptotic Puma selectively protects hematopoietic stem and progenitor cells against high-dose radiation," *Blood*, vol. 115, no. 23, 2010, doi: 10.1182/blood-2009-10-248872.
[246] D. G. Kirsch *et al.*, "P53 controls radiation-induced gastrointestinal syndrome in mice independent of apoptosis," *Science (1979)*, vol. 327, no. 5965, 2010, doi: 10.1126/science.1166202.
[247] M. Serrano, H. W. Lee, L. Chin, C. Cordon-Cardo, D. Beach, and R. A. DePinho, "Role of the INK4a locus in tumor suppression and cell mortality," *Cell*, vol. 85, no. 1, 1996, doi: 10.1016/S0092-8674(00)81079-X.
[248] A. Insinga *et al.*, "DNA damage in stem cells activates p21, inhibits p53, and induces symmetric self-renewing divisions," *Proc Natl Acad Sci U S A*, vol. 110, no. 10, 2013, doi: 10.1073/pnas.1213394110.
[249] M. Mohrin *et al.*, "Hematopoietic stem cell quiescence promotes error-prone DNA repair and mutagenesis," *Cell Stem Cell*, vol. 7, no. 2, 2010, doi: 10.1016/j.stem.2010.06.014.
[250] P. Kaur and C. S. Potten, "Cell Migration Velocities In the Crypts of the Small Intestine After Cytotoxic Insult Are Not Dependent On Mitotic Activity," *Cell Prolif*, vol. 19, no. 6, 1986, doi: 10.1111/j.1365-2184.1986.tb00761.x.
[251] C. S. Potten, "A comprehensive study of the radiobiological response of the murine (BDF1) small intestine," *International Journal of Radiation Biology*, vol. 58, no. 6. 1990. doi: 10.1080/09553009014552281.
[252] C. S. Potten, Y. Taylor, and J. H. Hendry, "The doubling time of regenerating clonogenic cells in the crypts of the irradiated mouse small intestine," *Int J Radiat Biol*, vol. 54, no. 6, 1988, doi: 10.1080/09553008814552421.
[253] A. J. Merritt *et al.*, "The Role of p53 in Spontaneous and Radiation-induced Apoptosis in the Gastrointestinal TVact of Normal and p53-deficient Mice," *Cancer Res*, vol. 54, no. 3, 1994.
[254] A. J. Merritt, T. D. Allen, C. S. Potten, and J. A. Hickman, "Apoptosis in small intestinal epithelia from p53-null mice: Evidence for a delayed, p53-indepdendent G2/M-associated cell death after γ-irradiation," *Oncogene*, vol. 14, no. 23, 1997, doi: 10.1038/sj.onc.1201126.
[255] I. Vitale, L. Galluzzi, M. Castedo, and G. Kroemer, "Mitotic catastrophe: a mechanism for avoiding genomic instability.," *Nat Rev Mol Cell Biol*, vol. 12, no. 6, 2011, doi: 10.1038/nrm3115.

[256] B. J. Leibowitz, W. Qiu, H. Liu, T. Cheng, L. Zhang, and J. Yu, "Uncoupling p53 functions in radiation-induced intestinal damage via PUMA and p21," *Molecular Cancer Research*, vol. 9, no. 5, 2011, doi: 10.1158/1541-7786.MCR-11-0052.
[257] V. Pant *et al.*, "Transient enhancement of p53 activity protects from radiation-induced gastrointestinal toxicity," *Proc Natl Acad Sci U S A*, vol. 116, no. 35, 2019, doi: 10.1073/pnas.1909550116.
[258] C. L. Lee *et al.*, "Sensitization of Vascular Endothelial Cells to Ionizing Radiation Promotes the Development of Delayed Intestinal Injury in Mice," *Radiat Res*, vol. 192, no. 3, 2019, doi: 10.1667/RR15371.1.
[259] H. M. Patt, E. B. Tyree, R. L. Straube, and D. E. Smith, "Cysteine protection against X irradiation," *Science (1979)*, vol. 110, no. 2852, 1949, doi: 10.1126/science.110.2852.213.
[260] C. Herskind, "Sulfhydryl protection and the oxygen effect on radiation-induced inactivation of r-chromatin in vitro. Influence of an OH scavenger: t-Butanol," *Radiat Res*, vol. 115, no. 1, 1988, doi: 10.2307/3577062.
[261] A. Mastromarino and R. Wilson, "Antibiotic radioprotection of mice exposed to supralethal whole body irradiation independent of antibacterial activity," *Radiat Res*, vol. 68, no. 2, 1976, doi: 10.2307/3574484.
[262] P. M. Calabro-Jones, R. C. Fahey, G. D. Smoluk, and J. F. Ward, "Alkaline phosphatase promotes radioprotection and accumulation of WR-1065 in v79-171 cells incubated in medium containing WR-2721," *Int J Radiat Biol*, vol. 47, no. 1, 1985, doi: 10.1080/09553008514550041.
[263] C. Savoye *et al.*, "Thiol WR-1065 and disulphide WR-33278, two metabolites of the drug Ethyol (WR-2721), protect DNA against fast neutron-induced strand breakage," *Int J Radiat Biol*, vol. 71, no. 2, 1997, doi: 10.1080/095530097144319.
[264] J. R. Kouvaris, V. E. Kouloulias, and L. J. Vlahos, "Amifostine: The First Selective-Target and Broad-Spectrum Radioprotector," *Oncologist*, vol. 12, no. 6, 2007, doi: 10.1634/theoncologist.12-6-738.
[265] M. I. Koukourakis and E. Maltezos, "Amifostine administration during radiotherapy for cancer patients with genetic, autoimmune, metabolic and other diseases," *Anti-Cancer Drugs*, vol. 17, no. 2. 2006. doi: 10.1097/00001813-200602000-00003.
[266] A. W. Beaven and T. C. Shea, "The effect of palifermin on chemotherapy- and radiation therapy-induced mucositis: A review of the current literature," *Supportive Cancer Therapy*, vol. 4, no. 4. 2007. doi: 10.3816/SCT.2007.n.014.
[267] P. J. Stiff, M. Leinonen, T. Kullenberg, M. Rudebeck, M. de Chateau, and R. Spielberger, "Long-Term Safety Outcomes in Patients with Hematological Malignancies Undergoing Autologous Hematopoietic Stem Cell Transplantation Treated with Palifermin to Prevent Oral Mucositis," *Biology of Blood and Marrow Transplantation*, vol. 22, no. 1, 2016, doi: 10.1016/j.bbmt.2015.08.018.
[268] D. Lauritano, M. Petruzzi, D. Di Stasio, and A. Lucchese, "Clinical effectiveness of palifermin in prevention and treatment of oral mucositis in children with acute lymphoblastic leukaemia: A case-control study," *Int J Oral Sci*, vol. 6, no. 1, 2014, doi: 10.1038/ijos.2013.93.
[269] A. Yuan and S. Sonis, "Emerging therapies for the prevention and treatment of oral mucositis," *Expert Opinion on Emerging Drugs*, vol. 19, no. 3. 2014. doi: 10.1517/14728214.2014.946403.

[270] D. K. Maurya and T. P. A. Devasagayam, "Ferulic acid inhibits gamma radiation-induced DNA strand breaks and enhances the survival of mice," *Cancer Biother Radiopharm*, vol. 28, no. 1, 2013, doi: 10.1089/cbr.2012.1263.
[271] M. B. Grace, W. F. Blakely, and M. R. Landauer, "Genistein-induced alterations of radiation-responsive gene expression," *Radiat Meas*, vol. 42, no. 6–7, 2007, doi: 10.1016/j.radmeas.2007.05.011.
[272] G. G. Nair and C. K. K. Nair, "Protection of cellular DNA and membrane from γ-radiation-induced damages and enhancement in DNA repair by sesamol," *Cancer Biother Radiopharm*, vol. 25, no. 6, 2010, doi: 10.1089/cbr.2010.0803.
[273] D. K. Maurya, V. P. Salvi, and C. K. Krishnan Nair, "Radioprotection of normal tissues in tumor-bearing mice by troxerutin," *J Radiat Res*, vol. 45, no. 2, 2004, doi: 10.1269/jrr.45.221.
[274] K. Min and S. E. Ebeler, "Quercetin inhibits hydrogen peroxide-induced DNA damage and enhances DNA repair in Caco-2 cells," *Food and Chemical Toxicology*, vol. 47, no. 11, 2009, doi: 10.1016/j.fct.2009.07.033.
[275] L. Liu *et al.*, "NOD2 agonist murabutide alleviates radiation-induced injury through DNA damage response pathway mediated by ATR," *J Cell Physiol*, vol. 234, no. 11, 2019, doi: 10.1002/jcp.28734.
[276] A. Chandra *et al.*, "PTH1-34 blocks radiation-induced osteoblast apoptosis by enhancing DNA repair through canonical Wnt pathway," *Journal of Biological Chemistry*, vol. 290, no. 1, 2015, doi: 10.1074/jbc.M114.608158.
[277] T. Affandi, A. M. Ohm, D. Gaillard, A. Haas, and M. E. Reyland, "Tyrosine kinase inhibitors protect the salivary gland from radiation damage by increasing DNA double-strand break repair," *Journal of Biological Chemistry*, vol. 296, 2021, doi: 10.1016/j.jbc.2021.100401.
[278] A. Kumar, S. Choudhary, J. S. Adhikari, and N. K. Chaudhury, "Sesamol ameliorates radiation induced DNA damage in hematopoietic system of whole body γ-irradiated mice," *Environ Mol Mutagen*, vol. 59, no. 1, 2018, doi: 10.1002/em.22118.
[279] D. K. Maurya, S. Balakrishnan, V. P. Salvi, and C. K. Nair, "Protection of cellular DNA from γ-radiation-induced damages and enhancement in DNA repair by troxerutin," *Mol Cell Biochem*, vol. 280, no. 1–2, 2005, doi: 10.1007/s11010-005-8052-3.
[280] J. Zhang *et al.*, "Quercetin Prevents Radiation-Induced Oral Mucositis by Upregulating BMI-1," *Oxid Med Cell Longev*, vol. 2021, 2021, doi: 10.1155/2021/2231680.
[281] Y. Nishiyama *et al.*, "Isorhamnetin promotes 53BP1 recruitment through the enhancement of ATM phosphorylation and protects mice from radiation gastrointestinal syndrome," *Genes (Basel)*, vol. 12, no. 10, 2021, doi: 10.3390/genes12101514.
[282] A. Nel, T. Xia, L. Mädler, and N. Li, "Toxic potential of materials at the nanolevel," *Science*, vol. 311, no. 5761. 2006. doi: 10.1126/science.1114397.
[283] A. Detappe, F. Lux, and O. Tillement, "Pushing radiation therapy limitations with theranostic nanoparticles," *Nanomedicine*, vol. 11, no. 9. 2016. doi: 10.2217/nnm.16.38.
[284] V. Jayaraman, G. Bhavesh, S. Chinnathambi, S. Ganesan, and P. Aruna, "Synthesis and characterization of hafnium oxide nanoparticles for bio-safety," *Materials Express*, vol. 4, no. 5, 2014, doi: 10.1166/mex.2014.1190.
[285] H. Sun, X. Wang, and S. Zhai, "The rational design and biological mechanisms of nanoradiosensitizers," *Nanomaterials*, vol. 10, no. 3. 2020. doi: 10.3390/nano10030504.

[286] L. M. Russell, C. M. Dawidczyk, and P. C. Searson, "Quantitative evaluation of the enhanced permeability and retention (EPR) effect," in *Methods in Molecular Biology*, vol. 1530, 2017. doi: 10.1007/978-1-4939-6646-2_14.
[287] N. N. Cheng *et al.*, "Chemical enhancement by nanomaterials under X-ray irradiation," *J Am Chem Soc*, vol. 134, no. 4, 2012, doi: 10.1021/ja210239k.
[288] X. D. Zhang *et al.*, "Ultrasmall glutathione-protected gold nanoclusters as next generation radiotherapy sensitizers with high tumor uptake and high renal clearance," *Sci Rep*, vol. 5, 2015, doi: 10.1038/srep08669.
[289] Y. Liu *et al.*, "Radiation-/hypoxia-induced solid tumor metastasis and regrowth inhibited by hypoxia-specific upconversion nanoradiosensitizer," *Biomaterials*, vol. 49, 2015, doi: 10.1016/j.biomaterials.2015.01.028.
[290] K. Stępień, R. P. Ostrowski, and E. Matyja, "Hyperbaric oxygen as an adjunctive therapy in treatment of malignancies, including brain tumours," *Medical Oncology*, vol. 33, no. 9. 2016. doi: 10.1007/s12032-016-0814-0.
[291] B. T. Oronsky, S. J. Knox, and J. Scicinski, "Six degrees of separation: The oxygen effect in the development of radiosensitizers," *Translational Oncology*, vol. 4, no. 4. 2011. doi: 10.1593/tlo.11166.
[292] J. Overgaard *et al.*, "Misonidazole combined with split-course radiotherapy in the treatment of invasive carcinoma of larynx and pharynx: Report from the DAHANCA 2 study," *Int J Radiat Oncol Biol Phys*, vol. 16, no. 4, 1989, doi: 10.1016/0360-3016(89)90917-6.
[293] R. C. Urtasun *et al.*, "Peripheral neuropathy related to misonidazole: incidence and pathology," *Br J Cancer*, vol. 37, no. SUPPL.3, 1978.
[294] J. Overgaard *et al.*, "A randomized double-blind phase III study of nimorazole as a hypoxic radiosensitizer of primary radiotherapy in supraglottic larynx and pharynx carcinoma. Results of the Danish Head and Neck Cancer Study (DAHANCA) Protocol 5-85," *Radiotherapy and Oncology*, vol. 46, no. 2, 1998, doi: 10.1016/S0167-8140(97)00220-X.
[295] J. Bentzen, K. Toustrup, J. G. Eriksen, H. Primdahl, L. J. Andersen, and J. Overgaard, "Locally advanced head and neck cancer treated with accelerated radiotherapy, the hypoxic modifier nimorazole and weekly cisplatin. Results from the DAHANCA 18 phase II study," *Acta Oncol (Madr)*, vol. 54, no. 7, 2015, doi: 10.3109/0284186X.2014.992547.
[296] J. Overgaard, "Improving radiotherapy of squamous cell carcinoma of the head and neck (HNSCC) through a continuous process of biological based clinical trials – a 40-year experience from the Danish Head and Neck Cancer Group – DAHANCA," *Eur J Cancer*, vol. 72, 2017, doi: 10.1016/s0959-8049(17)30416-1.
[297] J. T. T. Coates *et al.*, "The anti-malarial drug atovaquone potentiates platinum-mediated cancer cell death by increasing oxidative stress," *Cell Death Discov*, vol. 6, no. 1, 2020, doi: 10.1038/s41420-020-00343-6.
[298] M. Skwarski *et al.*, "Mitochondrial inhibitor atovaquone increases tumor oxygenation and inhibits hypoxic gene expression in patients with non-small cell lung cancer," *Clinical Cancer Research*, vol. 27, no. 9, 2021, doi: 10.1158/1078-0432.CCR-20-4128.
[299] Y. Huang *et al.*, "Wnt/β-catenin inhibitor ICG-001 enhances the antitumor efficacy of radiotherapy by increasing radiation-induced DNA damage and improving tumor immune microenvironment in hepatocellular carcinoma," *Radiotherapy and Oncology*, vol. 162, 2021, doi: 10.1016/j.radonc.2021.06.034.

[300] Y. Zheng, M. Xiao, J. Zhang, and F. Chang, "Micro RNA-640 Targeting SLIT1 Enhances Glioma Radiosensitivity by Restraining the Activation of Wnt/β-Catenin Signaling Pathway," *Br J Biomed Sci*, vol. 79, 2022, doi: 10.3389/bjbs.2022.10067.
[301] W. L. Liu *et al.*, "Targeting Phosphatidylinositide3-Kinase/Akt pathway by BKM120 for radiosensitization in hepatocellular carcinoma," *Oncotarget*, vol. 5, no. 11, 2014, doi: 10.18632/oncotarget.1978.
[302] S. Huang *et al.*, "Sym004, a novel anti-Egfr antibody mixture, augments radiation response in human lung and head and neck cancers," *Mol Cancer Ther*, vol. 12, no. 12, 2013, doi: 10.1158/1535-7163.MCT-13-0587.
[303] S. T. Durant *et al.*, "The brain-penetrant clinical ATM inhibitor AZD1390 radiosensitizes and improves survival of preclinical brain tumor models," *Sci Adv*, vol. 4, no. 6, 2018, doi: 10.1126/sciadv.aat1719.
[304] J. H. L. Fok *et al.*, "AZD7648 is a potent and selective DNA-PK inhibitor that enhances radiation, chemotherapy and olaparib activity," *Nat Commun*, vol. 10, no. 1, 2019, doi: 10.1038/s41467-019-12836-9.
[305] L. He and A. C. Dar, "Targeting drug-resistant mutations in ALK," *Nat Cancer*, vol. 3, no. 6, 2022, doi: 10.1038/s43018-022-00390-1.
[306] H. Xiao, Y. Zheng, L. Ma, L. Tian, and Q. Sun, "Clinically-Relevant ABC Transporter for Anti-Cancer Drug Resistance," *Frontiers in Pharmacology*, vol. 12. 2021. doi: 10.3389/fphar.2021.648407.
[307] D. B. Johnson *et al.*, "Acquired BRAF inhibitor resistance: A multicenter meta-analysis of the spectrum and frequencies, clinical behaviour, and phenotypic associations of resistance mechanisms," *Eur J Cancer*, vol. 51, no. 18, 2015, doi: 10.1016/j.ejca.2015.08.022.
[308] S. Bhattacharya and A. Asaithamby, "Repurposing DNA repair factors to eradicate tumor cells upon radiotherapy," *Translational Cancer Research*, vol. 6. 2017. doi: 10.21037/tcr.2017.05.22.
[309] A. Croset *et al.*, "Inhibition of DNA damage repair by artificial activation of PARP with siDNA," *Nucleic Acids Res*, 2013, doi: 10.1093/nar/gkt522.
[310] P. M. Girard *et al.*, "Evolution of tumor cells during AsiDNA treatment results in energy exhaustion, decrease in responsiveness to signal, and higher sensitivity to the drug," *Evol Appl*, 2020, doi: 10.1111/eva.12949.
[311] M. Quanz *et al.*, "Small-molecule drugs mimicking DNA damage: A new strategy for sensitizing tumors to radiotherapy," *Clinical Cancer Research*, 2009, doi: 10.1158/1078-0432.CCR-08-2108.
[312] N. Berthault *et al.*, "Comparison of distribution and activity of nanoparticles with short interfering DNA (Dbait) in various living systems," *Cancer Gene Ther*, 2011, doi: 10.1038/cgt.2011.39.
[313] M. Quanz, D. Chassoux, N. Berthault, C. Agrario, J. S. Sun, and M. Dutreix, "Hyperactivation of DNA-PK by double-strand break mimicking molecules disorganizes DNA damage response," *PLoS One*, 2009, doi: 10.1371/journal.pone.0006298.
[314] M. Quanz *et al.*, "Heat shock protein 90α (Hsp90α) is phosphorylated in response to DNA damage and accumulates in repair foci," *Journal of Biological Chemistry*, vol. 287, no. 12, 2012, doi: 10.1074/jbc.M111.320887.

[315] N. Coquery *et al.*, "Distribution and radiosensitizing effect of cholesterol-coupled Dbait molecule in rat model of glioblastoma," *PLoS One*, 2012, doi: 10.1371/journal.pone.0040567.
[316] S. Thierry, W. Jdey, S. Alculumbre, V. Soumelis, P. Noguiez-Hellin, and M. Dutreix, "The DNA repair inhibitor Dbait is specific for malignant hematologic cells in blood," *Mol Cancer Ther*, 2017, doi: 10.1158/1535-7163.MCT-17-0405.
[317] W. Jdey, S. Thierry, T. Popova, M. H. Stern, and M. Dutreix, "Micronuclei frequency in tumors is a predictive biomarker for genetic instability and sensitivity to the DNA repair inhibitor AsiDNA," *Cancer Res*, 2017, doi: 10.1158/0008-5472.CAN-16-2693.
[318] N. Berthault, P. Bergam, F. Pereira, P. M. Girard, and M. Dutreix, "Inhibition of DNA Repair by Inappropriate Activation of ATM, PARP, and DNA-PK with the Drug Agonist AsiDNA," *Cells*, vol. 11, no. 14, Jul. 2022, doi: 10.3390/cells11142149.
[319] W. Jdey *et al.*, "Drug-driven synthetic lethality: Bypassing tumor cell genetics with a combination of AsiDNA and PARP inhibitors," *Clinical Cancer Research*, 2017, doi: 10.1158/1078-0432.CCR-16-1193.
[320] I. M. Ward and J. Chen, "Histone H2AX Is Phosphorylated in an ATR-dependent Manner in Response to Replicational Stress," *Journal of Biological Chemistry*, vol. 276, no. 51, 2001, doi: 10.1074/jbc.C100569200.
[321] S. Hanasoge and M. Ljungman, "H2AX phosphorylation after UV irradiation is triggered by DNA repair intermediates and is mediated by the ATR kinase," *Carcinogenesis*, vol. 28, no. 11, 2007, doi: 10.1093/carcin/bgm157.
[322] B. Meyer, K. O. Voss, F. Tobias, B. Jakob, M. Durante, and G. Taucher-Scholz, "Clustered DNA damage induces pan-nuclear H2AX phosphorylation mediated by ATM and DNA-PK," *Nucleic Acids Res*, vol. 41, no. 12, 2013, doi: 10.1093/nar/gkt304.
[323] H. Lu, J. Saha, P. J. Beckmann, E. A. Hendrickson, and A. J. Davis, "DNA-PKcs promotes chromatin decondensation to facilitate initiation of the DNA damage response," *Nucleic Acids Res*, vol. 47, no. 18, 2019, doi: 10.1093/nar/gkz694.
[324] T. Stiff, M. O'Driscoll, N. Rief, K. Iwabuchi, M. Löbrich, and P. A. Jeggo, "ATM and DNA-PK Function Redundantly to Phosphorylate H2AX after Exposure to Ionizing Radiation," *Cancer Res*, vol. 64, no. 7, 2004, doi: 10.1158/0008-5472.CAN-03-3207.
[325] B. Mukherjee *et al.*, "DNA-PK phosphorylates histone H2AX during apoptotic DNA fragmentation in mammalian cells," *DNA Repair (Amst)*, vol. 5, no. 5, 2006, doi: 10.1016/j.dnarep.2006.01.011.
[326] E. P. Rogakou, D. R. Pilch, A. H. Orr, V. S. Ivanova, and W. M. Bonner, "DNA double-stranded breaks induce histone H2AX phosphorylation on serine 139," *Journal of Biological Chemistry*, vol. 273, no. 10, 1998, doi: 10.1074/jbc.273.10.5858.
[327] E. Moeglin *et al.*, "Uniform widespread nuclear phosphorylation of histone H2AX is an indicator of lethal DNA replication stress," *Cancers (Basel)*, vol. 11, no. 3, 2019, doi: 10.3390/cancers11030355.
[328] T. M. Marti, E. Hefner, L. Feeney, V. Natale, and J. E. Cleaver, "H2AX phosphorylation within the G1 phase after UV irradiation depends on nucleotide excision repair and not DNA double-strand breaks," *Proc Natl Acad Sci U S A*, vol. 103, no. 26, 2006, doi: 10.1073/pnas.0603779103.
[329] D. Ding *et al.*, "Induction and inhibition of the pan-nuclear gamma-H2AX response in resting human peripheral blood lymphocytes after X-ray irradiation," *Cell Death Discov*, vol. 2, no. 1, 2016, doi: 10.1038/cddiscovery.2016.11.

[330] W. Jdey *et al.*, "AsiDNA Treatment Induces Cumulative Antitumor Efficacy with a Low Probability of Acquired Resistance," *Neoplasia (United States)*, 2019, doi: 10.1016/j.neo.2019.06.006.
[331] N. I. Herath *et al.*, "The DNA repair inhibitor DT01 as a novel therapeutic strategy for chemosensitization of colorectal liver metastasis," *Mol Cancer Ther*, 2016, doi: 10.1158/1535-7163.MCT-15-0408.
[332] F. Devun *et al.*, "A preclinical study combining the DNA repair inhibitor Dbait with radiotherapy for the treatment of melanoma," *Neoplasia (United States)*, vol. 16, no. 10, 2014, doi: 10.1016/j.neo.2014.08.008.
[333] A. Schlegel *et al.*, "Pharmacokinetics and toxicity in rats and monkeys of coDbait: A therapeutic double-stranded DNA oligonucleotide conjugated to cholesterol," *Mol Ther Nucleic Acids*, vol. 1, no. 7, 2012, doi: 10.1038/mtna.2012.27.
[334] C. Le Tourneau *et al.*, "First-in-human phase I study of the DNA-repair inhibitor DT01 in combination with radiotherapy in patients with skin metastases from melanoma," *Br J Cancer*, 2016, doi: 10.1038/bjc.2016.120.
[335] C. Le Tourneau *et al.*, "A Phase 1 dose-escalation study to evaluate safety, pharmacokinetics and pharmacodynamics of AsiDNA, a first-in-class DNA repair inhibitor, administered intravenously in patients with advanced solid tumours," *Br J Cancer*, 2020, doi: 10.1038/s41416-020-01028-8.
[336] N. I. Herath *et al.*, "Potentiation of doxorubicin efficacy in hepatocellular carcinoma by the DNA repair inhibitor DT01 in preclinical models," *Eur Radiol*, vol. 27, no. 10, 2017, doi: 10.1007/s00330-017-4792-1.
[337] D. M. Ferreira S, Foray C, Gatto A, Larcher M, Heinrich S, Lupu M, Mispelter J, Boussin FD, Pouponnot C, "AsiDNA is a radiosensitizer with no added toxicity in medulloblastoma pediatric models," 2020, doi: 10.1158/1940-6207.CAPR-20-0054.
[338] F. Devun *et al.*, "Preclinical study of the DNA repair inhibitor Dbait in combination with chemotherapy in colorectal cancer," *J Gastroenterol*, vol. 47, no. 3, 2012, doi: 10.1007/s00535-011-0483-x.
[339] F. Devun, N. Herath, A. Denys, J. Sun, and M. Dutreix, "DNA repair inhibition by DT01 as an adjuvant therapy at each stage of hepatocellular cancer (HCC) treatment.," *Journal of Clinical Oncology*, vol. 33, no. 3_suppl, 2015, doi: 10.1200/jco.2015.33.3_suppl.303.
[340] N. I. Herath *et al.*, "Preclinical Studies Comparing Efficacy and Toxicity of DNA Repair Inhibitors, Olaparib, and AsiDNA, in the Treatment of Carboplatin-Resistant Tumors," *Front Oncol*, 2019, doi: 10.3389/fonc.2019.01097.
[341] N. Kotecki, C. Jungels, F. Hoerner, J. Canon, B. Colinet, and O. De Beaumont, *Long stabilization and disease control with AsiDNA TM , a first-in-class DNA Repair Inhibitor in combination with carboplatin with or without paclitaxel in patients with advanced solid tumors : A case report*, vol. 07, no. 2. 2021, pp. 1–6.
[342] L. Besse *et al.*, "Protocol for automated multivariate quantitative-image-based cytometry analysis by fluorescence microscopy of asynchronous adherent cells," *STAR Protoc*, vol. 4, no. 3, 2023, doi: 10.1016/j.xpro.2023.102446.
[343] S. Curras-Alonso *et al.*, "An interactive murine single-cell atlas of the lung responses to radiation injury," *Nat Commun*, vol. 14, no. 1, Dec. 2023, doi: 10.1038/s41467-023-38134-z.
[344] T. Xie *et al.*, "Single-Cell Deconvolution of Fibroblast Heterogeneity in Mouse Pulmonary Fibrosis," *Cell Rep*, vol. 22, no. 13, 2018, doi: 10.1016/j.celrep.2018.03.010.

[345] P. A. Reyfman *et al.*, "Single-cell transcriptomic analysis of human lung provides insights into the pathobiology of pulmonary fibrosis," *Am J Respir Crit Care Med*, vol. 199, no. 12, 2019, doi: 10.1164/rccm.201712-2410OC.
[346] L. M. Crosby and C. M. Waters, "Epithelial repair mechanisms in the lung," *American Journal of Physiology - Lung Cellular and Molecular Physiology*, vol. 298, no. 6. 2010. doi: 10.1152/ajplung.00361.2009.
[347] T. Tsukui *et al.*, "Collagen-producing lung cell atlas identifies multiple subsets with distinct localization and relevance to fibrosis," *Nat Commun*, vol. 11, no. 1, 2020, doi: 10.1038/s41467-020-15647-5.
[348] R. Peyser *et al.*, "Defining the activated fibroblast population in lung fibrosis using single-cell sequencing," *Am J Respir Cell Mol Biol*, vol. 61, no. 1, 2019, doi: 10.1165/rcmb.2018-0313OC.
[349] J. Chang *et al.*, "Circadian control of the secretory pathway maintains collagen homeostasis," *Nat Cell Biol*, vol. 22, no. 1, 2020, doi: 10.1038/s41556-019-0441-z.
[350] Z. Chen, Z. Wu, and W. Ning, "Advances in Molecular Mechanisms and Treatment of Radiation-Induced Pulmonary Fibrosis," *Translational Oncology*, vol. 12, no. 1. 2019. doi: 10.1016/j.tranon.2018.09.009.
[351] T. J. Koh and L. A. DiPietro, "Inflammation and wound healing: the role of the macrophage.," *Expert reviews in molecular medicine*, vol. 13. 2011. doi: 10.1017/S1462399411001943.
[352] T. T. Braga, I. C. Moura, A. P. Lepique, and N. O. S. Camara, "Editorial: Macrophages role in integrating tissue signals and biological processes in chronic inflammation and fibrosis," *Frontiers in Immunology*, vol. 8, no. JUL. 2017. doi: 10.3389/fimmu.2017.00845.
[353] T. S. Adams *et al.*, "Single-cell RNA-seq reveals ectopic and aberrant lung-resident cell populations in idiopathic pulmonary fibrosis," *Sci Adv*, vol. 6, no. 28, 2020, doi: 10.1126/sciadv.aba1983.
[354] H. Podgornik, M. Sok, I. Kern, J. Marc, and D. Cerne, "Lipoprotein lipase in non-small cell lung cancer tissue is highly expressed in a subpopulation of tumor-associated macrophages," *Pathol Res Pract*, vol. 209, no. 8, 2013, doi: 10.1016/j.prp.2013.06.004.
[355] H. Joshi *et al.*, "L-plastin enhances NLRP3 inflammasome assembly and bleomycin-induced lung fibrosis," *Cell Rep*, vol. 38, no. 11, 2022, doi: 10.1016/j.celrep.2022.110507.
[356] D. Hashimoto *et al.*, "Tissue-resident macrophages self-maintain locally throughout adult life with minimal contribution from circulating monocytes," *Immunity*, vol. 38, no. 4, 2013, doi: 10.1016/j.immuni.2013.04.004.
[357] C. Morse *et al.*, "Proliferating SPP1/MERTK-expressing macrophages in idiopathic pulmonary fibrosis," *European Respiratory Journal*, vol. 54, no. 2, 2019, doi: 10.1183/13993003.02441-2018.
[358] O. F. Hatipoglu *et al.*, "Osteopontin silencing attenuates bleomycin-induced murine pulmonary fibrosis by regulating epithelial–mesenchymal transition," *Biomedicine and Pharmacotherapy*, vol. 139, 2021, doi: 10.1016/j.biopha.2021.111633.
[359] L. Xu *et al.*, "Transforming growth factor β3 attenuates the development of radiation-induced pulmonary fibrosis in mice by decreasing fibrocyte recruitment and regulating IFN-γ/IL-4 balance," *Immunol Lett*, vol. 162, no. 1, 2014, doi: 10.1016/j.imlet.2014.06.010.

[360] L. Sun *et al.*, "New concepts of IL-10-induced lung fibrosis: Fibrocyte recruitment and M2 activation in a CCL2/CCR2 axis," *Am J Physiol Lung Cell Mol Physiol*, vol. 300, no. 3, 2011, doi: 10.1152/ajplung.00122.2010.
[361] D. Li *et al.*, "IL-33 promotes ST2-dependent lung fibrosis by the induction of alternatively activated macrophages and innate lymphoid cells in mice," *Journal of Allergy and Clinical Immunology*, vol. 134, no. 6, 2014, doi: 10.1016/j.jaci.2014.05.011.
[362] D. Schaue, E. L. Kachikwu, and W. H. McBride, "Cytokines in radiobiological responses: A review," *Radiation Research*, vol. 178, no. 6. 2012. doi: 10.1667/RR3031.1.
[363] R. Checker *et al.*, "Chemical and biological basis for development of novel radioprotective drugs for cancer therapy," *Free Radical Research*, vol. 55, no. 5. 2021. doi: 10.1080/10715762.2021.1876854.
[364] J. Biau *et al.*, "Combining the DNA repair inhibitor DBAIT with radiotherapy for the treatment of high grade glioma: Efficacy and protein biomarkers of resistance in preclinical models," *Front Oncol*, 2019, doi: 10.3389/fonc.2019.00549.
[365] S. Hume, G. L. Dianov, and K. Ramadan, "A unified model for the G1/S cell cycle transition," *Nucleic Acids Research*, vol. 48, no. 22. 2020. doi: 10.1093/nar/gkaa1002.
[366] T. K. Noah, B. Donahue, and N. F. Shroyer, "Intestinal development and differentiation," *Experimental Cell Research*, vol. 317, no. 19. 2011. doi: 10.1016/j.yexcr.2011.09.006.
[367] L. Wei *et al.*, "Inhibition of CDK4/6 protects against radiation-induced intestinal injury in mice," *Journal of Clinical Investigation*, vol. 126, no. 11, 2016, doi: 10.1172/JCI88410.
[368] M. Arroyo-Hernández, F. Maldonado, F. Lozano-Ruiz, W. Muñoz-Montaño, M. Nuñez-Baez, and O. Arrieta, "Radiation-induced lung injury: current evidence," *BMC Pulmonary Medicine*, vol. 21, no. 1. 2021. doi: 10.1186/s12890-020-01376-4.
[369] J. A. Rotolo *et al.*, "Regulation of ceramide synthase-mediated crypt epithelium apoptosis by DNA damage repair enzymes," *Cancer Res*, vol. 70, no. 3, 2010, doi: 10.1158/0008-5472.CAN-09-1562.
[370] H. Jin, Y. Yoo, Y. Kim, Y. Kim, J. Cho, and Y. S. Lee, "Radiation-induced lung fibrosis: Preclinical animal models and therapeutic strategies," *Cancers*, vol. 12, no. 6. 2020. doi: 10.3390/cancers12061561.
[371] M. P. Keane, J. A. Belperio, M. D. Burdick, and R. M. Strieter, "IL-12 attenuates bleomycin-induced pulmonary fibrosis," *Am J Physiol Lung Cell Mol Physiol*, vol. 281, no. 1 25-1, 2001, doi: 10.1152/ajplung.2001.281.1.l92.
[372] E. Dondossola *et al.*, "Self-targeting of TNF-releasing cancer cells in preclinical models of primary and metastatic tumors," *Proc Natl Acad Sci U S A*, vol. 113, no. 8, 2016, doi: 10.1073/pnas.1525697113.
[373] J. Shen *et al.*, "Anti-cancer therapy with TNFα and IFNγ: A comprehensive review," *Cell Proliferation*, vol. 51, no. 4. 2018. doi: 10.1111/cpr.12441.
[374] T. Sun *et al.*, "Inhibition of tumor angiogenesis by interferon-γ by suppression of tumor-associated macrophage differentiation," *Oncol Res*, vol. 21, no. 5, 2013, doi: 10.3727/096504014X13890370410285.
[375] L. Wall, F. Burke, C. Barton, J. Smyth, and F. Balkwill, "IFN-γ induces apoptosis in ovarian cancer cells in vivo and in vitro," *Clinical Cancer Research*, vol. 9, no. 7, 2003.
[376] S. Güttinger, E. Laurell, and U. Kutay, "Orchestrating nuclear envelope disassembly and reassembly during mitosis," *Nature Reviews Molecular Cell Biology*, vol. 10, no. 3. 2009. doi: 10.1038/nrm2641.

université PARIS-SACLAY | ÉCOLE DOCTORALE Cancérologie : biologie - médecine - santé (CBMS)

Résumé

Titre : Conséquences moléculaires et cellulaires d'AsiDNA™ combinée à la radiothérapie sur les tissus sains

Mots clés : AsiDNA™, tissue normal, radiothérapie, FLASH, radioprotection, cycle cellulaire

Résumé : La radiothérapie et la chimiothérapie sont couramment mises en œuvre dans les traitements du cancer à visée curative. Cependant, les effets secondaires sévères qui y sont associés interfèrent souvent avec l'achèvement du plan de traitement initial. Des études antérieures ont révélé que le radiosensibilisateur AsiDNA™ n'augmentait pas la sensibilité des tissus normaux, ce qui nous a amenées à évaluer le potentiel d'AsiDNA™ à protéger les tissus sains des toxicités induites par les radiations et à explorer son comportement dans les cellules normales.

Nos recherches ont révélé qu'in vitro, AsiDNA™ pénètre dans les cellules normales et tumorales avec une phosphorylation de H2AX se produisant uniquement dans la phase G1 du cycle cellulaire avec une forte réduction dans les cellules quiescentes par rapport aux cellules en division. AsiDNA™ induit un arrêt du cycle cellulaire G1/S dépendant de DNA-PK/p53/p21 uniquement dans les cellules normales. Un arrêt G1/S similaire a été identifié à la fois ex vivo et in vivo.

La combinaison d'AsiDNA™ avec la chimiothérapie ou la radiothérapie augmente la survie des cellules prolifératives saines in vitro et la radioprotection in vivo en réponse à la radiothérapie conventionnelle, sans impact additif une fois combinée avec la radiothérapie FLASH. Le séquençage de l'ARN sur cellule unique de poumon irradié a révélé une signature génétique pro-fibrotique présente dans les fibroblastes et les macrophages alvéolaires en réponse à la radiothérapie CONV qui a été réduite une fois combinée avec AsiDNA™.

Ces résultats suggèrent qu'en raison de l'arrêt du cycle cellulaire G1/S induit par AsiDNA™™ sur des cellules normales en division in vivo, la combinaison d'AsiDNA™ avec diverses modalités d'irradiation réduit la toxicité, offrant une opportunité unique d'utiliser AsiDNA™ en oncologie pour une augmentation bilatérale de la fenêtre thérapeutique.

université PARIS-SACLAY | ÉCOLE DOCTORALE Cancérologie : biologie - médecine - santé (CBMS)

Abstract

Title : The molecular and cellular consequences of AsiDNA™ combined with radiotherapy on healthy tissue

Keywords : AsiDNA™, Healthy tissue, radiotherapy, FLASH, radioprotection, cell cycle

Abstract : Radiotherapy and chemotherapy are customary implemented in cancer treatments with curative intent. However, the associated severe side effects often interfere with the completion of the initial treatment plan. Previous studies have uncovered that radiosensitizer AsiDNA™ displayed no increased normal tissue sensitivity, leading us to assess the potential of AsiDNA™ to protect healthy tissues from radiation-induced toxicities and explore its behaviour in normal cells.

Our research revealed that in vitro, AsiDNA™ penetrates normal and tumour cells with phosphorylation of H2AX only occurring in G1 phase of the cell cycle with strong reduction in quiescent cells compared to dividing cells. AsiDNA™ induces a DNA-PK/p53/p21-dependent G1/S cell cycle arrest only in normal cells. A similar G1/S arrest was identified both ex vivo and in vivo.

The combination of AsiDNA™ with chemotherapy or radiotherapy increases the survival of healthy proliferative cells in vitro and radioprotection in vivo in response to conventional radiotherapy with no additive impact once combined with FLASH radiotherapy. Single-cell RNA sequencing of irradiated lung revealed a pro-fibrotic genetic signature present in fibroblasts and alveolar macrophages in response to CONV radiotherapy which was reduced once combined with AsiDNA™.

These results suggest that due to the G1/S cell cycle arrest induced by AsiDNA™ on dividing normal cells in vivo, the combination of AsiDNA™ with various irradiation modalities reduces toxicity, offering a unique opportunity to use AsiDNA™ in oncology for a bilateral increase in the therapeutic window.